Tandem Mass Spectrometric Analysis of Bacterial Lipid A and Synthetic Glycosyl Donors Containing the 2-Amino-2-deoxy-D-Glucosaminyl Moiety

by:

Bashaeer Allehyane

**A thesis submitted to the School of Graduate Studies in partial fulfillment
of the requirements for the degree of Master of Science.**

Department of Chemistry

Memorial University of Newfoundland and Labrador

September 15, 2014

St. John's   Newfoundland and Labrador, Canada

Abstract

This study presents an interpretation of the mass spectrometry gas-phase fragmentation patterns of the extracted lipid A obtained from the native LPS extracts isolated from *Aeromonas Liquefaciencs*. This LPS SJ-19 is known to infect various fish species (Atlantic salmon and cod) which are cultivated in aquaculture ventures. The exact molecular structure of the lipid A and the core oligosaccharide region of this Rough bacterium have not yet been precisely established. This thesis presents the mass spectrometric fingerprint identification and structural elucidation of the lipid A from *A. Liquefaciencs,* which was accomplished via the use of electrospray ionization tandem mass spectrometry (ESI-MS/MS using FTICR, QIT, QHQ-MS/MS) and matrix assisted laser desorption ionization tandem mass spectrometry (MALDI-MS/MS).

In this work, tandem-in-time and tandem-in-space mass spectrometry was chosen for the structural elucidation of the lipid A isolated from *A. Liquefaciencs* SJ-19. The concomitant uses of high-energy and low-energy collision induced dissociation (CID-MS/MS) analysis were also used to elucidate the MS/MS fingerprints of this complex biomolecule and can be effectively used for any quantitative or qualitative studies.

In addition, a novel MS/MS study of a series of 2-acylated-2-deoxy-D-gluosamine glycosyl donors is also presented using ESI-MS/MS tandem-in-space and tandem-in-time mass spectrometry.

Acknowledgments

I would like to express my deep acknowledgement and appreciation to my supervisor Dr. Joseph Banoub who provided me with guidance and valuable directions during my degree program; I value him as a mentor and a father.

I would also like to thank Dr. Travis Fridgen my second supervisor for all his assistance and advice. In addition, I would like to thank Dr. Paris Georghiou for serving on my supervisory committee.

I would like to acknowledge the resources provided by Fisheries and Oceans (DFO), St. John's where I conducted my research. In addition, I would like to thank the government of Saudi Arabia Culture for their financial support for M.Sc. studies.

It would have been very difficult to complete the work associated with this document without the numerous discussions with my colleague and best friends Mervt Almostafa and Tasahil Albishi. I value their friendship and the time spent working together on my projects. I appreciate their support and assistance.

My life in Canada would have never been as pleasant without the support and the love of my family my husband Mousa Allahyani and my children. Mousa was always there for me when needed and has given me affection. I would like to express my love to my parents, sisters, and brothers. Their moral support will never be forgotten. And special thanks to all my friends in Saudi Arabia.

Last but not least, my great thanks to best friends in St. John's, Amaal Alharbi and Sarah Aljryan for the memorable moments that we have spent together.

Table of contents

List of Tables

List of Figures

*All the figures were drawn by me using CoreIDRAW Graphics Suite 12 software.

List of Abbreviations

Alternating current	AC
Atmospheric pressure	AP
Atmospheric pressure chemical ionization	APCI
Chemical ionization	CI
Collision activated Dissociation	CAD
Collision Induced Dissociation	CID
Desorption/ ionization	DI
Desorption electrospray ionization	DESI
Direct current	DC
Electron capture dissociation	ECD
Electron ionization	EI
Electrospray ionization	ESI
Electron transfer dissociation	ETD
Fast Atom Bombardment	FAB
Fourier transform	FT
Fourier transform ion cyclotron resonance	FT-ICR
Full widh at half maximum	FWHM
Galactose	Gal
Glucose	Glc
High performance liquid chromatography	HPLC
Infrared multiphoton dissociation	IRMPD
Inner membrane	IM
In-source decay	ISD

Ion trap	IT
Ion cyclotron resonance	ICR
Laser desorption ionization	LDI
L-*glycero*-D-manno-heptose	Hep
Lipopolysaccharude	LPS
Liquid chromatography	LC
Mass spectromety	MS
mass to charge ratio	*m/z*
Matrix assisted laser desorption ionization	MALDI
Outer membrane	OM
Phosphate-buffered salinc	PBS
Post-source decay	PSD
Quadrupole	Q
Quadrupole ion trap	QIT
Quadrupole orthogonal time-of-flight	Qq/TOF
Quadrupole-hexapole-Quadrupole	QhQ
Radio-frequency	RF
Secondry ionization mass spectrometry	SIMS
Select ion monitoring	SIM
Surface-induced dissociation	SID
Tandem mass spectrometry	MS/MS
Time-of-flight	TOF
Triple quadrupole	QqQ
Uridine diphosphate	UDP
α-3-deoxy-D-manno-oct-2-ulosonicacid	

Chapter 1

Introduction

1.1. Mass spectrometry

Mass spectrometry (MS) is one of the best analytical tools used for the structure elucidation of molecules and for the determination of molecular mass of chemical or biological compounds. Mass spectrometry has generated substantial interest due to its appealing properties such as providing precise results, analytical versatility, and high sensitivity. Typically, MS depends on the gas phase study of the produced fragment ions (- and + ion modes) that are separated electrically or magnetically according to their mass-to-charge ratio (*m/z*).[1]

In the late 1880s, mass spectrometry was first introduced by the physicist Eugen Goldstein, who discovered a new type of radiation, and called it "Kanalstrahlen", and he demonstrated that these new rays were merely positively charged particles.[2] Inspired by these discoveries, Sir Joseph John Thomson illustrated the value of this finding in 1913 by building the first mass spectrometer within the field of analytical chemistry.[3]

Mass spectrometry consists of three principal components; an ionization source, a mass analyzer and a detector, as schematically shown in Figure 1.1. The sample to be analyzed is first transferred into the ionization chamber of the spectrometer using the inlet. The sample molecules introduced in the source must be in the gas-phase; these are then ionized under a high vacuum atmosphere. The formed ions are expelled from the ionization chamber in a form of a beam of ions which is then accelerated

towards the mass analyzer by means of ion optics such as skimmer and focusing lenses.

The mass analyzer used in MS is plentiful and these can be: quadrupole, ion-trap, electric and/or magnetic fields, and time of-flight. The accelerated ions are sorted and separated in the analyzer, based on their mass-to-charge ratio (*m/z*) by maintaining a selected stable trajectory of each *m/z* ion.

Following the ion separation in the analyzer, the ions are detected by the detector and the resulting signal is converted into the data system to display the spectra. All of the major components of the MS are enclosed in vacuum system to minimize the collision between the ions and the molecules of other gases.

The ionization source, mass analyzer, and detector can be made in different configurations to create a variety of different geometries. However, the best choice of the combination of ionization source and mass analyzer relies on the sample characterization (polarity variance) and on data type desired (resolution, accuracy and mass range).[4,5]
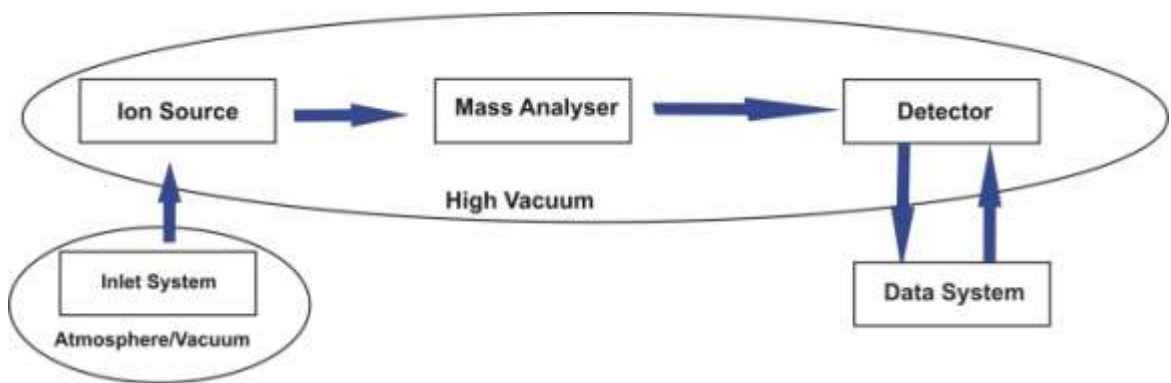
Figure 1.1: Schematic representation of the main components of mass spectrometry.

In this thesis, different types of mass spectrometer instruments have been used for the gas-phase study of lipid A of *Aeromonas Liquefaciencs* SJ-19 and for a series of synthetic compounds composed of 2-amino-2-deoxy-β-D- glycosides. The following ionization methods and the different analyzers were used: Matrix-assisted laser desorption/ionization time-of-flight (MALDI-TOF-MS), electrospray ionization with a quadrupole-hexapole-quadrupole (ESI-QhQ-MS) mass spectrometry, the hybrid electrospray ionization quadrupole/time-of-flight (ESI-QqTOF-MS) mass spectrometry, electrospray ionization quadrupole ion trap (ESI-QIT-MS), and Fourier transform ion cyclotron resonance mass spectrometry (FT-ICR-MS).

The diagnostic molecular ions were also studied by tandem mass spectrometry to identify their structures and to study their fragmentation routes.

In this chapter, the different ionization sources and an overview of the main MS and MS/MS techniques that were utilized in the context of this thesis will be presented.

1.1.1. Ionization techniques

Mass spectrometry allows the study of wide classes of molecules, ranging from small volatile, to polar and very large molecules. All possible types of analytes cannot be ionized by just one ionization technique, and a wide range of ionization techniques are available nowadays. The choice of the most suitable will depend on the physico-chemical properties of the analyte under investigation, its molecular weight, volatility and polarity, etc.[6,7] In this introduction two major types of ionization will presented namely hard and soft ionization techniques.

1.1.1.1. Hard ionization techniques

The first type to be discussed is the electron ionization (EI) method. In the ionization source the introduced gaseous molecules (vapor phase and high vacuum ≤10 Pa) are ionized by collisions with energetic electrons (typically 70 eV). Such interactions result in the generation of positive molecular radical ion and two electrons, as shown by the following equation:

$$M + e^- \longrightarrow M^{+\bullet} + 2e^-$$

The EI technique has a limitation that it is only effective in the study of volatile and thermally labile compounds due to the caveat that the sample must be introduced in the ionization chamber in its vapor state.[8]

Chemical ionization (CI) is another common type of mild ionization techniques. In this technique, the formation of the analyte ions is achieved by using ion-molecule reactions. In CI, a reagent gas such as hydrogen, methane, or ethane undergoes collisions in the ionization chamber with the electron beam to produce thermally stable gaseous ions, as illustrated in the following equation with methane (CH_4) as is an example:

$$CH_4 + CH_4 \longrightarrow CH_5^+ + CH_3^+$$

$$CH_3^+ + CH_4 \longrightarrow C_2H_5^+ + H_2$$
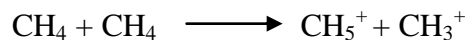
The gas ions then interact with the introduced sample molecules (M) resulting in the generation of the $[M+H]^+$ analyte ions. This analyte-ionizing gas interaction results in either the protonation (+ ion mode) or depronated (- ion mode) CI can be performed under various vacuum conditions according to the sample characterization.[8,9]

$$M + CH_5^+ \longrightarrow [M+H]^+ + CH_4$$

5

1.1.1.2. Soft ionization techniques

Soft ionization techniques have played an important role for studies of the structure determination and molecular mass identification of biomolecules and organic polymers. Numerous methods of desorption/ionization (DI) have been used to analyze large bimolecular masses and involve the impact on condensed-phase samples by an energetic projectile, which can include the following: [11,12]

- Photons (laser desorption, such as matrix-assisted laser desorption ionization (MALDI))[11]

- Excited atoms translationally (fast atom bombardment (FAB))[13]

- Energetic ions (secondary ion MS (SIMS))[14]

Electrospray ionization (ESI) has also been widely used to produce gas phase ions of thermally labile large biomolecules.

In the field of biotechnology, one of the most important applications for the analysis of insoluble biomolecules is MALDI-ionization. In contrast to MALDI- ionization, the ESI ionization method allows the analysis of analytes dissolved in solutions. MALDI and ESI are common techniques which have been used to volatize and ionize the proteins and peptides for mass spectrometric analysis.[15] A new combination between LDI and ESI is desorption electrospray ionization (DESI) which allows ambient MS for different applications including forensics, chemistry, and biology.[10] DESI permits the analysis of soluble and insoluble analytes.[16]

In 2002, the fourth Nobel Prize in mass spectrometry was awarded to John Fenn for developing ESI and Koichi Tanaka for developing MALDI.[17,18]

1.1.1.2.1. Electrospray ionization (ESI)

The development of ESI has allowed the analytical ionization of molecules with high molecular mass to be used in various applications including proteomics. Although a wide range of other analytes such as polar organic, inorganic, and metal-organic complexes have also been analyzed by using ESI with different mass analyzers.[19] These developments were first started in the late 1960s by the work of Dole and co-workers who were able to ionize a high molecular weight polymer into the gas phase as a charged species using the first ESI source which was coupled to a quadrupole mass analyzer.[18]

The main characteristic of ESI is the formation of multiple-charged ions of the analytes in solution under atmospheric pressure.

The sample in ESI must be diluted in a polar volatile solvent to make a solution which will be injected using a mechanical syringe pump through a hypodermic needle or stainless steel capillary, as shown in Figure 1.2. At low flow rate (typically 1-20 µl/min) the sample is constantly sprayed. In the chamber, the metal capillary surrounding the source sampling is subjected to high voltage (2-6 KV), resulting in the formation of highly-charged electrospray (ES) droplets (i.e. nebulization). Dry N_2 flows around the capillary in order to obtain better nebulization and to direct the spray emerging from the capillary into a mass analyzer, as well as to minimize the size of droplets by solvent evaporation.[20-23]
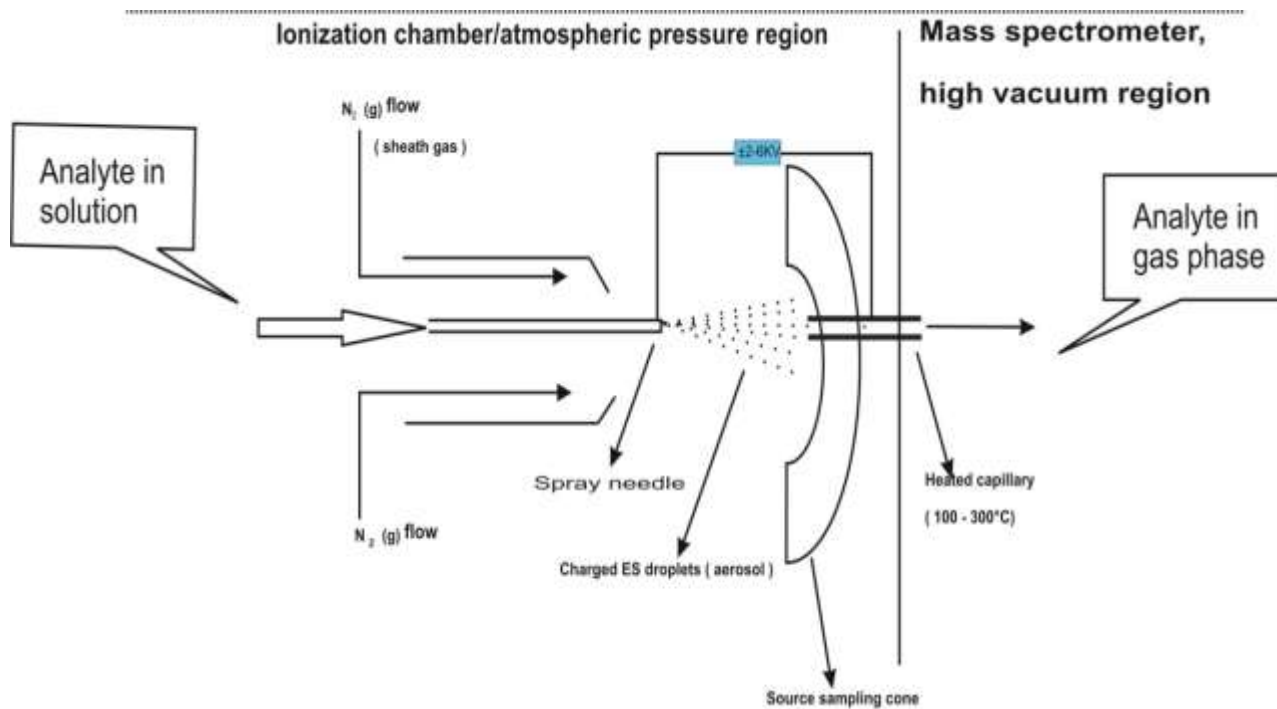
Figure 1.2: Apparatus for electrospray ionization.

There are two mechanisms that describe how the droplets are reduced, see Figure 1.3.[23] The first mechanism of ESI ion formation is called the ion evaporation method and is believed to favor ions with relatively low (m/z) values. Under the above condition, the droplets break down and their size is continuously being diminished while shifting inside the source. Eventually, the repulsive forces among the ions on the surface of the shrinking droplets become very high. As a result of the surface tension of the solvent from these forces, ions will desorb into the gas-phase.

The second theory is the charge residue model, which is predicted to be dominant in the case of ions with very high (m/z). The evaporation of the solvent is continuous and is accompanied by droplet fragmentation so that a single ion (probably multiply charged) is formed at the end of this process.[24]

ESI-MS has the advantage of being able to analyze biological analytes of non-covalent interactions. Samples of large masses can be handled, as well. On the other hand, ESI cannot be useful when using a sample which is a mixture and the results are considered to be unreliable.[25]
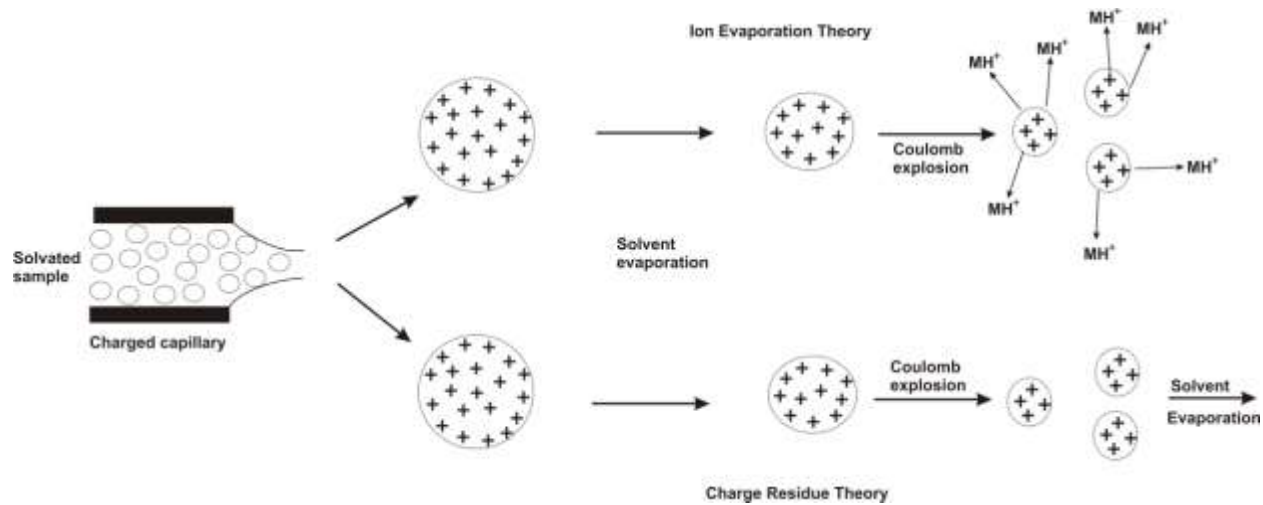
Figure 1.3: Schematic representation of the charged dropletes formation during ESI.

1.1.1.2.2. Matrix-assisted laser desorption ionization (MALDI)

MALDI is a soft ionization method used mainly in the analysis of biomolecules ranging from small (m/z<1000) to large (m/z>100 KDa) due to its wide range of applicability. As a result of its high sensitivity and tolerance for salt and other contaminants, MALDI has been used in various chemical studies such as proteomics, lipidomics and metabolomics. [26-30] For glycomics, it was noted that as the molecular mass of the sample is increased, the MALDI efficiency becomes higher in terms of natural carbohydrates. One of the main features of using MALDI for structural investigation is its preference for singly-charged ion formations.[31]

A sample to be tested in MALDI must be first dissolved in an appropriate solvent and then mixed with an excess amount of a suitable matrix in solution. This solution is then placed on a MALDI plate and, after the evaporation of the solvent; the matrix is co-crystallized with the analyte. After loading the plate into the MALDI instrument, the analytes are ionized into a gas phase via a laser beam, typically a nitrogen laser at a wavelength of 337 nm. The laser beam hits the sample-matrix crystal, leading to the absorption of the laser energy by the matrix and then transmitted to the energy absorbed to the analyte to initiate its ionization. Figure 1.4 illustrates how the laser energy ionizes the sample.[32]

To mass
spectrometer

Focussing
lens

Extraction
grid

Analyte
ions

Matrix
ions

Laser
beam

Cation

Analyte/matrix spot

Sample plate
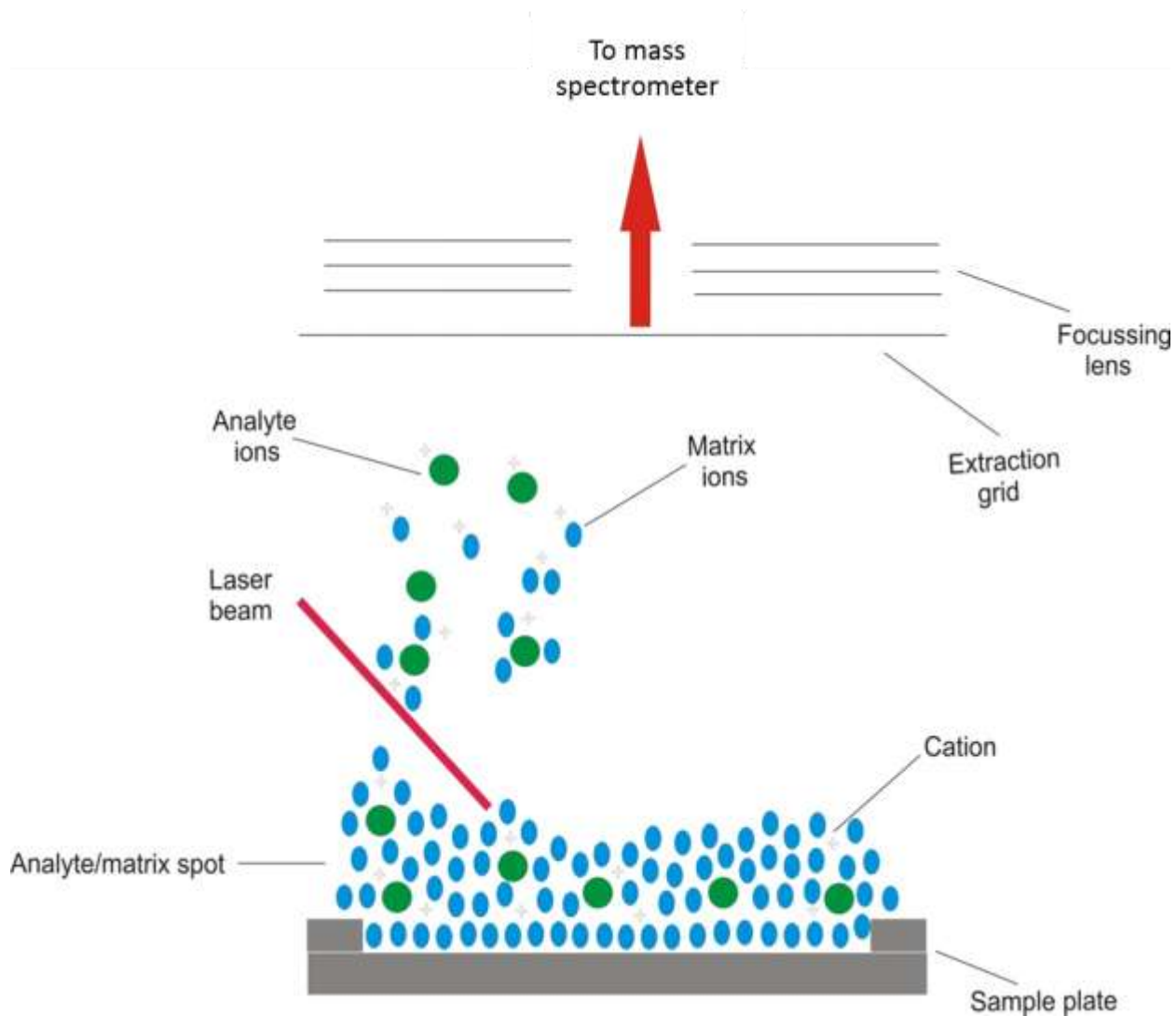
Figure 1.4: Representation showing the procedure of desorption/ionization of the analytes by a laser beam during MALDI.

The proper selection of the matrix is important and it depends on the nature of the analytes. The matrix selection can be influenced by the ionization mode, whether positive or negative ion modes are used. Basic matrices are favored in the latter case, while acidic ones are more efficient in the case of the former (i.e. proton donor).[33]

Various types of matrices are available including α-cyano-4-hydroxycinnamic acid (CHCA), sinapinic acid (SA), and 2,5-dihydroxybenzoic acid (DHB). MALDI was initially operated under vacuum; however, atmospheric pressure (AP) MALDI was developed in 2000. Operating in the atmospheric pressure AP-MALDI has several advantages, such as reduced cost, enhanced ease of operation and improved commercial production of mass spectrometers with interchangeable MALDI and ESI sources, such as a hybrid instrument of MALDI /ESI-QqTOF-MS.[34]

1.1.2. Mass analyzer techniques

The gas phase ions once produced in the ionization source are required to be sorted or separated based on their mass-to-charge (m/z) ratios. Several principles have been utilized to separate the ions including static or dynamic electric and magnetic fields which can be performed in a single mass analyzer or more combined together. The development of these mass analyzers has led them to be employed effectively in many areas of analysis especially in structural determinations.[35]

A new analyzer of orbitrap was available to use in 2005 which has a similar performance as in Fourier transform (FT) ion cyclotron resonance spectrometer; however, more modest size, complexity, and cost are the main limitations of its uses.[36].

The main criteria to evaluate the mass analyzer performance are the mass range limit, the transmission of ions, the analysis speed, the mass accuracy, and resolution. In this study, quadrupole (Q), time-of-flight (TOF), ion-trap (IT), and ion cyclotron resonance (ICR) mass analyzers are mainly focused upon.

1.1.2.1. Quadrupole (Q) analyzer

A quadrupole is a mass analyzer which separates the ions according to their (*m/z*) ratios, using the stability of the trajectories in oscillating electric fields. The quadrupole comprises four parallel rods of circular or hyberbolic section applying a potential to separate ions in the range of 5Kv, as shown in Figure 1.5. The simultaneous applications of a direct current (DC) potential and a radiofrequency (RF) potential between these rods leads to the ion oscillation in order for these ions to move along the z-axis. The followings equation describes the voltage across the rod:

$\Phi=_+(U+V\cos \omega t)$ and $\Phi=-(U-V\cos \omega t)$

where Φ is the voltage applied to the rods, ω is the frequency, U is the DC voltage, and V is the RF voltage amplitude.[37]

Ions with the appropriate values of U, V, and ω and close values of (*m/z*) will only possess the right trajectory and survive to reach the detector. Otherwise ions will be ejected since they collide with the similar charged rods.

The development of the Mathieu equation provides a deeper understanding of the ions' stabilities and trajectories. The key feature of a quadrupole is that it is well-suited to chromatographic coupling, as its scan speed can easily reach 1000 Ths[-1] and higher. Also it does not rely on the ions kinetic energy when they leave the source. On

the other hand, coupling more than a mass analyzer is required to perform MS/MS analysis. Although a quadrupole mass filter has excellent transmission efficiency, it cannot be applied to a large mass range and is characterized by having the narrowest mass range as compared to other multipoles.[38]

Quadrupole Mass Filter
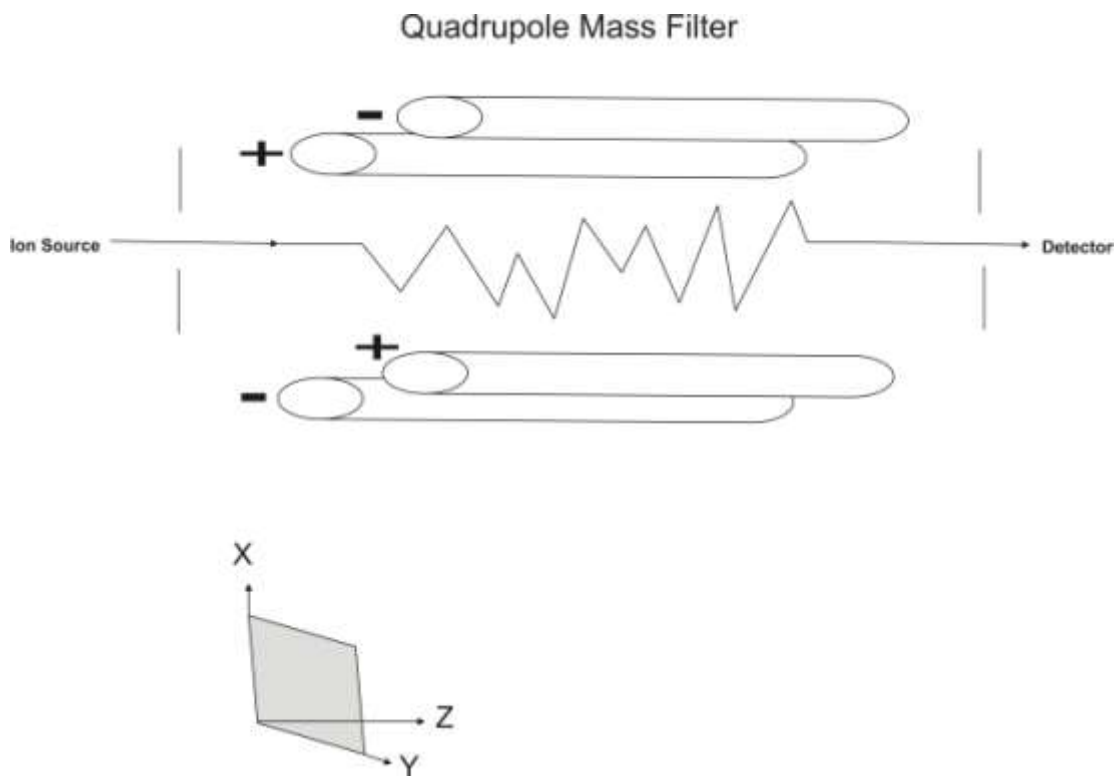
Figure 1.5: Schematic diagram of quadrupole mass analyzer and the x, y, and z axis where ions drift through the array of rods.

1.1.2.2. Time-of-flight (TOF) analyzer

The TOF analyzer separates ions based on their velocities after being accelerated by an electric field. The TOF instrumentation is demonstrated in Figure 1.6. When ions are expelled from the source by an intermittent process or a transient application, they accelerate into the flight tube as a potential difference is applied between an electrode and the extraction grid at a range of (10^3 to 10^4 V). Then ions travel into a field-free drift tube where they are separated according to their velocities as they are distributed by their masses and different kinetic energies. However, ions with the same kinetic energy will have different velocities in different directions. Hence, the lighter particles arrive at the detector earlier than the heavier ones. The flight time t_f is shown in following equation where L is the distance from the source to the detector. Typical flight times are (1 to 50 μs).[39]

$$t_f = L/v = L\sqrt{m \div 2zeV}$$
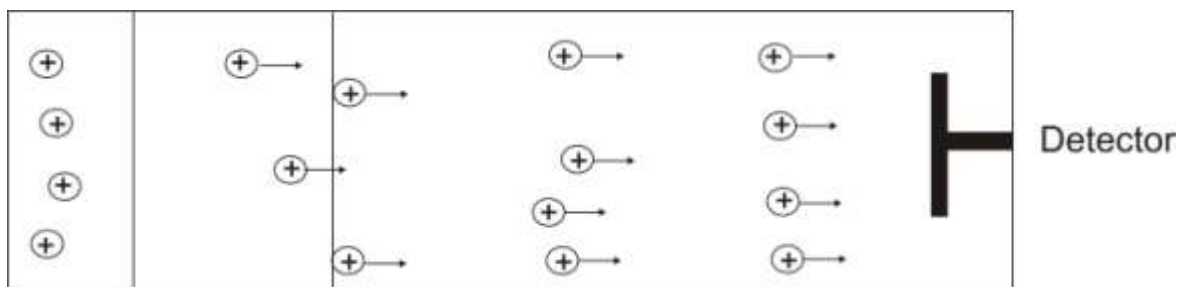
Figure 1.6: A schematic representation of the ions accelerating in the TOF.

One of the notable limitations of TOF is its resolution and sensitivity as ions reach the detector in microseconds. The resolution of the ions could be improved by the employment of an electrostatics ion mirror TOF, a reflectron, which increases the time to reach the detector as shown in Figure 1.7.[40] The reflectron consists of a decelerating and reflecting field to correct the temporal spread that results from the initial velocity of the ions. Thus ions with high kinetic energies will penetrate the decelerating region and spend more time within the reflecting region. On the other hand, a TOF analyzer possesses several advantages including simplicity, ruggedness, no limitation of upper mass range and ease of accessibility of the ion source.[41] The TOF analyzer is preferable and the most adapted for pulsed ionization methods such as MALDI, since the laser shot determines the starting time for the time measurement of the ions reaching the detector.
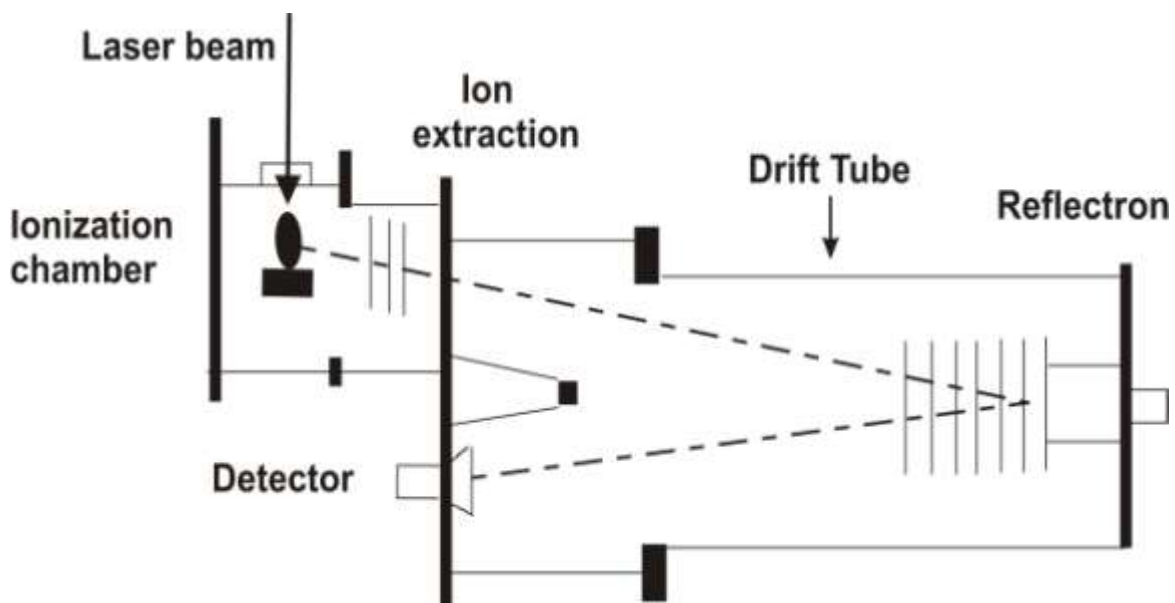
Figure 1.7: Schematic representation of the reflectron time of flight (TOF) analyzer.

1.1.2.3. Quadrupole ion trap (QIT)

A quadrupole ion trap (QIT) was developed by the physicists Wolfgang Paul and Hans Dehmelt to whom the Nobel Prize was awarded in 1989.[42] Figure 1.8 shows the main components of QIT, which includes a central doughnut-shape ring electrode and a pair of end cap electrodes with hyperbolic surfaces. A RF potential is applied to all the three electrodes of hyperbolic cross-section of trapped ions to create a dynamic parabolic region inside the trapping volume, so that ions are concentrated in the center. Ions with an appropriate m/z value circulate in a stable orbit within the trapping field. When the RF voltage is increased, the orbit of heavier ions becomes stabilized; however, for those of lighter ions which collided with the wall of the ring electrode and this orbit becomes destabilized. The ions' trajectories are expanded as a function of time due to the fact that ions repel each other in the trap. To avoid ion losses by this expansion, the trap must be maintained under a Helium gas pressure of around 10^{-3} Torr, which removes excess energy from the ions by collision.[43,44] The ions' trajectories are determined by solving Mathieu's equation in such a field similar to linear quadrupole.

The ion trap has the advantage of tapping ions for a relatively long time and stable ions can then be selected by a technique called mass- selective ejection. Increasing the radio-frequency voltage of the ring electrode causes destabilized ions which then leave the trapping region via an opening in the lower end-cap.[45]
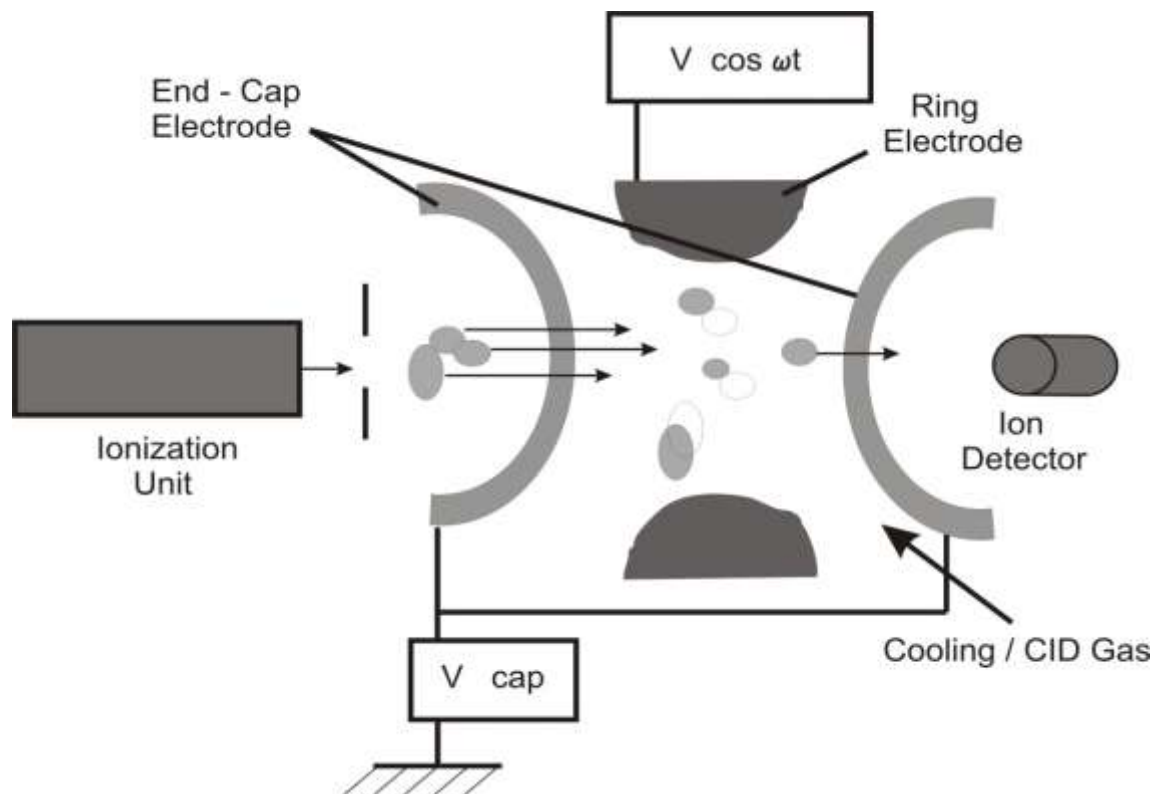
Figure 1.8: Schematic diagram of quadrupole ion trap mass analyzer (QIT).

The ion trap analyzer is a highly sensitive method that can achieve a low detection limit. Also, it is a compact, rugged, and less costly device capable of obtaining a high performance. High resolution can also be achieved by a slow scan mode ($>10^6$ at m/z >1000), but the mass measurement accuracy is relatively poor.[43]

1.1.2.4. Ion cyclotron resonance (ICR)

The interest in Fourier-transform ion cyclotron resonance mass spectrometry FT-ICR-MS has increased since its introduction in 1974 by Comisarow and Marshall. This technique consists of three basic components. These: a superconductive magnet; an ultrahigh vacuum, and an analyzer cell (ICR), as illustrated in Figure 1.9. The heart of FT-ICRMS is the analyzer cell which measures the mass-to-charge (m/z) ratio of an ion according to its frequency, since the ion is processed in a magnetic field.

The ICR cell is made up of three opposing pairs of plates, forming various shapes (cubic, cylindrical, orthorhombic, etc.), which are named as the trapping plate (one pair) which lies perpendicular to the magnetic field and the excitation and detection plates (2 pairs) which are parallel to the magnetic field.[46]
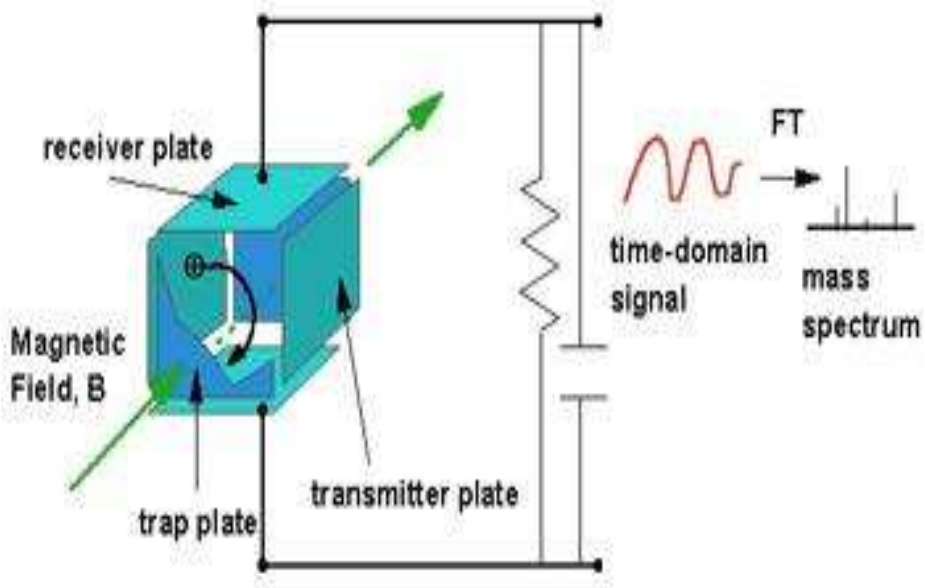
Figure 1.9: Schematic diagram of a ion cyclotron resonance (ICR) analyzer.

Ions pass into the ICR cell after being generated in the ionization source. Then they undergo harmonic oscillations in the electric field between the trapping plates to create a trapping motion. Since the magnetic field is strong, ions undergo stable cyclic motion in a plane perpendicular to the magnetic field, to obtain a cyclotron motion via a force known as the "Lorentz force". The cyclotron motion is represented by the cyclotron frequency ω_c because each ion rotates with its frequency. A magnetron motion is also positioned around the cell axis and is controlled by the magnetic and the electric field. All these three motions typically lead to a complex ion movement in the analyzer cell, as shown in Figure 1.10.[47] Typically, ions undergo two forces in the cell as can be illustrated in the following equations:

Centripetal force $F = qB/m$ (1)

Centrifugal force $F = mv^2/r$

Ions can be stabilized on a trajectory when the balance of these two forces occurrs:

$$q\upsilon B = m\upsilon^2/r \quad \text{or} \quad qB = m\upsilon/r \tag{2}$$

where q is the ion charge, m is the ion masses, and B is the strength of the magnetic field.

Ions complete a circular trajectory of $2\pi r$ with a frequency υ:

$$\upsilon = \omega/2\pi r \tag{3}$$

Thus the angular velocity ω is equal to:

$$\omega_c = 2\pi\upsilon = \upsilon/r = qB/m \tag{4}$$

As ω_c is proportional to m/q, the smaller that the mass–to-charge ratio is, the greater the cyclotron frequency becomes clearer.[47,48]
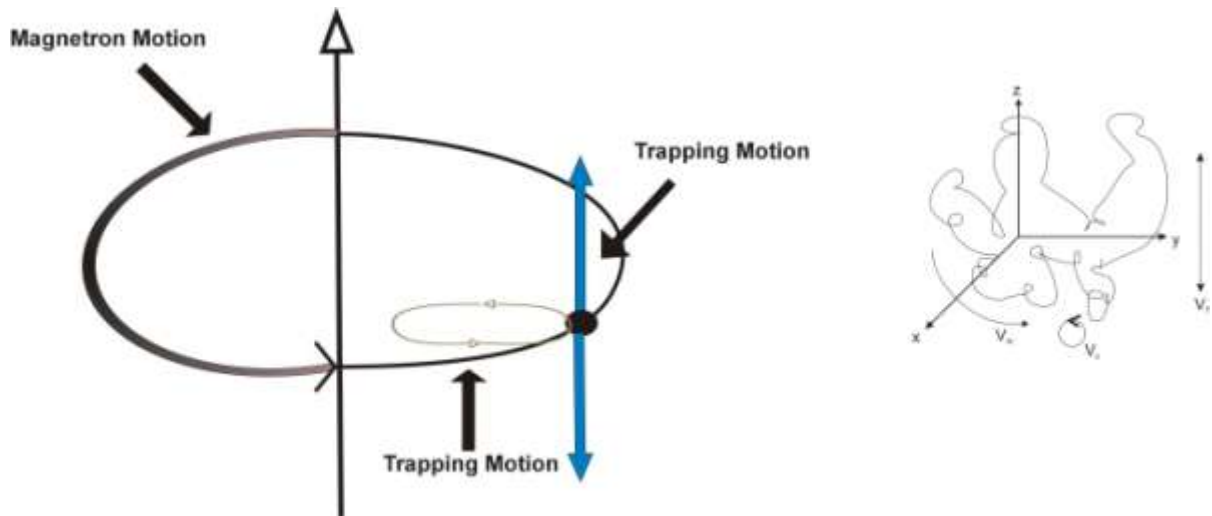
Figure 1.10: Ion motions within an ICR cell.

Since ions have kinetic energy when they move to the ICR cell, they are excited under the impact of the magnetic field and even at room temperature. However, ions are not detectable on the detection plate as they generally excited at room temperature. Under this condition, ions are statistically distributed in the cell as a result of their different velocities in their orbits provided by their different energies for ions of the same m/q. Thus, these ions must be coherently excited as "ion packets" to a larger radius in order to obtain a measurable signal via supplying a sinusoidal voltage to the excitation plates. An image current can be taken when the ions become close to the excitation plates by attraction (positive ion detection) or repulsion (negative ion detection). This is a simplified description of how ions can be generated in the ICR cell.[49]   ICR is a highly sensitive technique because of its ultra-high mass resolving power and mass accuracy. It can be used for high-throughput analysis if coupled with an autosampler.

1.2. Tandem mass spectrometry

Tandem mass spectrometry (MS/MS) is a powerful technique involving multiple steps rather than a single step mass spectrometry that allow ions or fragments to be analyzed, providing useful structural information. The basic components are illustrated in Figure 1.11. Ions or fragments, which are produced in a soft ionization source, pass through the first mass analyzer so that ions with particular m/z are selected. These ions, known as *the precursor ions*, are processed under gas collision or by an intense laser beam in the collision cell, to produce ions, called *the product ions.* These ions are then analyzed in the second mass analyzer and are detected by the ion detector.[50-52]
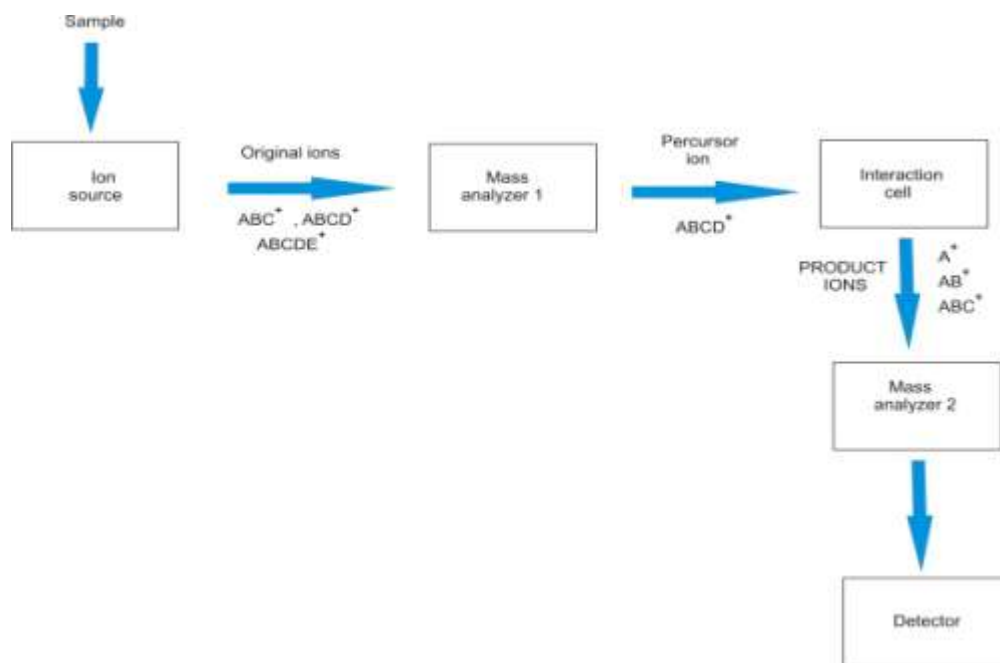
Figure 1.11: Schematic diagram of the main components of tandem mass spectrometry (MS/MS).

Various types of spectra can be identified from MS/MS experiments as illustrated in Figure 1.12. The product ion scanning is one of the four main scan experiments that can be performed. The product ion is isolated in the second mass analyzer and analyzed in the first mass analyzer to obtain the precursor ion. The precursor ion scan can be also obtained by isolating it in the first step followed by the ion fragment and scanned in the second mass analyzer. Additionally, a natural loss scan can be obtained by the first mass analyzer for all masses and also the second mass analyzer. However, the second mass analyzer must be at a set offset from the first one so that, it is not possible to be done in time tandem instruments. This scan is typically useful for closely related compounds, which often result in the same product ions. Finally, both

mass analyzers can be simultaneously measured a set of preselected analyte masses which gives a select ion monitoring scan (SIM).[53]

In tandem mass spectrometry, ion decomposition can be obtained by four main mechanisms: *a)* collisions of ions with a gas, generally nitrogen, helium, or argon: collision induced dissociation (CID), collision activated dissociation (CAD) experiments; *b)* interactions of ions with electrons: electron capture dissociation (ECD) and electron transfer dissociation (ETD); *c)* interactions of ions with photons by using infrared multiphoton dissociation (IRMPD); *d)* interactions of ions with surfaces: surface-induced dissociation (SID).[54-57]
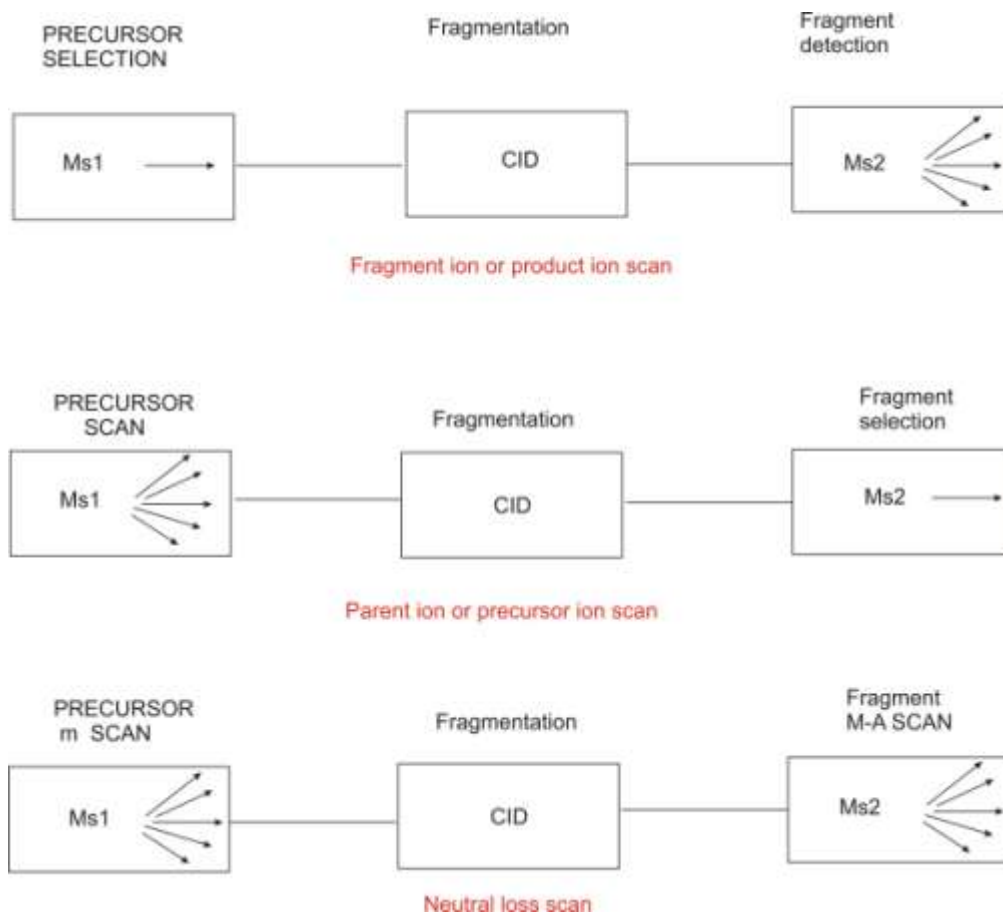
Figure 1.12: Block diagram of scan modes of MS/MS.

In fact, several combinations of mass analyzers can be assembled including sector, TOF, quadrupole, and ion trap. Tandem mass spectrometry can be performed in physically separated mass analyzers, called *tandem-in-space* or in single mass analyzer, called *tandem-in-time.* The most common type of tandem-in-space mass spectrometer is a triple quadrupole instrument. The mass analysis in tandem-in-time mass spectrometry is accomplished with ion trapped in a certain spatial region. Thus, the unwanted ions are expelled from the trapping place and the selected ion is kept, to be dissociated and analyzed.

QIT-MS^2 and FT-MS^2 instruments (tandem-in-time-MS) can be used with one analyzer and can perform multiple MS experiments (MS/MS), which are powerful tools for structural studies.[50,51]

In this work, both types of tandem mass spectrometry were employed; therefore, we have used a high collision energy tandem in space mass spectrometer is a MALDI-TOF/TOF-MS/MS spectrometer was used. In addition, several low-energy collision dissociation tandem mass spectrometers such as: the ESI-triple Quadrupole-hexapole-quadrupole (QhQ-MS/MS) and hybrid quadrupole orthogonal time-of-flight QqTOF-MS/MS instruments (tandem-in-space-MS); two low-energy collision dissociation tandem-in-time mass spectrometers which included the ESI-QIT-MS/MS, and ESI-FT-ICR-MS/MS instrumentations (tandem-in-time-MS) were used.

1.2.1. Tandem in space mass spectrometry

1.2.1.1. ESI-Quadrupole-hexapole-Quadrupole MS/MS

A triple QhQ mass spectrometer equipped with two quadrupoles and a central hexapole and is symbolized by two upper cases Qs and the lower case h, which represents the RF-only hexapole, Figure 1.13. The central hexapole is used as a collision cell where the selected ions from Q_1 undergo collision in Q_2 with a gas, usually a helium or argon.[58]

The product ions produced by CID have enough internal energy to convert a fraction of its kinetic energy to enhance fragmentations, and these ions are transmitted through the Q_3 to be separated. The kinetic energy of ions can be converted to the internal energy by increasing thier kinetic energy or/and using a more massive target to excite the electronic states in the precursor ions.

Several scan modes can be performed with different analysis. The efficiency of triple quadrupole fragmentation is high; however, reproducibility is low particularly between different mass spectrometers.[59]
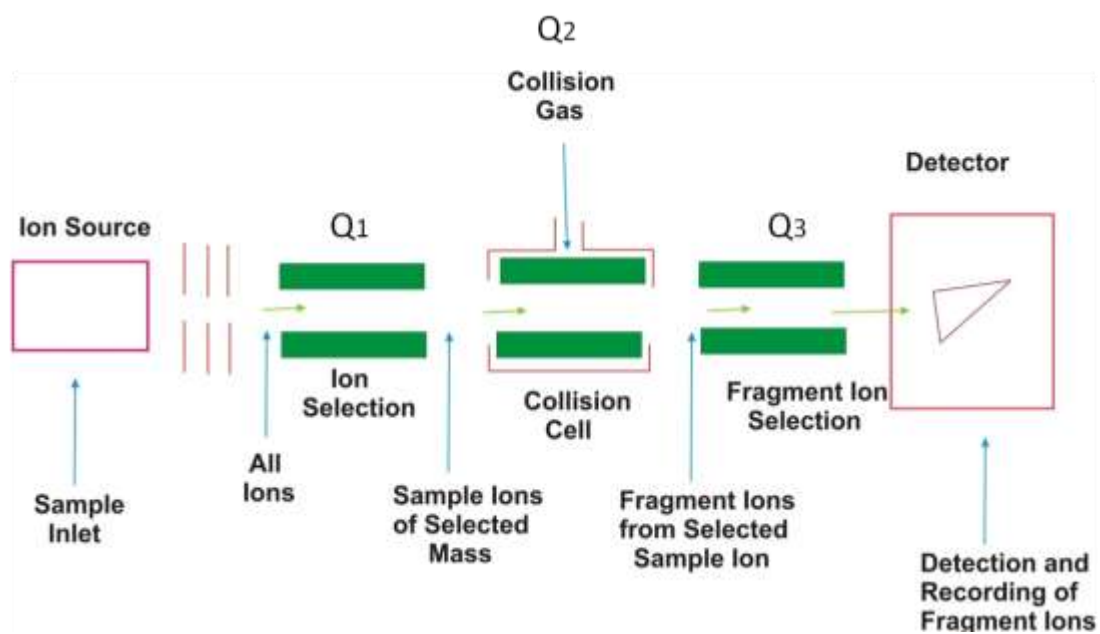
Figure 1.13: Triple Quadrupole mass spectrometry.

1.2.1.2. MALDI-TOF/TOF-MS/MS

A time-of-flight mass spectrometer can be utilized in tandem mass spectrometry by combining a linear TOF with a reflectron, (Figure 1.14). After ions have a sufficient internal energy, they can fragment to obtain product ion and neutral fragment.[60]

In the linear TOF, if the ions fragment during their flight path, they can be discriminated. The fragmentation which is called post-source decay (PSD) fragmentations first begins when the metastable decomposition occurs in the field-free region of the TOF flight tube.[61] This fragmentation is observed when the life-time induced by the internal energy of an ion is intermediate between its time spent in the source and its flight time.

Also, the fragmentations taking place in the source between two TOF are called in-source decay (ISD) fragmentations.[62] This is as a result of increasing the potential differences in the source to induce energetic collisions. In this situation, when the life-time of an ion is greater than its flight time, this ion reaches the detector before any fragmentation occurs. On the other hand, when the lifetime of an ion is shorter than its flight time, it fragments before leaving the source. These ions are accelerated in the flight tube that has a reflectron so that the lighter ions will spend more time than heavier onesin the reflectron region.

Collision-induced dissociation (CID) also can be utilized in MALDI-TOF/TOF-MS/MS.[63] In CID experiments, two main stages are required: collision activations and unimolecular dissociations, these two main stages are the two sequential time-of-flight analyzers. Accordingly, the selected precursor ions is isolated in the first stage and

following in the CID chamber collides with a neutral target gas, generally helium, nitrogen or argon, at a pressure such that ions undergoes one or more collisions. As a result, these ions are excited to higher energy states, which involve conversion of part of the translational energy of the ion to internal energy, with a consequent bond cleavage and dissociation.[64] At higher gas pressures, both the number of ions undergo collisions and the possibility for an individual ion to collide numerous times with the target gas molecules increases. Furthermore, the product ions formed by dissociation of the precursor ion can be further separated and analyzed in the second TOF analyzer.[65]
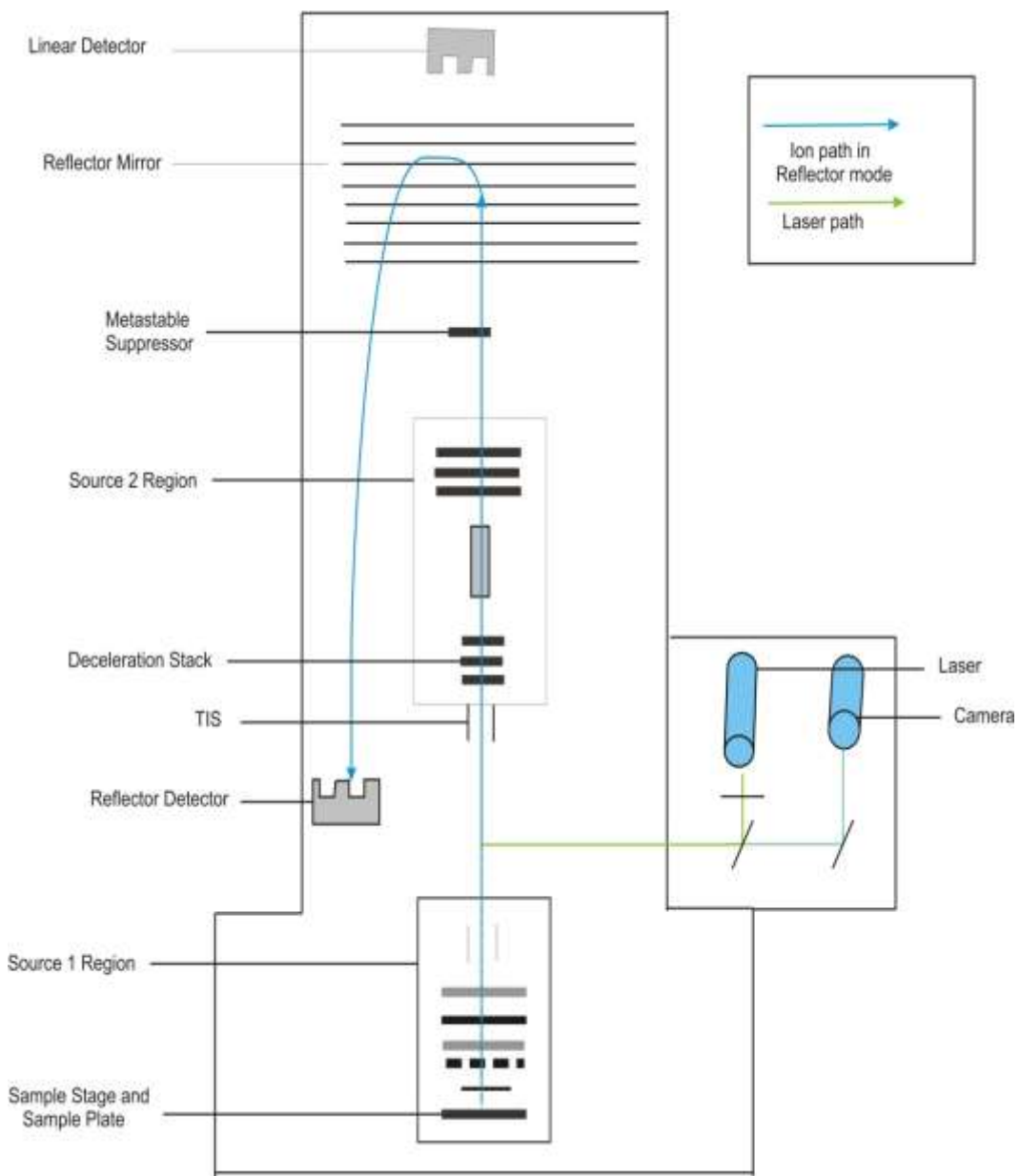
Figure 1.14: Schematic representation of MALDI-TOF/TOF-MS/MS

1.2.1.3. ESI-QqTOF-MS/MS

 The QqTOF instrument, shown in Figure 1.15, was first introduced in 1996 by Morris *et al* and was envisioned to be capable of linking both the scanning capabilities of a quadrupole and the resolving power of a TOF analyzer.

Owing to such properties, QqTOF has been capable of providing high-quality, informative, simple, one-stage MS and tandem MS/MS spectra. Figure 1.15 reveals the main components of the QqTOF-MS instrument, in which three quadrupoles are linked to a TOF analyzer aligned in the orthogonal configuration with respect to the quadrupoles; and, hence, the name QqTOF orthogonal mass spectrometry was assigned. The first quadrupole (Q_1) which operates in the RF mode is mostly employed to focus ions as well as to improve the quality of the ion beam by cooling the ions. The second quadrupole (Q2) is used during MS/MS and acts as the ion filter portion of the instrument for selection of the precursor ion (mass-resolving quadrupole). The third quadrupole (Q_3) is the collision cell in which low-energy CID fragmentation occurs. All of Q1 and Q3 quadrupoles share the property that they operate in the RF-only mode during simple single-stage MS analysis.[65,66]

The QqTOF possesses appealing advantages that it can be combined with either ESI or MALDI with little manipulation of the configuration. The interface of QqTOF with MALDI is substantial importance. QqTOF-MS/MS has also other merits such as high sensitivity and mass accuracy, ease of operation, and high resolution. The high sensitivity of QqTOF is seen when compared to a triple quadrupole, where the sensitivity of QqTOF is 100-fold greater than that of a triple quadrupole. However use of a triple quadrupole is still preferred for quantitative studies and high efficiency

functions such as those used for precursor ion scans in which the "parent" ion of a

specific fragment can be identified. [67]
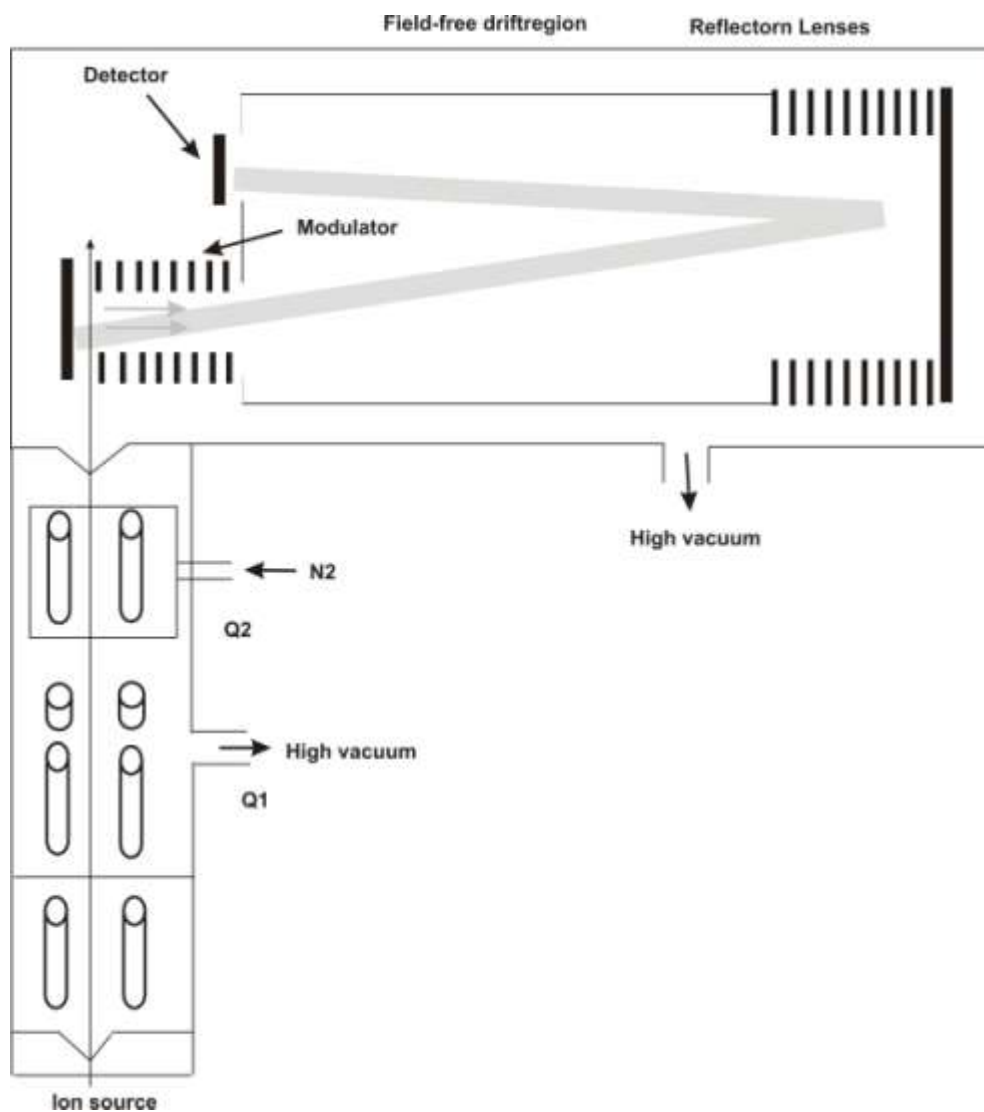
Figure 1.15: Schematic representation of the QSTAR hybrid QqTOF. It is also representative of a Hybrid quadrupole orthogonal time-of-flight mass spectrometer.

1.2.2. Tandem in Time mass spectrometry

1.2.2.1. ESI-QIT-MS/MS

The Quadrupole Ion Trap (QIT) is a tandem-in–time mass spectrometer, performing multiple cycles; a demonstration of up to 12 stages of (MS^{12}) is established in the same space-separated stages. Two stages are required: isolation and fragmentation. Isolation of a narrow range of *m/z* ions or species can be achieved in many ways; however, a forward scan followed by a reverse scan can be used to eject all the ions except the *m/z* of interest. Another method to isolate depends on the application the broad range supplementary AC frequencies to the end cap with a gap around the secular-frequency of the ions being isolated; (Figure 1.16). [68,69]

The precursor ions are selected after formation and storing in the first mass analysis by applying an RF waveform to eject all ions expect the precursor ions at the *m/z* of interest. Interring bath of collision gas states (continuous or pulse) is applied to facilitate the ions acceleration to a higher kinetic energy.

Fragmentation can be established via a derived-from-resonance ejection, called resonance excitation. Resonance excitation is similar to resonance ejection except that it uses a much lower amplitude AC waveform on the end-cap electrode. Waveforms with amplitudes differs from a few hundred millivolts to 1 V are usually applied for 10 millisecond at a frequency matching the secular frequency at which the isolated ions are being kept in the trap. Ions are excited at a frequency corresponding to q_z parameter values between (0.2 to 0.45). This destabilizes the trajectory of the ions and forces collision between the ions and the bath gas. Multiple collision lead to excitation of the ions, followed by dissociation and formation of product ions. The secular

frequencies of the product ions do not match the resonance excitation frequency and the product ions can therefore be recaptured at the center of the trap prior to a normal mass-instability scan to obtain the product ion mass spectrum. [69-71]

The conventional RF amplitude scan of the ring electrodes is performed to achieve mass analysis of the product ion. One possible way to isolate a precursor ion is to scan the basic RF-voltage in the reverse direction to eject all ions with *m/z* values greater than those of the precursor ions. Then, the basic RF-voltage is scanned in the forward direction to all low-mass ions. During these reverse and forward scans, an auxiliary resonance signal is also ramped. The other way of ion isolation is performed by applying broadband waveform supplementary AC frequencies to the end-cap with a gap around the secular-frequency of the ions being isolated.

Performing MS/MS in QITs using CID as described above is very efficient nearly 100% can be achieved; however, it usually offers low internal energy deposition and cannot always produce high energy fragmentation pathway. A number of different approaches have been suggested to try to improve conventional CID. A number of other approaches to perform CID have been attempted, including using DC offset or multiple combinations of waveform such as boundary –activated dissociation (BAD).

The major drawback of using QIT performs only a product-ion scans in tandem mass spectrometry. However, multi-stages of mass spectrometry (MS^n) can be achieved where the number of successive reaction or fragmentation stages can be very large. [71]
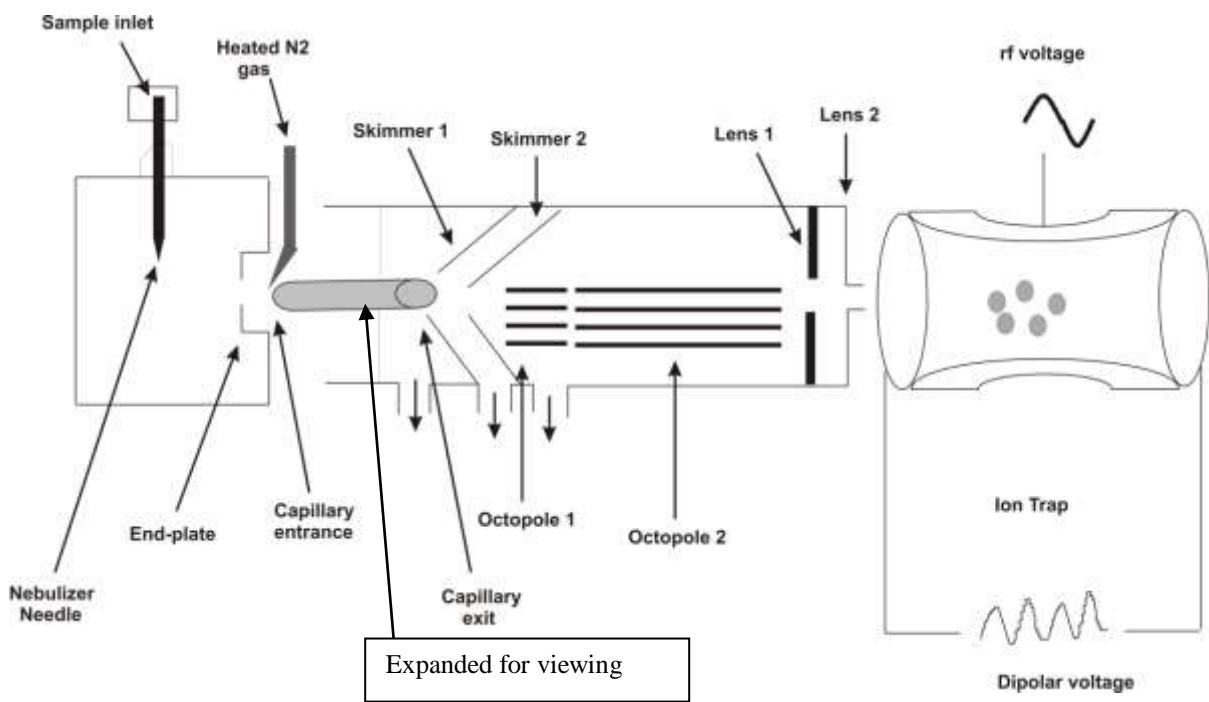
Figure 1.16: Schematic representation of the ESI-QIT-MS/MS.

1.2.2.2. FT-ICR-MS

The MS/MS experiment in FT-ICR is analogous to the QIT experiment; however, FT-ICR is limited to acquiring the product ion spectrum. Figure 1-17 is an illustration of a hybrid Q-FT-ICR-MS. Typically; the FT-ICR scan functions for the MS/MS operation are similar to those used in a QIT. First, a quench pulse is applied to eject from the cell any residual ion from the preceding experiment. Next, an ionization pulse is applied, and the precursor ion is isolated with a resonant excitation signal that contains all frequencies except the one that is related to the precursor ion; as a result, all other ions are ejected out of the FT-ICR cell.[72] After mass selection, a collision gas is pulsed into the ICR cell which causes the trapped ions to become collisionally activated and to obtain a bigger orbit. Since the CID is cannot be employed at zero atmospheric environment in the ICR cell, ions can be excited in the ICR cell by irradiating with a low-energy, off-resonance RF pulse. Then helium is pulsed into the cell concurrent with this excitation pulse to allow sustained off-resonance irradiation collision-induced dissociation (SORI-CID).

The CID products are mass analyzed as usual, that is, by excitation of the products to orbits of larger radius and detection of their image current. The FT-ICR has the unique distinction that in addition to SORI-CID, a variety of other fast and slow ion-activation methods can be performed.[73,74] Interactions of ions with electrons is also used including electron capture dissociation (ECD) and electron transfer dissociation (ETD). The first method on interactions of ions with electrons has been electron capture dissociation. ECD is generally used in Fourier transform ion cyclotron resonance FT-ICR mass spectrometers, due to the need of several milliseconds interactions between ions and

37

electron, and because ECD efficiency is highest for low-energy electrons (<1 eV) which are difficult to provide in quadrupole ion traps where strong RF. potentials affect the electrons' movement in the trap. Stabilization of the captured electron is faster than electron emission, which is usually on the time-scale of 10^{-14} s, so bond dissociation occurs faster than a typical bond vibration. [75,76]

Electron transfer dissociation (ETD) is based on ion-ion reactions, occurring in a quadrupole ion trap, between an electron-reach species, i.e. a radical anion of a polycyclic aromatic compound produced by chemical ionization, and a multiply charged ion.

In both ECD and ETD, the final result is the acquisition of an electron with a charge-state reduction of the ion and subsequent fragmentation. That is the reason why ECD and ETD can be applied to positive ions with at least a double charge, and electrospray is the most common ionization technique.

In both methods, the occurrence of direct bond cleavages only is observed with no, or minimal energy redistribution and randomization away from the reaction site. As a result, strong backbone N-C$_\alpha$ bonds of peptides are cleaved, forming c and z-type ions, complementary to b and y ions normally produced by low-energy CID. Moreover, interactions of ions with photons by using infrared multiphoton dissociation (IRMPD) or ion spectroscopy are applied to trapped ions in ion trap or FT-ICR analyzers. [77,79]

Ions can also be excited and subsequently fragmented by the absorption of one or more photons generally produced by using lasers of different wavelengths. In infrared wavelengths, multiphoton processes are consequently needed to excite ions sufficiently for efficient fragmentation.

ESI Capillary

Ion Funnel 1

Ion Funnel 2

Skimmer 2

Trap/Extract

GATE VALVE

Accumulation
Hexapole

ICR Cell

Deflector

Skimmer 2

10^{-2} mbar
Ar and/or
solvent

10^{-6} mbar

10^{-8} mbar

10^{-10} mbar

10^{-1} mbar

10^{-1} mbar

Source

Qh-Unit

Transfer

ICR Cell

3 mbar
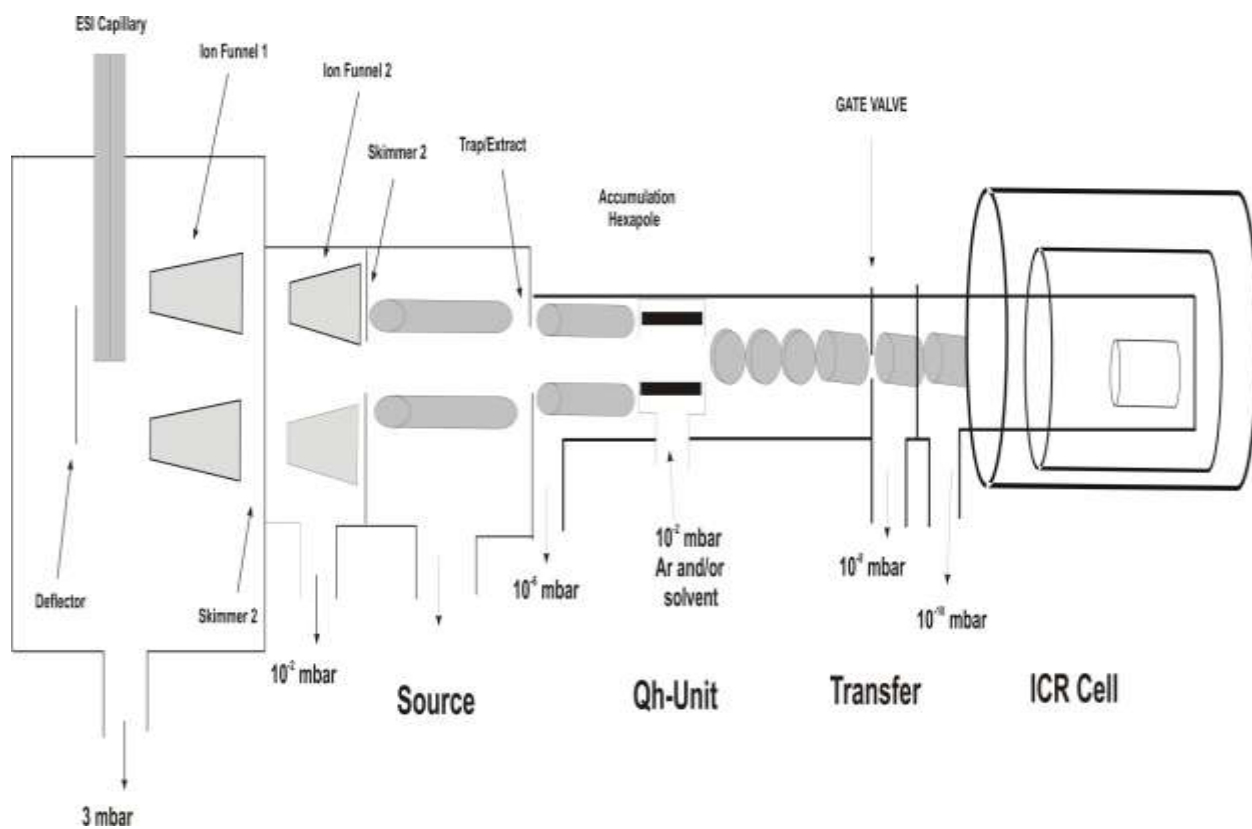
Figure 1.17: Schematic illustration of a Bruker FT-ICR-M

1.3. Bacterial cell membranes and lipopolysaccharides

1.3.1. Bacterial cell membranes

Bacteria cell envelopes are a complex multilayered component that surrounds their organisms and protects them from any unpredictable hostile environment. Generally, the cell membrane structure is composed of a phospholipid bilayer that contains the cytoplasm, as well as, proteins which serve as a fingerprint for each membrane. In the development of a staining process by Christian Gram, all bacteria since 1884 have been classified into two large groups. One group of bacteria is classified as Gram-negative bacteria (violet color) and the other as Gram-positive bacteria (red color).[80,82]

The fundamental Gram-negative bacterial cell envelope involves three layers; the outer membrane (OM), the peptidoglycan cell wall, and the cytoplasmic or inner membrane (IM). The outer membrane is a unique feature of Gram-negative bacteria which is basically a glycolipid or lipopolysaccharide (LPS), and functions as a protective barrier for the bacteria. LPSs can be connected with one other via neutralization of the negative charge of the phosphate groups present in the molecule if cations such as Mg^{++} are present.

Additionally, proteins are exited in the cell membrane and can be divided into, lipoproteins and β-barrel proteins types. The basic roles of all these components are to prevent any environmental toxic molecules from penetrating the bacterial organisms and to provide an additional stabilizing layer around the cell. [83]

The Gram-positive bacteria cell envelope is different from Gram-negative bacteria in several ways. Their structures differ, mostly in their outer membranes which are

absent. Thus, the Gram-positive organisms are surrounded by layers of peptidoglycan to make it many times thicker. Figure 1.18 shows the differences between the Gram-negative and the Gram- positive bacteria cell envelope. [84,85]
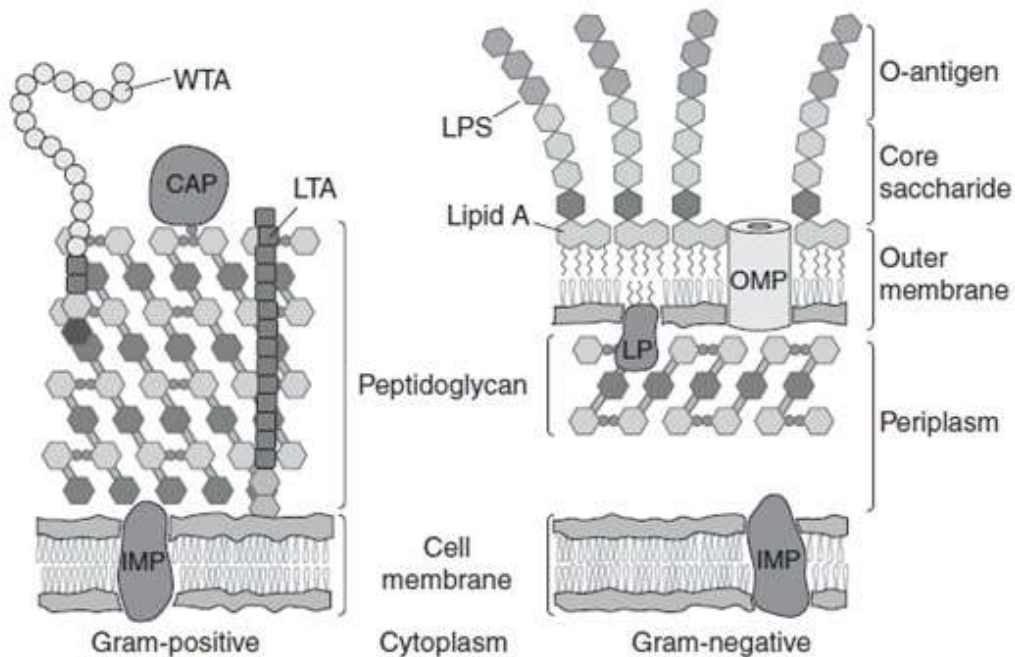
Figure 1.18: Illustration showing the structure of the Gram-negative and the Gram-positive bacteria cell envelop where WTA = wall teichoic acid, CAP = covalently attached protein, IMP = integral membrane protein, LP = lipoprotein, LPS = lipopolysaccharide, LTA = lipoteichoic acid, OMP = outer membrane protein and is adopted with the permission of reference 85.

1.3.2. Lipopolysaccharides

Lipopolysaccharides (LPSs) are amphiphillic macromolecules components in the outer leaflet of the external membranes of gram-negative bacteria and are considered as the virulence factor or endotoxins of the human and animal pathogenic bacteria. LPSs are normally comprised of two parts: a polysaccharide and lipid A. The polysaccharide fraction contains the O-antigen (O-chain) and the core oligosaccharides which are anchored in the membrane via the lipid A. The oligosaccharide antigen is covalently linked to the core oligosaccharide, which is in turn, linked covalently to the lipid A. LPS is known to causing endotoxic shock, and for their pyrogenic activity. In addition, LPSs can also activate and compliment the macrophages. [86,87]

However, the endotoxic properties of LPS reside largely in the lipid A components. Therefore, the main characteristics of lipid A are to display great toxic properties and also its structure is responsible for the biological activities of endotoxins that contributes to the different cells of the immune system. [88]

1.3.2.1. The O-specific chain

The O-specific chain is composed of repeating oligosaccharides, up to 50 units, whose structure and composition are different among numerous genera and bacterial serotypes. Moreover, these oligosaccharide units themselves contain one to eight sugar residues which only occur in smooth types of LPS, as opposed to rough-type LPSs that lack this functionality.[89] Rough LPS usually contain units of the O-antigen linked to the core oligosaccharide, which in turn glycosylate the lipid A. The O-antigen constituents cause the differences in lipid A structure for various types. Since the O-chains are considered as a fingerprint for distinguishing several types of bacteria, they are used to identify the specificity of each bacteria serotype. In pathogentic of Gram-negative bacteria, the O-chain serves as the host, while the infection and as the protective of the central integrity from the surrounding environment. This feature results from the variety of glycosides connections, sugar substitution, and genetic capacities to provide a unique structure of an O-chain with linear and/or branched linkages.[90]

The O-chains are responsible for O-antigenic properties that typically produce linking of species-specific antibodies. They also protect the bacteria from the effect of numerous antibiotics as shown by the relative sensitivity of rough-type strains as compared to smooth-type bacteria. The O-chains of *Actinobacillus pleuropneu moniae* and of some other LPSs have been shown to be responsible for adhesion to mammalian tissues, thus favouring infection. In lung tissues, the LPS of A. *pleuropneumoniae* is the main adhesion. Some O-chains can even adhere to a mineral surface as in the case of *Shewanella algae* LPS (this LPS was the first bacterial polysaccharide found to contain a residue of malic acid).[91]
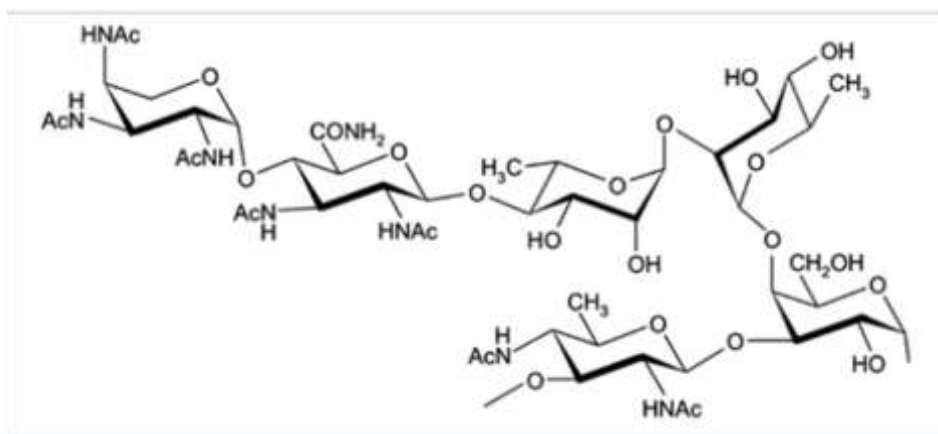
Figure 2.19: Illustration showing the structure of the O-specific chain.[91]

1.3.2.2. The core oligosaccharide

The core oligosaccharide is divided into two regions namely the outer core, which includes hexoses (primarily glucose), galactose, and *N*-acetyl-D-glucosamine. In addition, the inner core of the oligosaccharide is composed of specific residues characteristic of LPS, such as L-glycero-D-manno-heptose (LD-Hep) and 3-deoxy-D-manno-octulosonic acid (Kdo) which is linked to the O-6'position of lipid A via an α-ketosidic linkage. The Kdo is a unique and specific 8-carbon sugar present in the lipopolysaccharide (LPS) of a wide variety of Gram-negative bacteria. It has been demonstrated that it has significant biological activities in LPS. [92]

Similar to other sugars within the LPS moiety, Kdo can be substituted with reactive groups such as phosphate or phosphoethanolamine. Another unique sugar within the LPS inner core region is *L-glycero-D-manno*-heptose (Hep), which is a 7-carbon sugar; some bacteria, however, lack Hep residues.

In the three best-studied species of the genus *proteus* (*vulgaris*, *penneri*, and *mirabilis*), the inner core of almost all strains have their Kdo-I residue substituted at the C-8 position by 4-amino-4-deoxy-β-L-arabinose otherwise this part of the core

resembles that of other species. The outer cores, however, vary considerably. A partial list of their unusual constituents includes a Kdo linked to Hep, a galactouronic residue Gal-Amide linked to an aliphatic amine or to the α–amino group of L-lysine, 2-glycylamino-2-deoxy-D-glucose, the open-chain from of GalNAc glycosidically linked to GaIN in the form of a cyclic acetal. [93]
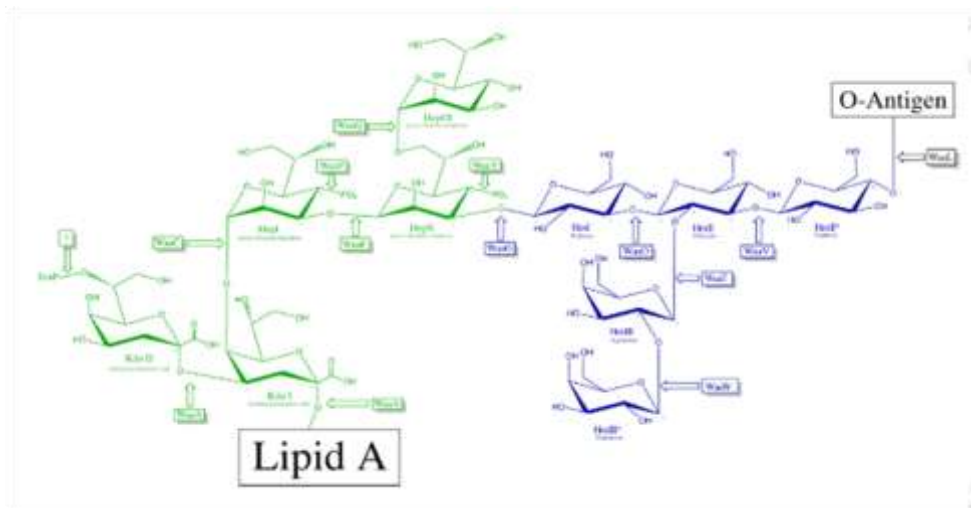
Figure 1.20: Illustration showing the structure of the core-oligosaccharide.[91]

1.3.2.3. Lipid A

Lipid A is a hydrophobic anchor of lipopolysaccharide (LPS) which is a glucosamine disaccharide with six or seven acyl chains. It has a conserved architecture consisting of a bisphophorylated β-(1→6)-linked D-glucosamine (2-amino-2-deoxy-D-glucopyranose; Glc$p$N) disaccharide backone. Both ester and amide serve as linking backbone units with fatty acids at positions O-3 and O-3′ for the ester and N-2 and N-2′ for the amide in the hydroxylated form of these fatty acids that are peculiar, as they bear a 3-OH group which, in turn, can be esterified via other fatty acids residues.[94,95] Identifying numerous species of lipid A depends on the number and the length of lipid A's fatty acids. The lipid A fraction is intrinsically heterogeneous due to the different

degree of phosphorylation and acylation, the distribution and the type of acyl residues. Consequently, lipid A structure changes, and these changes are the cause of the pathogenesis of a number of diseases. [96]

Despite the fact that lipid A fatty acids usually contain 10-16 carbon atoms, it has been shown that other unusual chains such as a 20-carbon chain exist within some isolates; for example, they are associated with the lipid A isolated from *Chlamydia*. As well as, the presence of a C16 fatty acid in *Salmonella* LPS is governed by the PhoP-PhoQ system. PhoP-PhoQ is a two-component system that regulates virulence, mediates the adaptation to Mg^{2+} limiting environments, and governs several cellular activities in numerous Gram-negative bacteria.

Other observations in such variations in lipid A structure are responses to specific factors of the growth condition (PH, Mg^{2+} concentration, and presence of cationic peptides). Moreover, these aspects can result in modification of the fatty acid chains or substitution of the phosphate group. A mixture of three or four molecular species in a single preparation often results from heterogeneity in the degree of fatty acid substitution. This heterogeneity can occur due to underacylation, or to post-synthesis degradation. [97]

1.4. Mass spectrometric analysis of carbohydrates

Mass spectrometry analysis of carbohydrates usually allows for obtaining structural information on their constituent units to obtain structure and post-translational modification. The carbohydrate chains are made up of sugar units which are linked via glycoside bonds to build a polymer, in principle similar to the peptide

bonds in protein.[98] During MS and MS/MS analysis, it was observed that not only the breakages of a glycoside bond occurred, but in addition, inner-sugar cleavages could occur, which produce diagnostic fragment ions, that allowed to the study of the structures of carbohydrate chains. [99]

The CID analysis of the protonated molecules of complex glycoconjugates was first described by Domon and Costello as they proposed the systematic nomenclature for carbohydrate fragmentation of complex glycoproteins during FAB-MS/MS analysis.[100]

The simple disaccharide lactose is used to illustrate the possible fragmentations where the reducing end is Glc (glucose) and the non-reducing unit is Gal (galactose). Figure 1.19 displays the units produced as the consequence of cleavages of the reducing end elimination; ions of the non-reducing end formation are termed A, B, and C, with A being related to inner sugar fragments. On the other hand, the fragments that stem from the reducing end are referred to as Z, Y, and X with the latter being connected with inner-sugar fragments. As well, the A, B, C, Z, Y, and X letters can also be numbered according to the exact position of where the sugar residue is located. Specifically, the non-reducing end starts with the number 1 for the case of A, B, and C ions, whereas, the reducing end are numbered from 1 in the case of Z, Y ions. However, the Y_0 ion is numbered 0 if it is the aglycone of the reducing end group.
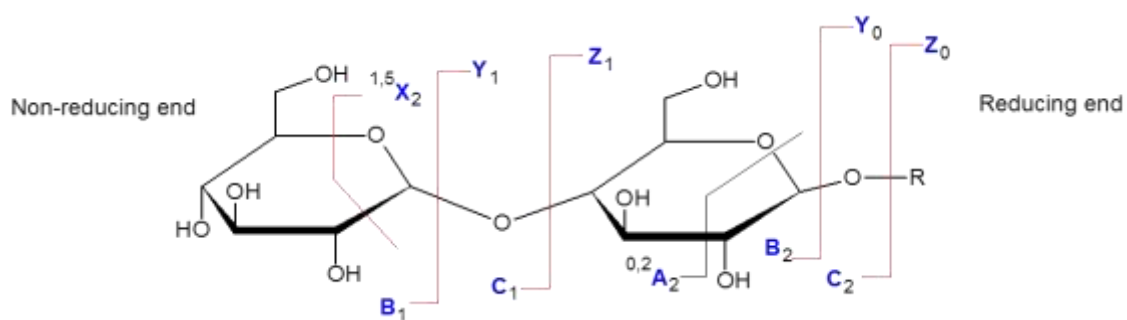
Figure 1.21: Possible fragmentation pathways during CID-MS/MS of a glycoconjugate corresponding to lactose according to the Domon & Costello Nomenclature and is adopted with the permission of reference 100.

Chapter 2

Materials and Methods

2.1. Lipopolysaccharides

2.1.1. Bacterial culture

The rough mutant-type strain of *Aeromonas liquefaciens* was obtained from Dr. T.P.T. Evelyn (Department of Fisheries and Oceans, Nanaimo, British Columbia, Canada). It was isolated originally from Sockeye salmon, and is numbered as "Strain SJ-19, rough mutant, of the collection of the Northwest Atlantic Fisheries Centre, St. John's, NL". The cultures were grown to medium-to-late stationary phase in Trypticase Soy Broth without added glucose (Baltimore Biological Laboratories Inc.) for almost 20 h at 25°C and aeration at 20-1/min in a New Brunswick MF-128S fermentor. They were then killed by the addition of 0.3 % formalin with continuous agitation for 16 h at room temperature. Cells were subsequently collected by centrifugation at 20,000 rpm in a Sorvall SS-34 rotor (48,200 xg), washed with NaCl (0.15 M) and finally lyophilized and stored at -50° C until required.

2.1.2. Purification of the lipopolysaccharides

LPS was extracted by the hot-phenol method and freeze-dried. Basically, stored cells (10 g) were suspended in deionized water (175 ml) and heated to 70° C.[101] An equal volume of heated phenol (90 %) was added and the mixture was stirred for 20 min at 70° C. The mixture was then cooled on ice and centrifuged using Sorvall SS-34 rotor (3500 rpm, 1475 x g). The aqueous layer was isolated by aspiration and the procedure

was repeated twice. The aqueous layers were combined and dialysed against water to remove any traces of phenol. Furthermore, the volume of the combined water mixture was reduced by evaporation (under vacuum) and finally centrifuged at 39,000 rpm (105,000 x g) for 3 h. The LPS pellet was resuspended in water and centrifugation was repeated twice; LPS was finally lyophilized. LPS isolates were further purified using polymyxin-coated Affi-prep beads (Bio-Rad Laboratories, Richmond, CA, USA). Fifteen milligrams of LPS was suspended in 15 ml of phosphate-buffered saline (PBS, PH=7.4). LPS solution was then mixed with washed polymyxin beads (the beads were originally washed first with 0.1 M NaOH and then with distilled water. The mixture was incubated overnight with agitation using an orbital shaker (1500 rpm). The mixture was then centrifuged (2500 x g) for 10 min and the supernatant was collected. The beads were then washed twice with 15 ml and 5 ml 0.1 M NaOH. The supernatants were combined and LPS was dialysed against water and finally lyophilized.

2.1.3. Hydrolysis of the lipopolysaccharides

LPS (100 mg) was hydrolyzed with 1% acetic acid for 90 min at 100°C. Centrifugation at 3000 x g for 30 min resulted in the precipitation of lipid A, while the polysaccharide was present in aqueous media. Lipid A was removed and washed with water, and the core oligosaccharide was recovered from the supernatant by chromatography on Sephadex G-50 (Pharmacia Ltd.). Fractions were visualized using a differential refractive index monitor (Waters Associates).

2.2. Mass spectrometric analysis of lipid A

2.2.1. Electrospray quadrupole Fourier transform ion cyclotron mass spectrometry

Mass spectrometry was performed using an An Apex Qe 7.0 Bruker Fourier Transform Ion Cyclotron Mass Spectrometer (FT-ICR-MS) with an Apollo II electrospray source was presented in this work. The FT-ICR MS can be broadly separated into four segments: the gas-phase ion source, quadrupole region, ion transfer optics, and ICR cell. The gas-phase ions are initially generated from the solution phase using electrospray ionization (ESI), and are subsequently accelerated through a quadrupole mass filter into a hexapole collision cell. Solvated ions can be prepared in this cell by minimizing the collision Ar gas flow and introducing solvent (10^{-2} mbar) through a microvalve that separates the collision cell from a degassed solvent reservoir.

Lipid A of the *Aeromonas Liquefaciens* bacteria was diluted in chloroform and methanol (1:1) and 0.1% TMA/ pure Milli-Q water and then electrosprayed underivatized in negative (-ve) ion mode.

The conditions employed were: dry gas 8.00 l/min, trap drive 51.5, quadrupole amplitude RF 177.2 V, skimmer 40.0 volt, Oct 1 DC 12 volt, quadrupole DC 1.70 volt , scan begins at *m/z* 500 and end at *m/z* 2000, max accumulation time 200000 µs.

2.2.2. Electrospray quadrupole-hexapole-quadrupole mass spectrometry

The ESI mass spectra (negative ion mode) were recorded with a Micromass Quattro II quadrupole-hexapole-quadrupole mass spectrometer equipped with a megaflow ESI source capable of analyzing ions up to *m/z* 4000. A personal computer (Compaq PII 266

MHz processor running Windows NT 4, service pack 3) equipped with Micromass MASSLYNX 3.2.0 Mass Spectrometry Data System software was used for data acquisition and processing. The temperature of the ESI source was maintained at 75°C. The operating voltage of the ESI capillary was 3.00 kV and the high voltage lens was set to 0.40 throughout the whole operation. ESI-MS were recorded with a cone voltage of 25V.

2.2.2.1. ESI-QhQ-MS of partial de-acylation of ester-linked to the acyl group of lipid A with sodium methoxide (NaOMe)

The partial liberation of the O-linked ester fatty acids from lipid A was released from intact LPS by treatment with sodium methoxide (CH_3ONa) in methanol. Following neutralization with dry ice, the obtained sample was analyzed using ESI-MS using the previous conditions. CID-MS/MS experiments were conducted using the same instrument. Product ion scans of selected masses were induced by collision with argon in the (RF-only) hexapole. The resulting product ions were analyzed by the second quadrupole. Collision energies varying from 20 to 35 eV and a collision gas pressure in the collision cell varying from 3.5 x 10"4 to 6.5 x 10"4 mbar (1 bar = 105 Pa) were used in all MS/MS experiments. The collision gas (N_2) pressure was increased to induce the dissociation of the sodium adduct ions. Precursor ion scans were performed when needed of mass-selected ions which were induced by collision with argon in the (RF-only).

2.2.3. Matrix-assisted laser/desorption ionization time-of-flight mass spectrometry (MALDI-TOF-MS)

α-Cyano-4-hydroxycinnamic acid (α-CHCA) matrix was used at a concentration of 5 mg/ml in a 2:2:1 mixture (v/v/v) of methanol, acetonitrile, and water. Lipid A was used at a concentration of 2 mg/ml in a (1:1) mixture (v/v) of chloroform and methanol. The sample was prepared by mixing equal volumes of α-CHCA solution and lipid A solution. The spot was done by using 1 μl of this mixed solution and spotted onto a MALDI plate and then left to crystallize and dry in desiccators before being loaded into the MALDI-MS instrument.

Mass spectra of the lipid A isolated from *Aeromonas liquefaciens* SJ-19 were acquired in reflectron negative ion mode. The MALDI-TOF/TOF-MS spectrometer (MALDI 4800, Applied Bioscience) was used for this experiment. The MS data was acquired in the mass range 600 to 1900 *m/z*. The MALDI-TOF/TOF-MS instrument was equipped with a nitrogen laser (337 nm). All the spectra were accumulated as 600 individual laser shots. The accelerating potential was 25KV. The focusing guide wire was held at a potential 0.18%. The laser intensity of 4200 was used. The MALDI-TOF/TOF-MS possessed a high mass accuracy (5 ppm) and resolution of 15000-25000 (FWHM). The minimum signal to noise ratio was 35.

High-energy collision dissociation MS/MS (CID-MS/MS) experiments were conducted using the same instrument. Product ion scans of selected masses were induced by a high CID collision cell. The resulting product ions were analyzed by the second TOF analyzer. The tandem mass spectrometric analyses were achieved with air

as collision gas and at collision energy of 1 kV, which corresponds to the difference between the accelerating potential (8 kV) and the floating cell (7 kV).

2.3. The synthesis of oligosaccharides of 2-amino-2-deoxy-β-D-glycosides

N-Alkoxycarbonyl derivatives of 2-amino-2-deoxy-β-D-glycoside A and B (Figure 2.1) have been used as valuable glycosylation donors since they allowed chemioselective preferential deprotection of the amino protective group. It was anticipated that the carbamate protective group could be involved in C-2 anchimeric assistance to afford the cyclic azadioxocarbenium intermediate F'' the formation of which should be more favored than the corresponding oxazolinium ion which has already been described in the oxazoline procedure.[102]

The first example reported in the literature involved a glycosylation using the 3,4,6-tri-*O*-acetyl-2-(benzyloxycarbonylamino)-2-deoxy-α-D-glucopyranosyl bromide as donor, and methanol in excess as acceptor, in the presence of Ag$_2$CO$_3$ as promoter to afford the corresponding β-methyl glycoside in moderate yield. It was shown that using the same donor and benzyl 2-acetamido-4,6-*O*-benzylidene-2-deoxy-α-glucopyranoside as acceptor, in the presence of mercuric cyanide as the promoter, the oxazolidinone D was obtained in almost quantitative yield together with the 3-*O*-benzyl ether derivative (8%) of the acceptor alcohol.[103-107] Nevertheless, when a 2-(benzyloxycarbonylamino) cyclohexanol acceptor was used in the same conditions, the expected β-glycoside was obtained.[104,108]

In this thesis, the 2,2-allyloxycarbonylamino derivative D (R=All) was studied in more detail for the Lewis acid-catalyzed glycosylation reaction reported by Banoub and

coworkers. The amino function of the so-formed β-glycosides could be easily deprotected in a chemiospecific manner [Pd(0) complexes] after the glycosylation step to afford the free amino group containing glycoside.[109,110]. Thus, following the 2-(allyloxycarbonyl) procedure several monosaccharide or oligosaccharide acceptors were efficiently glycosylated to afford structural units of antigenic fragments, glycans building blocks or glycopeptides.[111]

The alkoxycarbonyl approach has been successfully applied for the synthesis of lipid A intermediates. Thus the donors (X= Br, C1; R=CH$_2$CC$_4$, Bn) were reacted with D-glucosamine acceptors (with free HO-6 or free HO-6 and HO-4) in the presence of mercuric cyanide as the promoter to afford the expected disaccharides in good to very good yields (40-94 %) Compound A (X = α-Br; R = CH$_2$CCl$_3$) was shown to be a 1,2-trans and a 1,2-cis glycosylation donor as well, depending on the promoter used.[112,113] Thus, when zinc chloride (1 equiv) combined with trityl chloride (1 equiv) was used as a promoter, very good yields and high β-stereoselectivities *(β:α = 99:l)* were observed. In contrast, when zinc chloride (or bromide) only was used as the promoter, the α-glycosides were obtained stereoselectively *(α: β = 99.1)* in good yields[114].
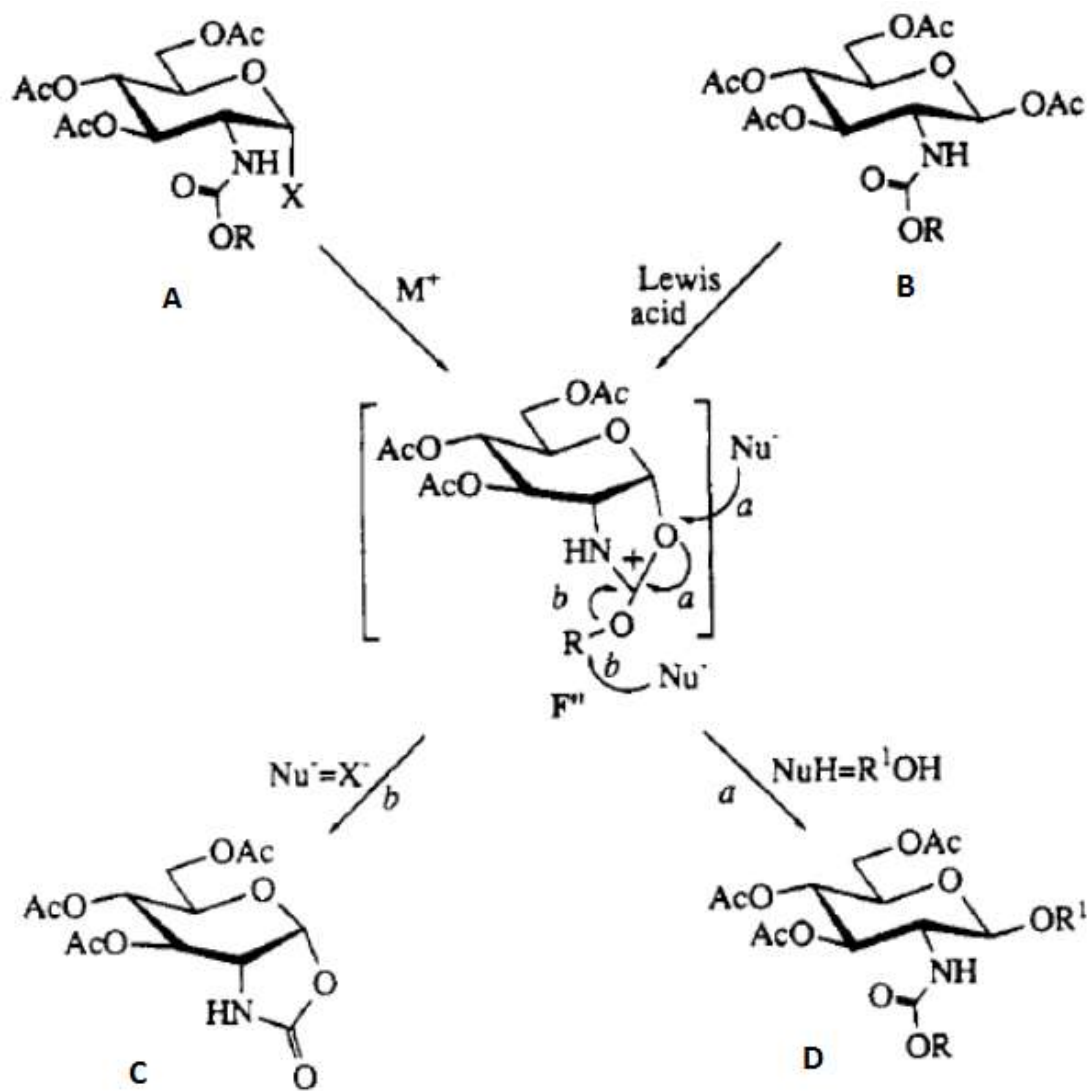
Figure 2.1: The synthesis of oligosaccharides of 2-amino-2-deoxy-β-D-glycoside figure D is adopted with the permission of reference 108.

2.3.1. 3-D Quadrupole ion traps mass spectrometry (QIT-MS) of the synthesis of oligosaccharides of 2-Amino-2-deoxy-β-D-glycosides

The mass spectra of the glycosides were acquired in the positive ion mode for the mass range 100 to 600 *m/z* using the orthogonal-spray ion source Agilent 1100 Series LC/MSD Trap SL spectrometer. For the positive ion mode analysis, samples were dissolved in acetonitrile: methanol (2:2). Over its standard *m/z* 50 - 2200 mass range, the LC/MSD Trap can maintain better than 0.6 u (FWHM) mass resolutions at a 13,000 u/s scan speed. Over the same mass range, the LC/MSD Trap can achieve better than 0.3u (FWHM) resolution at over 1600 u/s.

A high performance liquid chromatography (HPLC) system is the most common form of sample delivery for the Ion Trap. A small syringe pump is also included with the ion trap system to introduce samples directly to either the electrospray (ESI) or APCI ion sources. When used with the ESI interface, two modes of operation are available to inject the sample in solution directly to the nebulizer under low-flow conditions (typically 1–10 μL/min), or to inject the sample in solution into the HPLC system main flow through a T-connector.

Samples (1 mg ml^{-1}) were directly infused into the QIT-MS under the low-flow condition; this combined operation is particularly convenient for the optimization of instrument parameters and the development of MS/MS methods.

The condition employed were: dry gas 8.00 l/min, trap drive 51.5, octapole amplitude RF 177.2 V, skimmer 40.0 volt, Oct 1 DC 12 volt, Oct DC 1.70 volt, scan begins at *m/z* 100 and end at *m/z* 600, max accumulation time 200000 μs. For low masses, the trap analyzer was calibrated using penta-*O*-acetyl-β-D-galactopyranose and

checking for the exact masses of the $[M+H-AcOH]^+$ ion $C_{14}H_{19}O_9$ at *m/z* 331.1024 and octa-*O*-acetyl-β-D-lactopyranose and checking for the $[M+H-AcOH]^+$ ion $[C_{26}H_{33}O_{17}]^+$ at *m/z* 617.1712.

2.3.2. Electrospray quadrupole orthogonal time-of-flight mass spectrometry of the synthetic oligosaccharides of 2-amino-2-deoxy-β-D-glycosides

Mass spectrometry was performed using an Applied Biosystems API QSTAR XL MS/MS quadrupole orthogonal time-of-flight (QqTOF)-MS/MS hybrid instrument capable of analyzing a mass range of *m/z* 100-40,000 with a resolution of 10,000 in the positive mode. ESI was performed with a Turbo Ion spray source operated at 5.5 kV at a temperature of 80 °C. 1 mg of the synthetic oligosaccharides of 2-amino-2-deoxy-D-glycoside was dissolved in 2 ml of acetonitraile/methanol (2:2) so that the final concentration was 0.5 mg/ml. The solution was then electrosprayed underivatized in the negative ion mode. Aqueous 0.5% taurocholic acid solution (Applied Biosystems, Foster City, CA) was added to the sample for TOF calibration (exact mass $[M-H]^- =$ 514.2838). Nitrogen was used as the collision gas for MS/MS analysis with collision energies (CE) varying between -35 to -100 eV. The samples were infused into the mass spectrometer with an integrated Harvard syringe pump at a rate of 10 pL/min using the Turbo Ion spray source; operated at 5.5 kV at a temperature of 80-100°C. The positive ion mode of the ToF analyzer was calibrated with rennin (Applied Biosystems, Foster City, CA), exact mass $[M+H]^+ = 1\,758.9326$; $[M+2H]^{2+} = 879.9699$. For CID MS/MS, the CE was set so that the selected precursor ion remained abundant (10 to 100 eV), and CID gas pressure was varied between 4 and 12.

Chapter 3

ESI-FT-ICR-MS Analysis (Tandem-in-Time Mass Spectrometry) for Verifying The Structure of Lipid A of *A. Liquifaciens*. Proof of the Incomplete Biosynthesis Lipid A

3.1. Overview of lipid A biosynthesis

Most Gram-negative bacteria synthesize lipid A to make up the external cellular monolayer of the outer membrane (OM), (Figure 3.1). Lipid A biosynthetic pathway can be described as being formed from either a conserved (constitutive) and/or variable (modification) components. The constitutive lipid A backbone is synthesized from intracellular enzymes that are present in virtually all Gram-negative bacteria and are not subjected to regulation. On the other hand, the variable lipid A whose backbone is synthesized from mostly extra-cytoplasmic enzymes may vary from organism to organism.[117]

The further biochemical modification of lipid A are formed by enzymes which are either located on the periplasmic surface of the inner membrane and/or in the outer membrane.[118] These enzymes are induced due to changes in the bacterial growth conditions, such as, changes in pH, divalent cation concentrations, and/or the presence of anti-microbial peptides.
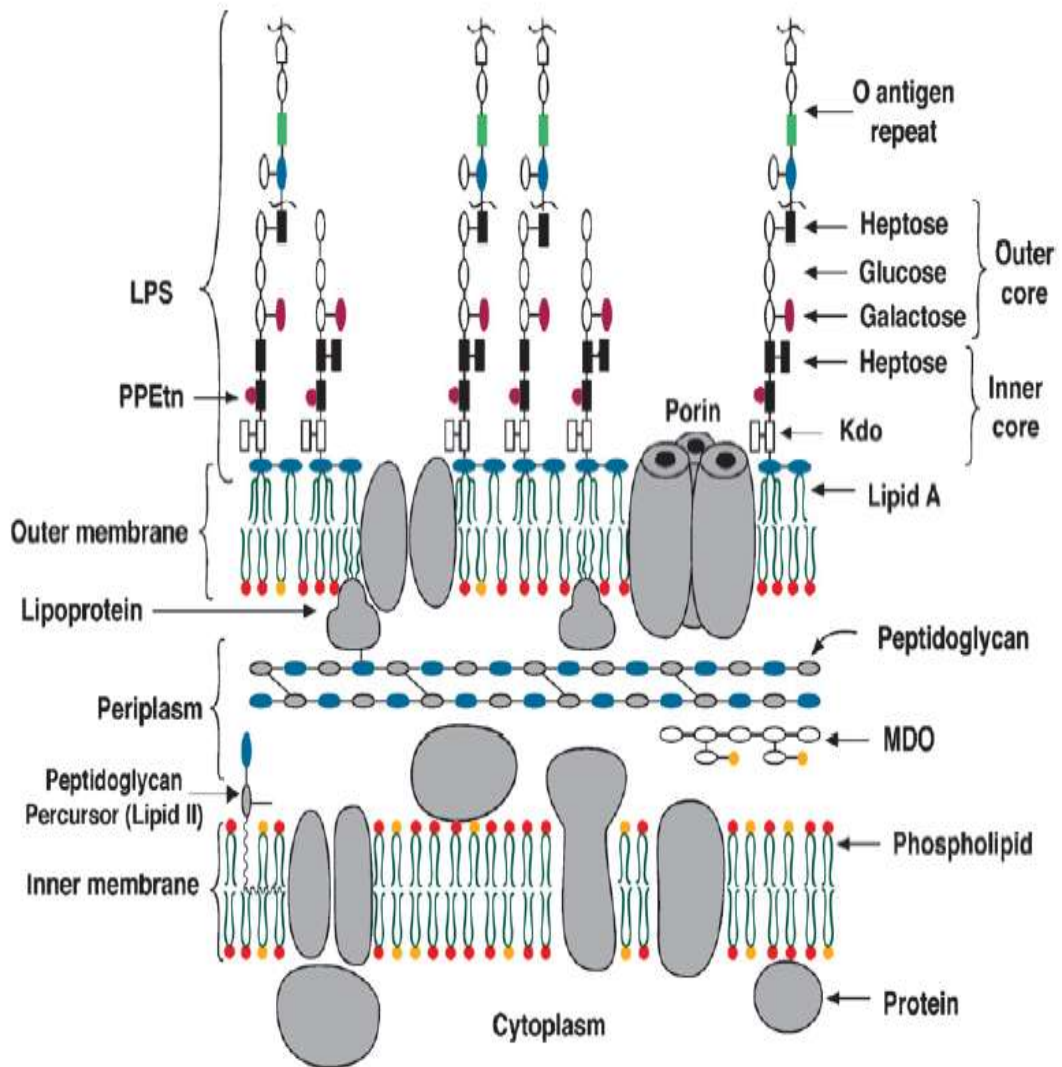
Figure 3.1: Schematic structure of the *E. coli* K-12 cell envelope and is adopted with the permission of reference 118.

3.1.1. The constitutive enzymatic pathway of lipid A biosynthesis of *E. coli*

There are nine enzymes of the constitutive lipid A pathway and single-copy genes encoding these enzymes, which are conserved in the Gram-negative bacteria like *E. coli*. However, for an organism like *Sphingomonas,* it was found that it was formed by biosynthesis of the bioactive sphingolipids instead of lipid A.[119-121] The discovery of 2,3-diacylglucosamine 1-phosphate (lipid X) facilitates the systematic determination of the constitutive pathway of lipid A biosynthesis.

Figure 3.2 represents the constitutive pathway of lipid A biosynthesis in which LpxA, C and D are soluble proteins, and LpxB and LpxH are peripheral membrane proteins; their chemical structures have not yet been reported.[122]

The first step of lipid A biosynthesis occurs by the fatty acylation of UDP-GlcNAc, (Figure 3.2), which is catalyzed via LpxA. In the case of *E. coli* the thioester *R*-3-hydroxymyristoyl acyl carrier protein (ACP) is the selective donor substrate.[123] The active location of *E. coli* LpxA functions as a precise β-hydrocarbon ruler that connects the C14 hydroxyacyl by chains two orders of magnitude faster than for the C12 or C16 chains. The equilibrium constant (~0.01) for UDP-GlcNAc acylation by the E. coli LpxA mechanism is unfavorable. Therefore, it was shown that the deacetylation of UDP-3-*O*-(acyl)-GlcNAc by LpxC is the committed step.[124,125]

LpxC is a Zn^{2+}-dependent enzyme which is greatly conserved in all Gram-negative bacteria.[126] As well, it has no sequence similarity to other deacetylases or amidases and efficiently functions as a target for antibiotics. Recently, LpxC slow, tight-binding inhibitors with low nM affinity named *N*-aroyl-L-threonine hydroxamates have been

reported. Next, a second *R*-hydroxymyristate chains is added via LpxD to build the UDP-2,3-diacyl-GlcN.

The X-ray LpxD structure shows that it is a homotrimer constructed around multiple contiguous hexad repeats, like LpxA.[127-128] Following the addition of the second *R*-hydroxymyristate chains, the pyrophosphate linkage of UDP-2,3-diacyl-GlcN is cleaved by LpxH. At this stage, the LpxH forms the 2,3-diacyl-GlcN-1-phosphate (Lipid X), which catalyzes the attack of water on the α-phosphorus atom of the UDP.

The integral inner membrane proteins LpxK, LdtA, LpxL, and LpxM catalyze the last five steps of the constitutive pathway in *E. coli*. In addition it was shown that one predicted membrane-spanning segment appears for each protein at its N-terminus and its active sites are presumed to face the cytoplasmic surface of the inner membrane. Then, LpxK phosphorylates the 4′-position to make the intermediate lipid A IV_A, which serves as the endotoxin antagonist in human cells; however, the endotoxin is agonist in mouse.[129]

This variable pharmacology of lipid A has been identified by the presence of the lipid A receptor of the mammalian innate immune system known as the TLR4/MD2 complex.[130]

Furthermore, the biosynthesis of lipid A is completed by the incorporation of two Kdo residues by the bi-functional enzyme KdtA. Please note that the labile nucleotide CMP-Kdo, derived from arabinose 5-phosphate, is the Kdo donor.[131]

Finally, the last step of *E. coli* lipid A biosynthesis involves the addition of the secondary laurate and myristate chains by LpxL and LpxM, which displays sequence similarity to each other and are related to the lysophosphatidic acid acyltransferases.[132]
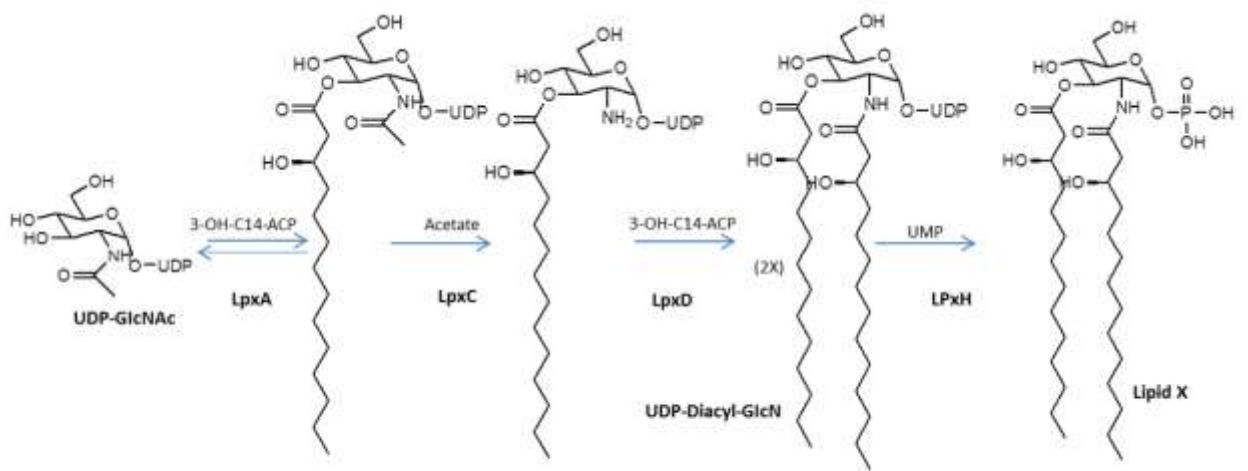
Figure 3.2: The constitutive pathway for Kdo_2-lipid A biothynthesis on *E. coli*.
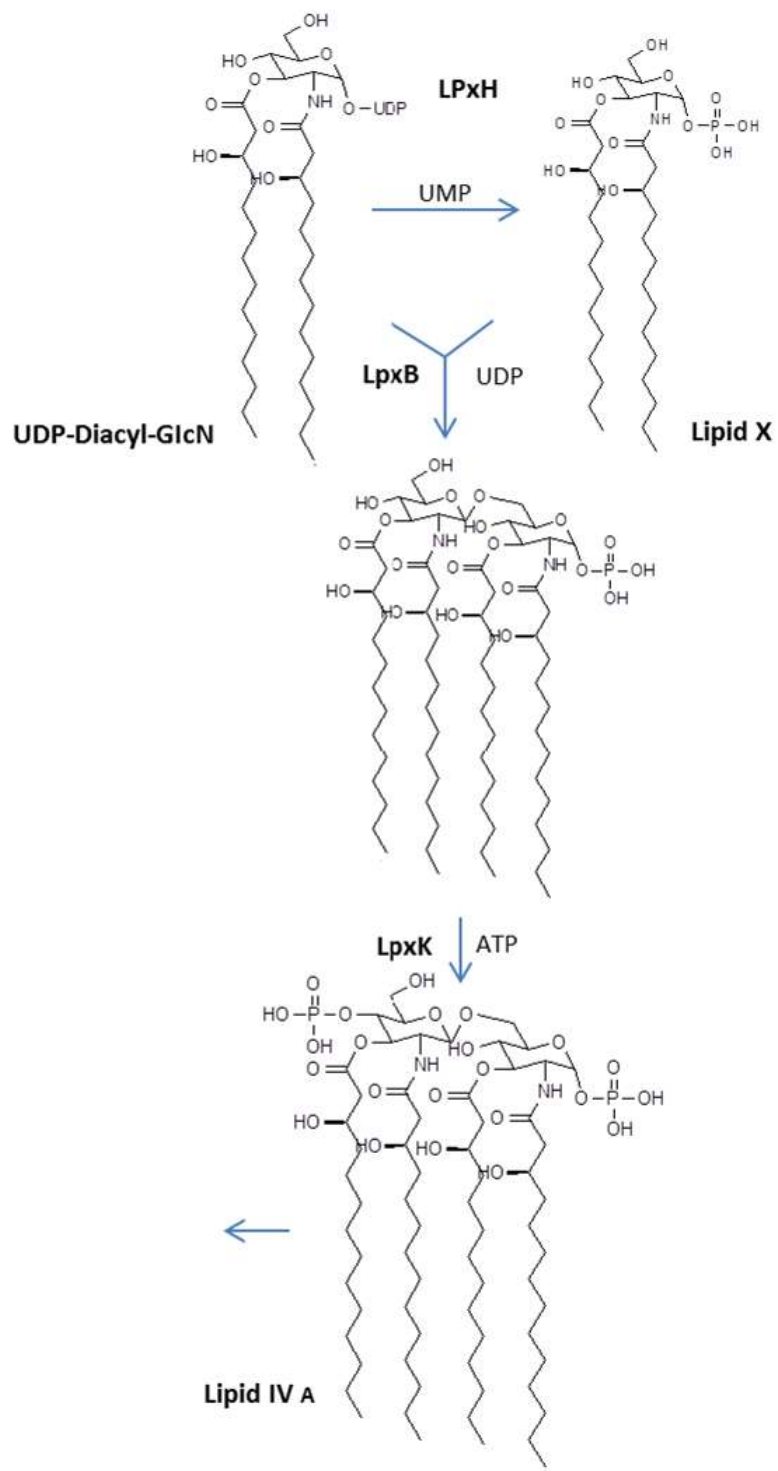
Figure 3.2, continued: The constitutive pathway for Kdo2-lipid A biothynthesis on *E. coli*.
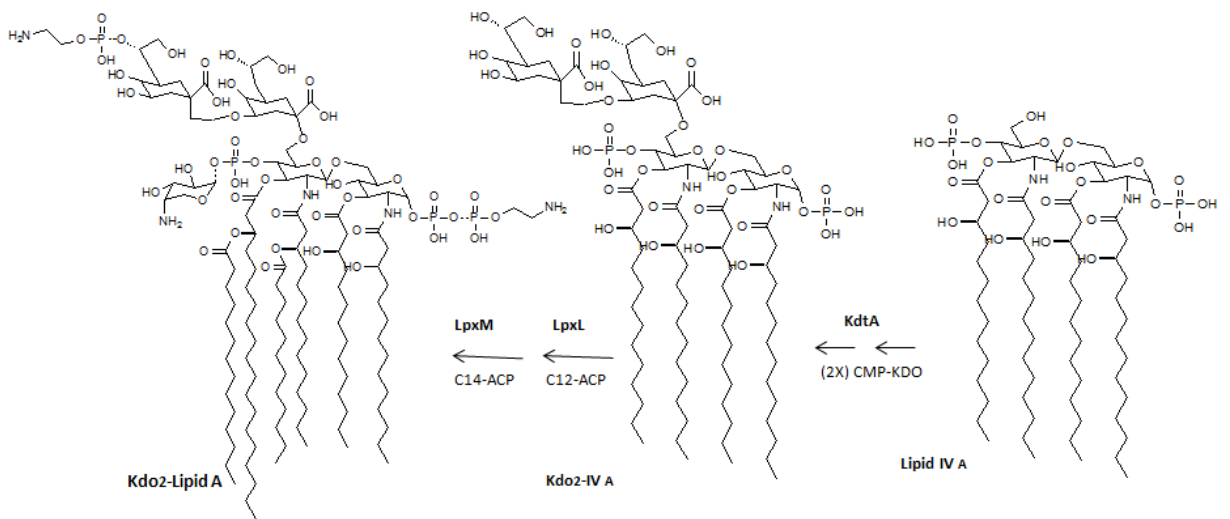
Figure 3.2, continued: The constitutive pathway for Kdo2-lipid A biothynthesis on *E. coli*.

3.1.2. The Modification of the enzymatic pathway of lipid A biosynthesis of *E. coli* and *Salmonella*

It was found that the Lipid As of both *E. coli* K-12 and *S. typhimurium* could be also modified by some enzymes such as phosphoethanolamine, L-Ara4N, and/or palmitate; these structures are represented in Figure 3.3.[133] In the case of *S. typhimurium* which contain two selective deacylases and a dioxygenese, many of these modifying enzymes are regulated by the responses to changes in their growth conditions.[134]

The attachment of L-Ara4N by the enzyme ArnT is induced by the activation of the PmrA transcription factor due to the exposure of cells to mild acid or the constitutive mutations of *pmrA*. The biosynthesis and the mechanism of its attachment to Lipid A have been determined.[135] The first step is the oxidative decarboxylation of UDP-glucuronic acid by the *C*-terminal domain of ArnA to form the UDP-4-ketopentose. Following this step, UDP-L-Ara4N is obtained when UDP-4-ketopentose is transaminated by ArnB and this is formed by formylation of its *N*-terminal domain to form ArnA. Both ArnA and ArnB are soluble proteins and their structures are identified using X-ray crystallography.[136,137] However, the mechanism by which they interact and transfer their products between their active sites is still unknown. The EptA enzyme facilitates the transfer of phosphoethanolamine to lipid A, predominantly to the 1-phosphate group on the outer surface of the inner membrane. Likewise, EptA can modify the lipid A at the O-4′ position with a second phosphoethanolamine moiety under certain growth conditions or in the absence of L-Ara4N. The roles of the phosphoethanolamine modifications are uncertain, compared to the L-Ara$_4$N group that is critical for polymyxin resistance.
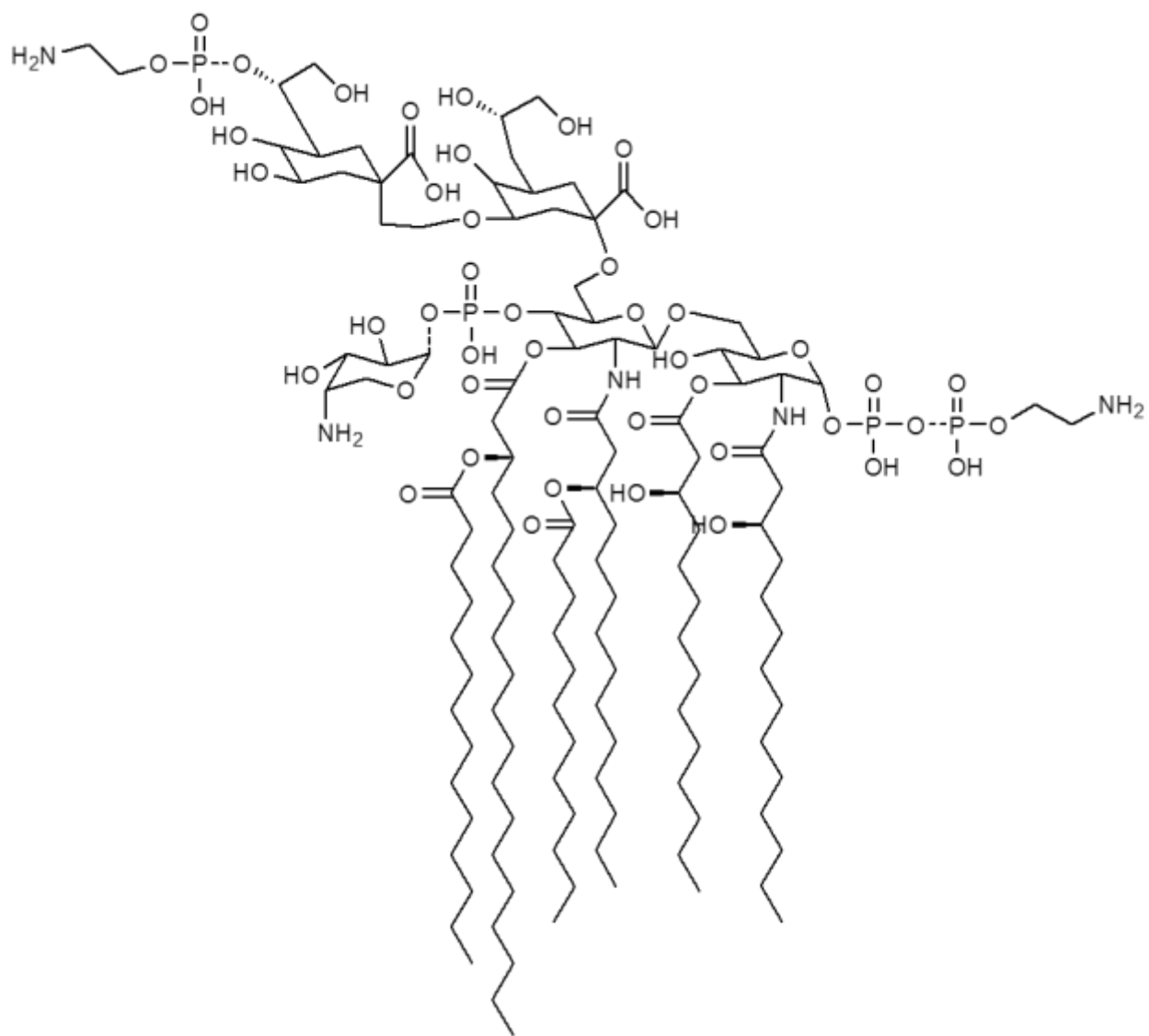
Figure 3.3: Covalent modifications of Kdo$_2$-lipid A in *E. coli* K-12 and *Salamonella.*

It is very important to understand that lipid A extracts are usually formed as a micro-heterogeneous mixture composed of a major lipid A component, in addition to other minor products. This heterogeneity is most likely a result of complete and incomplete lipid A biosynthesis and differs mainly in the composition of fatty acid length and saturation and substitution of the phosphate by ethanolamine or various glycosyl groups.[97]

In this chapter, low-energy collision dissociation ESI-FT-ICR-MS (tandem-in-time mass spectrometry) was used to differentiate and elucidate the molecular structure of the main constituent of native lipid A constituents isolated from the bacterial species *A. liquefaciens* SJ-19.

In addition, low-energy sustained off-resonance irradiation-collision induced dissociation (SORI-CID, herein called CID) analysis has illustrated the gas-phase fragmentation routes of the various constituents of this incompletely biosynthesized lipid A mixture and has defined the major diagnostic fingerprint ions. It is apparent that the structural identification data of this biological compound can be used in the future to evaluate related lipid As and to perform quantitative studies for its potential formulations.

3.2. ESI-FT-ICR-MS analysis

ESI-FT-ICR-MS (negative ion mode) obtained for lipid A of *A. liquefaciens* SJ-19 displayed an incomplete biosynthesis as illustrated by the multiple molecular ions shown in Figure 3.5. The ESI-FT-ICR-MS showed *inter alia* four different deprotonated molecules having related structures of the lipid A at *m/z* 1716.1491 LipA1, at *m/z*

1688.2209 lipA2; and two most abundant ions at *m/z* 1506.0511 LipA3 and at *m/z* 1279.8596, LipA4

Therefore, lower intensity ions at *m/z* 1716.1491 LipA1 and at *m/z* 1688.2209 LipA2 were assigned to the deprotonated molecules of the mono-phosphorylated hexa-acylated forms of lipid A carrying four (*R*)-14:0 (3-OH) (primary fatty acid) on the lipid A disaccharide.

In addition, two most abundant ions at *m/z* 1506.0511 LipA3 and at *m/z* 1279.8596 LipA4 were tentatively attributed to the mono-phosphorylated penta-acylated forms for the deprotonated molecule LipA3 at *m/z* 1506.0511 carrying four (*R*)-14:0(OH) (primary fatty acid) and, one 12:0 branched fatty acid at position of l4:0(3-(*R*)-*O*-12:0. The deprotonated molecule at *m/z* 1279.8596 LipA4 attributed to the mono-phosphorylated tetra-acylated forms carrying four (*R*)-14:0 (OH) (primary fatty acid) on the one 12:0 branched fatty acid on position l4:0(3-(*R*)-*O*-12:0) of the lipid A (Figure 3.4). It should be note that the mass difference of 228 Da between the ions at *m/z* 1506.0511 LipA3 and the ions at *m/z* 1279.8596 LipA4 could indicate the elimination of a C14-acid at the O-3′ position from the ions at *m/z* 1506.0511 LipA3.
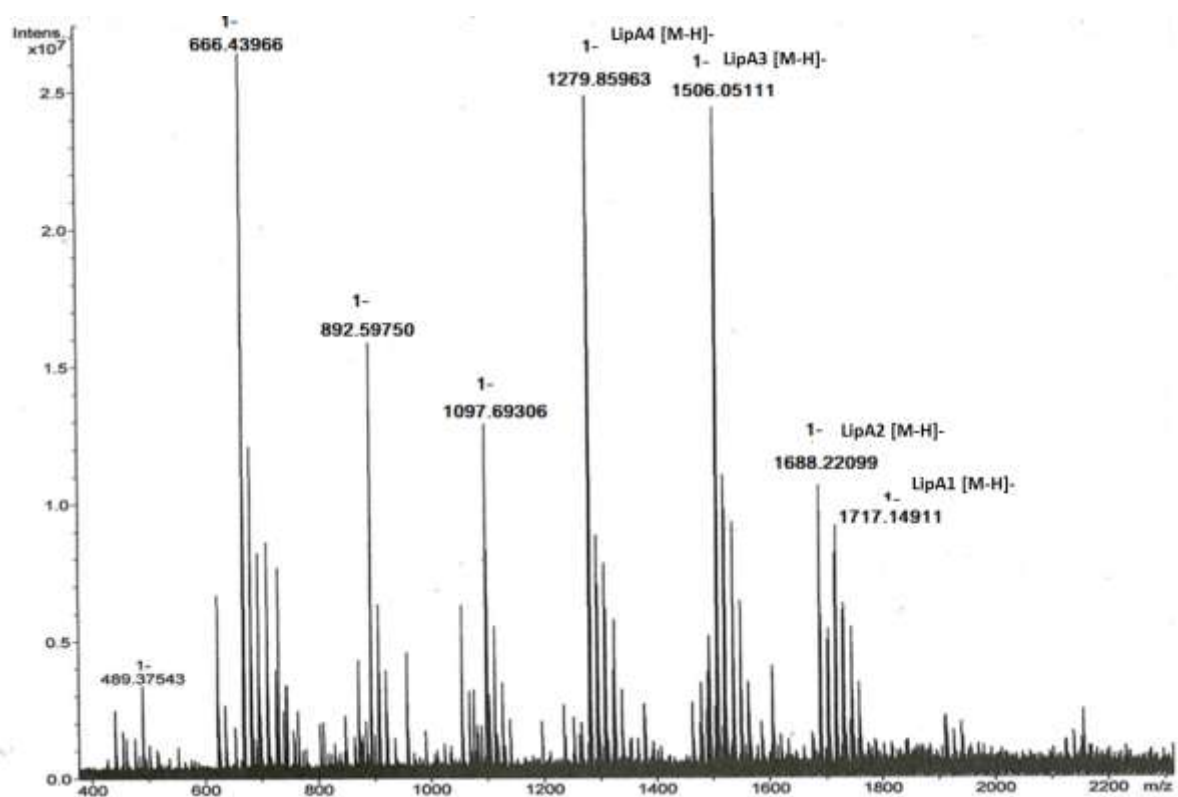
Figure 3.4: Negative ion FT-ICR-MS of the native lipid A extract from *A. liquefaciens* SJ-19.

Table 3.1: Assignments of the diagnostic ions observed in FT-ICR spectrum of native

lipid A extracted from *A. liquefaciens* SJ-19.

Diagnostic ions	Empirical formula	*m/z* Calculated; Observed	Abundance (%)
[M-H]⁻	$C_{94}H_{177}N_2O_{22}P$	1716.1491	27.52
[M(C14:0(3OH))keteneH]⁻	$C_{92}H_{173}N_2O_{25}P_2$	1688.2209	30.73
[M-(C14:0) ketene-H]⁻	$C_{80}H_{149}N_2O_{21}P$	1506.0511	95.5
[M-(C12:0)ketene (C14:0(3OH))ketene-H]⁻	$C_{66}H_{124}N_2O_{19}P$	1279.8596	97.3
[M-(C14:0)ketene-(C14:0(3-OH))ketene-(C12)-H]⁻	$C_{54}H_{102}N_2O_{18}P$	1097.6930	36.40
[M-(C14:0)ketene-(C14:0(3-OH))ketene-(C12:0)Ketene)-H]⁻	$C_{53}H_{102}N_2O_{16}P$	1053.352	21.26
[C-(C14:0)ketene-H]⁻	$C_{46}H_{87}NO_{13}P$	892.5975	46.81
[C- (C14:0(3-0(14:0)))ketene - H]⁻	$C_{32}H_{61}NO_{11}P$	666.2209	100

The proposed structures of the monophosphorylated lipid A and its distinctive ions observed in the FT-ICR-MS are illustrated in Table 3.1 and Figure 3.4. It should be noted, that at this stage of this study, the positions of the esterified fatty acids were tentatively assigned and that there were many other possible structures for this lipid A. The theoretical structure shown in Figure 3.5 corresponds to a monophosphorylated lipid A with a theoretical [M-H] $^-$ at m/z 1506.0511 LipA3 and at m/z 1279.8596 LipA4 respectively. The structures shown in Figure 3.4 were however, confirmed with a detailed analysis MS/MS analysis of selected molecular anions, as described in the following sections.

The different proposed structures of the deprotonated molecules attributed to LipA1 to LipA4, which were obtained in the conventional single stage, have been tentatively proposed.

The ions at lower m/z values and intensities were tentatively assigned as different mono-phosphorylated lipid A species devoid of 14:0 acid m/z 1097.6930, 14:0 acid and 14:0(3-OH) acid m/z 1053.3525 or mono-phosphorylated species containing one D-GlcN devoid of 14:0 acid and 14:0(3-OH) acid m/z 892.5934, 12:0(3-OH) acid m/z 386.2501. These lower m/z value ions could be explained by the partial degradation of lipid A during work-up and acid liability of some acylchains and phosphate group at O-1 position during the acid hydrolysis.
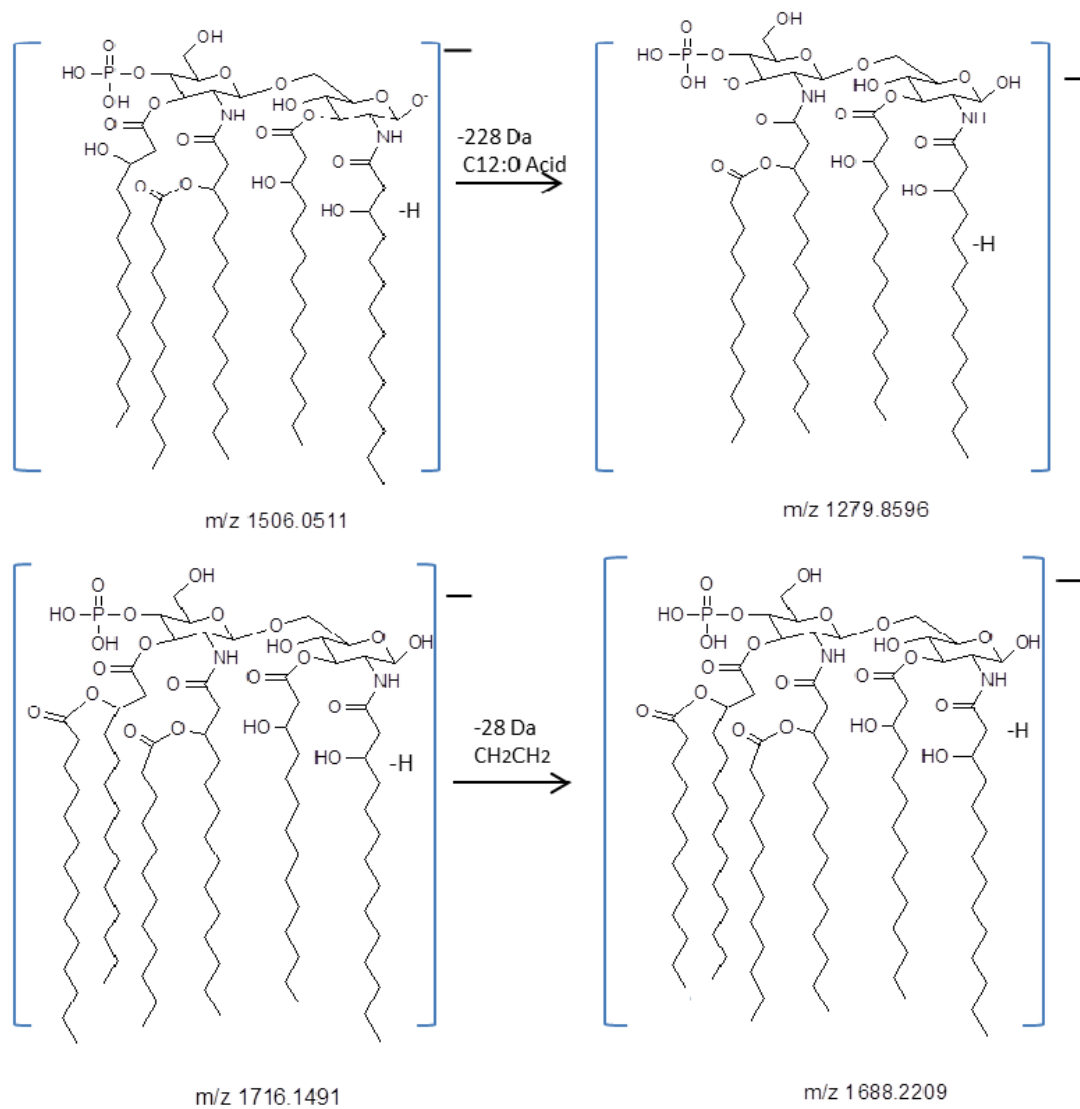
Figure 3.5: The four proposed structures of the native lipid A extract from *A. liquefaciens* SJ-19.

It is important to note that some of these low value m/z ions can also be explained by their gas-phase fragmentation in the conventional scan. Thus, it was noted that the glycosidic cleavages could be induced by the MS provided, hence providing useful structural information and sugar sequencing of complex carbohydrates. In the ESI-MS, two distinctive ions, at m/z 892.5975 and m/z 386.2501 were observed and were assigned as the [C-H]$^-$ and [Y-H]$^-$ ions, respectively, which are shown in Figure 3.6. In this thesis the carbohydrate nomenclature used by Domon and Costello was employed.[100]

The assignment of the ions observed in the simple one-stage high-resolution MS analysis is based on the exact molecular masses only, and additional evidence is usually required to validate these assignments. Therefore, without further confirmation, it would be impossible to suggest various constitutional isomer structures for this lipid A mixture. For example, all the proposed ion structures shown in Table 3.1 and Figure 3.4, could also be correct if, instead, the fatty acid acylation on the disaccharide backbone were reversed.

For this reason, the use of tandem mass spectrometry permitted the identification of the diagnostic product ions and also confirmed the proposed molecular structure.

Figure 3.6: Schematic representation of the one of the common structure of lipid A and the diagnostic ions of [C-H]⁻ and [Y-H]⁻ observed in the FT-ICR-MS spectrum.

3.2.1. CID- FT-ICR-MS/MS analysis

The distribution of the fatty acids was determined for the lipid A isolated from *A. liquefaciens* SJ-19 by multiple-stage ESI-MS^n (n=2) CID. The detected product ions were interpreted according to the rules described previously in the ESI-CID-MS^n studies of lipid A.[138] ESI-MS^2 of the precursor ions at *m/z* 1716.14910 LipA1 Figure 3.7, *m/z* 1688.2209 LipA2 Figure 3.9, *m/z* 1506.0511 LipA3, Figure 3.11, *m/z* 1279.8596 (LipA4) Figure 3.13, and *m/z* 1097.6930 Figure 3.16, were performed to determine the distribution of fatty acids on the disaccharide lipid A backbone.

Moreover, to determine the exact location of the phosphate group at *m/z* 892.5932 Figure 3.11 and *m/z* 666.4396 Figure 3.12 similar CID-MS^2 experiments were performed. Please note that we have compared our data with that of the already published data for *Salmonicida*-SJ-83-type structure.[139]

The investigation of the fatty acid acyl group distributions was performed by MS^2 of the ion at *m/z* 1716.1491 LipA1 observed in CID analysis of lipid A preparations from *A. liquefaciens* SJ-19 as illustrated in Figure 3.7. On the basis of chemical structure proposed for this lipid A constituents as shown in Figure 3.8, this ion was assigned to the monophosphorylated, hexa-acylated lipid A form containing two GlcN residues, one P group, four (*R*)-14:0(3-OH) on the N-2, O-3, N-2′, and O-3′ positions, one C14:0 fatty acid on the l4:0(3-(*R*)-*O*-14:0) at the O-3′ position and one 12:0 fatty acids on the l4:0(3-(*R*)-*O*-12:0) at the N-2′ position.

The most abundant product ions at *m/z* 1488.1165 indicated the elimination of the 14:0 fatty acid from the l4:0(3-(*R*)-*O*-14:0) at the O-3′ position from the precursor ion of *m/z* 1716.1491. The product ion at *m/z* 1244.7851 corresponds to the loss of a 14:0 fatty

acid from the l4:0(3-(R)-O-14:0) from the O-3′ position and a 14:0 acid at the C-3 position from the precursor ion at *m/z* 1716.1491. Also, the elimination of a 14:0 fatty acid from the l4:0(3-(R)-O-14:0) at the O-3′ position, a 14:0 ketene from the branched fatty acid at the O-3′ position and 14:0 acid from the O-3 position acid was appeared in the product ion at *m/z* 1035.6162.

In contrast to the CID analysis of the precursor ion at *m/z* 1716.1491 LipA1, the CID analysis of the precursor ion at *m/z* 1688.2209 LipA2 is shown in Figure 3.9 gave the product ions at *m/z* 1488.1165, at *m/z* 1244.7851, and at *m/z* 1035.6162, Figure 3.10. These product ions were also observed in the MS^2 of the precursor ion at *m/z* 1716.1491 LipiA1. Nevertheless, it is important to stress that the product ion at *m/z* 1444.9572 was only observed in the MS^2 of the precursor ion at *m/z* 1688.2209 LipA2. The mass difference between the ions at *m/z* 1688.2209 LipA2 and at *m/z* 1444.9572 is of (-244 Da), indicates the elimination of 14:0(3-OH) acid, present from either the reducing end or non-reducing end from the O-3 and O-3′ positions of the disaccharide backbone of the lipid A.
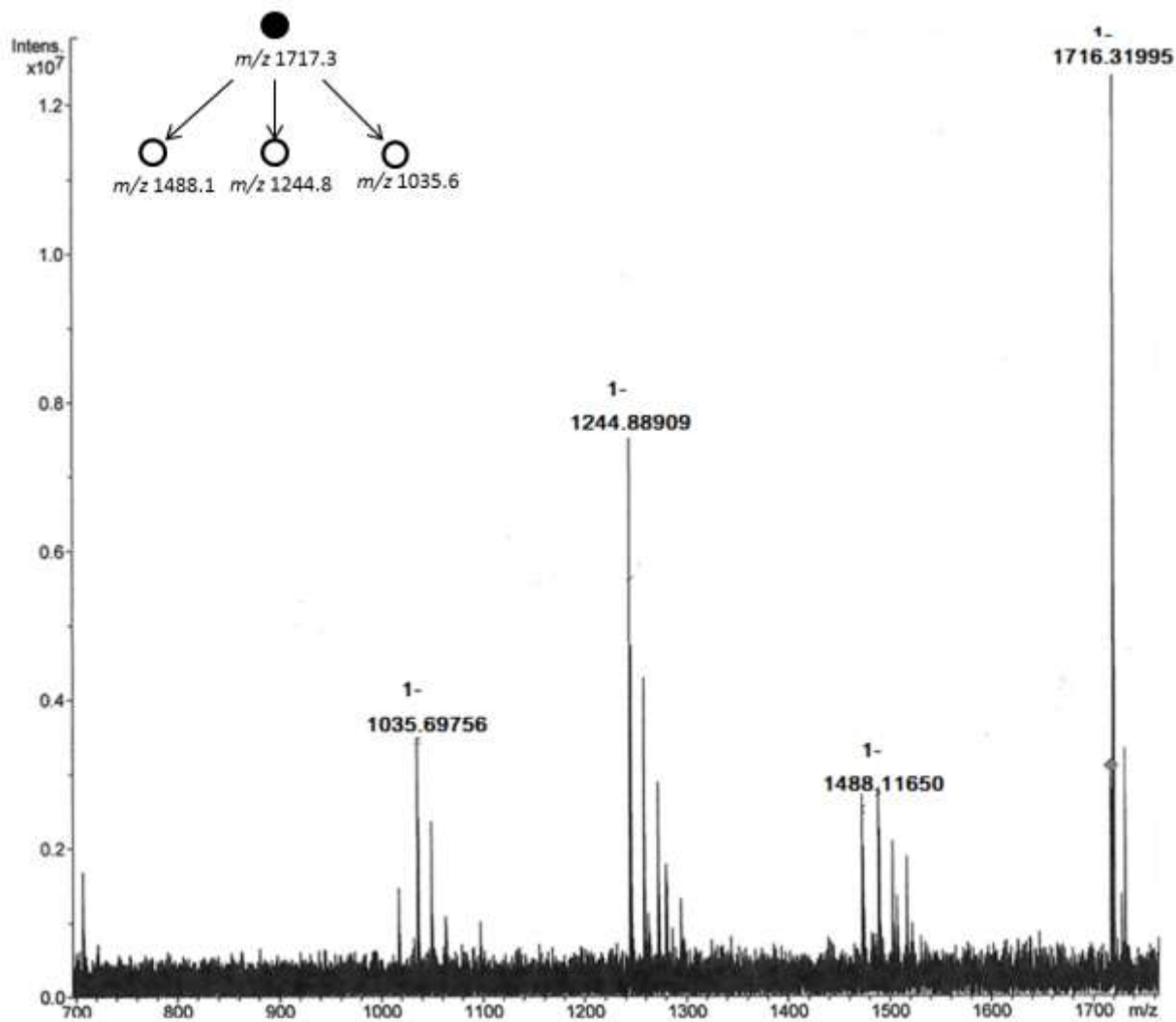
Figure 3.7: Negative ion MS/MS of the singly charged monophosphorylated lipid A [M-H]⁻ ion A at *m/z* 1716.3199.

Figure 3.8: The proposed MS/MS fragmentation pathway of the selected ion at *m/z* 1716.3199.

Figure 3.9: Negative ion MS/MS of the singly charged monophosphorylated lipid A [M-H]⁻ ion A at *m/z* 1688.1230.
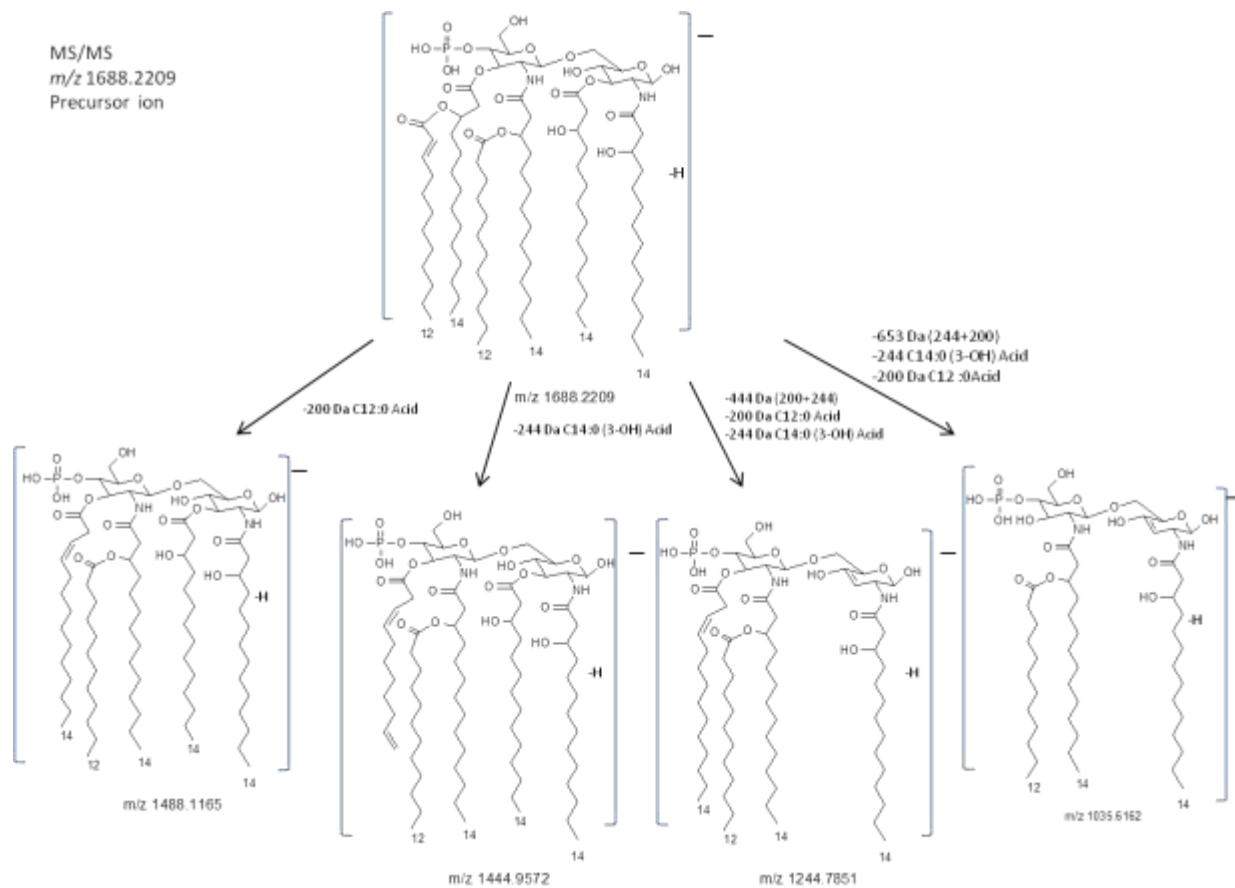
Figure 3.10: The proposed MS/MS fragmentation pathway of the selected ion at *m/z* 1688.1230.

To determine the possible structures of the most abundant ions shown in the ESI-MS, the precursor ion at *m/z* 1506.0511 LipA3 was subjected to a MS^2 experiment, and as shown in Figure 3.11; it gave the major product ion at *m/z* 1261.7949. This product ion was formed by elimination of the 14:0(3-OH) acid from the O-3′ position (-244 Da differences) from the precursor ion at *m/z* 1506.0511. As a result of this elimination, ion at *m/z* 1261.7949 was attributed to the monophosphorylated, penta-acylated lipid A form with one phosphate group on the non-reducing end, three (*R*)-14:0(3-OH) acid on the N-2, O-3, and N-2′ positions, and one a 12:0 fatty acid at position of l4:0(3-(*R*)-*O*-12:0) at N-2′. This elimination is illustrated in Figure 3.12 could in fact occur from either at the O-3 and O-3′ positions located respectively in the reducing end (ion A), or non-reducing end (ion B) of the lipid A disaccharide backbone.

Additionally, the CID analysis of the second most abundant precursor ion at *m/z* 1279.8596 LipA4 Figure 3.13 afforded the product ion at *m/z* 1079.6387. This product ion indicates the elimination of 12:0 fatty acid at l4:0(3-(*R*)-*O*-12:0) group from the N-2′ position (-200 Da). As a result of this elimination, this latter was assigned to the monophosphorylated, tetra-acylated lipid A form containing one phosphate group, three 14:0(3-OH) located at the N-2, O-3, and N-2′ positions, one a 12:0 located on the l4:0(3-(*R*)-*O*-12:0) group at the N-2′ position. It should be noticed that this product ion of at *m/z* 1035.6523 could derive from either the loss of 12:0(3-OH) acid molecules from the N-2 and N-2′ positions of the disaccharide lipid A backbone from the reducing end or non-reducing end of the lipid A disaccharide backbone, (Figure 3.14).
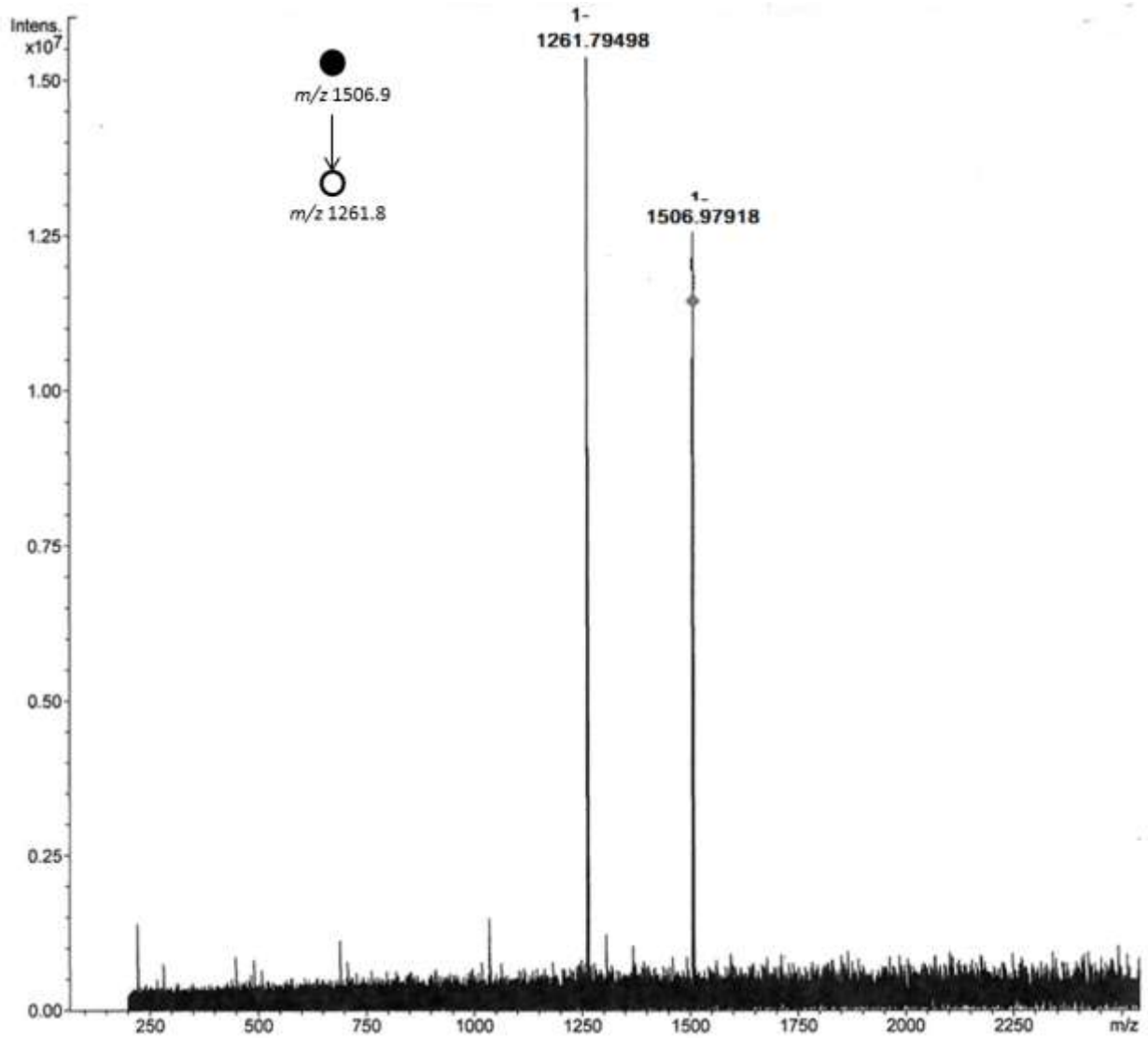
Figure 3.11: Negative ion MS/MS of the singly charged monophosphorylated lipid A [M-H]⁻ ion at *m/z* 1506.9791.
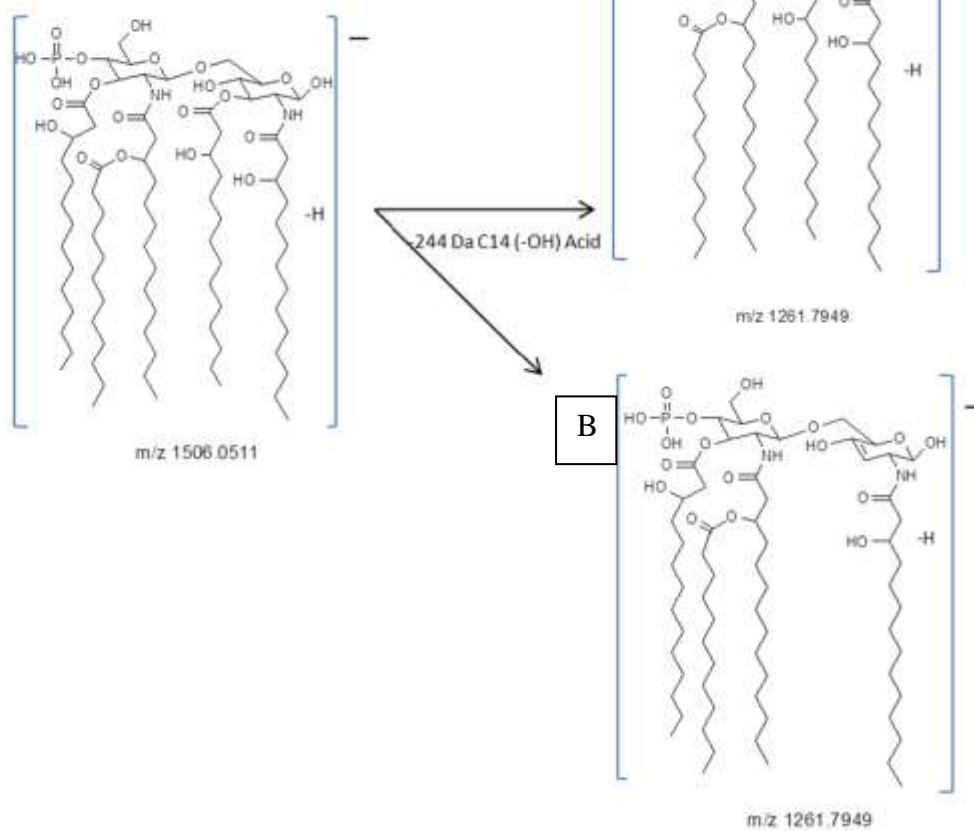
Figure 3.12: The proposed MS/MS fragmentation pathway of the selected ion at *m/z* 1506.9791.
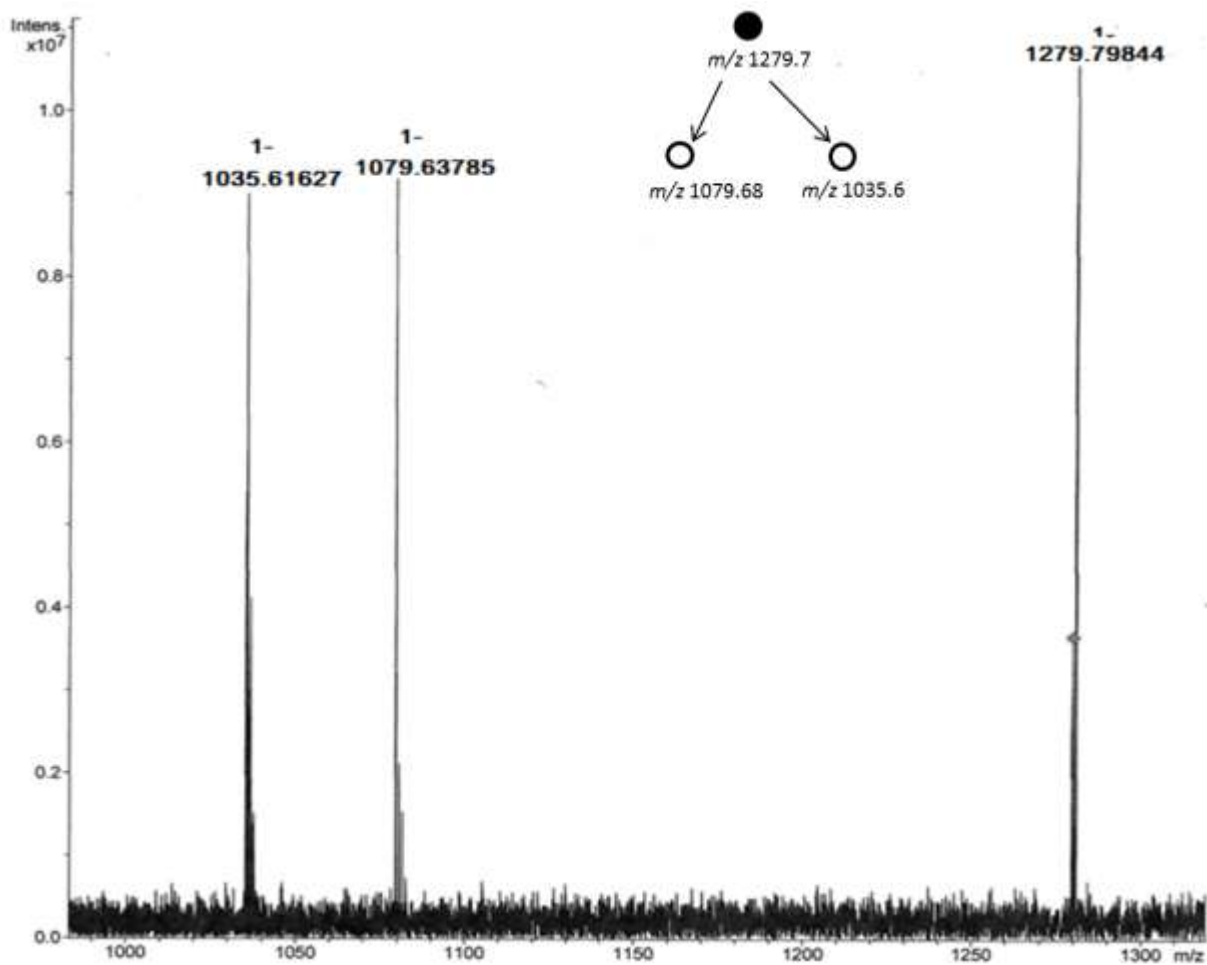
Figure 3.13: Negative ion MS/MS of the singly charged monophosphorylated lipid A [M-H]⁻ ion at *m/z* 1279.79844.
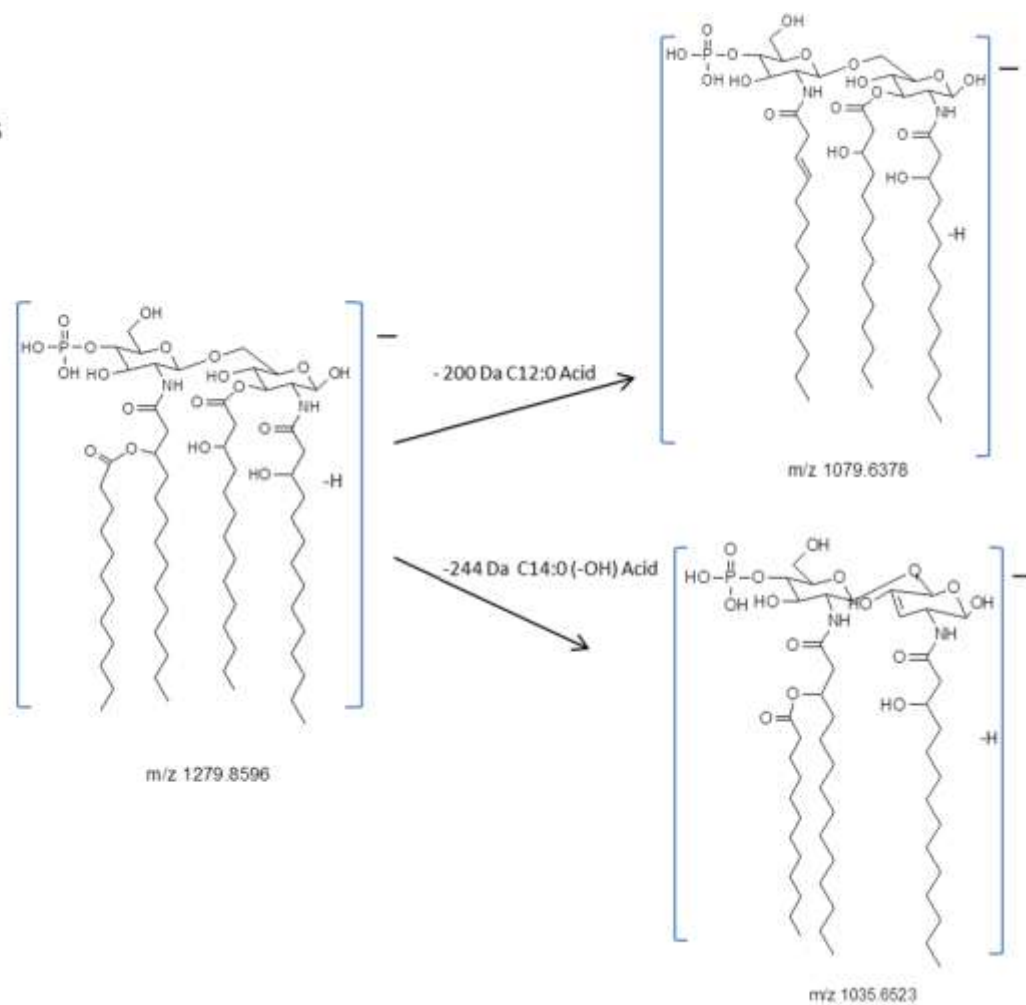
Figure 3.14: The proposed MS/MS fragmentation pathway of the selected ion at *m/z* 1279.7984.

Figure 3.15 illustrates the product ion at *m/z* 853.4597 was produced from the precursor ion at *m/z* 1097.6930. This ion was formed from the elimination of the 14:0(3-OH) ketene at the O-2′ position that was connected to the amido group at the N-2′ position (-244 Da) as shown in Figure 3.16.

To confirm the presence of the phosphate group position, the precursor ion at *m/z* 892.5932 was isolated and subjected to a CID analysis Figure 3.17. The most abundant product ion at *m/z* 648.3745 was formed by loss of the 14:0 fatty acid on the l4:0(3-(*R*)-*O*-14:0) group at the O-3′ position (-244 Da) of the disaccharide backbone of lipid A. The suggested structure of the product ion at *m/z* 648.3745 appears to indicate that the position of the phosphate group could exist in either the C-1 position on the reducing end sugar or on the O-4′ of the non-reducing end sugar of the disaccharide backbone, which is presumably acylated with the 14:0 located at the branched fatty acid of N-2′ and a 12:0 fatty acid from the l4:0(3-(*R*)-*O*-12:0) group at the N-2′ position exited at either the reducing end or non-reducing end as shown in Figure 3.18.

Moreover, this CID of the precursor ions at *m/z* 466.2131 and at *m/z* 448.2035 indicate the elimination of the 14:0(3-OH) acid located at the N-2′ position (-244 Da) and the 12:0 ketene (-182 Da) located at the l4:0(3-(*R*)-*O*-12:0) from N-2′ position in both cases and H_2O in the case of *m/z* 448.2035 only.

As well, the precursor ion at *m/z* 666.4396 was isolated and analyzed by CID-MS^2 (Figure 3.19), to produce the product ion at *m/z* 649.4235 by loss of a molecule of H_2O at the O-3′ position, as shown in Figure 3.20.
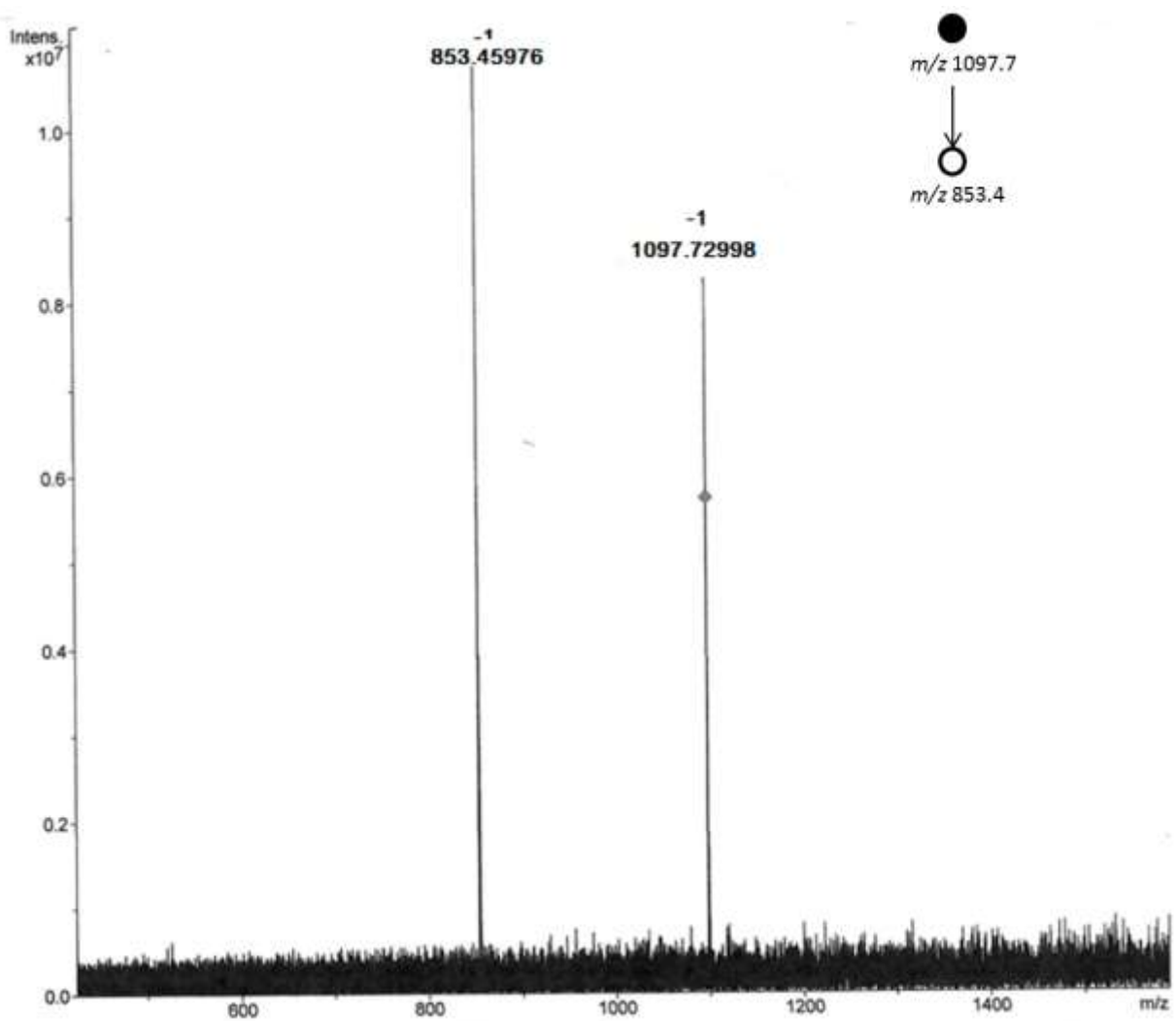
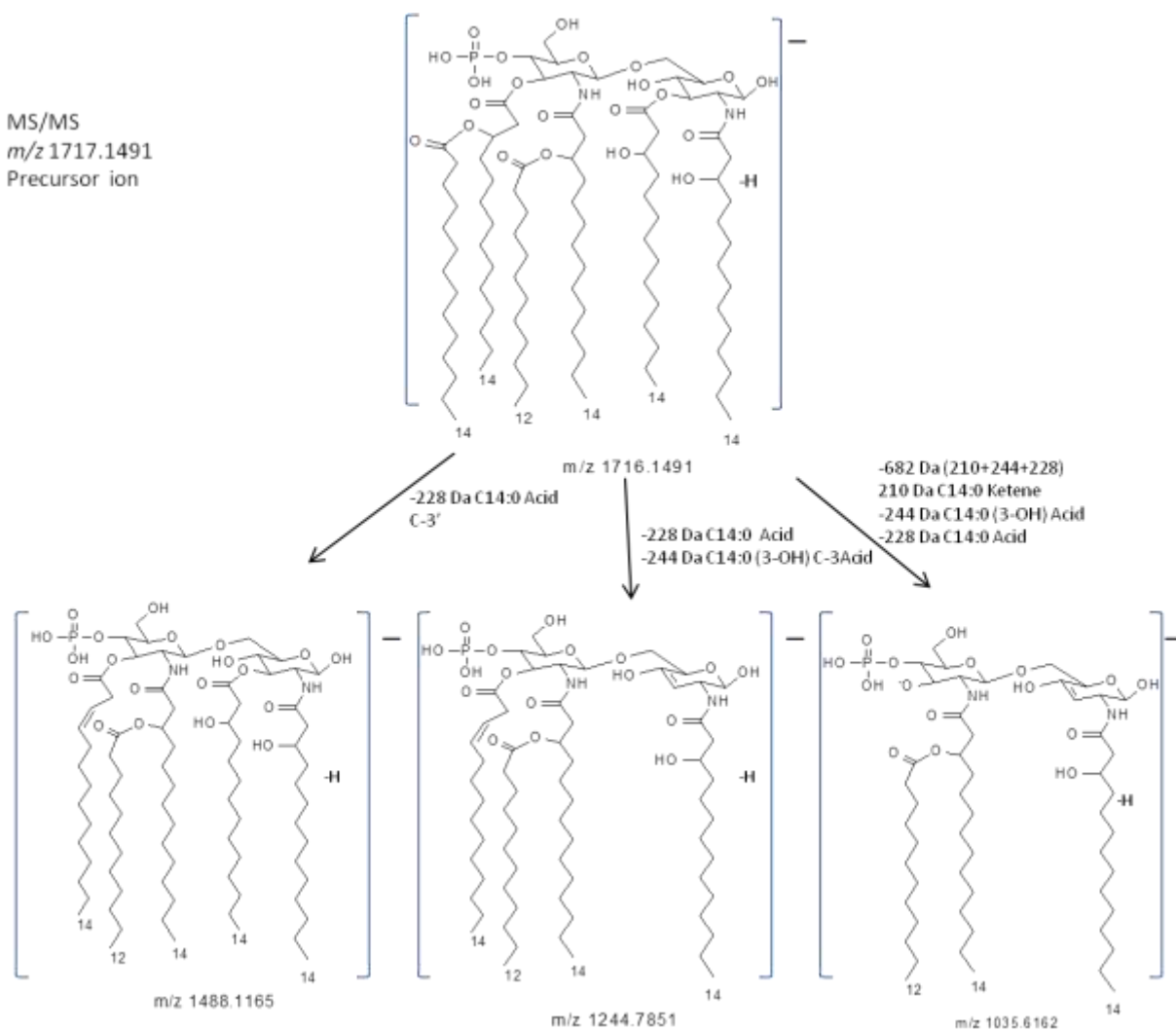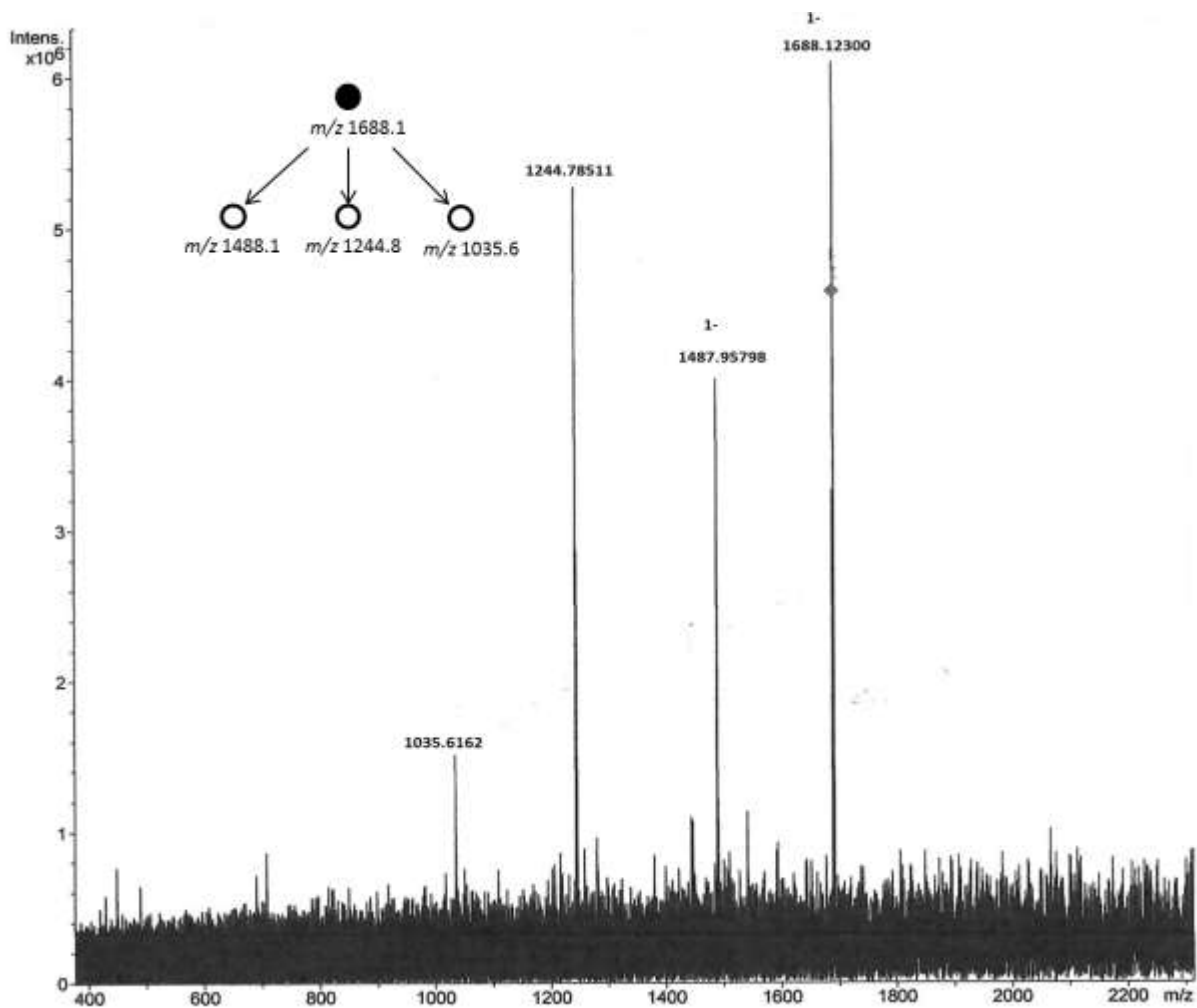**Figure 3.15:** Negative ion MS/MS of the singly charged monophosphorylated lipid A [M-H]⁻ ion at *m/z* 1097.7299.

Similarly, in the CID-MS2 of the precursor ion at *m/z* 666.4396, were noted, which the presence of the product ions at *m/z* 386.2501 and at *m/z* 326.2873 indicated the elimination of the branched fatty acid 12:0 located at the O-3′ position (-200 Da) and HPO_3 (-80 Da) from the non-reducing end as shown in Figure 3.19. This product ions suggests that the phosphate group and the 12:0 fatty acid at the l4:0(3-(*R*)-*O*-12:0) group at the N-2′ position are at similar backbone as could be shown in both sides of the lipid A backbone.
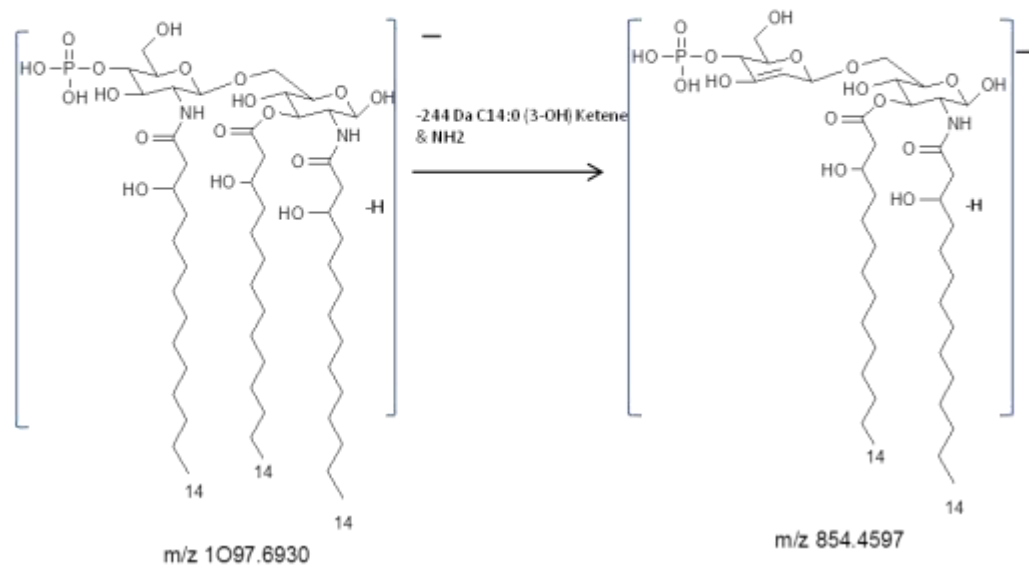
Figure 3.16: The proposed ms/ms fragmentation pathway of the selected ion at *m/z* 1097.6930.

3.2.2. CID analysis of the [C-H]⁻ and [Y-H]⁻ ions

As mentioned earlier, two diagnostic ions, namely [C-H]⁻ and [Y-H]⁻; associated with the glycosidic cleavages of the β-D-(l→6) of the D-GlcN disaccharide were observed in the conventional FT-ICR-MS scan, at *m/z* 892.5932 and at *m/z* 386.2501, respectively, (Figures 3.6). To confirm the proposed structure of these ions, MS/MS were acquired. The product ion scan of the selected ion [C-H]⁻ at *m/z* 892.5932 showed the loss of a l4:0 acid chain from the C-3′ to yield the product ion assigned as [C-(C14:0) (3-OH) acid-H]⁻ observed at *m/z* 648.3745 which can further fragment by losing a 12:0 ketene molecule located at the l4:0(3-(*R*)-*O*-12:0) at the N-2′ position to afford the product ion observed at *m/z* 466.2131. This latter loss probably takes place from the labile *O*- linked fatty acid rather than the more stable *N*-linked one.

It is well-accepted that during CID analysis of the lipid A moiety, the elimination of the fatty acid derivatives occur mainly from the *O*- linked fatty acid esters. Therefore, it was projected that the major ion observed at *m/z* 648.3745 would be associated with the loss of the 14:0(3-OH) acid form the O-3' position, rather than a loss of 12:0 ketene at the l4:0(3-(*R*)-O-12:0) group at the N-2′ position from the product ion observed at *m/z* 466.2131; note that it is very possible that these two processes occur simultaneously, as mentioned earlier. This latter product ion could further fragment by losing another molecule of H_2O to produce the distinctive product ions [C-(C12:0) acid-(C14:l)acid-(C12:0)acid-H-H_2O]⁻ appearing at *m/z* 448.2035, (Figure 3.18) for proposed structures. These product ions confirmed the proposed structure of lipid A bearing two secondary ions and one phosphate group at its non-reducing end of the lipid A backbone.
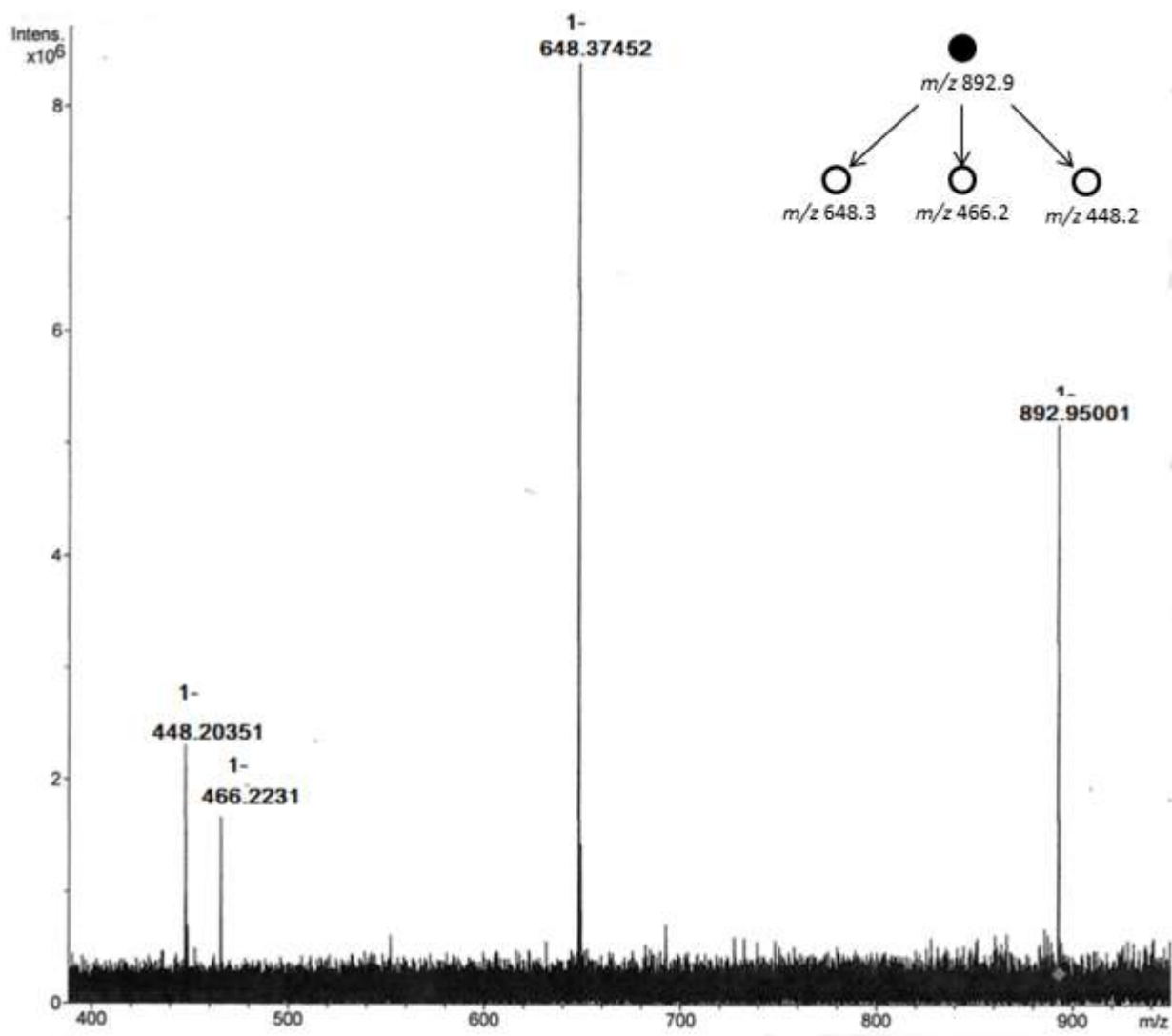
Figure 3.17: Negative ion MS/MS of the singly charged monophosphorylated lipid A [M-H]⁻ ion at *m/z* 892.9500.
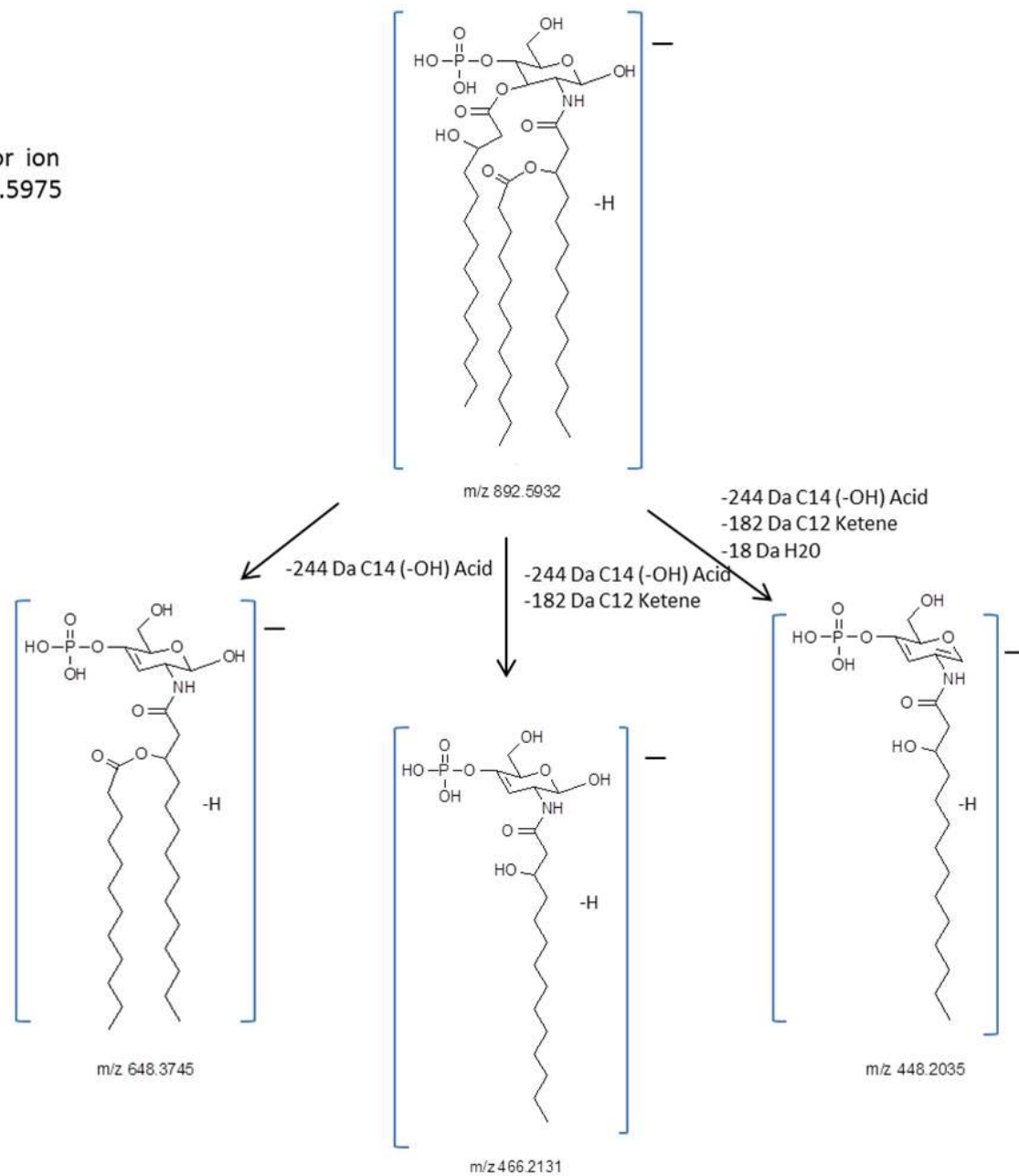
Figure 3.18: The proposed MS/MS fragmentation pathway of the selected ion at *m/z* 892.5932.

On the other hand, as shown in Figure 3.19, CID analysis of the [Y-(C12:0(3-0(14:0))) ketene-H]$^-$ ion at *m/z* 666.38 was also rationalized and is presented in the self-explanatory Figure 3.20. Despite the many possible fragmentation routes that can lead to the formation of the same ions observed in this CID, the fragmentation pattern presented in Figure 3.20 was confirmed by using product ion scan analysis.

The product ion scan of the ion at *m/z* 666.4396 assigned as [C-(C14:0(3-0(12:0))ketene-H]$^-$ is shown in Figure 3.20, and it clearly illustrates that this ion indeed produced the major product ion observed at *m/z* 386.2501 formed by losing 12:0 acid at the l4:0(3-(*R*)-*O*-12:0) group at the N-2′ position and H_2O_2P from the non-reducing end and the secondary product ion at *m/z* 326.2873 produced by the loss of the 12:0 acid at the l4:0(3-(*R*)-*O*-12:0) group at the N-2′ position, C_3H_6 from the C14 chain, and HPO_3 from the non-reducing end; eliminating the theoretical possibility that this ion was obtained from the ion reducing end sugar losing 14:0(3-OH) ketene.

The rationale presented in Figure 3.20 further confirms the proposed structure, and illustrates, once more, that this product ion retains the 12:0 fatty acids at the non-reducing end due to the appearance of the diagnostic product ions observed at *m/z* 649.4235 that indicate the elimination of H_2O.
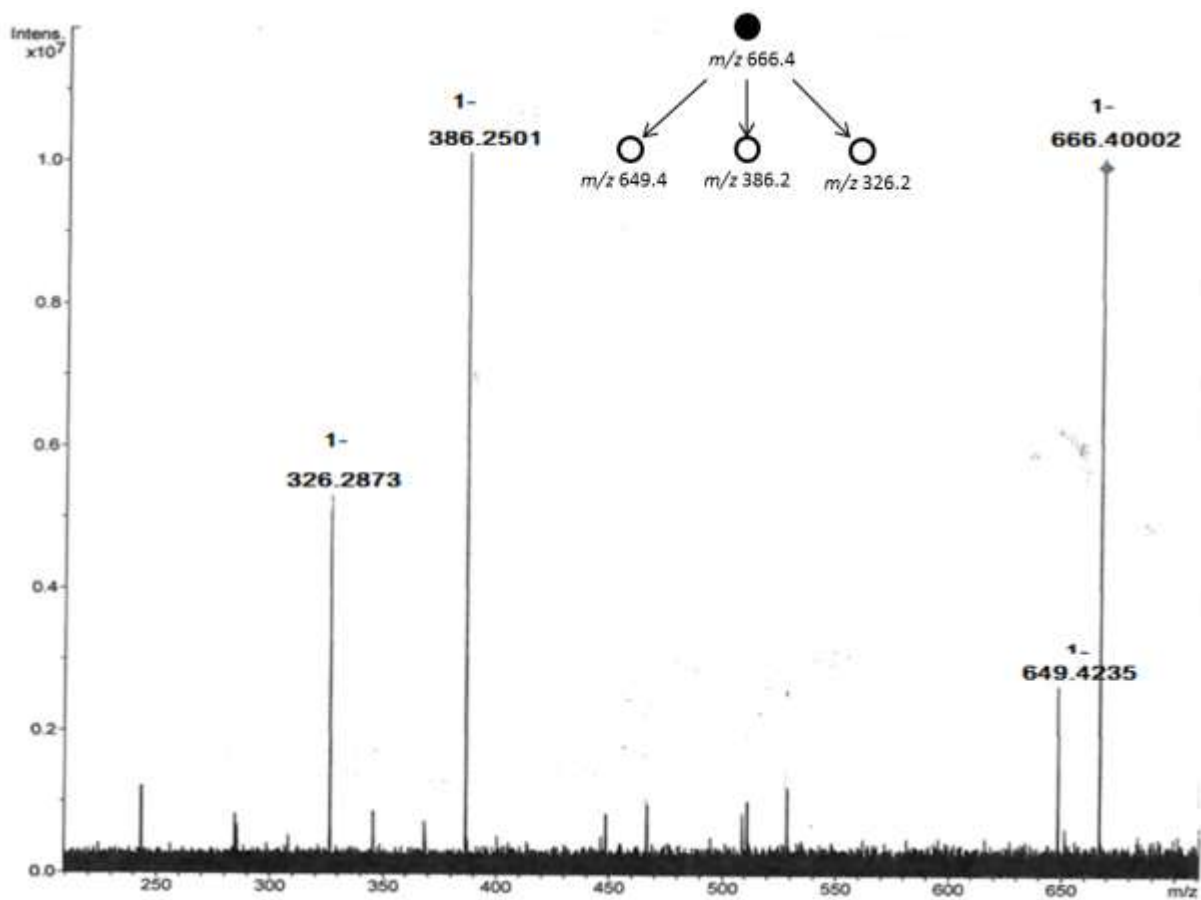
Figure 3.19: Negative ion MS/MS of the singly charged monophosphorylated lipid A [M-H]⁻ ion at *m/z* 666.40002.
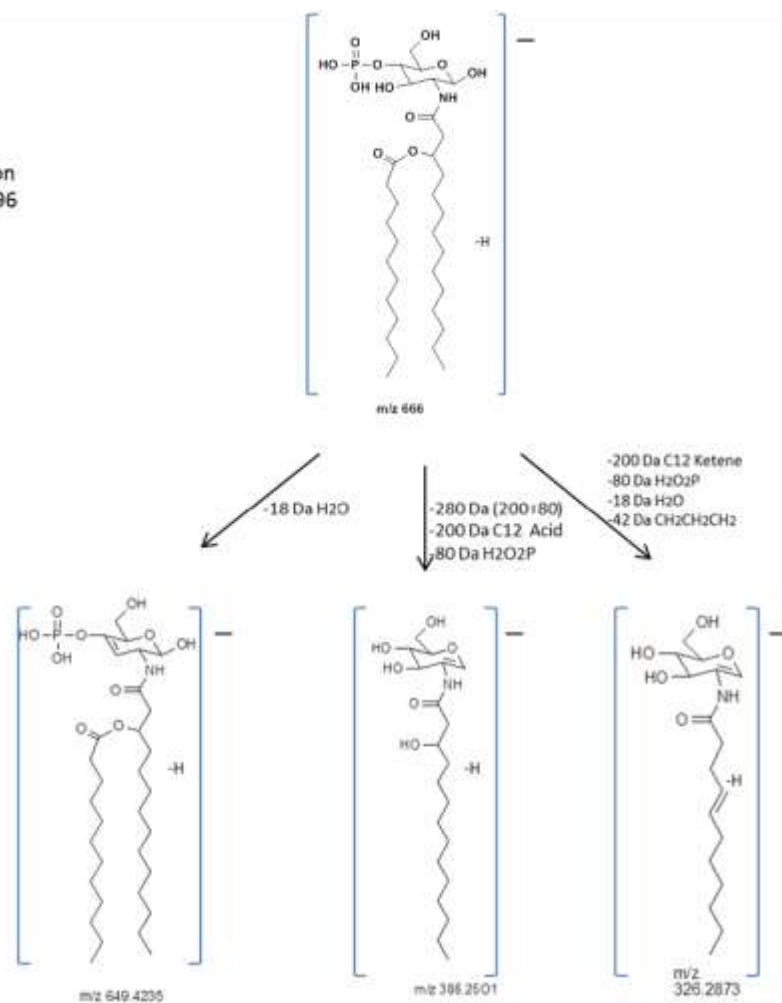
Figure 3.20: The proposed MS/MS fragmentation pathway of the selected ion at *m/z* 666.4396.

3.3. Summary:

The chemical structure of lipid A, isolated by mild acid hydrolysis from *Aeromonas liquefaciens* lipopolysaccharide, was investigated using electrospray ionization FTICR hybrid tandem in time mass spectrometry low collision-energy (CID) and illustrated a great degree of microheterogeneity. The chemical structure of the main constituent of this heterogeneous mixture was identified as a D-(l→6) linked glucosamine disaccharide substituted by one phosphate group, being bound to the non-reducing end at position O-4' of the D-glucosamine disaccharide.

The location of the fatty acids linked to the disaccharide backbone was established by identifying diagnostic ions in the conventional FT-ICR-MS scan. Low-energy collision (CID) tandem mass spectrometry analysis of the selected precursor diagnostic ions confirmed, unambiguously, their proposed molecular structures. It was established that myristyloxylauric 14:0(3-(*R*)-*O*-12:0) acid residues were both N-2' and O-3' linked to the non-reducing end of the D-GlcN residue, whereas two 3-hydroxy myristic (R)-14:0(3-OH) acid chains acylated the remaining positions of the reducing end.

The MS and MS/MS data obtained allowed us to determine the complex molecular structure of lipid A. In addition, the fragmentation patterns were clearly illustrated and established for this biologically-active compound.

Chapter 4

ESI-QhQ-MS/MS and MALDI-TOF/TOF-MS/MS analysis (Tandem-in-Space Mass Spectrometry) for verifying the structure of Lipid A of the Gram negative bacteria *A. Liquifaciens.*

4.1. Background

Lipid A extracts are usually formed as a micro-heterogeneous mixture composed of a major lipid A component, in addition to other minor products. This heterogeneity is most likely a result of complete and incomplete lipid A biosynthesis and differs mainly in either the composition of fatty acid length and/or position and saturation, in addition to the substitution of the phosphate by ethanolamine or various glycosyl groups.[97]

In this chapter, conventional single stage ESI-MS (-ion mode) was recorded with the QhQ-mass spectrometer in order to investigate the lipid A structure. In this work, it was noticed that the ESI-MS measured with different cone voltages, were similar to the ones recorded with the FT-ICR-MS instrument, in term of distribution of the deprotonated molecules of the heterogenous lipid A. Nevertheless, low-energy collision CID-MS/MS of the selected different precursor ions failed to fragment and to produce diagnostic product ions, even with collision energies = 100eV. These discrepancies were attributed to the inefficiency of the hexapole collision to fragment such ions.

In order to obtain another efficient ionization method, which could be used for comparison with the FT-ICR-MS (tandem-in-time mass spectrometry) described in Chapter 2, the MALDI- ionization in a TOF/TOF tandem mass spectrometer was used. This tandem mass spectrometer allows the measuring of high-energy CID-MS/MS

analysis (tandem-in-space mass spectrometry). Therefore, the CID-MS/MS analyses will permit the differentiation and elucidation of the molecular structure of the fundamental constituent of native lipid A isolated from the bacterial species *A. liquefaciens* SJ-19.

Furthermore, this series of MS/MS analysis will decipher the gas-phase fragmentation pattern and the mass spectrometric fingerprints of the various incompletely biosynthesized lipid A. The data obtained can be used in future medicinal experiments to evaluate lipid A and to perform quantitative studies on its formulations.

4.2. ESI-QhQ-MS analysis

The negative ESI-MS with the QhQ-MS instrument of the lipid A was acquired with a declustering potential (DP) value of -60V, Figure 4.1. This MS showed a cluster of high molecular ions between *m/z* 1650-1850, and two major abundant ions at *m/z* 1506.05 and *m/z* 1279.85, all of which were considered to be singly charged species. This series of incomplete biosynthetic series was tentatively assigned as shown in Figure 4.1 and Table 4.1.

The presences of *inter alia* five different deprotonated monophosphorylated molecules assigned as [M-H]⁻ and having related structures of the lipid A were observed at *m/z* 1716.36 LipA1, *m/z* 1687.91 LipA2, *m/z* 1505.60 LipA3, *m/z* 1279.42 LipA4, and *m/z* 892.08 LipA5. However, it is important to mention that the deprotonated molecule at *m/z* 892.08 designated as LipA-5 was only observed in QhQ-MS as a major peak, as illustrated in Figure 4.1.
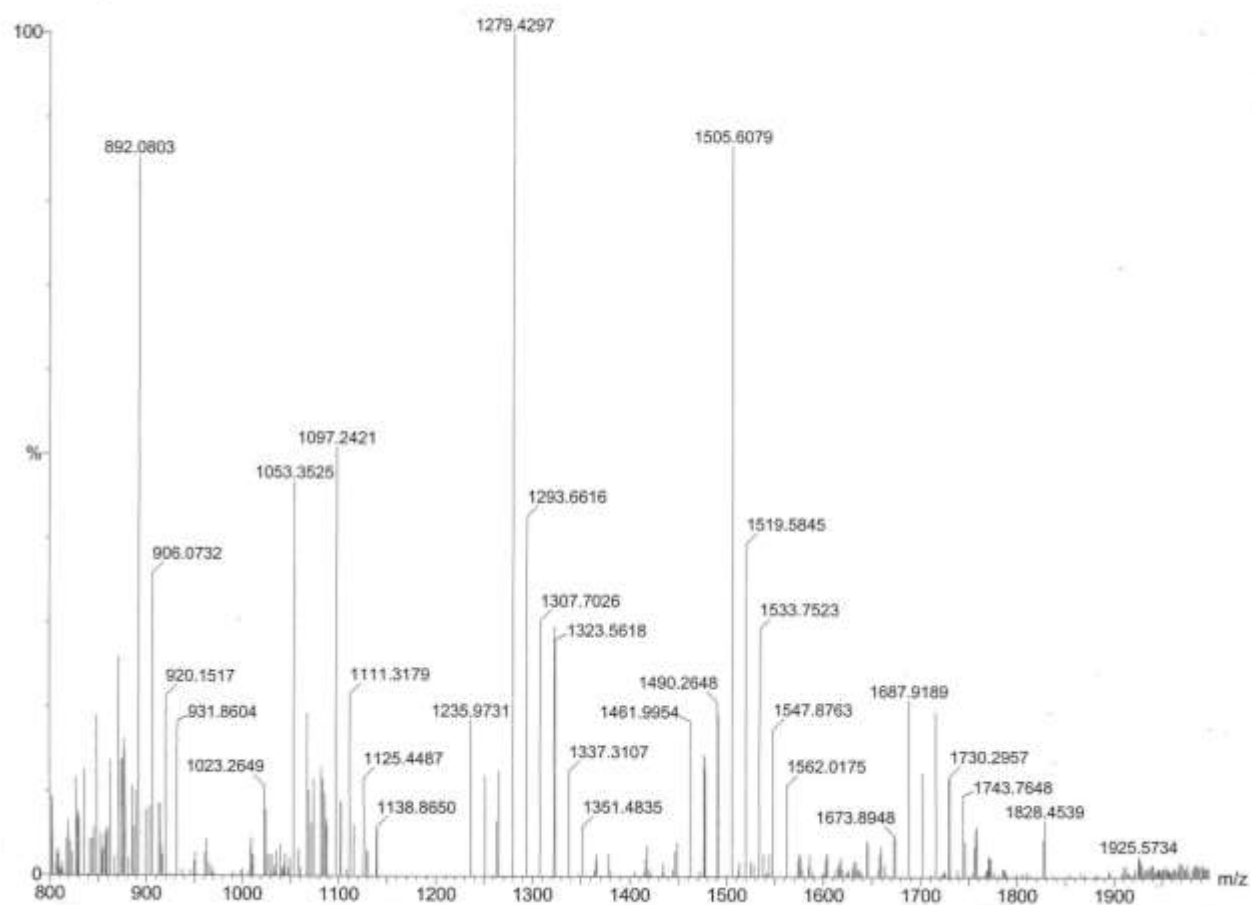
Figure 4.1: Negative ions QhQ-MS of the native lipid A extract from *A. liquefaciens* SJ-19.

Consequently, the lower-intensity deprotonated molecular ion at *m/z* 1716.36 was assigned as LipA1, which was tentatively described as being the mono-phosphorylated hexa-acylated forms of lipid A carrying four (*R*)-14:0(3-OH) on the N-2, O-3, N-2', and O-3' positions of the lipid A disaccharide. In addition, *m/z* 1716.36 contained one branched fatty acid l4:0(3-(*R*)-*O*-12:0) attached to the N-2 and one branched fatty acid l4:0(3-(*R*)-*O*-14:0) at the O-3' positions of the D-GlcN residues.

On the other hand for the deprotonated molecular ion at *m/z* 1687.93 LipA2, was carried four (*R*)-14:0(3-OH) acyl groups at the N-2, O-3, N-2', and O-3' positions and two branched 12:0 fatty acids of the l4:0(3-(*R*)-*O*-12:0) located at the O-3' and N-2' position of the lipid A disaccharide.

The two most abundant deprotonated molecular ion at *m/z* 1505.60 LipA3 and at *m/z* 1279.73 LipA4 were tentatively assigned as follows. The deprotonated molecular ion at *m/z* 1505.60 LipA3 was assigned as the mono-phosphorylated pentaacylated forms carrying four (*R*)-14:0(OH) on the N-2, O-3, N-2' and O-3' positions, one branched 12:0 fatty acid of the l4:0(3-(*R*)-*O*-12:0 at the N-2′ position of the lipid A disaccharide.

The deprotonated molecule at *m/z* 1279.42 LipA4 attributed to the mono-phosphorylated tetra-acylated forms carrying four (*R*)-14:0(OH) at the N-2, O-3, N-2' and O-3' positions, and one branched of the 12:0 fatty acids of the l4:0(3-(*R*)-*O*-12:0) at the O-3' and N-2' position of the lipid A disaccharide, see Figure 4.1.

Table (4-1): Assignment of the diagnostic ions in QhQ mass spectrum of native lipid A.

Diagnostic ions	Empirical formula	m/z Calculated; Observed	Abundane (%)
[M-H]$^-$ (Lip A1)	$C_{94}H_{177}N_2O_{22}P$	1716.149	18.52
[M-(C14:0(3-OH))ketene-H]$^-$ (Lip A2)	$C_{92}H_{173}N_2O_{25}P_2$	1687.918	20.73
[M-(C13:0) ketene-H]$^-$	$C_{81}H_{152}N_2O_{21}P$	1519.584	39.18
[M-(C14:0) ketene-H]$^-$ (Lip A3)	$C_{80}H_{149}N_2O_{21}P$	1505.607	88.92
[M-(C12:0)ketene-(C14:0(3-OH))ketene-H]-	$C_{92}H_{173}N_2O_{25}P_2$	1293.6616	23.81
[M-(C12:0)ketene-(C14:0(3-OH))ketene-H]$^-$ (Lip A4)	$C_{66}H_{124}N_2O_{19}P$	1279.429	100
[M-(C14:0)ketene-(C14:0(3-OH))ketene-(C12)-H]$^-$	$C_{54}H_{102}N_2O_{18}P$	1097.242	52.40
[M-(C14:0)ketene-(C14:0(3-OH))ketene-(C12:0)Ketene)-H]$^-$	$C_{53}H_{102}N_2O_{16}P$	1053.352	49.26

To confirm the proposed structure of the various components of the Lipid A, low-energy CID-MS/MS analysis was attempted in order to determine the distribution of the fatty acid and to identify all the deprotonated molecules at *m/z* 1716.149, *m/z* 1687.91, *m/z* 1519.58, and *m/z* 1293.66 (Table 4.1). Unfortunately, the MS/MS analysis performed on our conventional quadrupole-hexapole-quadrupole tandem instrument, failed to fragment the selected precursor ions using different collision energies and gas pressure conditions in the collision cell. This major discrepancy was due to the inefficiency of this hexapole collision cell to fragment the selected precursor deprotonated molecules.

4.3. MALDI-TOF-MS analysis

The MALDI-TOF-MS (- ion mode) of the lipid A obtained from *A. liquefaciens* SJ-19 was measured in the reflector mode with the TOF/TOF instrument and high laser power (Figure 4.2). Once more as previously shown, it was noticed that the MALDI-MS showed similar spectra to the ones measured with the ESI-QhQ-MS and FT-ICR-MS instruments. Again the ESI-MS indicated that the biosynthesis of lipid A was incomplete. Accordingly, we have assigned for this lipid A mixture, the original five common structures of the lipid A as suggested previously were assigned, as shown in Figure 4.3.

Accordingly, the MALDI-TOF-MS measured in the reflector mode showed *inter alia* five different deprotonated monophosphorylated molecular ions [M-H]⁻ having related structures at *m/z* 1716.3613 LipA1, *m/z* 1688.0341 LipA2, *m/z* 1505.906 LipA3, *m/z* 1279.7390 LipA4, and *m/z* 915.1865 LipA5.

It is important to note that the ion at *m/z* 915.1865 LipA5 was only observed in the MALDI-TOF-MS as a major peak, as illustrated in Figure 4.2. Therefore, the lower intensity ions at *m/z* 1716.3613 LipA1 and at *m/z* 1688.0341 LipA2 were assigned to the deprotonated molecules of the mono-phosphorylated hexa-acylated forms of lipid A carrying four (*R*)-C14:0(3-OH) on the N-2, O-3, N-2', and O-3' positions of the lipid A disaccharide; in addition of the branched fatty acyl group composed of a l4:0(3-(*R*)-*O*-12:0) at the N-2 and l4:0(3-(*R*)-*O*-12:0) to O-3' positions. On the other hand for the deprotonated molecule LipA2 at *m/z* 1688.0341 LipA2 two 12:0 fatty acids of the l4:0(3-(*R*)-*O*-12:0) at the O-3' and N-2' position, (Figure 4.3).

In addition, the most abundant deprotonated molecules at *m/z* 1505.9106 LipA3 and at *m/z* 1279.7390 LipA4 were tentatively described as containing the mono-phosphorylated penta-acylated forms for the deprotonated molecule LipA3 at *m/z* 1505.9106 carrying four (*R*)-14:0(OH) on the N-2, O-3, N-2' and O-3' positions and one branched 12:0 fatty acid at position of l4:0(3-(*R*)-*O*-12:0 at the N-2' position of the lipid A disaccharide.

The deprotonated molecular ions LipA3 at *m/z* 1279.7390 was attributed to the mono-phosphorylated tetra-acylated forms carrying four (*R*)-14:0(OH) on the N-2, O-3, O-2' and O-3' positions and one branched 12:0 fatty acid of l4:0(3-(*R*)-*O*-12:0) at position O-3' and N-2' of the lipid A disaccharide, see Figure 4.3.
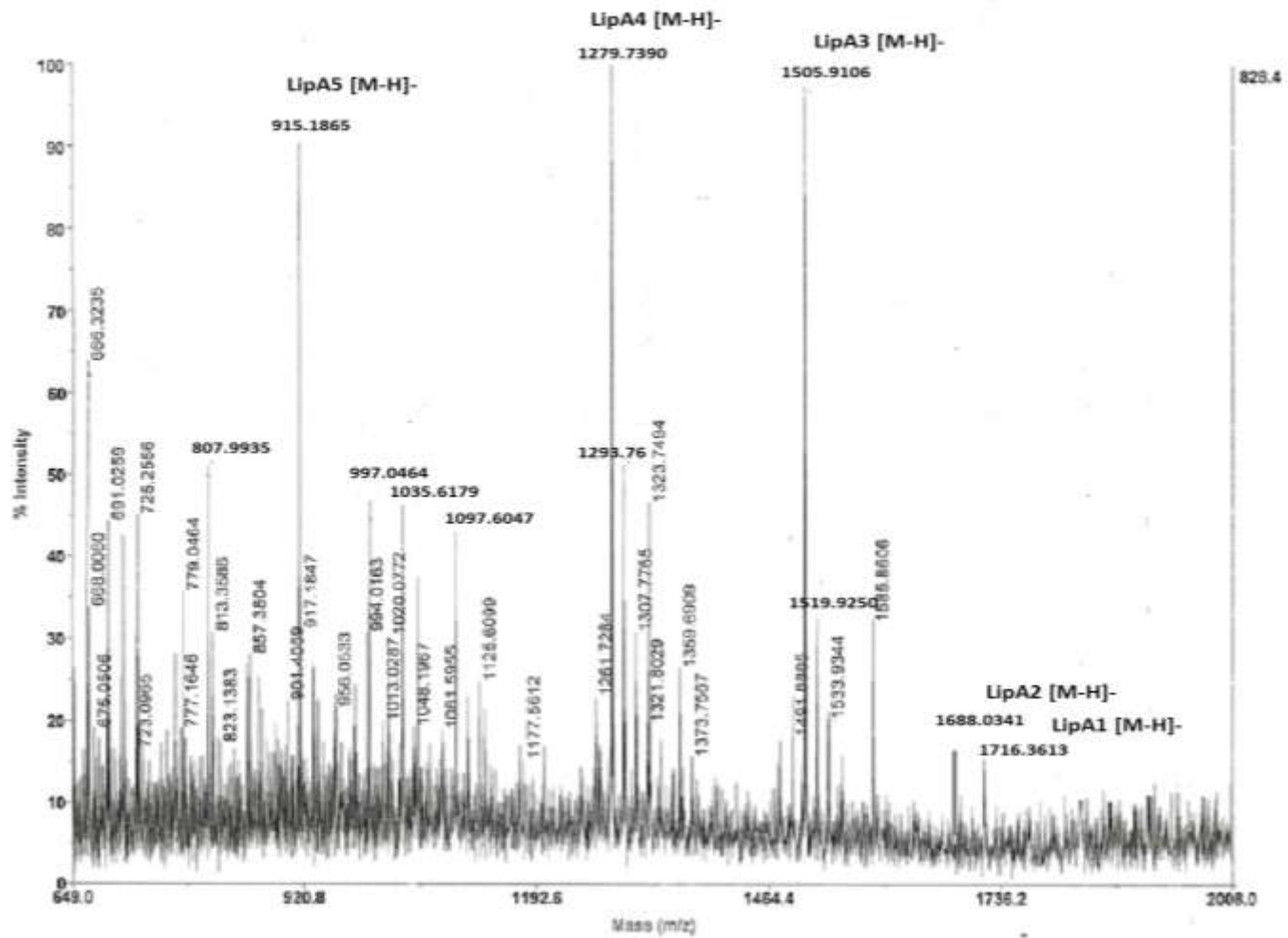
Figure 4.2: Negative ions MALDI-TOF-MS spectra of the native lipid A extracted from *A. liquefaciens* SJ-19.

m/z 1717.1491

m/z 1688.0341

m/z 1505.9106

m/z 1279.7390

m/z 915.1865
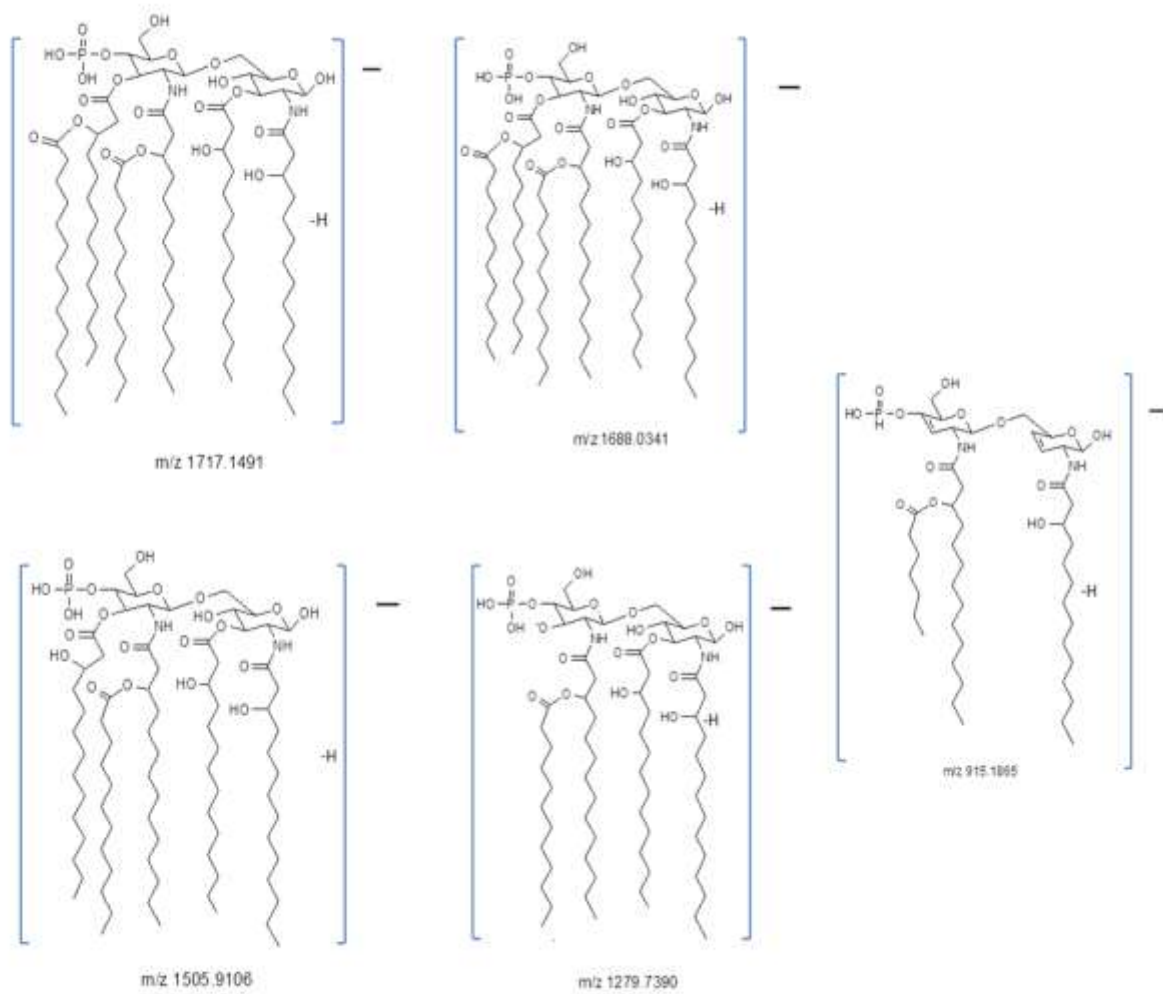
Figure 4.3: The five proposed structures of lipid A extracted from *A. liquefaciens* SJ-19.

It should be noted that the mass difference of 228 Da between the ions at *m/z* 1505.9106 LipA3 and the ions at *m/z* 1279.7390 LipA4 could indicate the elimination of 14:0 acid on the C-3' from the ions at *m/z* 1505.9106 LipA3, Figures 4.9 and 4.10. Also, the ion at *m/z* 915.1865 LipA5 corresponds to a lipid A with two (*R*)-14:0(3-OH) acyl groups on the O-3 and O-3' positions, in addition to, one branched 7:0 acid of the l4:0(3-(*R*)-*O*-7:0) at the N-2' position, (Figure 4.3).

The proposed structures of the monophosphorylated lipid A and its distinctive ions observed in the MALDI-TOF-MS are illustrated in Table 4.2 and Figure 4.2. It should be noted, that at this stage of this study, the position of the esterified fatty acids was tentatively assigned and that there were many possible structures for the lipid A.

The MS shown in Figure 4.2 were, however, confirmed with a detailed analysis of the high energy CID-TOF/TOF-MS/MS analysis of selected molecular anions, as described in the following sections.

It is important to note that some of this series of anions having low *m/z* values ions can be explained by their gas-phase fragmentation in the conventional MS scan. Thus, as reported it is known that MS could induce the glycoside cleavages, hence providing useful structural information and sugar sequencing of complex carbohydrates.[100] In the MALDI-TOF-MS, one diagnostic anion at *m/z* 807.9935 was observed and was assigned as the [C-H]⁻ ion (Figure 4.4). In this chapter, the carbohydrate nomenclature, which was developed by Domon and Costello was used.[100]

Diagnostic ions	Empirical formula	m/zCalculad; Observed	Abundane (%)
[M-(C14:0(3-OH))ketene-H]$^-$ (Lip A1)	$C_{92}H_{173}N_2O_{25}P_2$	1688.0341	30.7
[M-(C13:0) ketene-H]$^-$	$C_{81}H_{152}N_2O_{21}P$	1519.9250	32.6
[M-(C14:0) ketene-H]$^-$ (Lip A2)	$C_{80}H_{149}N_2O_{21}P$	1505.9106	95.5
[M-(C12:0)ketene-(C14:0(3-OH))ketene-H]$^-$ (Lip A3)	$C_{66}H_{124}N_2O_{19}P$	1279.7390	97.3
[M-(C14:0)ketene-(C14:0(3OH))ketene-(C12)-H]$^-$	$C_{54}H_{102}N_2O_{18}P$	1097.6047	36.4
[M-(C14:0)ketene-(C14:0(3-OH))ketene-(C12:0)ketene)-H]$^-$	$C_{53}H_{102}N_2O_{16}P$	1053.5668	29.2
[C-(C14:0)ketene-H]$^-$	$C_{52}H_{96}N_2O_{16}P$	1035.6179	46.8
[M-2((C14:0(3-OH)))acid-(C14:1)ketene-H]$^-$	$C_{52}H_{90}N_2O_{13}P$	997.0464	40.4
[M-(C14:0(3-OH))acid-(C12:0)acid-(C14:1)ketene-H]$^-$	$C_{47}H_{83}N_2O_{13}P$	915.1865	75.8
[C-(C14:0(3-O(C12:0)))ketene-H]$^-$	$C_{40}H_{74}N_2O_{13}P$	807.9935	45.4

Table (4-2): Assignment of the diagnostic ions in MALDI-TOF mass spectrum of native lipid A.

The assignment of the ions observed in the simple one-stage high resolution MS analysis is based on the exact molecular mass only, and additional evidence is usually required to validate these assignments. Therefore, without further confirmation, it would be impossible to suggest various constitutional isomers structures for this lipid A mixture. For example, all of the proposed ion structures shown in Table 4.2 and Figure 4.2 could also be correct, if the fatty acid acylation on the disaccharide backbone were reversed. For this reason, the use of tandem mass spectrometry permitted the identification of the diagnostic product ions and also confirmed the proposed molecular structure.

[C-H]-
807.9935
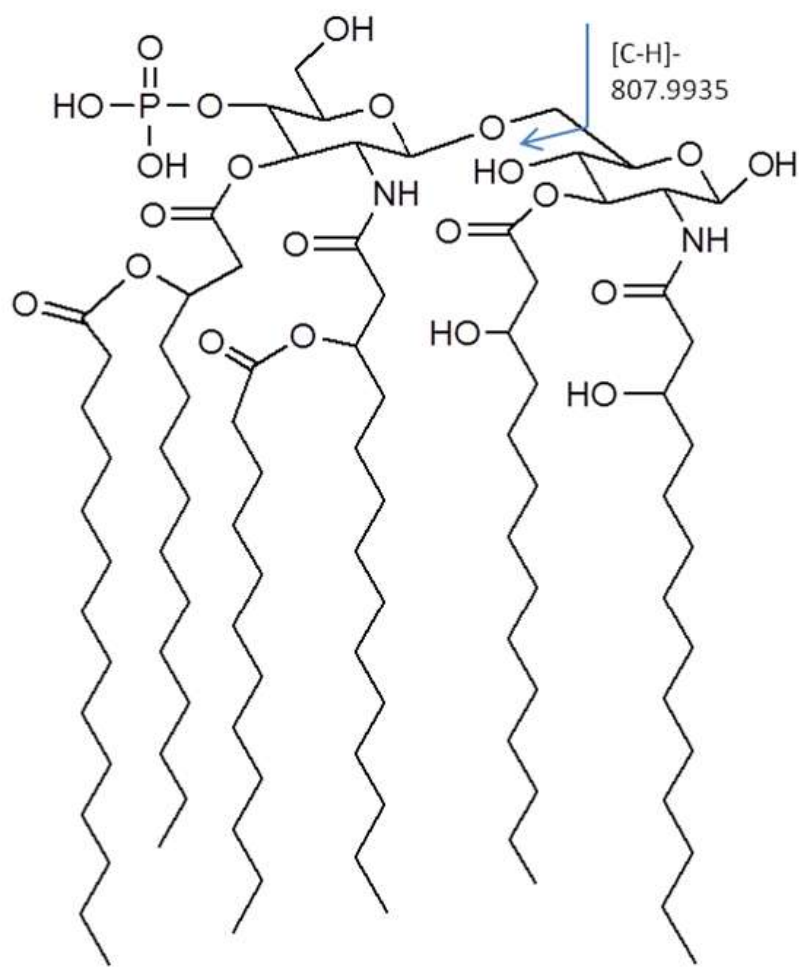
m/z 1716.3613

Figure 4.4: Schematic representation of the one of the common structure of lipid A and the diagnostic ion of [C-H]⁻ observed in the MALDI-MS spectrum.

4.3.1. MALDI-CID-TOF/TOF-MS/MS analysis

The distribution of the fatty acids was determined for the lipid A isolated from *A. liquefaciens* SJ-19 by high-energy CID-TOF/TOF/-MS/MS. The structures of the detected product ions were deduced as previously described in Chapter 3 for the ESI-MS/MS studies of lipid A.

Accordingly, the study of the fatty acid distribution was performed by the high-energy CID-TOF/TOF-MS/MS on the selected precursor anions to determine the distribution of fatty acids at *m/z* 1716.1491 LipA1, at *m/z* 1688.0341 LipA2, *m/z* 1505.9106 LipA3, at *m/z* 1279.7390 LipA4, at *m/z* 1488.0753, and *m/z* 915.1865 LipA5.

Moreover, for the determination of the phosphate group position at O-1 or O-4, the product ion scan of the anion at *m/z* 807.9935 was measured (Figure 4.14). It is noteworthy that the obtained MALDI-MS/MS data suggested that the structures of studied lipid A were comparable with ESI-CID-MS/MS analyses previously described in Chapter 3 for the same lipid A mixture.

High-energy CID-TOF/TOF/-MS/MS of the anion at *m/z* 1716.9491 LipA1 is illustrated in Figure 4.5A. On the basis of this MS/MS analysis, it was concluded that the precursor anion was a monophosphorylated, hexaacylated lipid A form containing two GlcN, one phosphate group, four (*R*)-14:0(3-OH) on the N-2, O-3, N-2', and O-3' positions of the lipid A disaccharide, one branched 14:0 fatty acids of the l4:0(3-(*R*)-*O*-14:0) at the O-3' position and one branched 12:0 fatty acid of the l4:0(3-(*R*)-*O*-12:0) group at the N-3' position.

In contrast to the ESI-FT-ICR-MS^2 of the anion at *m/z* 1716.1491 LipA1, the only product ion which was observed is the anion at *m/z* 1488.1165 indicating the elimination of 14:0 acid of the l4:0(3-(*R*)-*O*-14:0) at the O-3' position (Figure 4.6).

Second-generation MS/MS, also known as *quasi-* MS^3 of the anion at *m/z* 1488.0753 was performed to obtain similar product anions of *m/z* 1261.8041, *m/z* 1244.7851, *m/z* 1035.6162, and *m/z* 976.721, (Figure 4.5B). The product anion at *m/z* 1261.7949 was formed by the loss of the 14:0 acid from position O-3' and the product anion at *m/z* 1244.8624 was produced by loss of the 14:0 acid and H$_2$O from position O-3'. Moreover, the product anion at *m/z* 1244.8624 is formed by the loss of the 14:0(3-OH) acid at position O-3' and the 14:0 ketene molecule from position O-3. Finally, the product anion at *m/z* 976.7049 was produced by elimination of the 14:0 acid from position O-3', loss of a molecule of 14:0 ketene from O-3, and loss of a molecule of C$_4$H$_{10}$ from the branched fatty acid located at N-2' position.
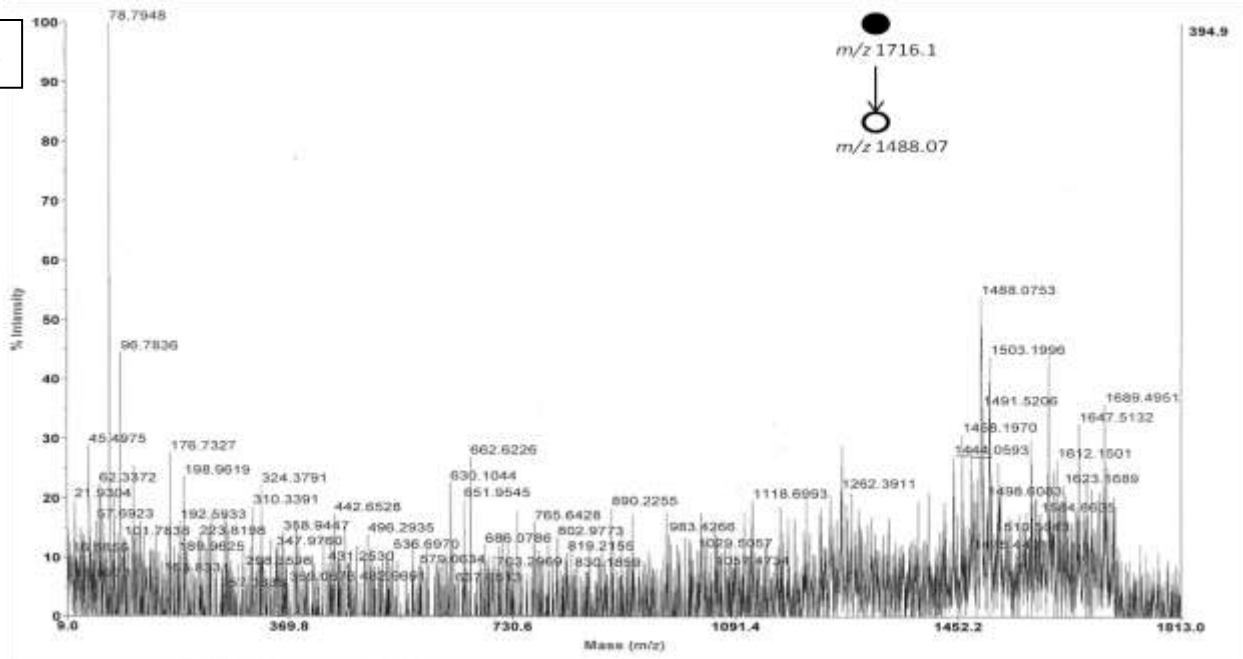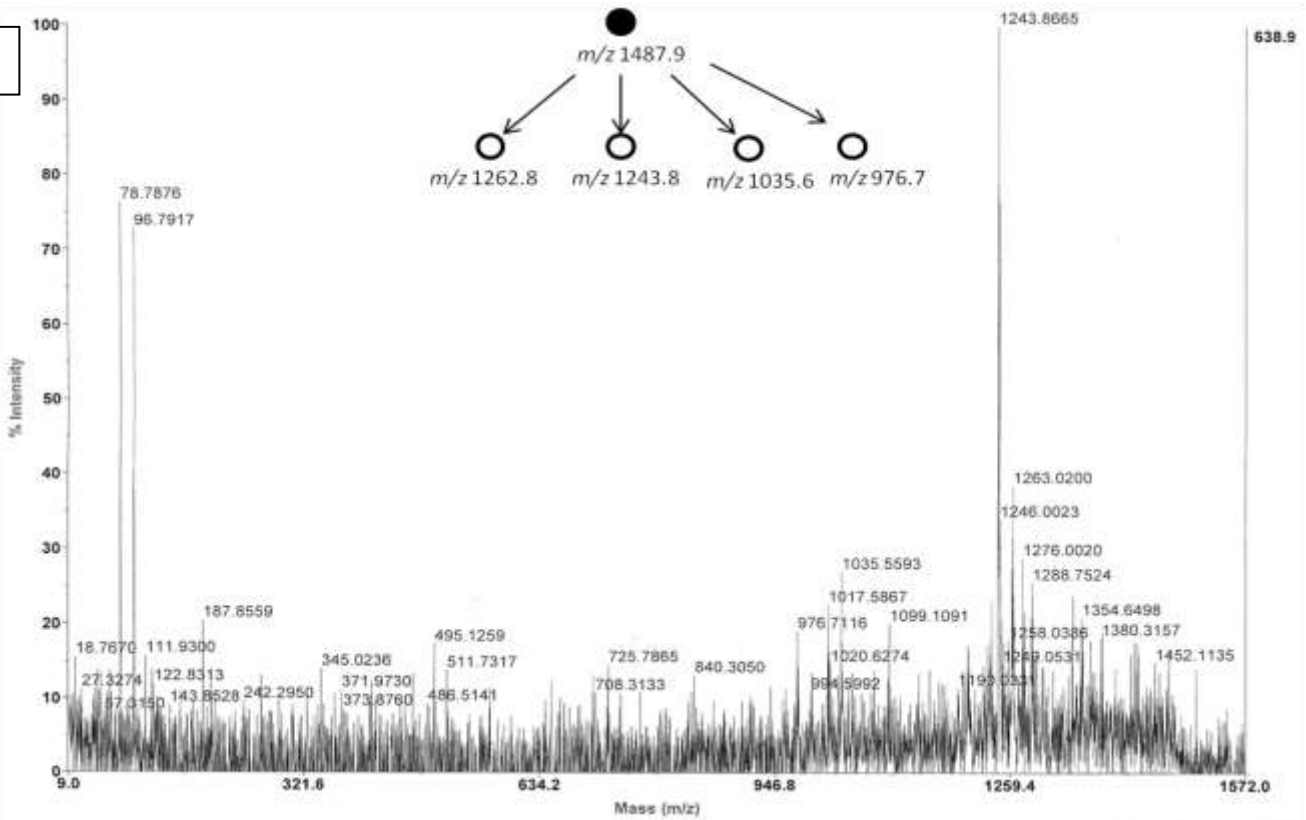
Figure 4.5: Negative ion CID-MS/MS of the singly charged monophosphorylated lipid A [M-H]⁻ ion (A) at *m/z* 1716.9491 and B *quasi-* MS³ at *m/z* 1488.1.

113

MS/MS
Precursor ion
m/z 1716.9491

m/z 1716.9491

-228 Da C14:0 Acid
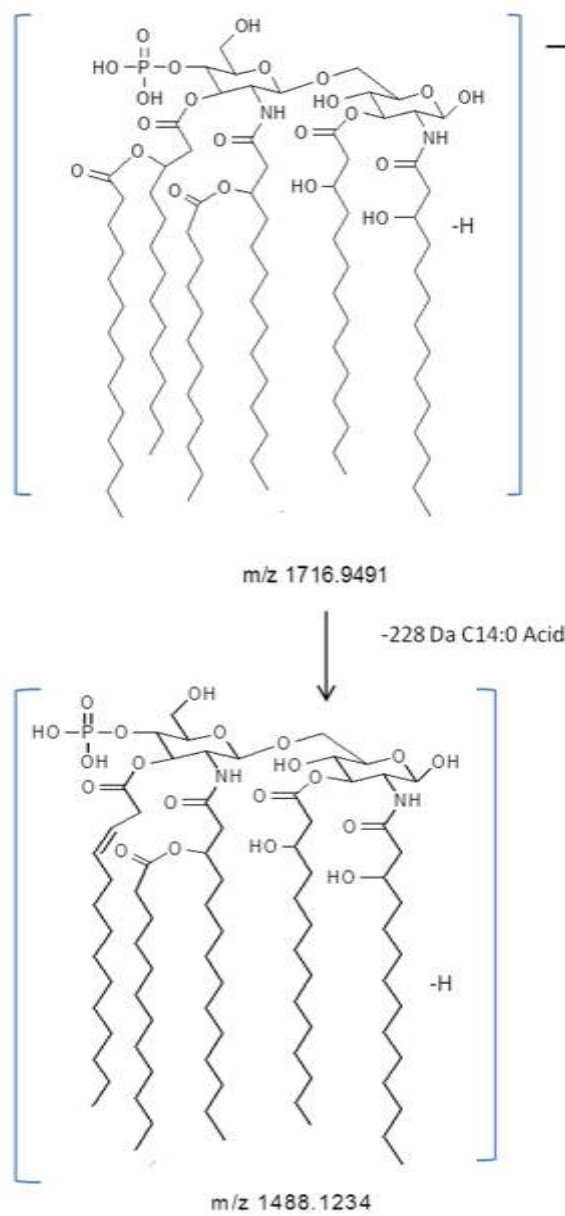
m/z 1488.1234

Figure 4.6: The proposed CID-fragmentation pathway of the selected precursor anion at *m/z* 1716.9491.
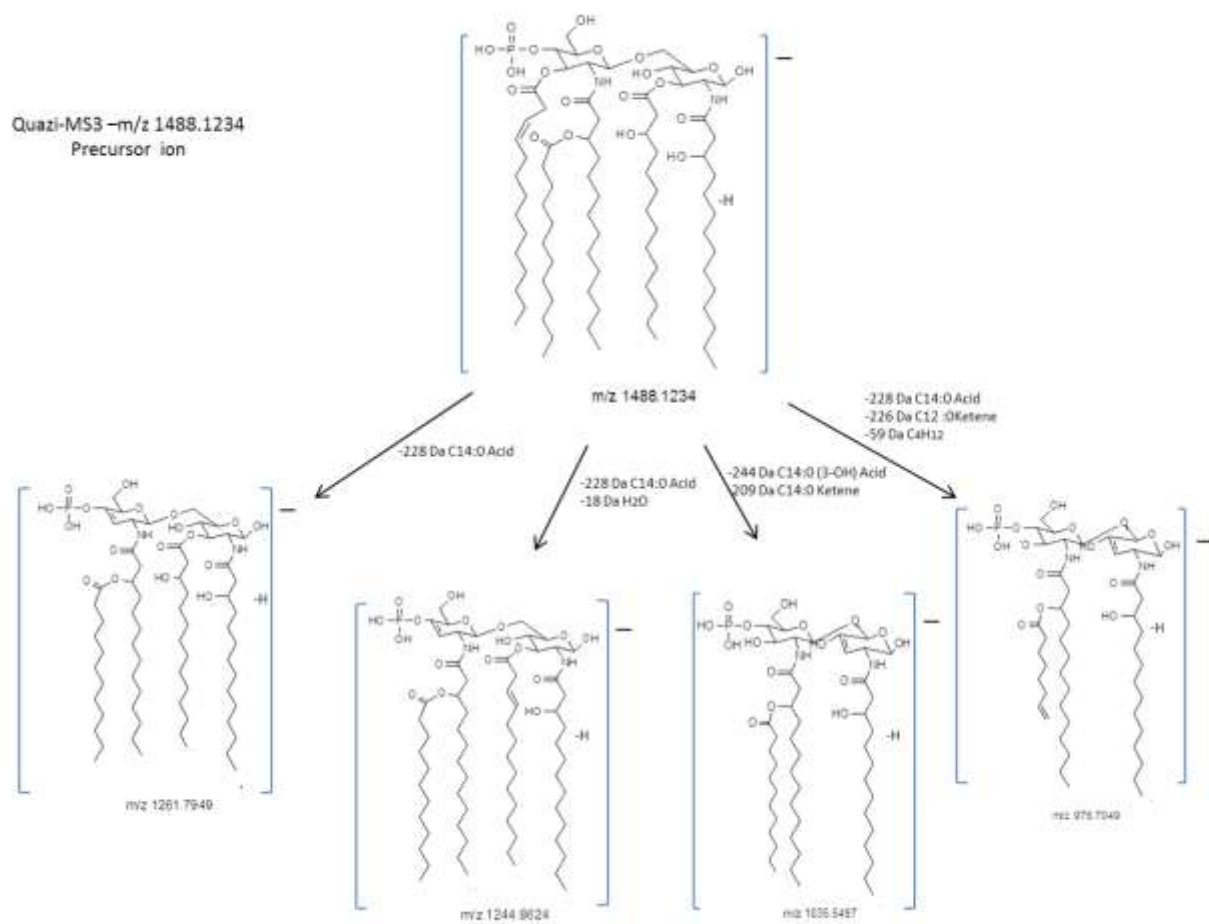
Figure 4.7: The proposed CID-fragmentation pathway of the selected *quasi-* MS[3] at *m/z* 1488.12.

Similar to the FT-ICR-MS^2 of *m/z* 1688.2209 analysis, high energy CID-TOF/TOF-MS/MS of the precursor anion at *m/z* 1688.0923 LipA2 afforded the product anions at *m/z* 1488.1075 and *m/z* 1244.8624, (Figure 4.8A). The product ion at *m/z* 1488.1075 indicate the elimination of the 14:0 acid of the l4:0(3-(*R*)-*O*-14:0) acyl group located at the O-3' position. Also, the product anion at *m/z* 1244.8624 is formed by loss of the 14:0(3-OH) acid from the O-3' position and 14:0 acid at the position of l4:0(3-(*R*)-*O*-14:0) at the O-3' position. It is important to reiterate that these product anions were observed in the FT-ICR-MS^2 of *m/z* 1688.0923; though, the product ion of *m/z* 1444.1765 was only observed in the CID-TOF/TOF-MS/MS of *m/z* 1688.2209. The mass difference between the anions *m/z* 1688.2209 and *m/z* 1444.1765 (-244 Da) indicates the elimination of the 14:0(3-OH) acid located at the O-3 position as shown in Figure 4.9.

To determine the structure of the most abundant anion *m/z* 1505.9511 LipA3, this precursor anion was isolated in TOF-1 and following CID, fragmented in TOF-2 (Figure 4.8B) to give the main product anion of *m/z* 1261.8793. This CID analysis suggested that this anion was composed of the monophosphorylated and pentaacylated lipid A containing one phosphate group located at O-4', two (*R*)-14:0(3-OH) groups located at the N-2 and O-3. In addition, the N-2' position is substituted with the branched l4:0(3-(*R*)-O-12:0) group (Figure 4.10). The product anion at *m/z* 1261.7949 was formed by elimination of the 14:0(3-OH) acid on the O-3' position (-244 Da); this product ion was identical to the FT-ICR-MS^2 of the same precursor anion. This elimination could occur either at the reducing end or the non-reducing end sugar. In contrast to the low-energy CID-MS/MS analysis done with the FT-ICR-MS^2, further

fragmentations of the precursor anions were observed in the high-energy CID-TOF/TOF-MS/MS.

It is worthwhile mentioning that contrary to the FT-ICR-MS[n] studies of this lipid A mixture, the MALDI-CID-TOF/TOF-MS/MS showed a series of unique diagnostic anions which were absent in the anions studied in Chapter 3. These anions are described as following. For example the product ion scan of the anion *m/z* 1505.9511 LipA3 gave the product ion at *m/z* 1488.2014, which was formed by losing a molecule of H_2O at the C-3' position. The product ion at *m/z* 1244.8057 ion was formed by the loss of the (*R*)-14:0 (3-OH) acids at the C-3' position (-244 Da) of the branched acyl group, and a molecule of H_2O from the O-3 position of the precursor ion. In addition, the product ion at *m/z* 1035.7547 was observed by loss of the 14:0(3-OH) acid located at O-3' (-244 Da) and 14 acid located at O-3 (-228 Da), and the product ion at *m/z* 1017.6693 by losing the 14:0 acid located at the C-3' position (-228 Da), a 12:0 ketene of the l4:0(3-(*R*)-*O*-12:0) at the N-2' position (-182 Da), and H_2O_2P (-80 Da), as illustrated in Figure 4.9.
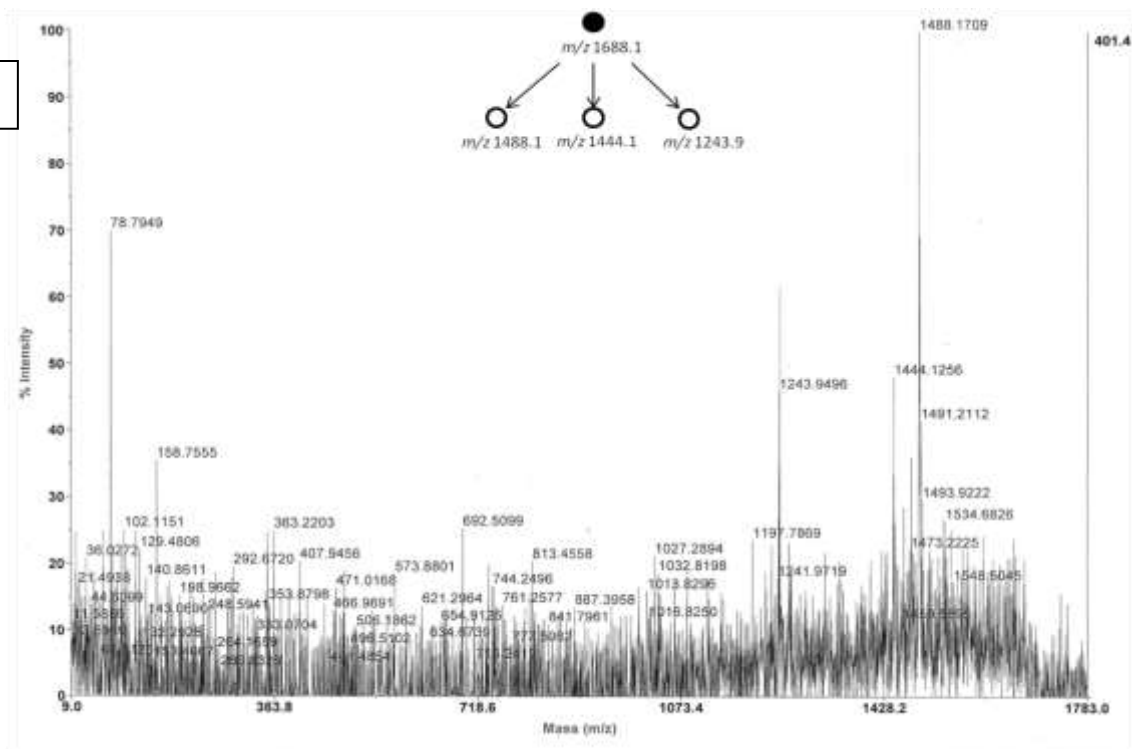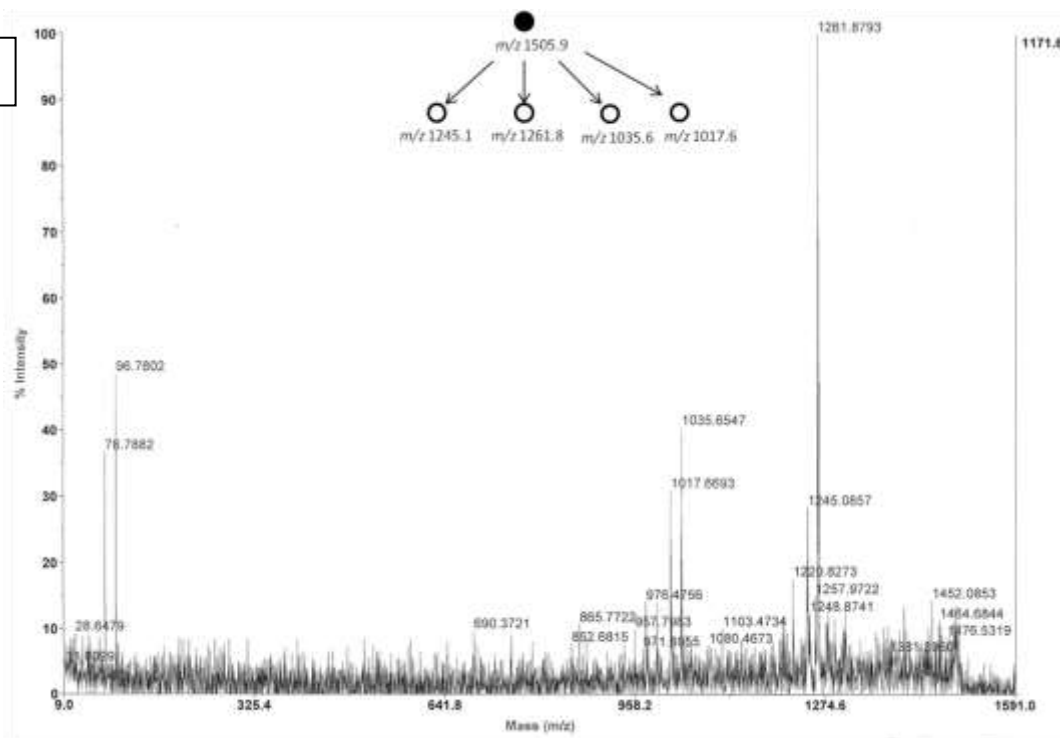
Figure 4.8: Negative ion CID-MS/MS of the singly charged monophosphorylated lipid A [M-H]⁻ ion A at *m/z* 1688.1 and (B) at *m/z* 1505.9511.

Figure 4.9: The proposed CID fragmentation pathway of the selected precursor anion at *m/z* 1688.96.

MS/MS
m/z 1505.0511
Precursor ion

−228 Da C14:0 Acid
−182 Da C12:0 Ketene
−80 Da H2O2P

m/z 1506.9511

−244 Da C14:0 (3-OH) Acid
−228 Da C14:0 Acid

−244 Da C14:0 (3-OH)Acid

−244 Da C14:0 (3-OH)Acid
−18 Da H₂O

m/z 1017.6693

m/z 1261.7949

m/z 1244.8624

m/z 1035.6547
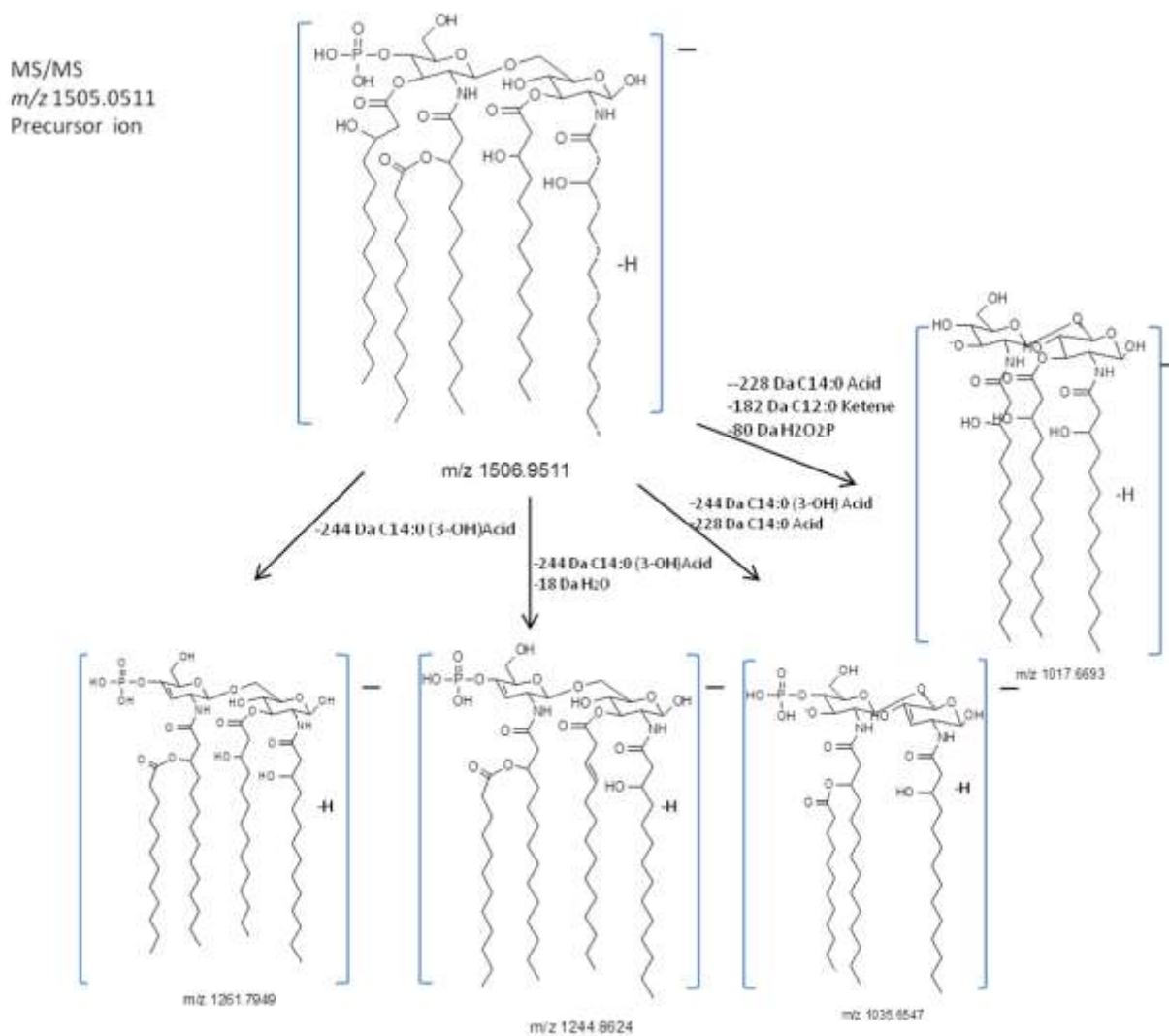
Figure 4.10: The proposed CID-fragmentation pathway of the selected anion at *m/z* 1505.9.

The structure of the precursor anion at 1279.8596 LipA4 was tentatively assigned as the tetra-acylated form which contains, one phosphate group at C-1, three (*R*)-14:0(3-OH) located at the N-2, O-3, and N-2' positions and one branched C12:0 fatty acid of l4:0(3-(*R*)-*O*-12:0) located at the N-2' position. Thus, high-energy CID-TOF/TOF/-MS/MS of the most abundant anion at *m/z* 1279.8596 LipA4 gave two major product anions at *m/z* 1035.6523 and at *m/z* 1079.6387 (Figure 4.11B). The product anion at *m/z* 1035.6523 resulted from the loss of the 14:0(3-OH) acid from the O-3 position of the precursor anion (-244 Da), as shown in Figure 4.12. Also, the product ion of *m/z* 1079.6387 indicates the elimination of the 12:0 acid from the O-3 position of the branched fatty acid of the l4:0(3-(*R*)-*O*-12:0) at the N-2' position (-200 Da).

It is important to note that the CID-MS/MS fragmentations from the precursor anions at *m/z* 1505.9511 LipA3 and at *m/z* 1279.8596 isolated from LipA4 gave the same series of the product ions, (Figure 4.11).

Thus, the MS/MS of the precursor anion at *m/z* 1279.8596 afforded the product anion at *m/z* 1261.8041, which had the same structure assigned as [M-(C14:0(3-OH)) acid-(C12:0)ketene-H]⁻ shown in Figure 4.12. The formation of this product anion at *m/z* 1261.7949 can be explained by the elimination of a molecule of H_2O from the fatty acid at the O-3' position. In addition, the product anion at *m/z* 1035.7547 was formed by the loss of the 14:0 fatty acid from the O-3 position (-228 Da) and the loss of the 14:0(3-OH) acid located at the O-3' position (-244 Da). In addition, the product anion at *m/z* 1079.5653 was formed by the loss of the 12:0(3-OH) acid located at the branched fatty acid of the O-3 position (-200 Da). Finally, the product anion at *m/z* 994.5394 was

formed by loss of the 14:0(3-OH) acid located at the O-3' position (-244 Da) and C_4H_8 located at the branched fatty acid of the N-2′ position.

The MALDI-MS high abundance anion at *m/z* 915.1865 assigned as LipA5 was isolated and subjected to high energy CID-TOF/TOF-MS/MS. The structure of this precursor anion was assigned as [M-(C14:0)ketene-2((C14:O)(3-OH))Acid-$(C_7H_{18}CHO_2)]^-$ and is shown in Figure 4.13.

In contrast to FT-ICR-MS[2], high energy MALDI-CID-MS/MS indicated further fragmentations of the carbon chain of the fatty acid acyl groups. This is evident in the presence of the product anion at *m/z* 820.1091, whose formation indicated the elimination of H_2PO_3 at the reducing end of the GLcN-1 residue. In addition, the product anion at *m/z* 614.7172 indicated the elimination of H_2PO_3 from the C-1 reducing end sugar and elimination of the 6:0 portion of the chain l4:03-(*R*)-*O*-6:0 at the N-2' position. Finally, the product anion at *m/z* 514.6216 is formed by loss of H_2PO_2 which was located at the O-4' position and by loss of a molecule of C6:0 ketene from the branched fatty acid of O-3', and another loss of a molecule of 14:0(3-OH) ketene from the N-2' position.
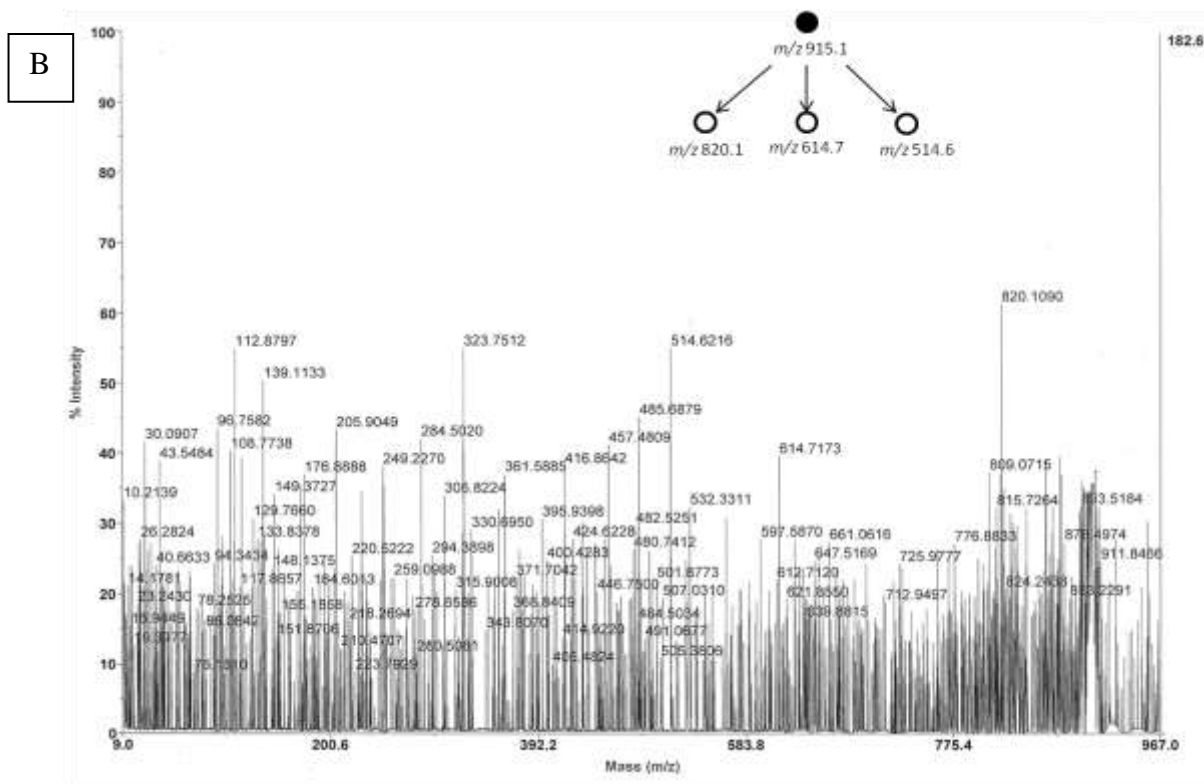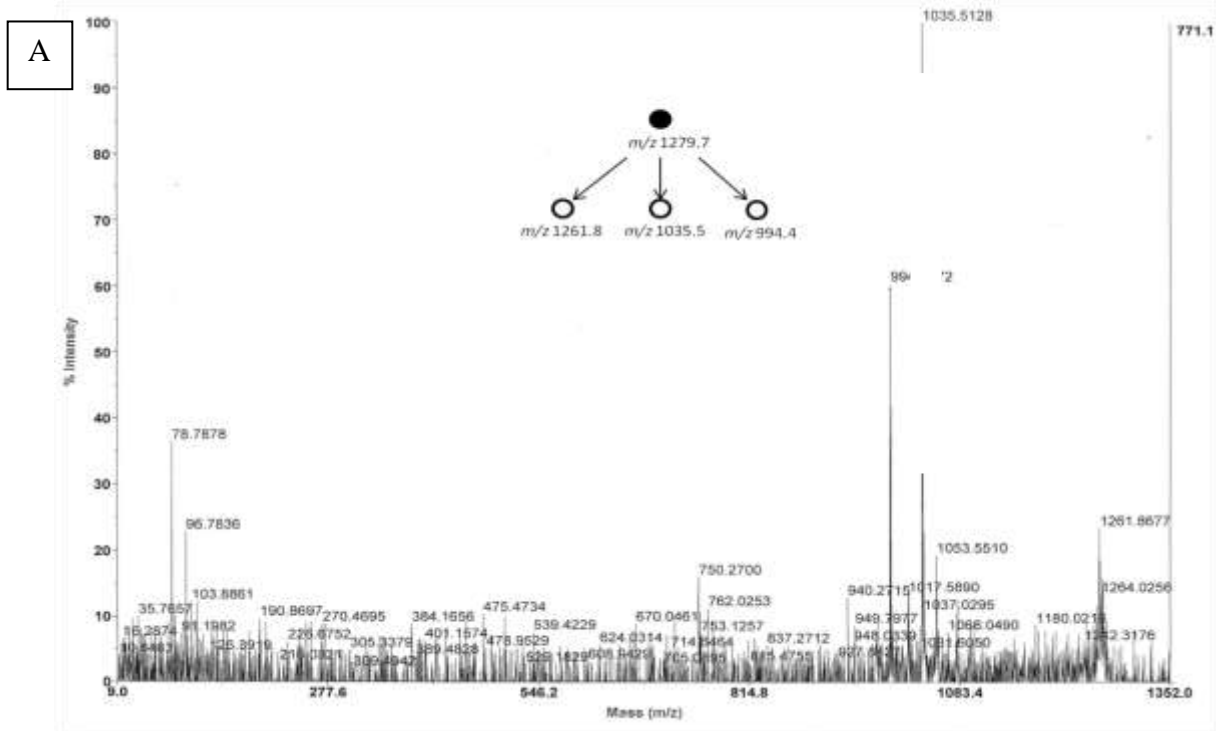
Figure 4.11: Negative ion CID-MS/MS of the singly charged monophosphorylated lipid A [M-H]⁻ ion A at *m/z* 1279.2 and B at *m/z* 915.18.

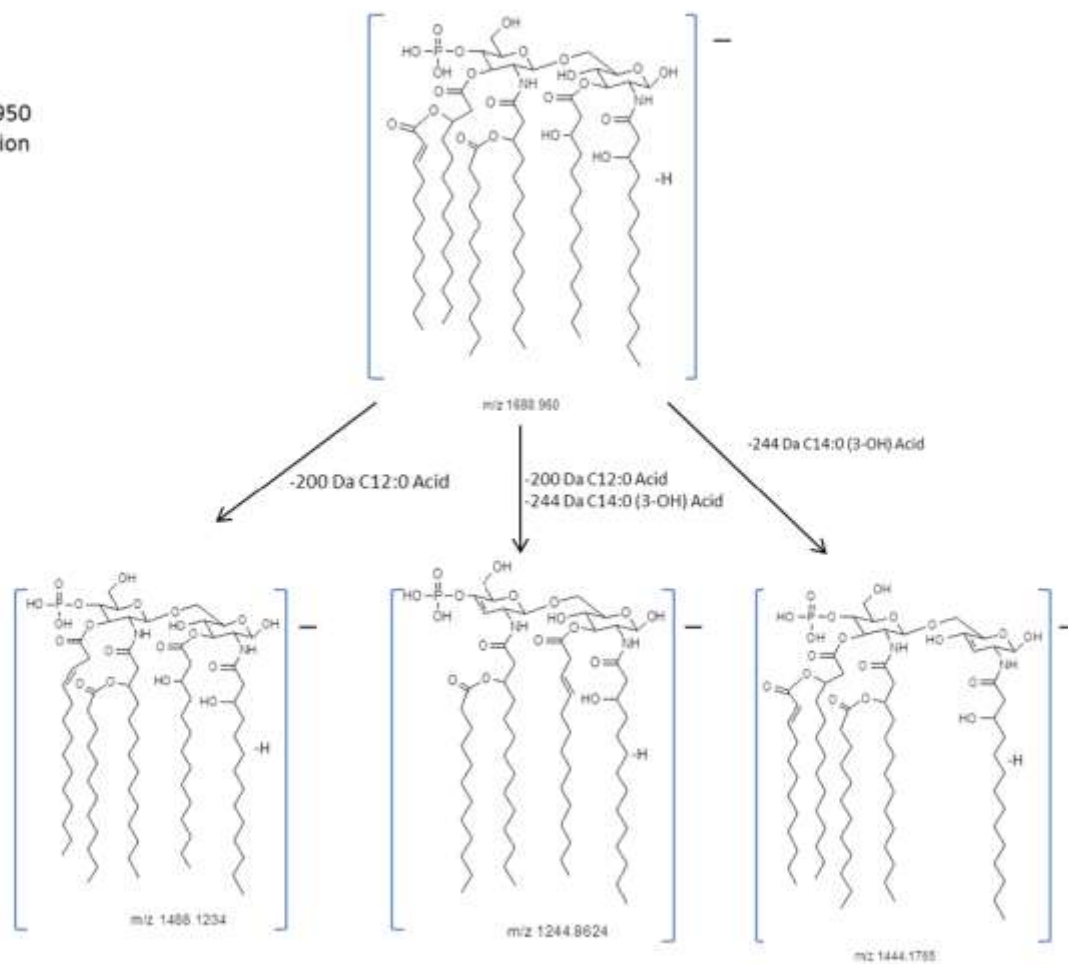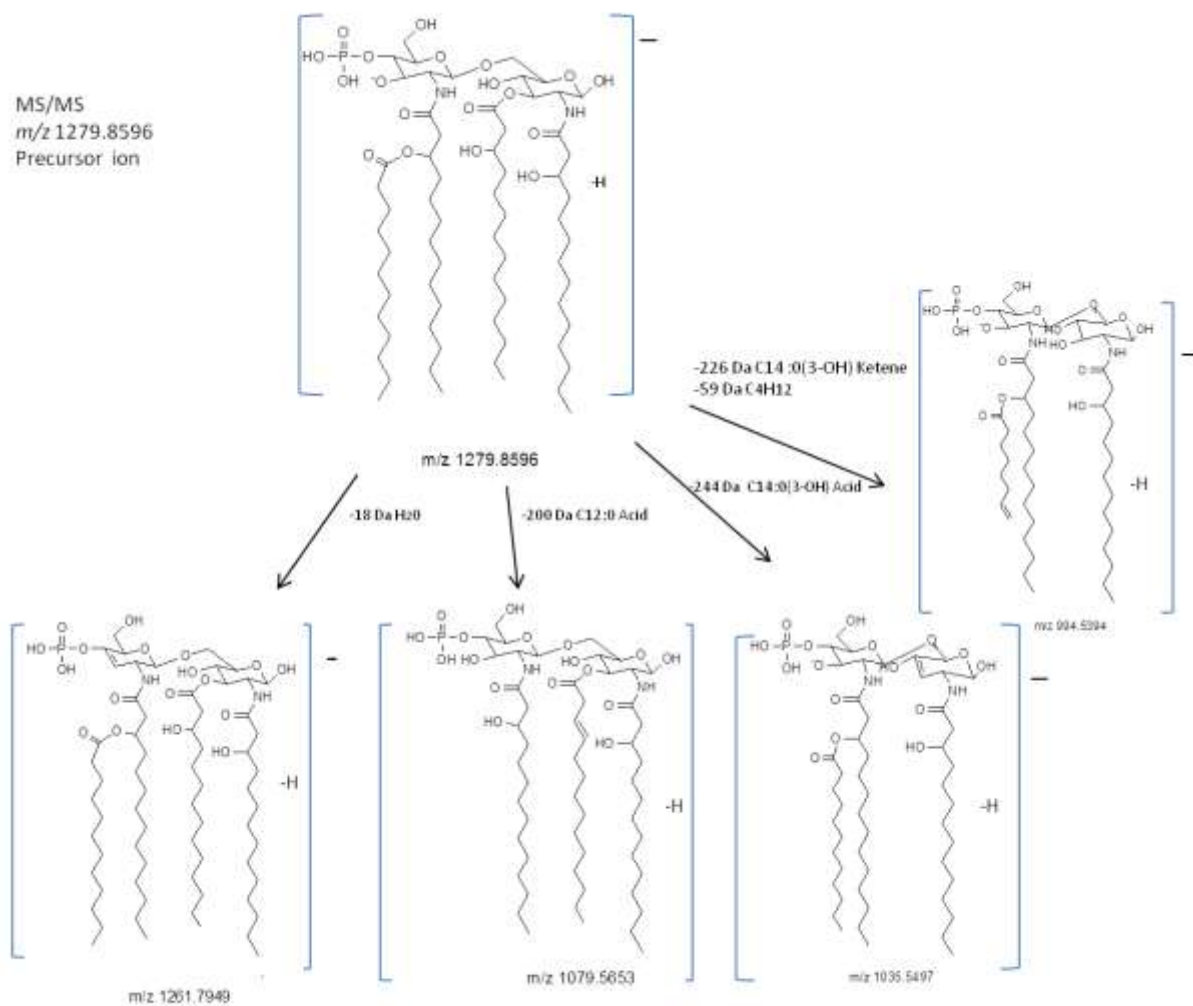**Figure 4.12:** The proposed CID-fragmentation pathway of the selected precursor anion at *m/z* 1279.8.
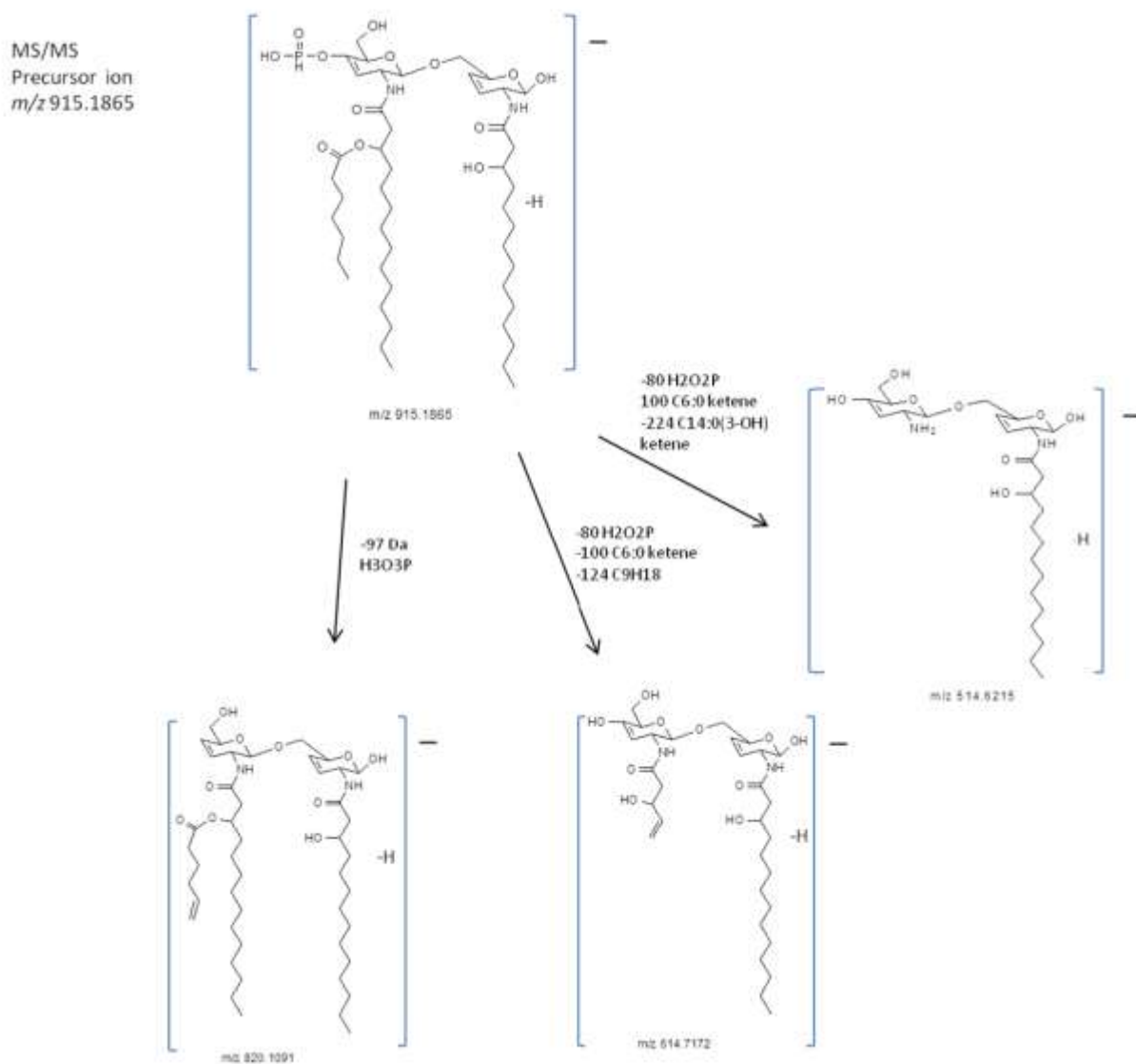
Figure 4.13: The proposed CID-fragmentation pathway of the selected precursor anion at *m/z* 915.1865.

4.3.2. MS/MS analysis of the [C-H]⁻ and [Y-H]⁻ ions

As mentioned earlier in the distinctive carbohydrate signature product anion, namely the [C-H]⁻ anion, resulted from the glycosidic cleavage of the β-D-(1→6) of the D-GlcN disaccharide. This [C-H]⁻ anion at *m/z* 807.9935 was identified in the conventional MALDI-TOF-MS. To confirm its proposed structure, MS/MS was acquired and is shown in Figure 4.14. The structure of this precursor anion [C-H]⁻ at *m/z* 807.9935 was tentatively assigned as containing one l4:0(-OH) acyl group located at the N-2' position, one molecule of the branched l4:0(3-(*R*)-*O*-12:0) acyl group located at the N-2' position, and one 6:0 acid located at the O-3' position.

The high-energy CID-TOF/TOF-MS/MS analysis of the precursor anion [C-H]⁻ at *m*/z 807.9935 demonstrated the elimination of a molecule of 12:0 ketene from the branched fatty acid l4:0(3-(*R*)-*O*-12:0) at the N-2' position to yield the product anion observed at *m/z* 625.7056 which can further fragment by loss of H_2O at the N-2' position to afford the product anion at *m/z* 609.9285 as shown in Figure 4.15. It is proposed that the loss of a $CH_2=CH_2$ molecule probably takes place form most probably the labile *O*-linked fatty acyl group rather than from the more stable *N*-linked one.
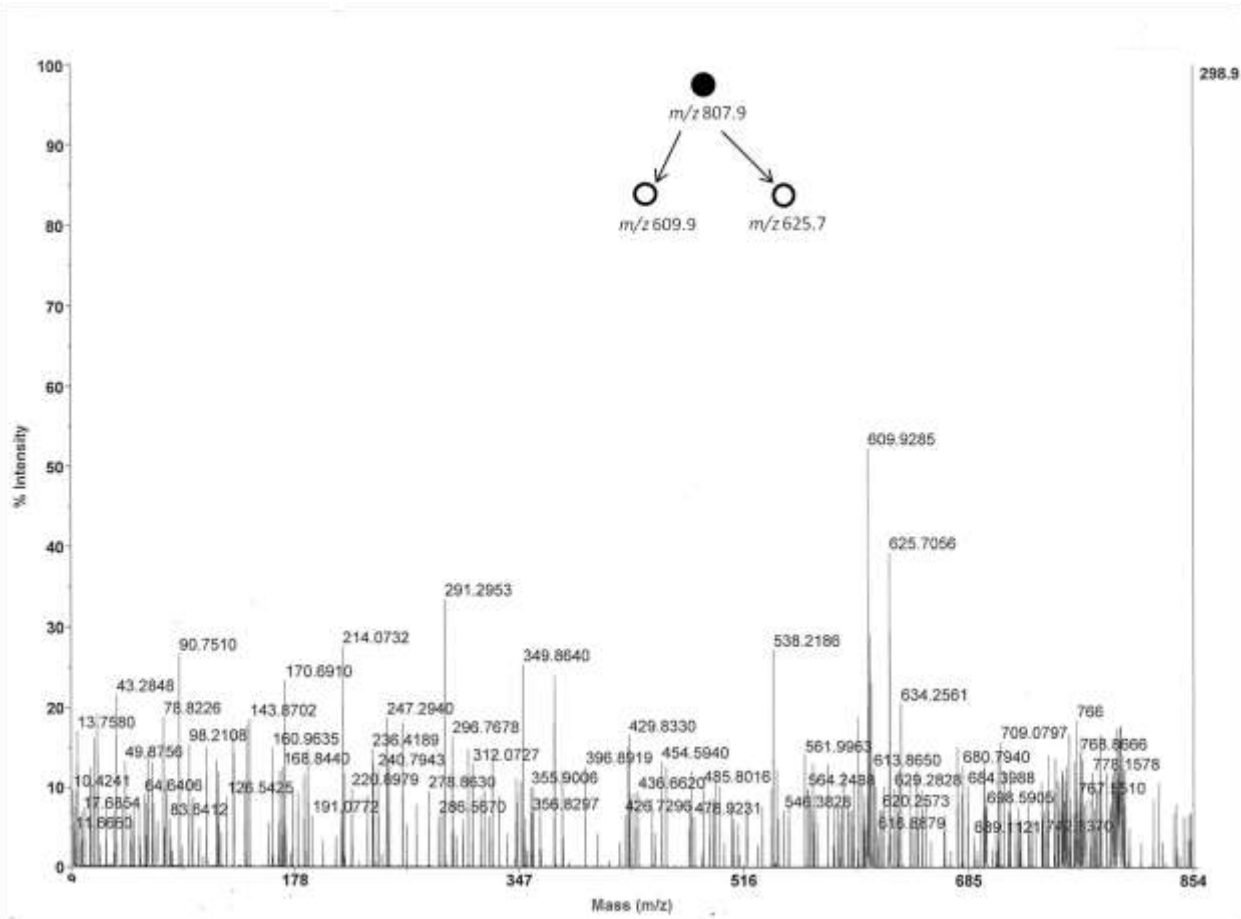
Figure 4.14: Negative ion CID-MS/MS of the singly charged monophosphorylated lipid A [M-H]⁻ ion at *m/z* 807.9935.
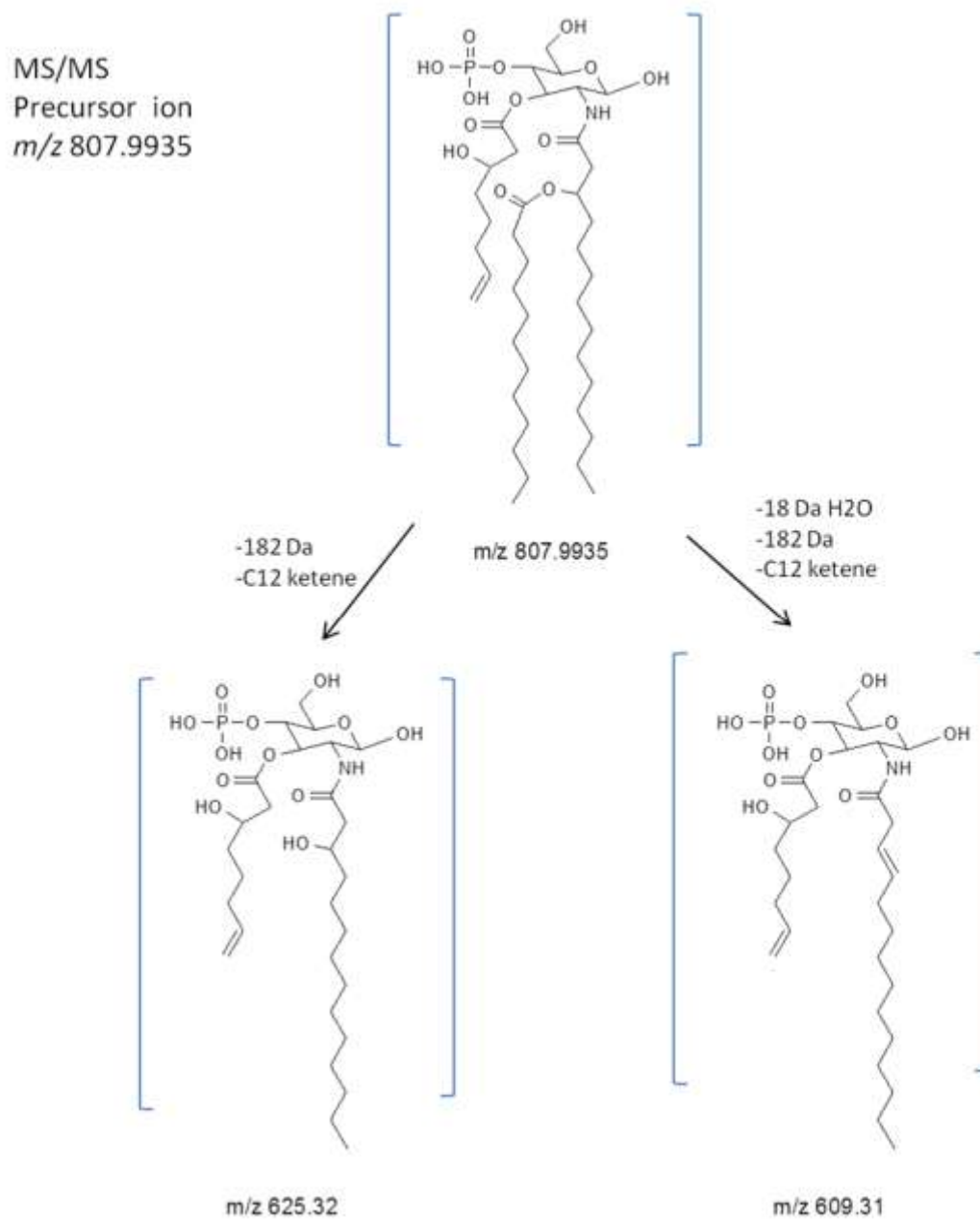
Figure 4.15: The proposed CID-fragmentation pathway of the selected precursor anion at *m/z* 807.9935.

4.4. ESI-QhQ-MS analysis of partial de-acylation of ester linked to the acyl group of lipid A

The ESI-QhQ-MS (+ ion mode) was used for this de-estaified lipid A and CID-MS/MS analysis of partially de-acylated lipid A samples allowed the determination of type and location of the six fatty acyl groups of the hexa-acylated forms of lipid A. The catalytic CH_3ONa treatment caused the partial liberation of the *O*-ester-linked acyl and acyloxyacyl residues.[138] ESI-MS (+ ion mode) of the partially de-acylated lipid A indicated the presence of a series of anions at *m/z* 792.6, *m/z* 682.6, *m/z* 572.6, *m/z* 462.7, and *m/z* 352.6 are shown in Figure 4.16.

CID-MS/MS analysis on the precursor ions at *m/z* 792 is illustrated in Figure 3.17. These series of MS/MS analysis permitted to further confirmations concerning the identities of the hexa-acylated forms of lipid A from *A. liquefaciens* SJ-19. It is noteworthy that all these different singly-charged precursor ions gave exactly the same series of product ions at *m/z* 792.7645, *m/z* 683.0242, *m/z* 572.9725, and *m/z* 352.4959 which confirmed the presence of the acyl groups on both O-3 and O-3' positions.
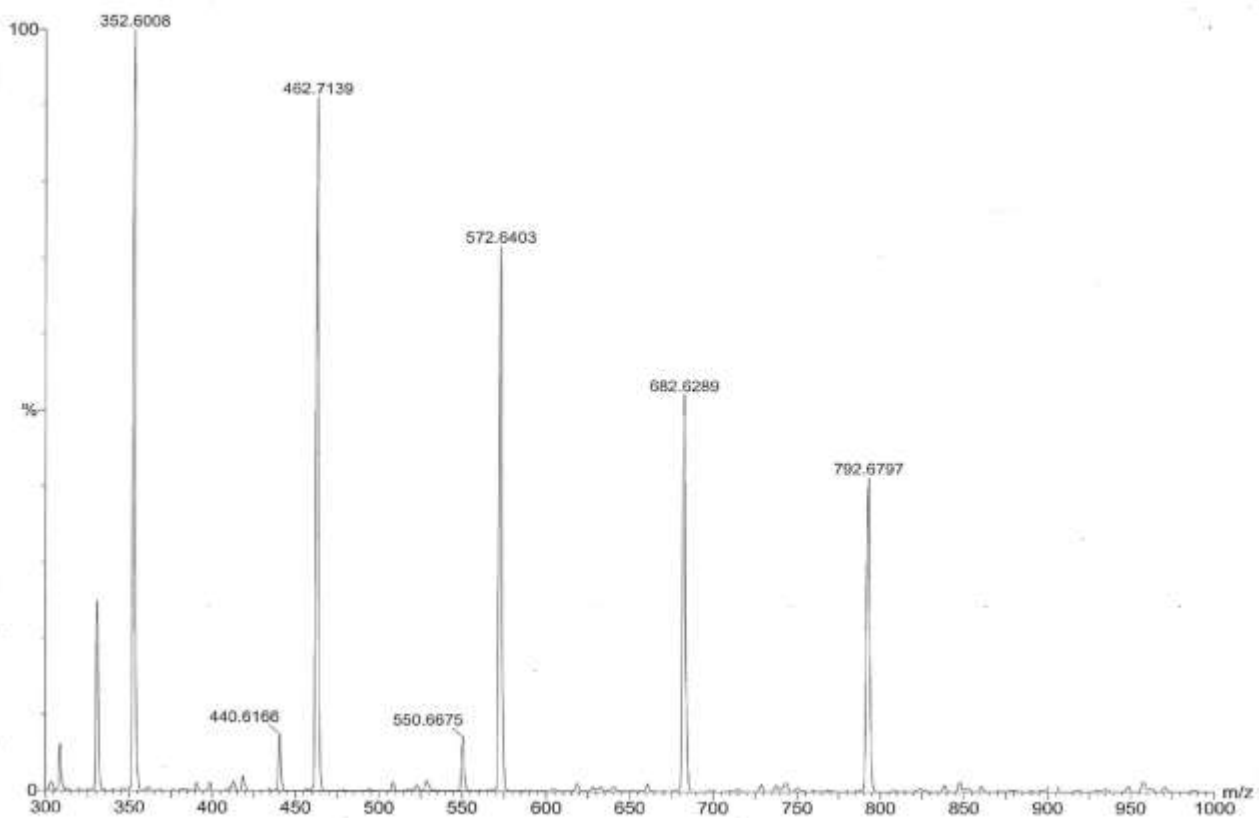
Figure 4.16: ESI-MS (+ ion mode) of the partially deacylated lipid A extract from *A. liquefaciens* SJ-19.

To confirm the presence of 14:0 acid as the fatty acids at N-2 and N-2′ CID-MS/MS analysis of the precursor ion at *m/z* 792.7645 was performed (Figure 4.16). The CID-fragmentation pattern permitted representation of the structure showed in Figure 4.17. This corresponded to the GlcN disaccharide, which was monophosphorylated at the O-4′ position and substituted with two branched fatty acid acyl groups, 14:0(3-O-14:0), and one 14:0(3-OH) acyl group located at the O-3, N-2′, and O-3 positions, respectively. In addition, the product ion at *m/z* 682.0242 was formed by elimination of the C_5H_{10} (-70 Da) molecule from the carbon chain of the branched fatty acid acyl group from the N-2′ position and two molecules of H_2O from the C-1 and O-3′ positions, as shown in Figure 4.18.

Likewise, the product ion at *m/z* 572.9725 was formed by loss of the 12:0(3-OH) acyl group (-182 Da) molecule from the acyl groups at the N-2′ position and 2 molecules of H_2O from the C-1 and C-3' positions. In addition, the elimination of a 14:0 (OH) ketene molecule (-204 Da) from the N-2′ position, and 4 molecules of H_2O from O-1, O-4, O-3′, and O-4′ were observed for the product ion at *m/z* 462.9210. The distinctive ion, namely [C-H]⁻ associated with the glycosidic cleavages of the β-D-(l→6) of the D-GlcN disaccharide was shown in the CID-MS/MS at *m/z* 352.4959, *m/z* 243.0121, and *m/z* 132.8726. The product ion at *m/z* 352.4959 corresponds to the elimination of 2 molecules of H_2O from the fatty acid and O-1 positions. Moreover, the product ion at *m/z* 243.0121 indicates the loss of CH_2CH_2OH (45 Da) molecule located at O-6, 3 molecules of H_2O from the C-1, O-3, and C-4 positions, and 2 molecules of H_2 from the fatty acid chain. Finally, the product ion at *m/z* 132.8726 indicates the loss of (C_8H_{16}) molecule located at N-2 from the precursor ion at *m/z* 243.0121.
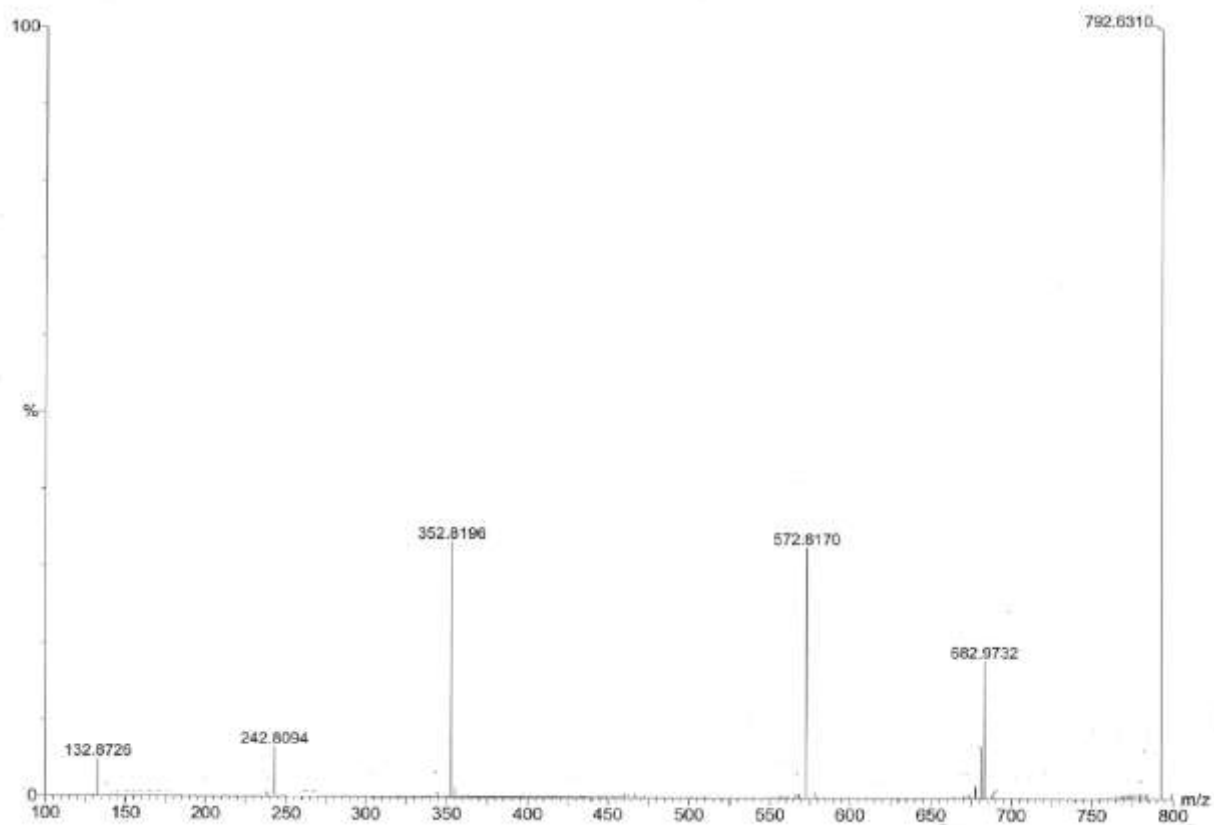
Figure 4.17: Positive ion of high collision energy CID-MS/MS of the singly charged lipid A [M-H]⁻ ion at *m/z* 779.6310.
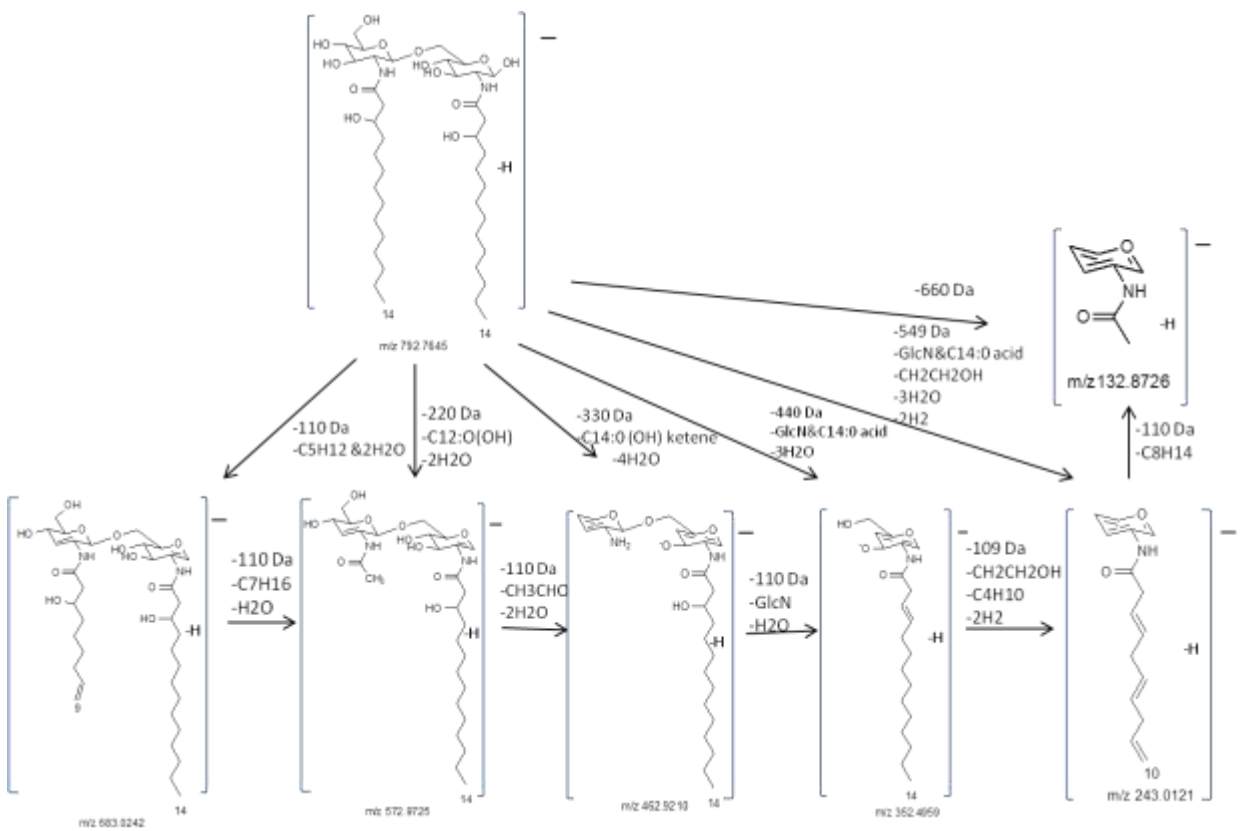
Figure 4.18: The proposed fragmentation pathway of the selected ion at *m/z* 792.7645

4.5. Summary:

The chemical structure of lipid A, isolated by mild acid hydrolysis from *Aeromonas liquefaciens* lipopolysaccharide, was investigated using ESI-QhQ-MS. It was observed that the selected precursor ions failed to fragment during low-energy CID-MS/MS analysis.

On the other hand, MALDI-TOF/TOF-MS/MS (tandem-in-space mass spectrometry) performed with a hybrid instrument was successful and allowed for MS/MS analysis. The MS/MS analysis performed with the hybrid TOF/TOF/-MS/MS Instrument is, by definition, high-energy collision dissociation and is tandem-in-space MS. This is the main objective of why this work was done. It permitted a direct comparison with the low-energy CID-MS/MS performed with the FT-ICR-MS, whose ion separation and gas-phase fragmentation are considered as tandem-in-time MS.

In contrast to our FT-ICR-MS study using tandem in time mass spectrometry, the chemical structure of this Lipid A mixture indicated that it was a heterogeneous mixture formed probably by incomplete biosynthesis. The main constituents of this mixture were formed by a D-(l→6) linked D-glucosamine disaccharide substituted by one phosphate groups which was bound to the non-reducing end at position O-4' of the D-glucosamine disaccharide. The location of the fatty acids linked to the disaccharide backbone was proposed by identifying the diagnostic ions in the conventional TOF-MS scan.

High-energy collision (CID) tandem mass spectrometry analysis of the various selected precursor diagnostic ions confirmed, unambiguously, their proposed molecular structures. It was established that myristyloxylauric 14:0(3-*O*-12:0) acid residues were

both attached to the N-2' and O-3' positions of the non-reducing end of the D-GlcN residue, whereas two 3-hydroxy the branched fatty acid at the 14:0(3-OH) acid chains acylated the remaining positions of the reducing end.

Chapter 5

Tandem Mass Spectrometry of the 2-amino-2-deoxy-β-D-glucosaminyl donors

5.1. Background

The complex glycostructures are well-recognized in the pathogenesis of deadly diseases such as cancer, meningitis, AIDS, pneumonia, and hepatitis. The carbohydrate antigens are well known as potential targets for modern therapeutics. This knowledge has been translated into an appreciation of the roles of carbohydrates with respect to human diseases.[140,141] Numerous kinds of biologically significant carbohydrates are made up mainly of oligosaccharide residues of the 2-amino-2-deoxy-β-D-glucopyranosyl (D-glucosamine) series, which are also known as prokaryotic and eukaryotic glycoconjugates.[142] A linear homopolymer, "chitin", composed of 2-acetamido-D-glucosamine (GIcNAc) polymer is a component of fungal cell walls and arthropod integuments and the linear sulfated polysaccharide "heparin" comprising of alternating GIcNAc and L-iduronic acid units is a major factor in diverse biological procedures, including blood coagulation, cell growth, viral infection, etc.[143,144]

Moreover, the lipid A region of antigenic lipopolysaccharides is an amphiphilic macromolecule consisting of two D-glucosamine residues that has been illustrated to impact several inflammatory processes. Multiple glycosamino residues have been further found in several tumor-associated glycosphingolipids.[145,146]

Amino sugars are widely distributed in living organisms, and occur as constituent glycoproteins, glycolipids, bacterial lipopolysaccharides, and proteoglycans. The presence of these high number of naturally-occurring glycosaminyl residues, are usually

N-acetylated, and linked by 1,2-*trans*-β-D-gluco- and/or galacto-linkages to form the antigenic moiety.

However, it has been determined that during the Koenigs-Knorr glycosylation reaction, the introduction of the 2-acetamido-2-deoxy-glucosaminyl portion (obtained from the glycosyl halides donors) e.g. 1a or 1b (Figure 5.1) during a glycosylation reaction with complex aglycones (glycosyl acceptors) was usually impractical.[147] The reactive acyloxonium intermediate formed by participatory assistance of the 2-acetyl moiety of GlcNAc leads to the formation of the 1,2-*O,N*-oxazoline end product which is more stable, and the effective yield of this glycosylation reaction is reduced. This side-reaction significantly decreases the rate of glycosylation and this is very evident when sterically-hindered glycosyl donors are utilized.[148]
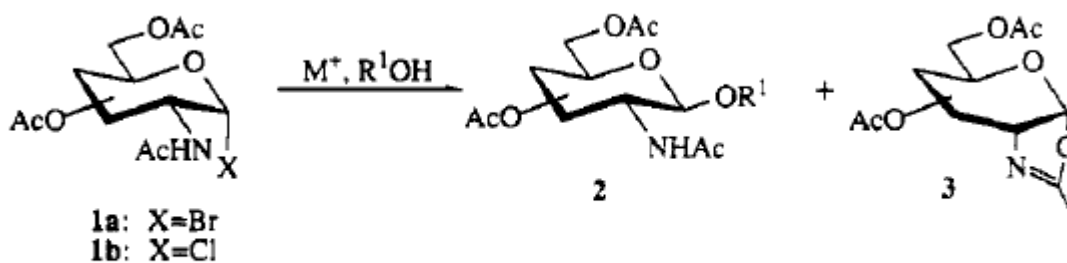
Figure 5.1: Schematic illustration of the full structure of the glycosyl acceptors or donors and is adopted with the permission reference 110.

This is the main reason why a series of fully-acylated derivatives of the 2-amino-2-deoxy glucosamine have been used in Lewis acid-catalyzed glycosylations to avoid the formation of the 1,2-*O,N*-oxazoline end product (Figure 2.1 , Chapter 2).

The initial purpose of the work reported herein was to study the gas-phase MS/MS fragmentations of the acylated glycosides of 2-amino-2-deoxy-β-D-glucosamine derivatives (Figure 5.2) used as glycosyl donors. This will permits the confirmation of their new structures using tandem mass spectrometry.

In this Chapter, the low-energy CID-MS/MS gas-phase fragmentations using two types of tandem mass spectrometry analysis of the precursor ions obtained from this series of GlcN compounds are reported using (tandem-in-time MS) including an ESI-QIT-MS^2 and with an quadrupole orthogonal time-of-flight QqTOF-MS/MS hybrid instrument (tandem-in-space MS).

Figure 5.2: The main four structures of the synthetic compounds are indicated as such: A) methyl-2-(acetylamino)-3,4,6-tri-*O*-acetyl-2-deoxy-β-D-glucopyranoside, B) isopropyl-2-(acetylamino)-3,4,6-tri-*O*-acetyl-2-deoxy-β-D-glucopyranoside, C) tri-chloroethyl 2-(*N*-allyloxy)-3,4,6-tri-*O*-acetyl-2-deoxy-β-D-glucopyranoside, and D) benzyl 3,4,6-tri-*O*-benzyl-2-(acetylamino)-2-deoxy-β-D-glucopyranoside.

5.2. ESI-QIT-MS and ESI-QIT-MS^2 (tandem-in-time mass spectrometry)

5.2.1 ESI-QIT-MS analysis of methyl-2-(acetylamino)-3,4,6-tri-*O*-acetyl-2-deoxy-β-D-glucopyranoside

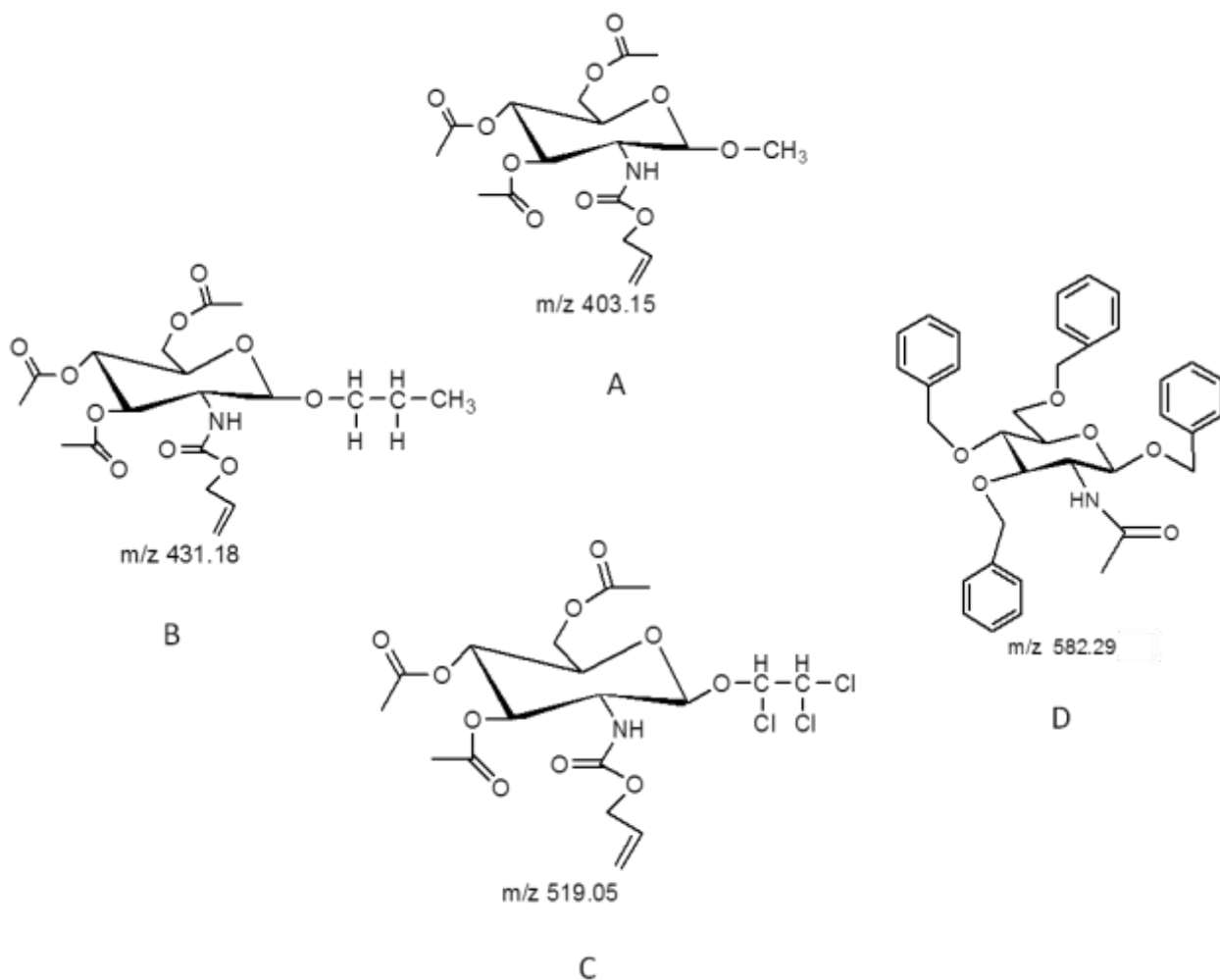The ESI-MS (+ ion mode) of the synthetic compound of methyl-2-acetylamino-3,4,6-tri-*O*-acetyl-2-deoxy-β-D-glucopyranoside was performed using ESI-QIT-MS in order to study its gas phase fragmentations. The major sodiated molecular ion [M+Na]$^+$ was observed at *m/z* 426.21 as shown in Figure 5.3A. In addition the ESI-MS showed the presence of the ion at *m/z* 372.01 which was formed by elimination of the methoxyl radical group from the C-1 position (-31 Da). The ion at *m/z* 252.12 was formed by the consecutive loss of a formaldehyde molecule (CH$_2$O -30 Da) from the C-1 position, a molecule of acetic acid from the C-3 position, and 2 ketene molecules (CH$_2$=C=O) from the C-4 and C-6 positions. It is important to note that these losses are not sequentially in that order.

The above assignments are tentative as they were observed in the single-stage MS and additional evidence is usually required to validate these assignments.

For this reason, the use of tandem mass spectrometry permitted the identification of the diagnostic product ions and also allowed the verification of the proposed molecular structure.

5.2.1.1 ESI-QIT-MS^2 analysis of methyl-2-(acetylamino)-3,4,6-tri-*O*-acetyl-2-deoxy-β-D-glucopyranoside

The low-energy-CID-MS^2 analysis of the precursor [M + Na]$^+$ at *m/z* 426.21 is shown in Figure 5.3B. The product ion scan of the precursor ion at *m/z* 426.21 indicated the

presence of the major sodiated ion at *m/z* 366.23 produced by eliminations of a molecule of acetic acid from the C-3 position.[149] In addition, the sodiated product ion at *m/z* 252.12 was formed by the consecutive losses of a formaldehyde molecule (CH_2O - 30 Da) from the C-1 position, a molecule of acetic acid from the C-3 position, and 2 ketene molecules ($CH_2=C=O$) from the C-4 and C-6 positions, (Figure 5.4). Needless to say, the exact order of these eliminations is not exactly known.
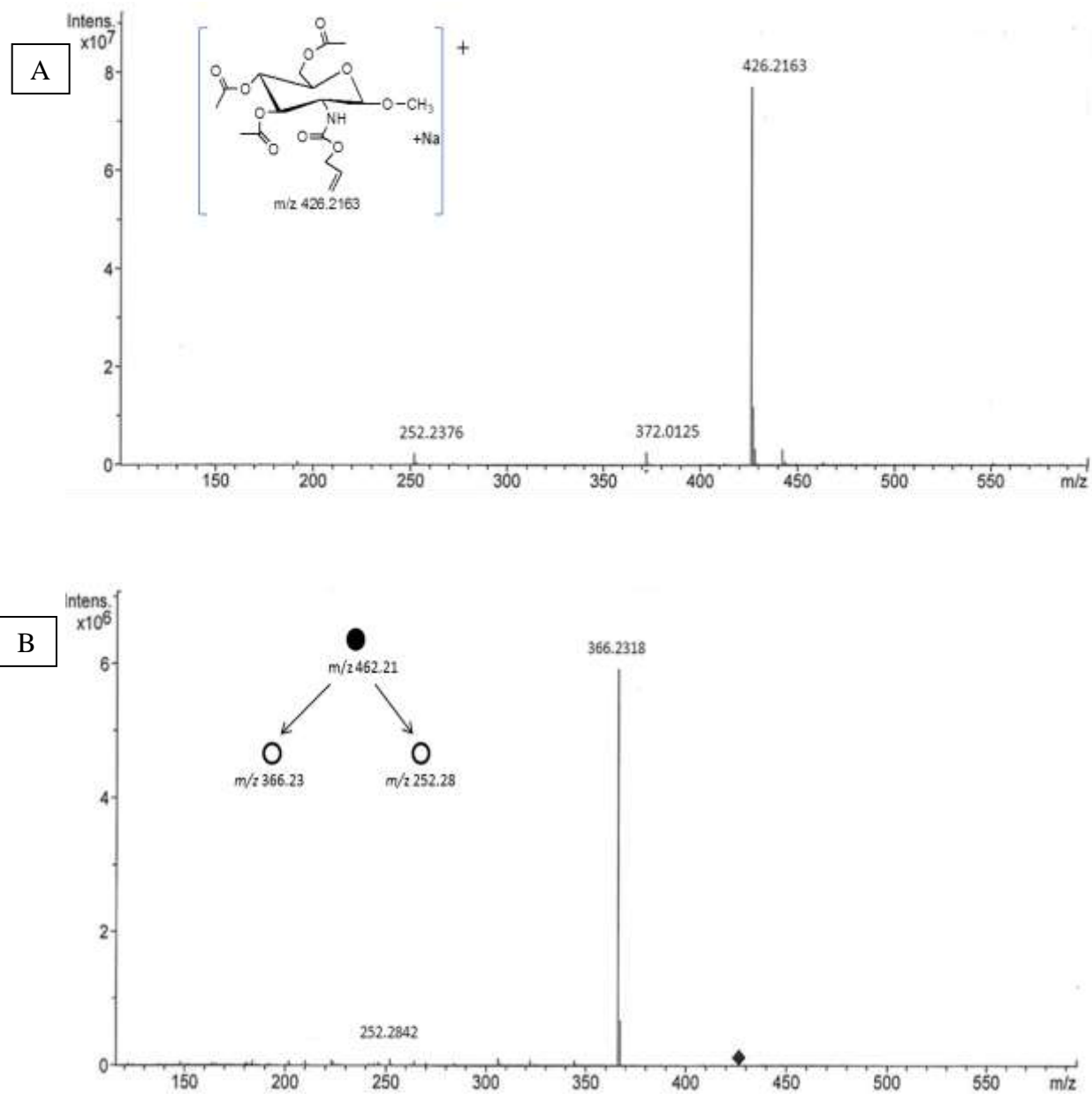
Figure 5.3: A) ESI-QIT-MS of the methyl-2-acetylamino-3,4,6-tri-*O*-acetyl-2-deoxy-β-D-glucopyranoside and B) Low-energy CID-MS^2 of the precursor ion precursor [M + Na]+ at *m/z* 426.21.
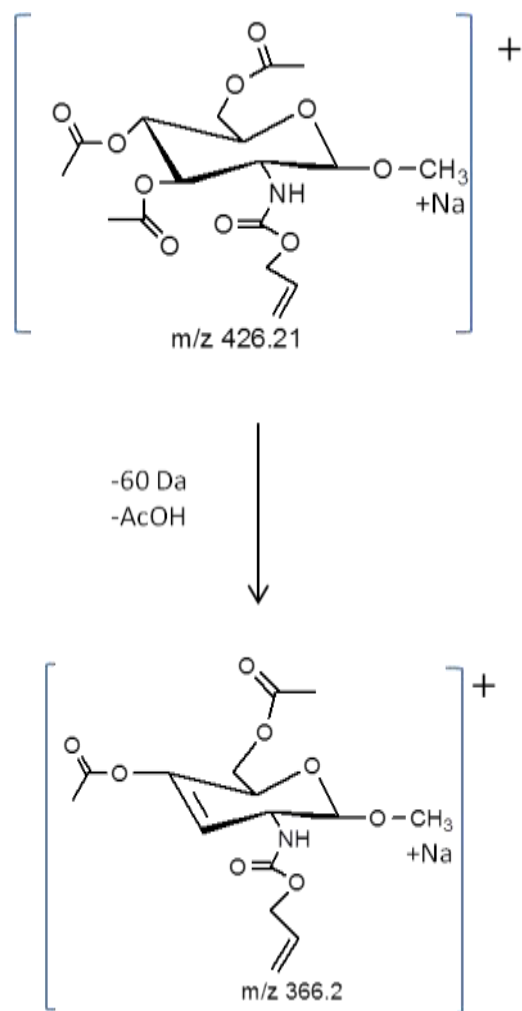
Figure 5.4: The low-energy-CID-MS^2 fragmentations pathway for the precursor ion [M+Na]$^+$ at *m/z* 426.21.

5.2.2. ESI-QIT-MS analysis of trichloroethyl 2-(*N*-allyloxy)-3,4,6-tri-*O*-acetyl-2-deoxy-β-D-glucopyranoside

The ESI-MS (+ ion mode) of trichloroethyl 2-(*N*-allyloxy)-3,4,6-tri-*O*-acetyl-2-deoxy-β-D-glucopyranoside gave the sodiated molecular ion [M+Na]+ at *m/z* 542.06 (100%), and showed the presence of the adduct ion [M+K]$^+$ at *m/z* 560.01. This ESI-MS also contained the ion at *m/z* 372.01 which was formed by elimination of the aglycone trichloroethanol ($Cl_2CHCCHClOH$) from the C-1 position (-148 Da). In addition, the ion at *m/z* 252.10 was formed by the consecutive elimination of a molecule of trichloroethanol from the C-1 position followed by 2 molecules of acetic acid from the C-4 and C-6 positions (-120 Da). Moreover, the ion at *m/z* 192.16 was formed by elimination of a molecule of trichloroethanol and the 3 molecules of acetic acid resulting from the C-3, C-4, and C-6 positions.

5.2.2.1. ESI-QIT-MS^2 analysis of trichloroethyl 2-(*N*-allyloxy)-3,4,6-tri-*O*-acetyl-2-deoxy-β-D-glucopyranoside

The low-energy CID-MS^2 was performed on the sodiated [M+Na]$^+$ ion at *m/z* 542.03 and the MS/MS is shown on Figure 5.5B. The product scan of this precursor ion gave the major ion at *m/z* 394.21, which was formed by the consecutive elimination of the aglycone moiety ($Cl_3C_2H_2OH$, -148 Da). In addition, the product ion at *m/z* 506.1206 was formed by elimination of a HCl molecule, and was assigned as [M +Na-HCl]$^+$. An interesting elimination noteworthy of mention, was the formation of the protonated ion at *m/z* 484.011 produced by the loss of NaCl form the [M+ Na]$^+$ precursor ion to give the product ion [M+ NaCl]$^+$, specifically, the carbocation C-1

(Figure 5.5B). In addition, the formation of the major sodiated product ion observed at m/z 394.21 from the precursor ion at m/z 542.03 was formed by the elimination of the trichloroethanol aglycone moiety ($Cl_3C_2H_2OH$, -148Da), (Figure 5.6). Also, the product ions at m/z 372.10 formed by the loss of a molecule of trichloroethanol aglycone (-148 Da) from the C-1 position. The sodiated product ion at m/z 334.14 was formed by the elimination of a ketene molecule ($CH_2=C=O$) (-120Da) resulting from the C-3 position and a molecule of trichloroethanol from the C-1 position. The sodiated product ion at m/z 274.05 was formed by the elimination of 2 ketene molecules ($CH_2=C=O$) from the C-3 andC-6 positions; not necessarily in that order; followed by a molecule of aglycone trichloroethanol. Finally, the protonated ion at m/z 252.02 was created by the expulsion of Na^+ ion, 2 ketenes molecules ($CH_2=C=O$) from the C-3 and C-6 positions, and trichloroethanol.
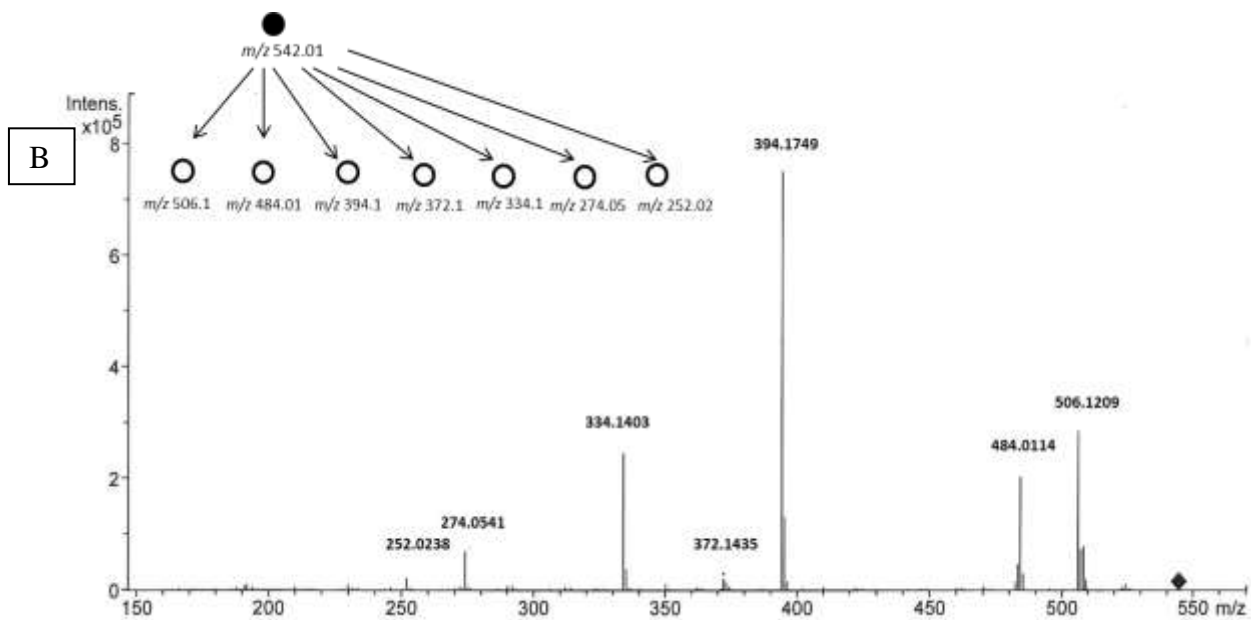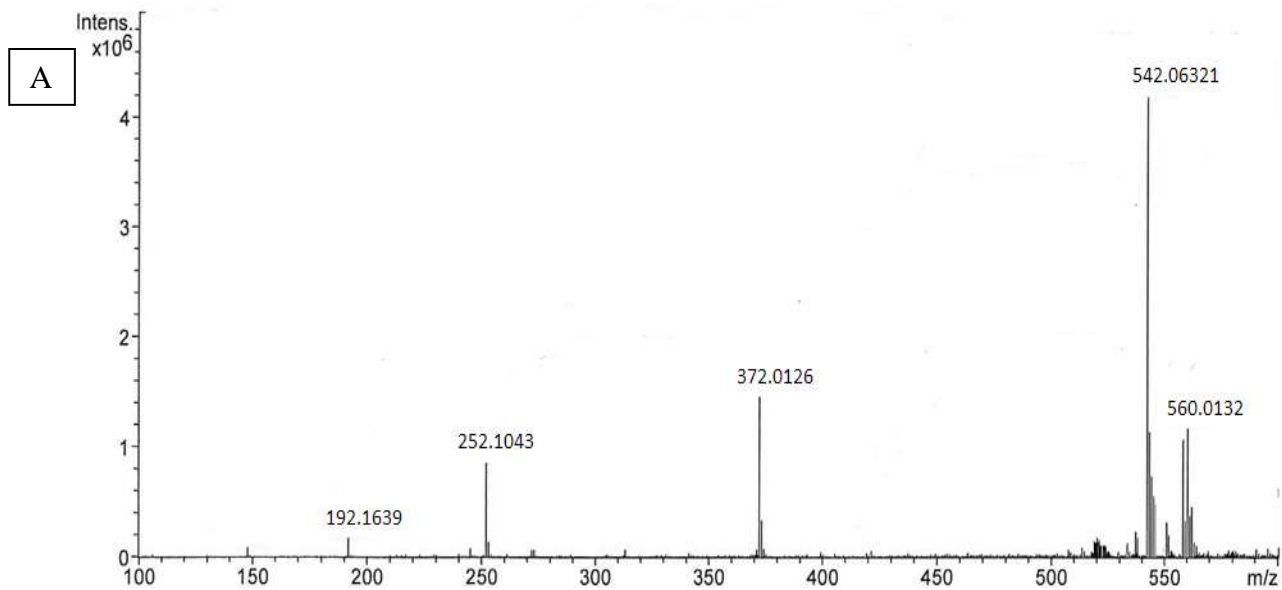
Figure 5.5: A) ESI-QIT-MS of the trichloroethyl 2-*N*-allyloxy-3,4,6-tri-*O*-acetyl-2-deoxy-β-D-glucopyranoside and B) Low-CID-MS^2 of the precursor ion [M+Na]$^+$ at *m/z* 542.06.
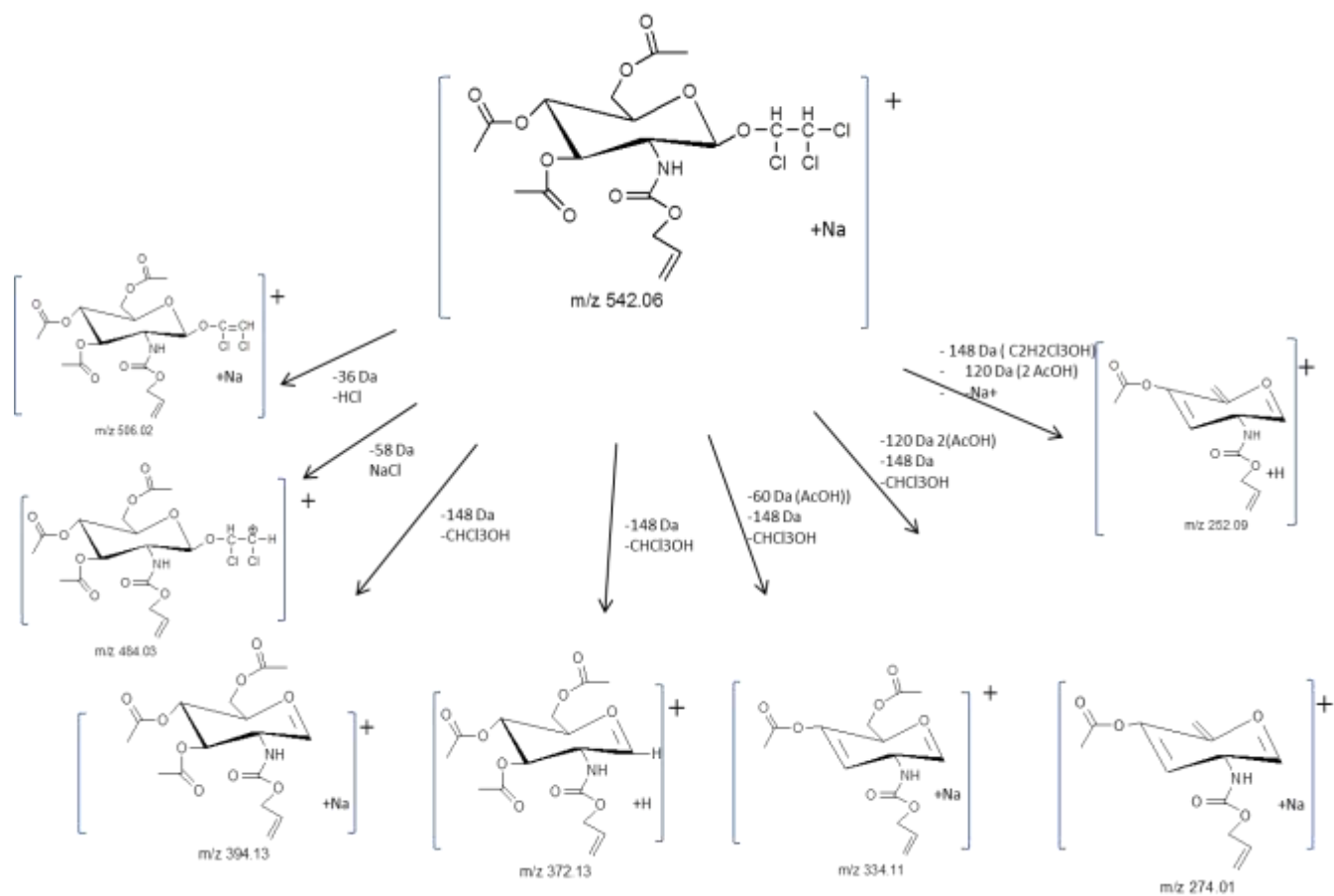
Figure 5.6: The low-energy-CID-MS^2 fragmentations pathway for the precursor ion [M+Na]$^+$ at *m/z* 542.06.

5.2.3. ESI-QIT-MS of the benzyl 3,4,6-tri-*O*-benzyl-2-(acetylamino)-2-deoxy-β-D-glucopyranoside

The ESI-MS (+ ion mode) of the synthetic compound benzyl 3,4,6-tri-*O*-benzyl-2-(acetylamino)-2-deoxy-β-D-glucopyranoside was measured, and it showed the presence of the protonated molecular ion at *m/z* 582.29. It should be noted that the formation of the [M + Na]$^+$ sodiated molecular ion was not observed in this case, (Figure 5.7A). The ion at *m/z* 474.35 was formed by elimination of the benzyl alcohol from the C-3 position of the precursor protonated molecule. Further elimination of an additional molecule of benzyl alcohol gave the product ion at *m/z* 366.23. This latter ion in its turn eliminated another molecule of benzyl alcohol to yield the ion at *m/z* 260.24.

5.2.3.1. ESI-QIT-MS^2 analysis of benzyl 3,4,6-tri-*O*-benzyl-2-(acetylamino)-2-deoxy-β-D-glucopyranoside

Low energy-CID-MS^2 was measured for the precursor ion at *m/z* 582.36, Figure (5.7B). The ion at *m/z* 474.35 was formed by the elimination of the benzyl alcohol from the C-3 position of the precursor protonated molecule. The product ion scan showed the presence of the product ions at *m/z* 366.03 and *m/z* 260.02, respectively. These product ions were respectively formed by elimination of one and two molecules of benzyl alcohol at the C-1 and, the C-1 and C-2 positions, respectively (Figure 5.8).

The second-generation product ion scan of *m/z* 474.35 was measured using low energy-CID-MS^3, Figure (5.9A). This product ion scan showed the presence of the product ions at *m/z* 366.03 and *m/z* 260.02, respectively, which were formed by the

elimination of one and two molecules of benzyl alcohol from the C-1 and, the C-1 and

C-2 positions, respectively (Figure 5.9B).
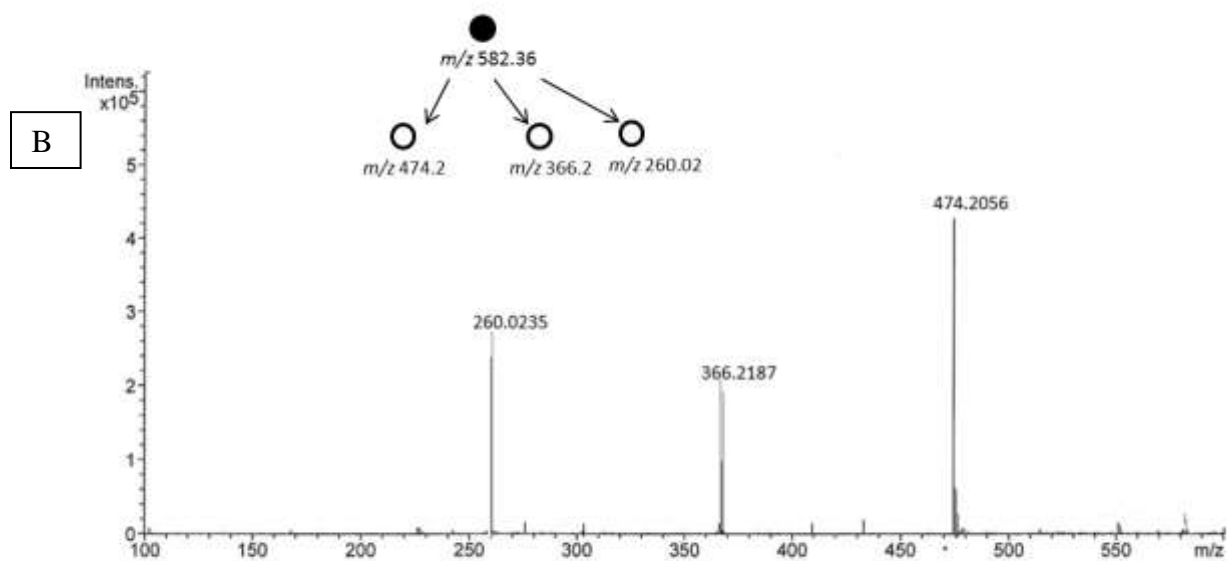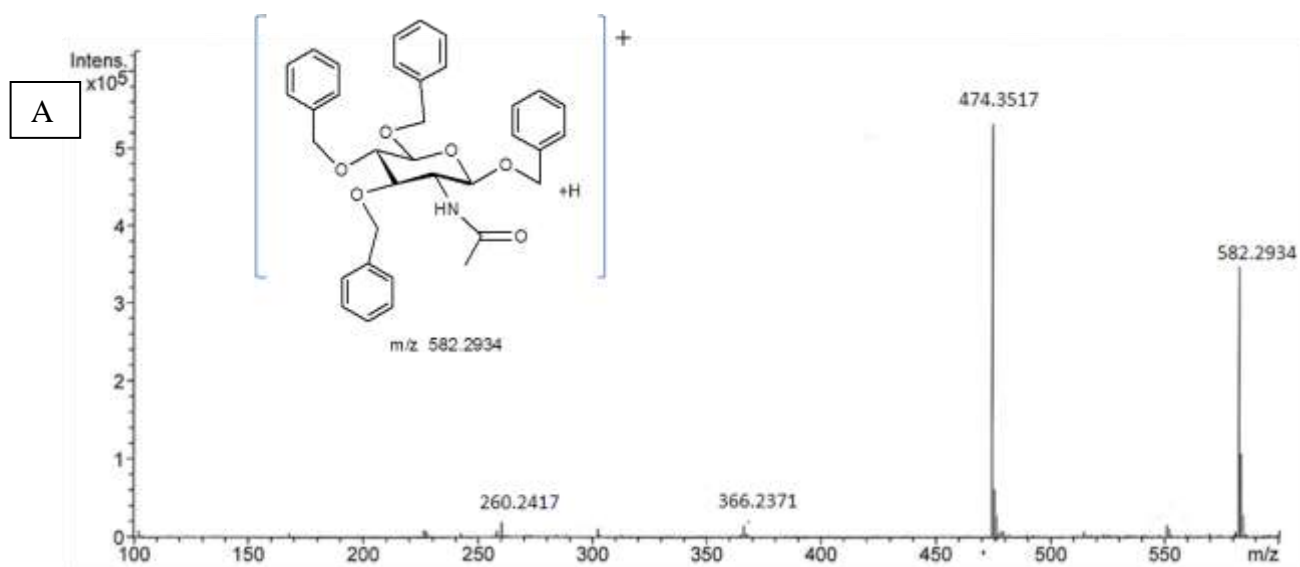
Figure 5.7: A) ESI-QIT-MS of benzyl 3,4,6-tri-*O*-benzyl-2-(acetylamino)-2-deoxy-β-D-glucopyranoside and B) low-CID-MS^2 of the precursor ion [M +H]$^+$ *m/z* 582.2.
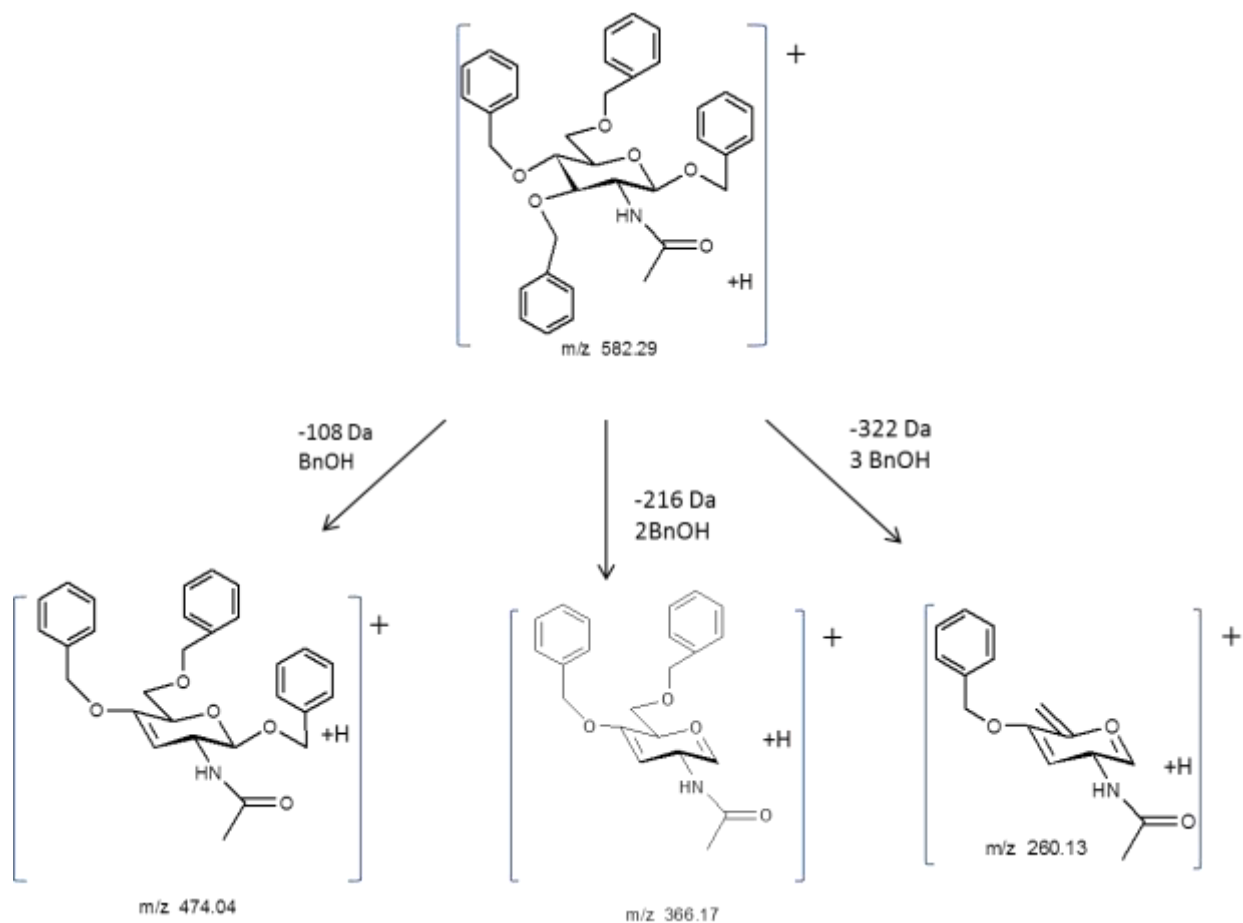
Figure 5.8: The low-energy-CID-MS^2 fragmentations pathway for the precursor ion [M+ H]$^+$ at *m/z* 582.2.
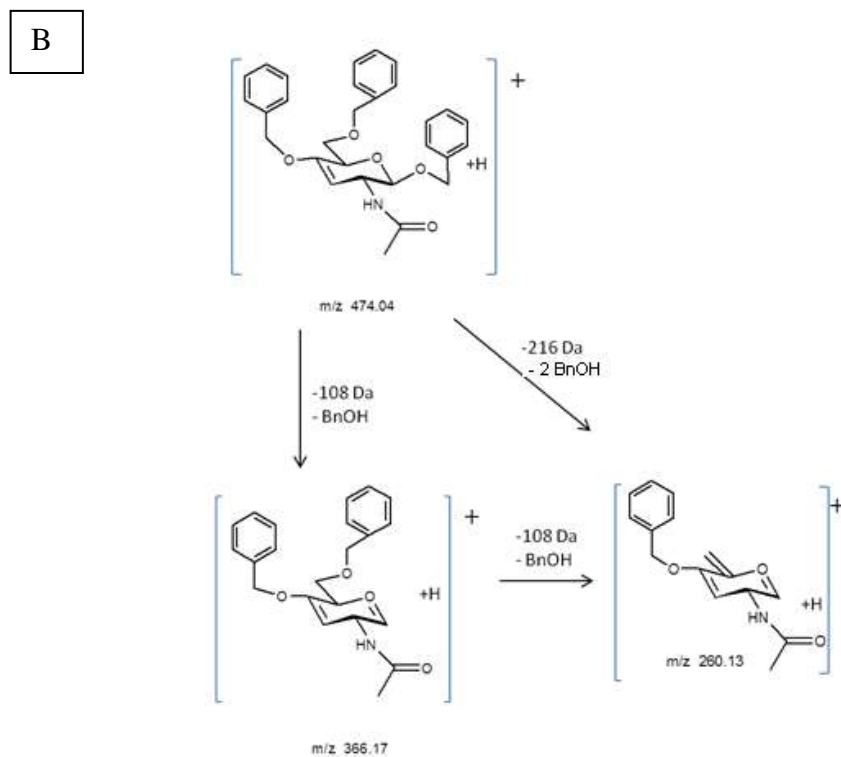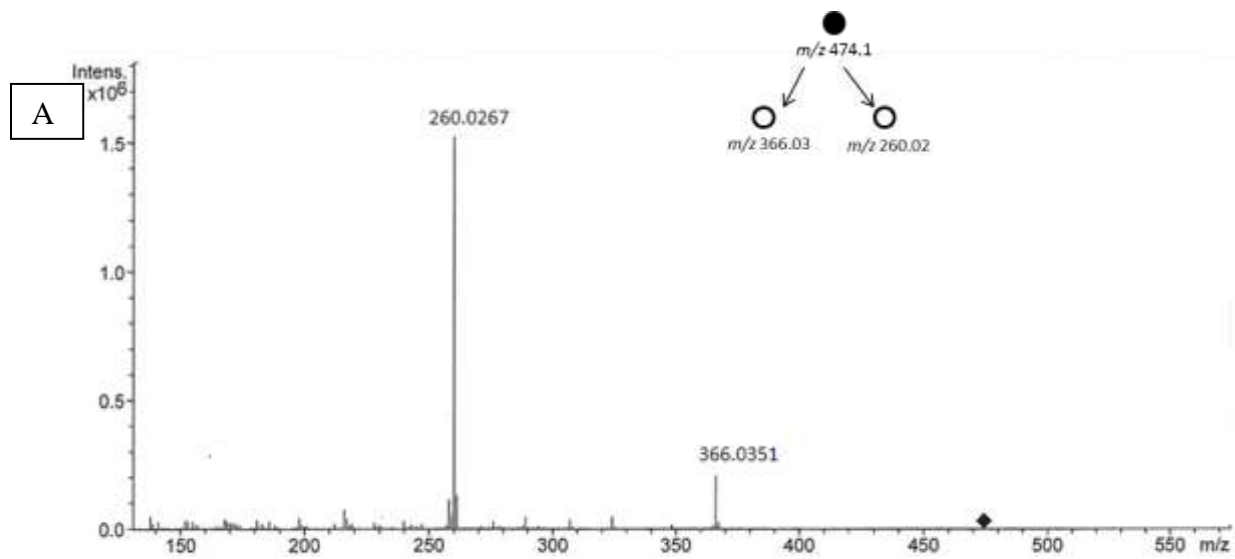
Figure 5.9: A) the low-energy-CID-MS^2 of the precursor ion [M +H]$^+$ *m/z* 474.3517 and B) is fragmentation pathway for MS^3 of the precursor ion [M+ H]$^+$ at *m/z* 474.04.

5.3. ESI-QqTOF-MS CID-MS/MS (tandem-in-space MS)

5.3.1. ESI-QqTOF-MS analysis the methyl-2-(acetylamino)-3,4,6-tri-*O*-acetyl-2-deoxy-β-D-glucopyranoside

The ESI-MS (+ ion mode) of the synthetic methyl-2-acetylamino-3,4,6-tri-*O*-acetyl-2-deoxy-β-D-glucopyranoside was measured with the ESI-QqTOF-MS hybrid instrument. The sodiated molecular ion $[M + Na]^+$ at *m/z* 426.14 and the protonate molecular ion $[M + H]^+$ at *m/z* 404.17 confirmed the exact molecular structure of the methyl-2-acetylamino-3,4,6-tri-*O*-acetyl-2-deoxy-β-D-glucopyranoside as shown in (Figure 5.10). It is important to note that the protonated molecule $[M + H]^+$ at *m/z* 404.17 was only formed during the ESI-QqTOF-MS, which is different than when measured with the ESI-QIT-MS instrument. Similarly, the major ion at *m/z* 372 was created by elimination of the methoxy radical group from of the C-1 position (-31 Da). The product ion at *m/z* 252.12 was formed by the consecutive loss of a molecule of formaldehyde (CH_2O -30 Da) from the C-1 position, a molecule of acetic acid from the C-3 position, and 2 ketene molecules ($CH_2=C=O$) from the C-4 and C-6 positions. The product ion at *m/z* 192.01 was created by the consecutive elimination of three molecules of acetic acid and a molecule of methanol.

The assignment of all the ions observed in the single-stage MS analysis confirmed the respective structure of this glycosyl donor, and additional evidence is usually required to validate these assignments.
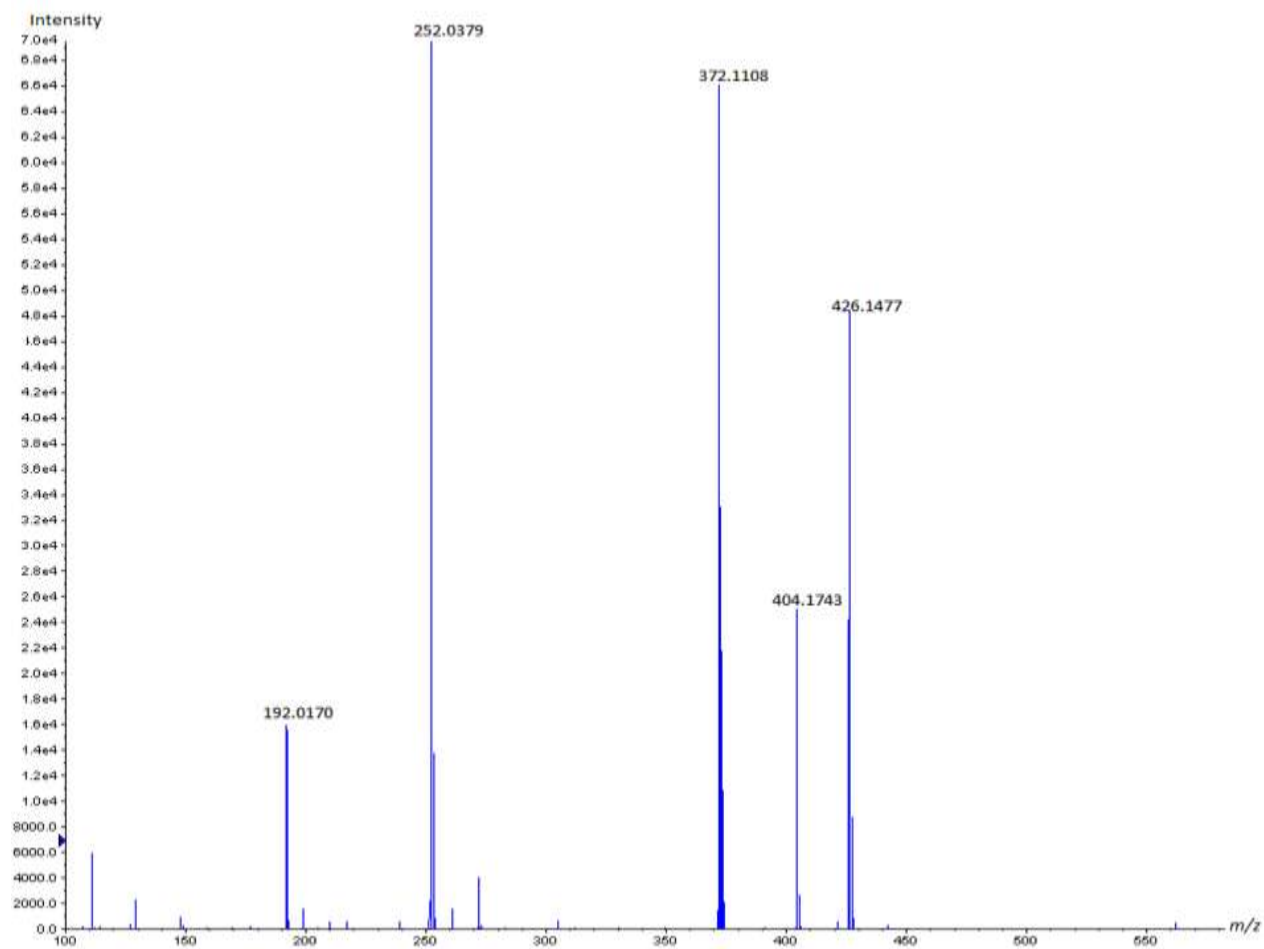
Figure 5.10: The ESI-QqTOF-MS of the methyl-2-acetylamino-3,4,6-tri-*O*-acetyl-2-deoxy-β-D-glucopyranoside.

5.3.1.1. CID-MS/MS analysis of methyl-2-(acetylamino)-3,4,6-tri-*O*-acetyl-2-deoxy-β-D-glucopyranoside

The low-energy-CID-MS/MS analysis of [M+Na]$^+$ at *m/z* 426.16 is shown in Figure 5.11A. Similar to the CID-MS^2 performed with the QIT-MS instrument, the sodiated product ion scan gave the major product ion at *m/z* 366.12 which was formed by elimination of acetic acid from the acetyl group of the C-3 position (-60 Da) as illustrated in Figure 5.12A.

Likewise, the low energy-CID-MS/MS was performed on the protonated molecular ion [M + H]$^+$ at *m/z* 404.15, (Figure 5.11B). This product ion scan showed the formation of the product ion at *m/z* 372.12 which was created by the loss of methanol from the C-1 position. The product ion at *m/z* 252.12 was formed by the consecutive losses of molecule of formaldehyde (CH_2O -30 Da) from the C-1 position, a molecule of acetic acid from position of C-3, and 2 ketene molecules ($CH_2=C=O$) from the C-4 and C-6 positions, (Figure 5.12B).
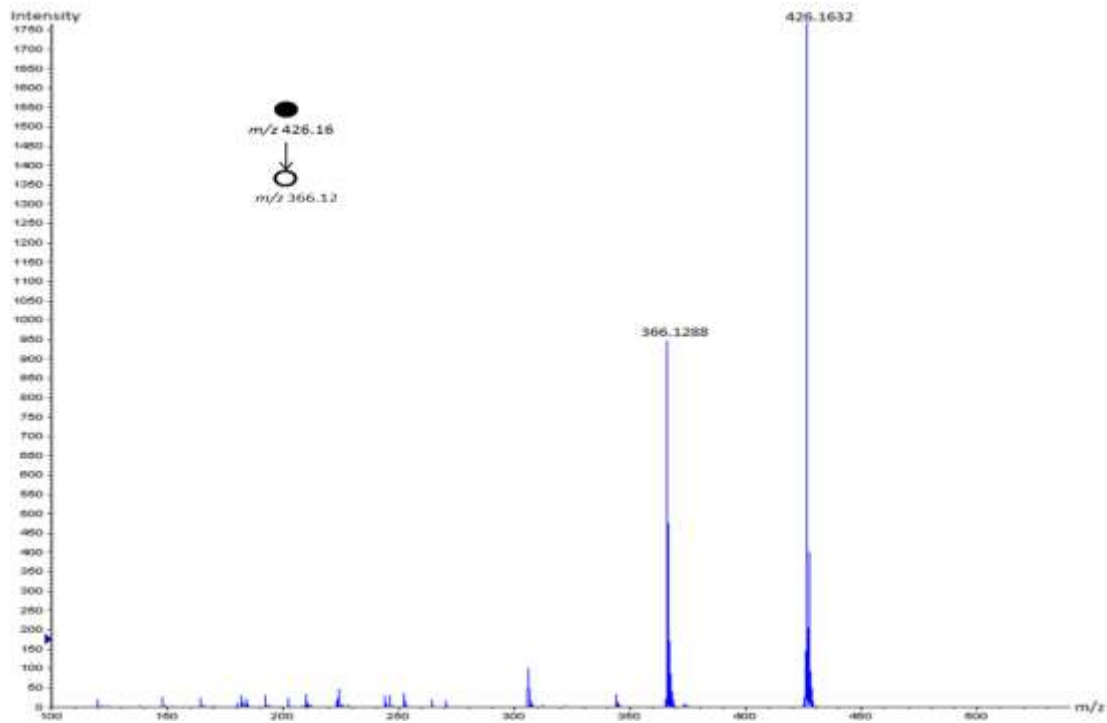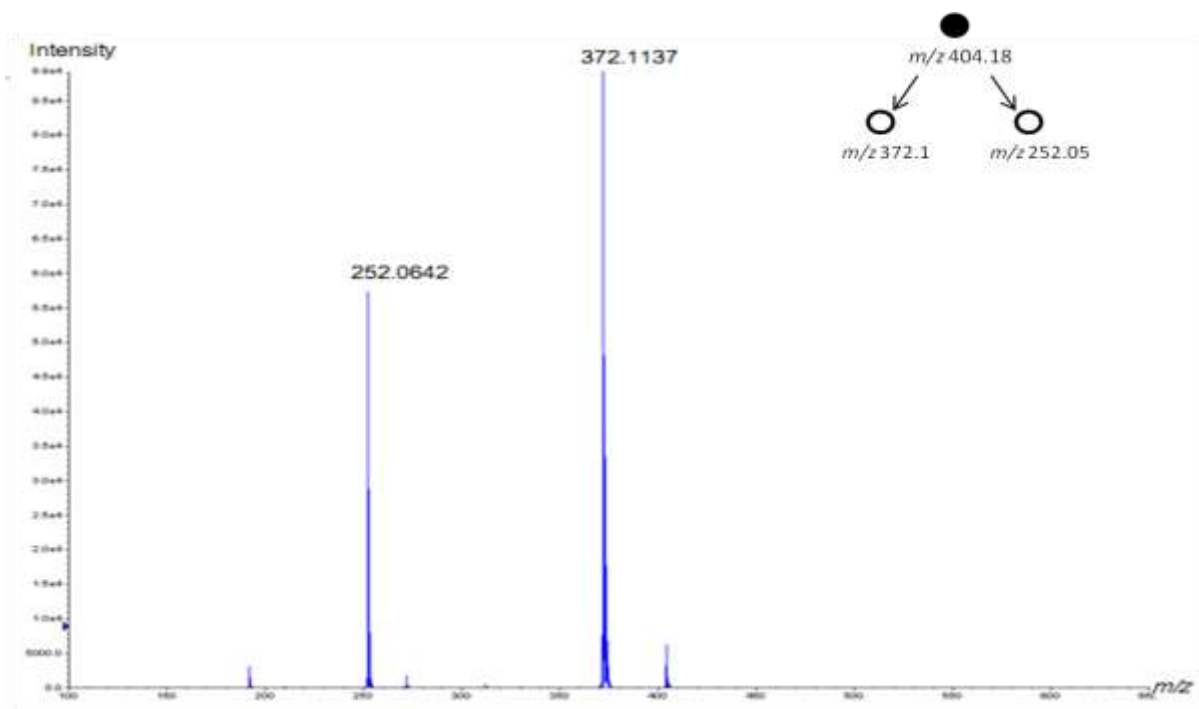
Figure 5.11: A) CID-MS/MS of the precursor sodiated molecule [M+ Na]$^+$ at *m/z* 426.21 isolated from methyl-2-acetylamino-3,4,6-tri-*O*-acetyle-2-deoxy-β-D-glucopyranoside d B) the CID-MS/MS of the precursor protonated molecule ion [M+H]$^+$ at *m/z* 404.18.

Figure 5.12: A) Low-energy-CID-MSMS fragmentations pathway for the precursor ion [M+Na]$^+$ at *m/z* 426.21 and B) the low-energy-CID-MSMS fragmentations pathway for the precursor ion [M+H]$^+$ at *m/z* 404.15.

5.3.2. ESI-QqTOF-MS Analysis of isopropyl-2-(acetylamino)-3,4,6-tri-*O*-acetyl-2-deoxy-β-D-glucopyranoside

The ESI-MS (+ ion mode) of the isopropyl-2-(acetylamino)-3,4,6-tri-*O*-acetyl-2-deoxy-β-D-glucopyranoside was established using the ESI-QqTOF-MS hybrid instrument. Two major product ions assigned as [M+Na]$^+$ and [M+H]$^+$ observed at *m/z* 454.20 and *m/z* 432.20, respectively which verified its molecular structure (Figure 5.13A). The ion at *m/z* 372.12 was formed by the loss of a molecule of acetic acid from the acetyl group from the C-3 position. The product ion at *m/z* 252.10 was formed by the elimination of the three molecules of acetic acid from the acetyl group from the C-3, C-4, and C-6 positions (-180 Da). Also, the ion at *m/z* 192.32 was formed by the loss of $CH_3CH_2CH_2OH$ aglycone (- 60 Da) from C-1 position and the three molecules of acetic acid from the acetyl group from the C-3, C-4, and C-6 positions (-180 Da).

5.3.2.1. CID-MS/MS analysis of isopropyl-2-(acetylamino)-3,4,6-tri-*O*-acetyl-2-deoxy-β-D-glucopyranoside

The low energy-CID-MSMS analysis of the protonated molecular ion [M+H]$^+$ at *m/z* 432.20 is shown in Figure 5.13B. The product ion at *m/z* 372.12 was formed by the loss of a molecule of acetic acid from the C-3 position. The product ion *m/z* 252.10 was formed by the elimination of the three molecules of acetic acid from the C-3, C-4, and C-6 positions (-180 Da), as shown in Figure 5.14.
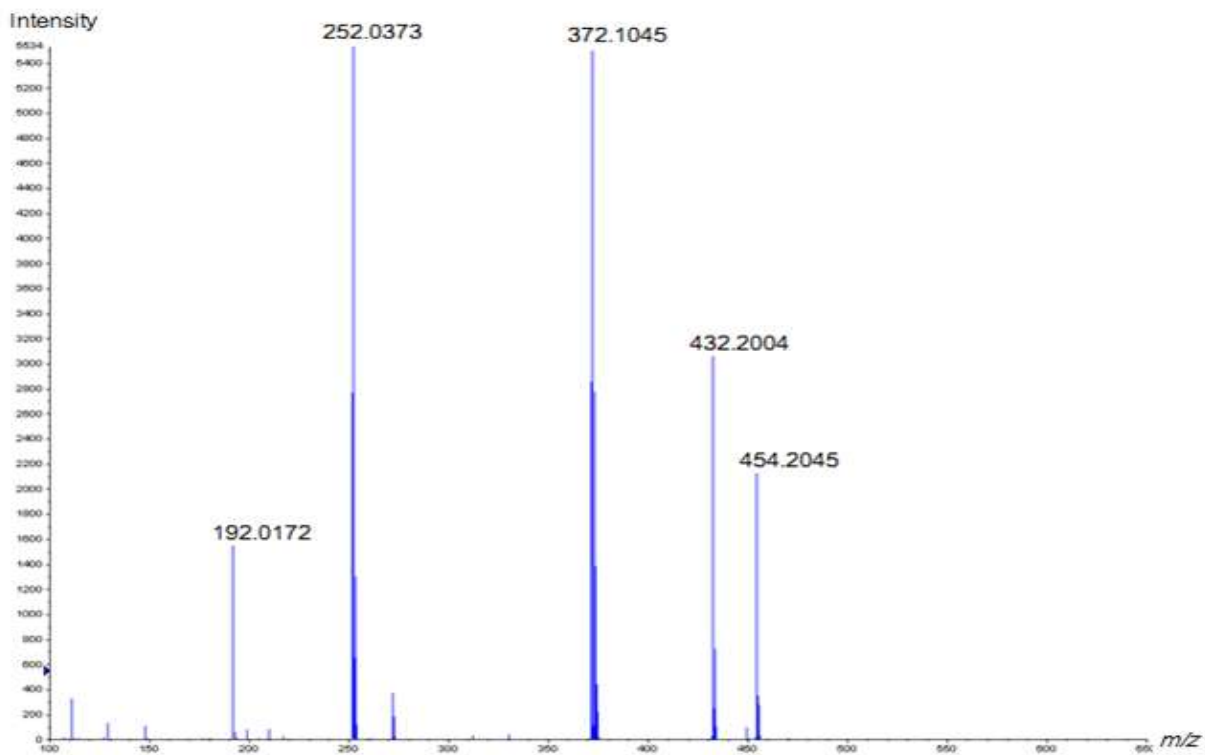
Figure 5.13: A) ESI-QqTOF-MS of the isopropyl -2-acetylamino-3,4,6-tri-*O*-acetyl-2-deoxy-β-D-glucopyranoside and B) Low-CID-MS/MS of the protonated molecule [M+H]$^+$ at *m/z* 432.2.
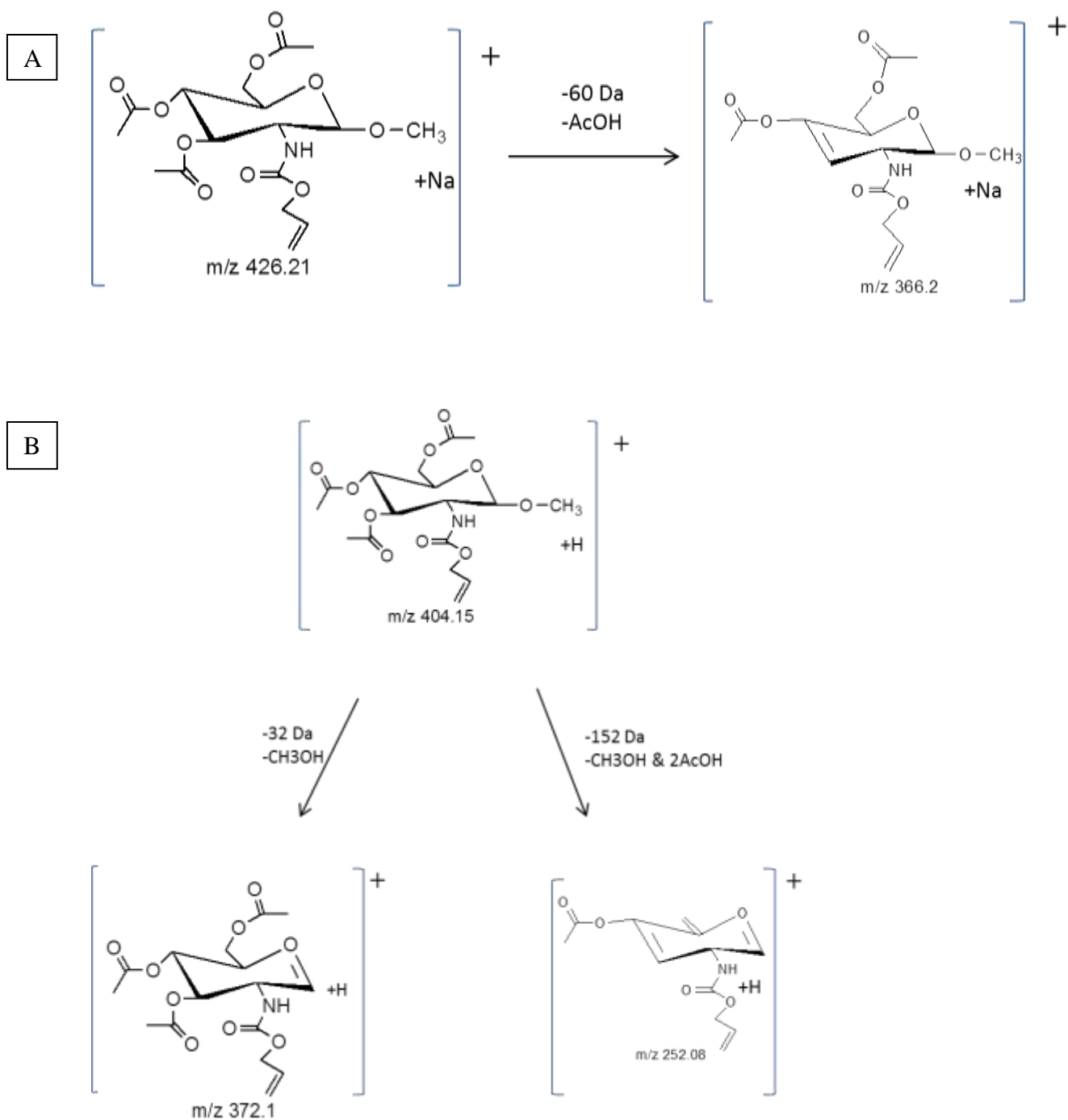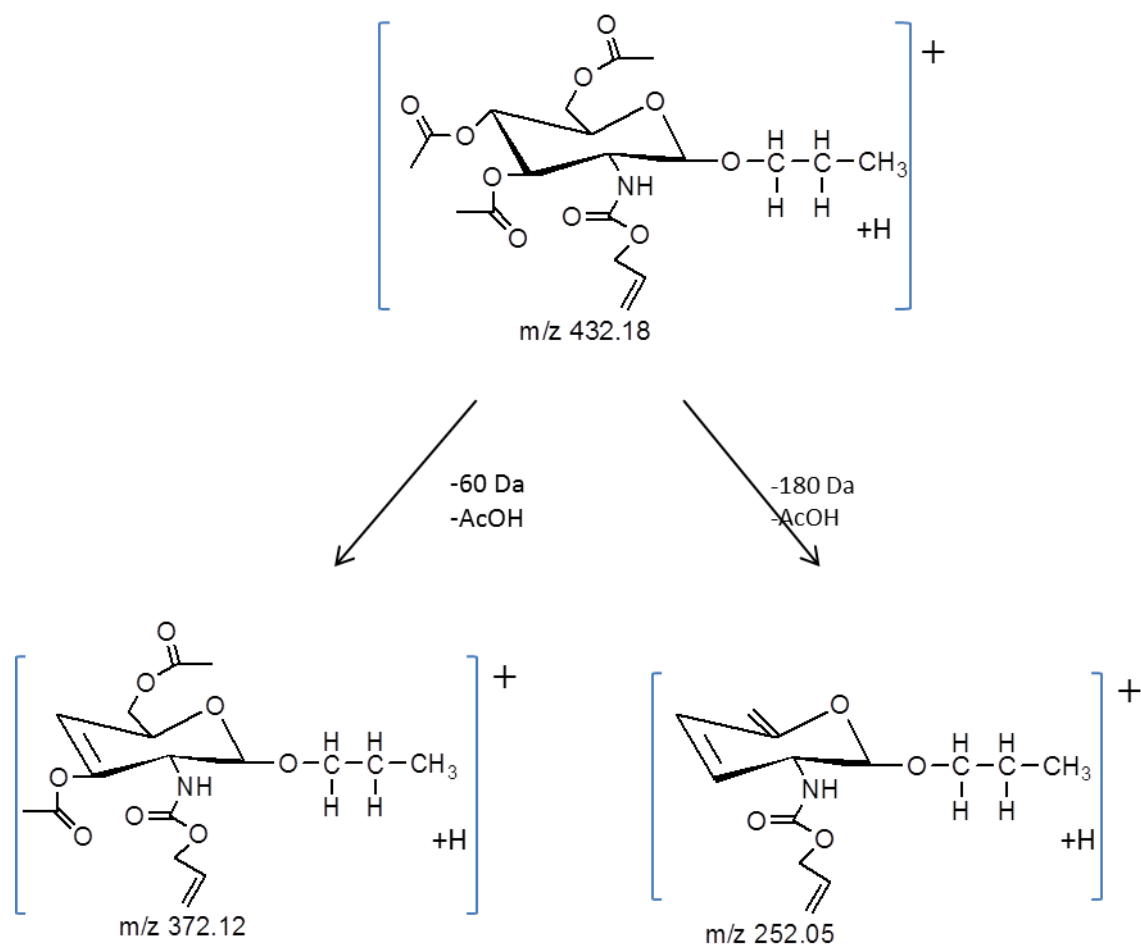
Figure 5.14: The low-energy-CID-MSMS fragmentations pathway for the protonated molecule [M+H]$^+$ at *m/z* 432.18.

5.3.3. ESI-QqTOF-MS analysis of trichloroethyl 2-(*N*-allyloxy)-3,4,6-tri-*O*-acetyl-2- deoxy-β-D-glucopyranoside

The positive ESI -MS of trichloroethyl 2-(*N*-allyloxy)-3,4,6-tri-*O*-acetyl-2-deoxy-β-D-glucopyranoside was established using ESI-QqTOF-MS. The major ion was observed at *m/z* 542.09 and the ion at *m/z* 520.38 confirmed its molecular structure. It is important to note that in that respective case and contrary to the QIT-MS the formation of the diagnostic protonated ion of $[M+H]^+$ was noted, and which was absent as described earlier, (Figure 5.15A).

The ion at *m/z* 252.10 indicates the elimination of a molecule of trichloroehanol from the trichloroethyl group from the C-1 position and a molecule of acetic acid from the C-3 and C-4 positions (-120 Da). Moreover, the ion at *m/z* 192.16 was formed by elimination of the trichloroehanol aglycone from the C-1 position and three molecules of acetic acid from the acetyl groups from the C-3, C-4, and C-6 positions.

5.3.3.1 CID-QqTOF-MS/MS Analysis of trichloroethyl 2-(*N*-allyloxy)-3,4,6-tri-*O*-acetyl-2-deoxy-β-D-glucopyranoside

The low energy-CID-MS/MS was performed on the sodiated molecular ion [M+Na]+ at *m/z* 542.03 as illustrated in Figure 5.15B. The product ion scan of this ion gave the major ion at *m/z* 394.2114, which was formed by elimination of the three molecules of acetic acid from the C-3, C-4, and C-6 positions (-180 Da).

Similar to the low energy-CID-MS[2] measured with the QIT-MS instrument, this precursor ion scan gave the product sodiated ion at *m/z* 506.12, which was formed by

the elimination of a HCl from the C-1 position and assigned as dichloroethyl-2-acetylamino-3,4,6-tri-O-acetyl-2-deoxy-β-D-glucopyranoside.

Once more, we have noticed the formation of the protonated ion at m/z 484.011 assigned as dichloroethyl-2-acetylamino-3,4,6-tri-O-acetyl-2-deoxy-β-D-glucopyranoside, which was created from by elimination of a HCl molecule and the Na$^+$ ion from the precursor ion from the C-1 position. The formation of the major sodiated product ion observed at m/z 394.21, which was formed by the consecutive elimination of the trichloroethanol aglycone moiety (Cl$_3$C$_2$H$_2$OH, -148Da) from the C-1 position, (Figure 5.16).

In addition, the sodiated product ion at m/z 334.14 was formed by the elimination of a ketene molecule (CH$_2$=C=O) from the C-3 position and a molecule of trichloroethanol from the C-1 position. The sodiated product ion at m/z 274.05 was formed by the elimination of 2 ketene molecules (CH$_2$=C=O) from the C-3 and C-6 positions; followed by a molecule of aglycone trichloroethanol. Finally, the protonated ion at m/z 252.02 was created by the expulsion of Na$^+$ ion, 2 ketenes molecules (CH$_2$=C=O) from the C-3 and C-6 positions and trichloroethanol, not necessarily in this order. However, the product ion at m/z 192.08 was only observed in the low energy-CID-MSMS of the QqTOF-MSMS instrument, which was formed by the elimination of the trichloroethanol from the trichloroethyl group from the C-1 position and 3 ketene molecule (CH$_2$=C=O) from the C-3, C-4, and C-6 positions.
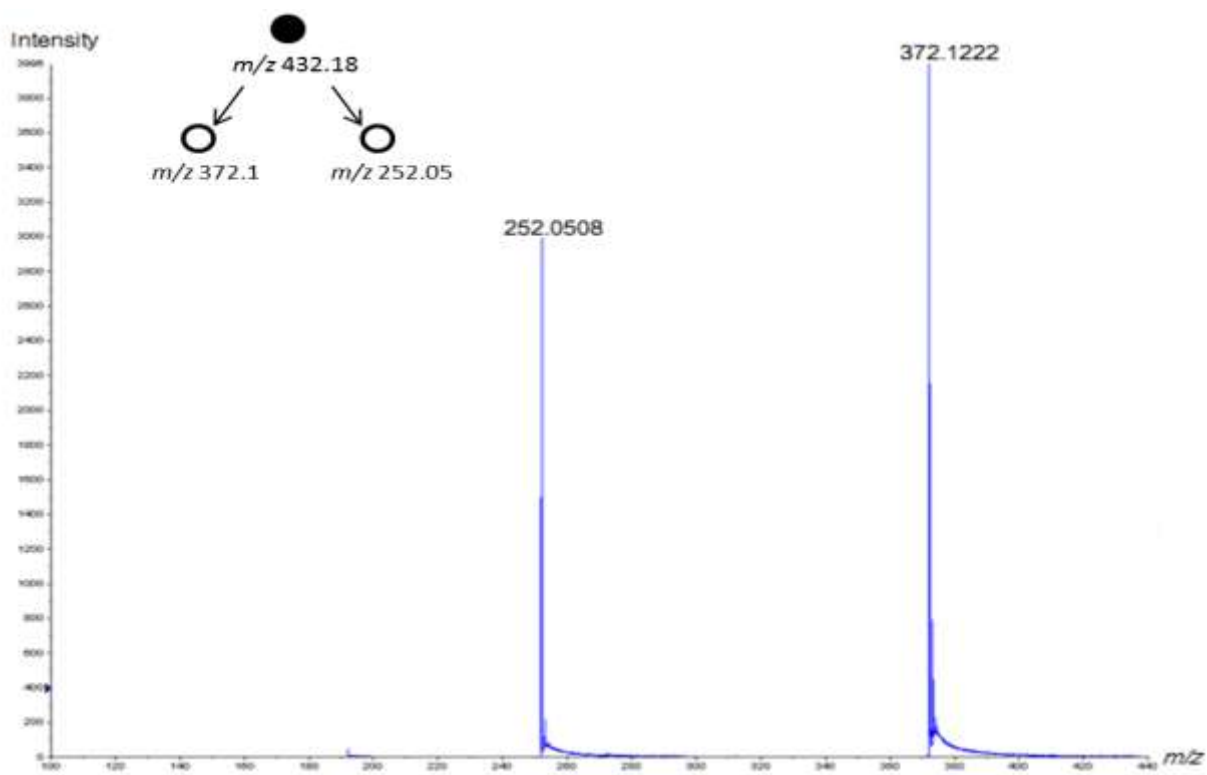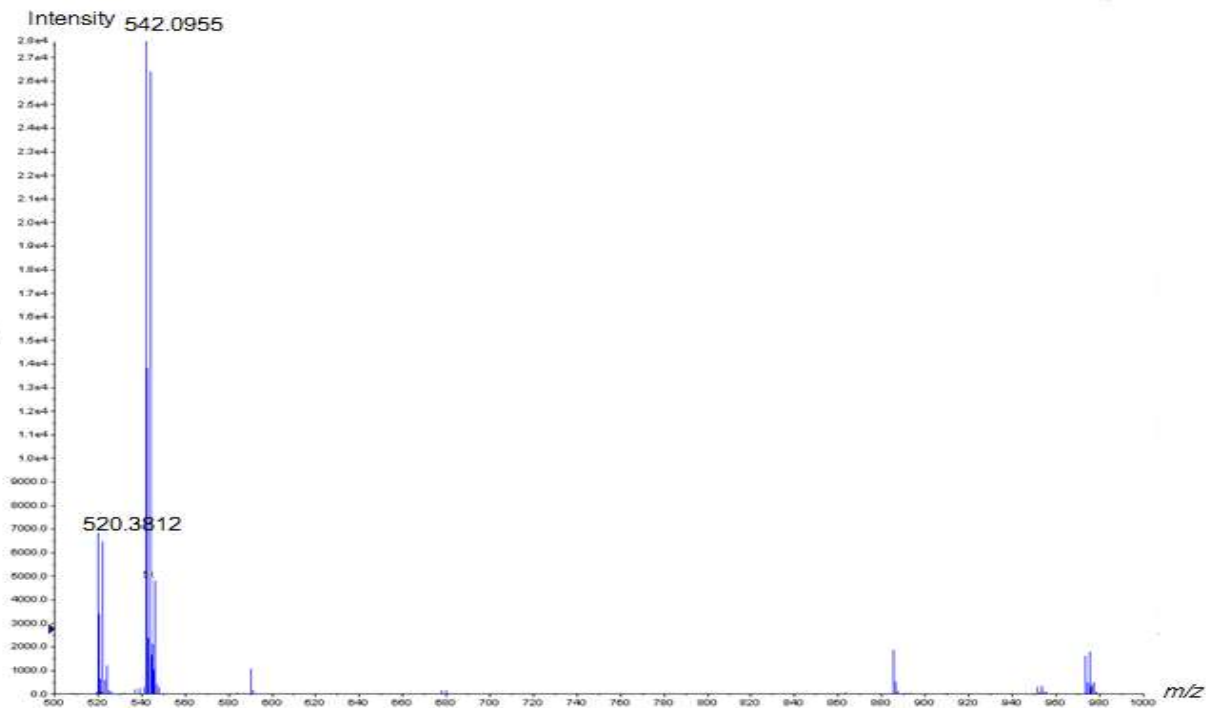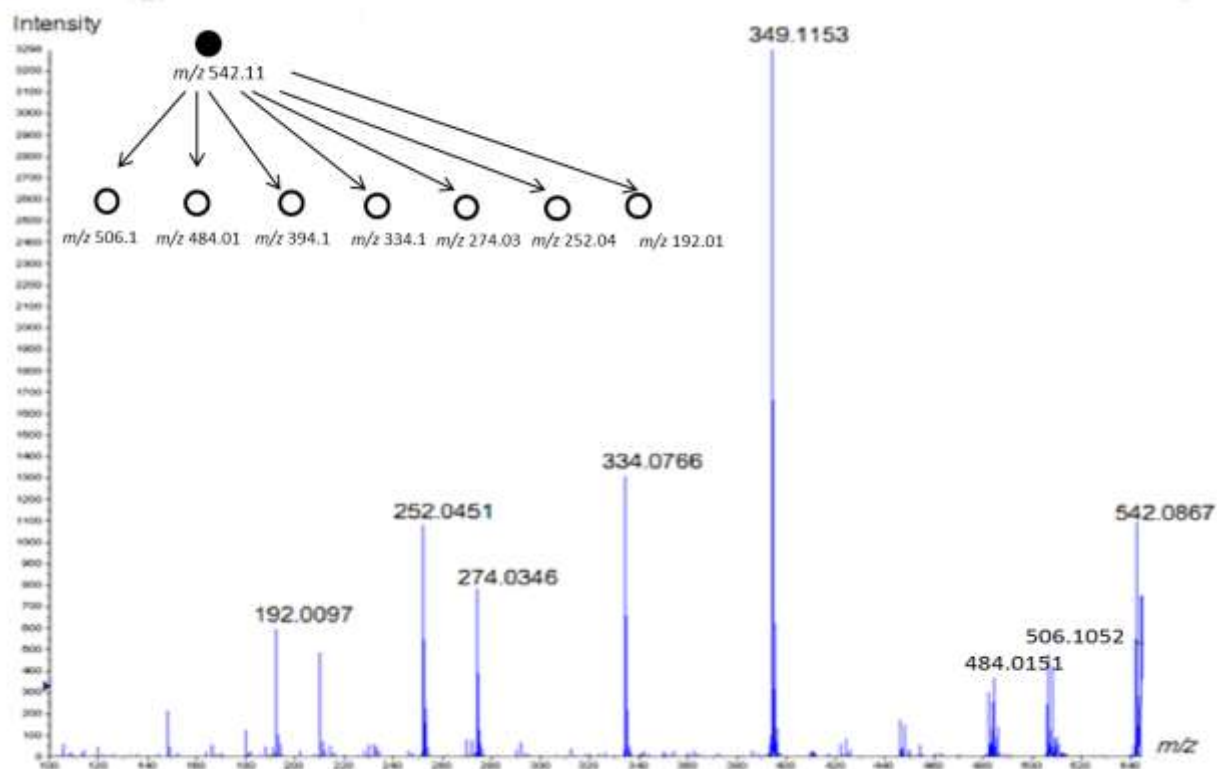
Figure 5.15: A) ESI-QqTOF-MS of the trichloroethyl 2-*N*-allyloxy-3,4,6-tri-*O*-acetyl-2-deoxy-β-D-glucopyranoside and B) low-CID-MS/MS of the precursor ion [M+Na]$^+$ at *m/z* 542.09.
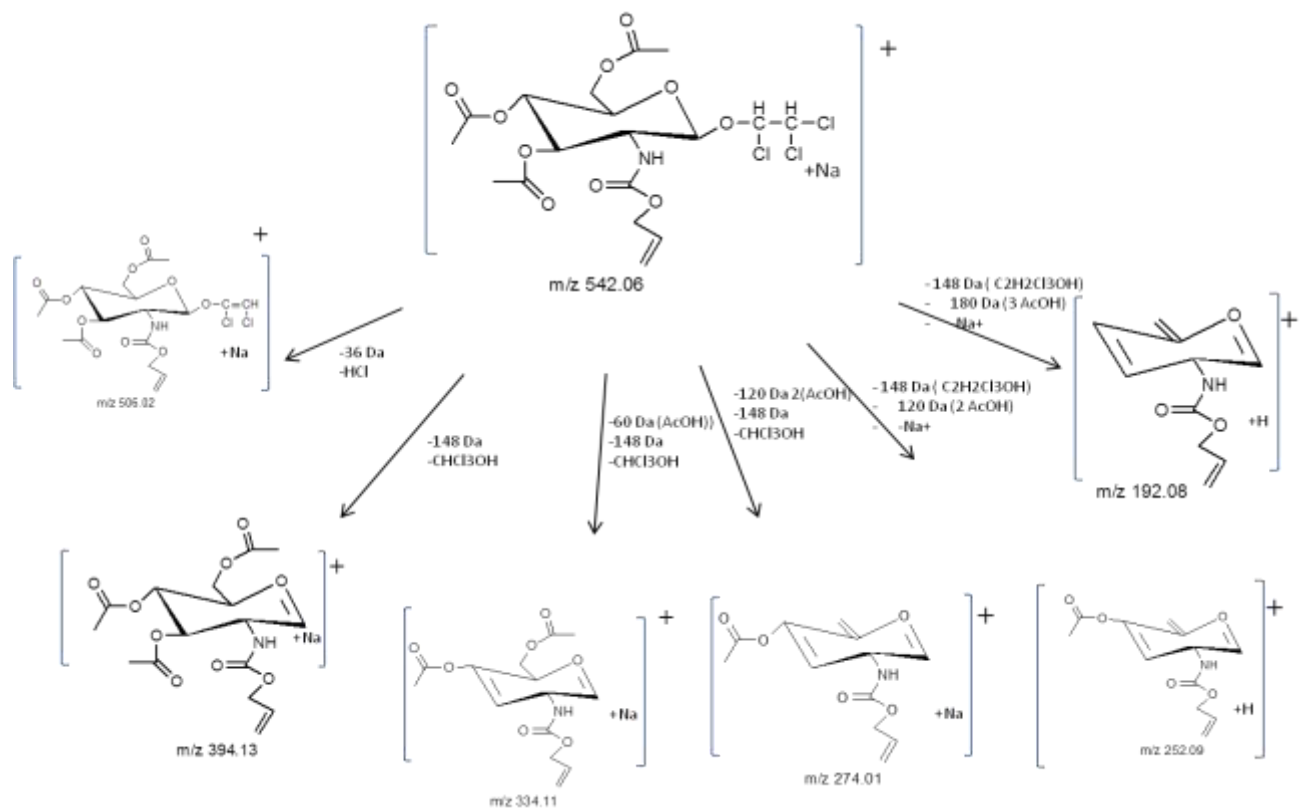
Figure 5.16: The low-energy-CID-MSMS fragmentations pathway for the precursor ion [M+Na]$^+$ at *m/z* 542.06.

5.3.4. ESI-QqTOF-MS analysis of benzyl 3,4,6-tri-*O*-benzyl-2-(acetylamino)-2-deoxy-β-D-glucopyranoside

The ESI-MS (+ ion mode) of the synthetic compound of benzyl 3,4,6-tri-*O*-benzyl-2-(acetylamino)-2-deoxy-β-D-glucopyranoside was established using ESI-QqTOF-MS to study its gas phase fragmentations. Figure 5.17A shows its mass spectrum which gave the sodiated molecular ion $[M+Na]^+$ at *m/z* 604.37 and the protonated ion $[M+H]^+$ *m/z* 582.37, which confirmed the molecular structure. It is important to note that the sodiated ion at *m/z* 604.37 was only diagnostic in the ESI-QqTOF-MS. The major ion was observed at *m/z* 474.24 was formed by the elimination of benzyl alcohol from the C-3 position.

5.3.4.1. CID-QqTOF-MS/MS analysis of benzyl 3,4,6-tri-*O*-benzyl-2-(acetylamino)-2-deoxy-β-D-glucopyranoside

Low energy-CID-MS/MS analysis the protonated ion $[M+H]^+$ *m/z* 582.37 is shown in Figure 5.17B. Similar to low CID-MS^2 measured with the QIT-MS instrument, the major ion at *m/z* 474.24 was formed by elimination of benzyl alcohol from the C-3 position.

Moreover, the product ion scan for *m/z* 582.37 gave the product ion at *m/z* 366.03 and *m/z*-260.02. The product ion at *m/z* 366.03 was formed by the loss of a molecule of benzyl alcohol from the C-3 position. Once more, *m/z* 260.02 formed by the loss of an additional molecule of benzyl alcohol from the C-3, C-4, and C-6 positions, as shown in Figure 5.18.
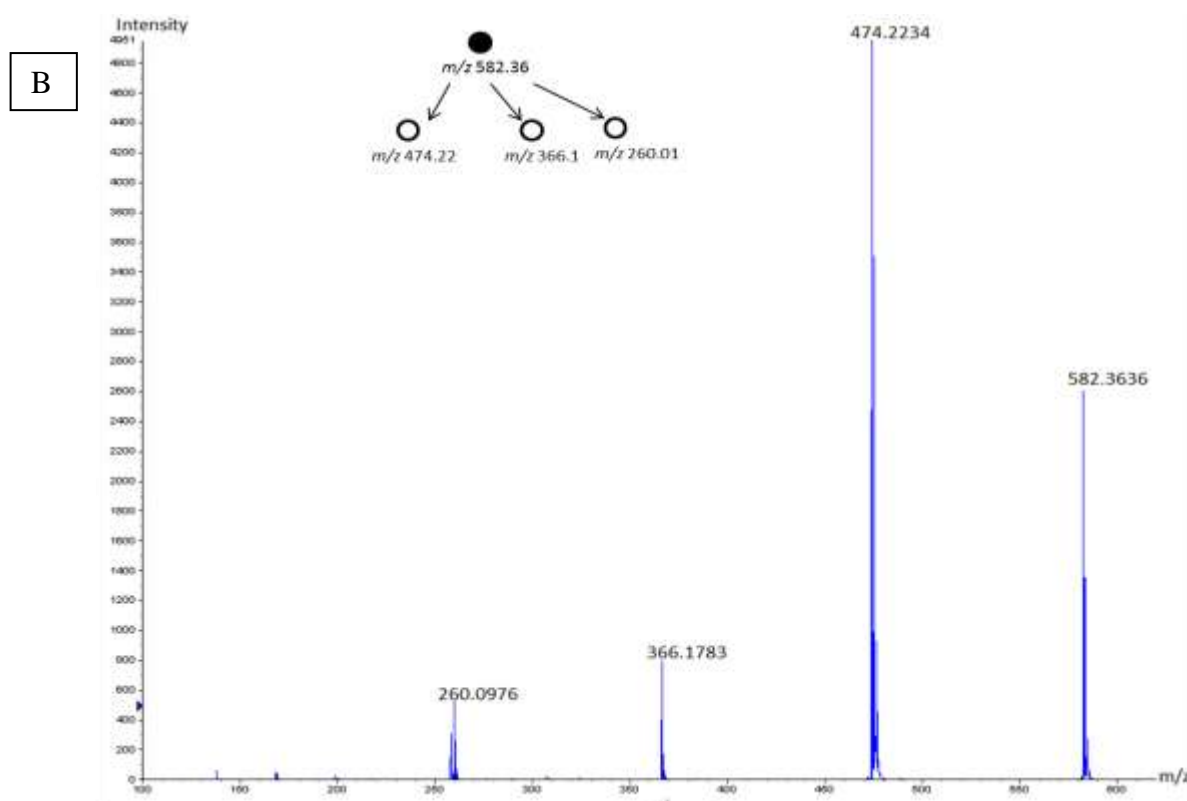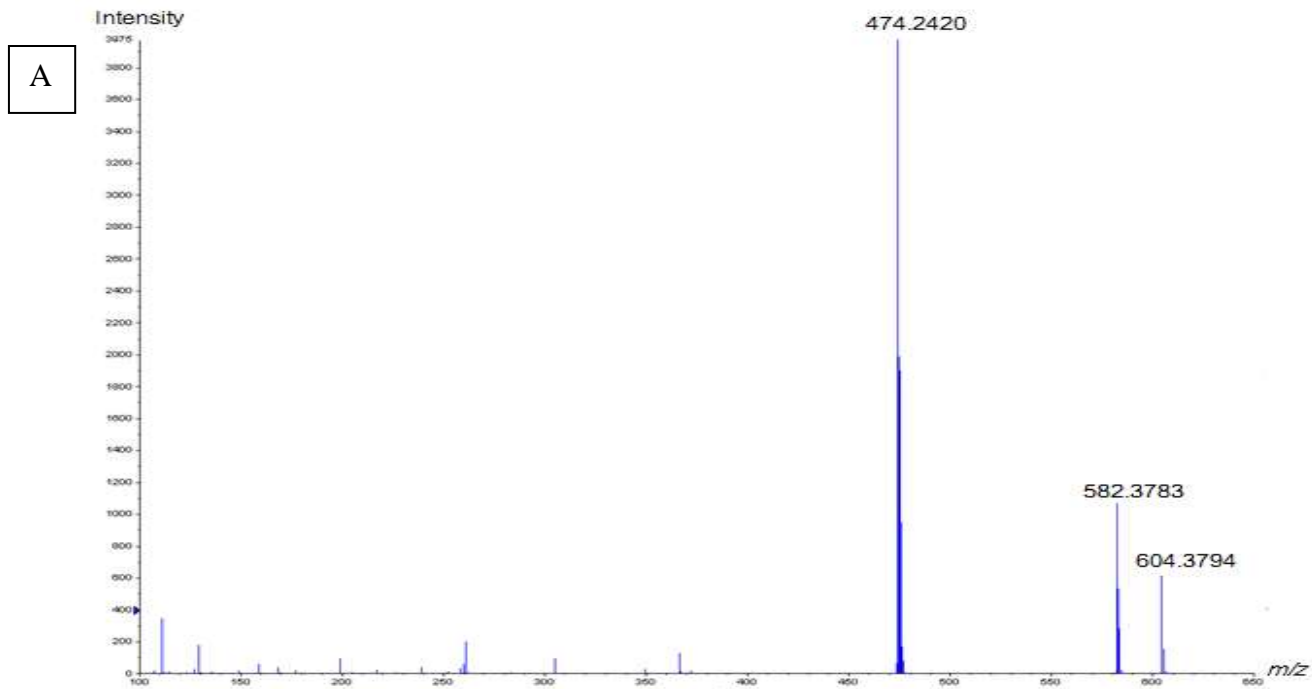
Figure 5.17: A) ESI-QqTOF-MS of the benzyl 3,4,6-tri-*O*-benzyl-2-(acetylamino)-2-deoxy-β-D-glucopyranoside and B) the low-CID-MS/MS of the precursor ion [M+H]$^+$ at *m/z* 582.36.
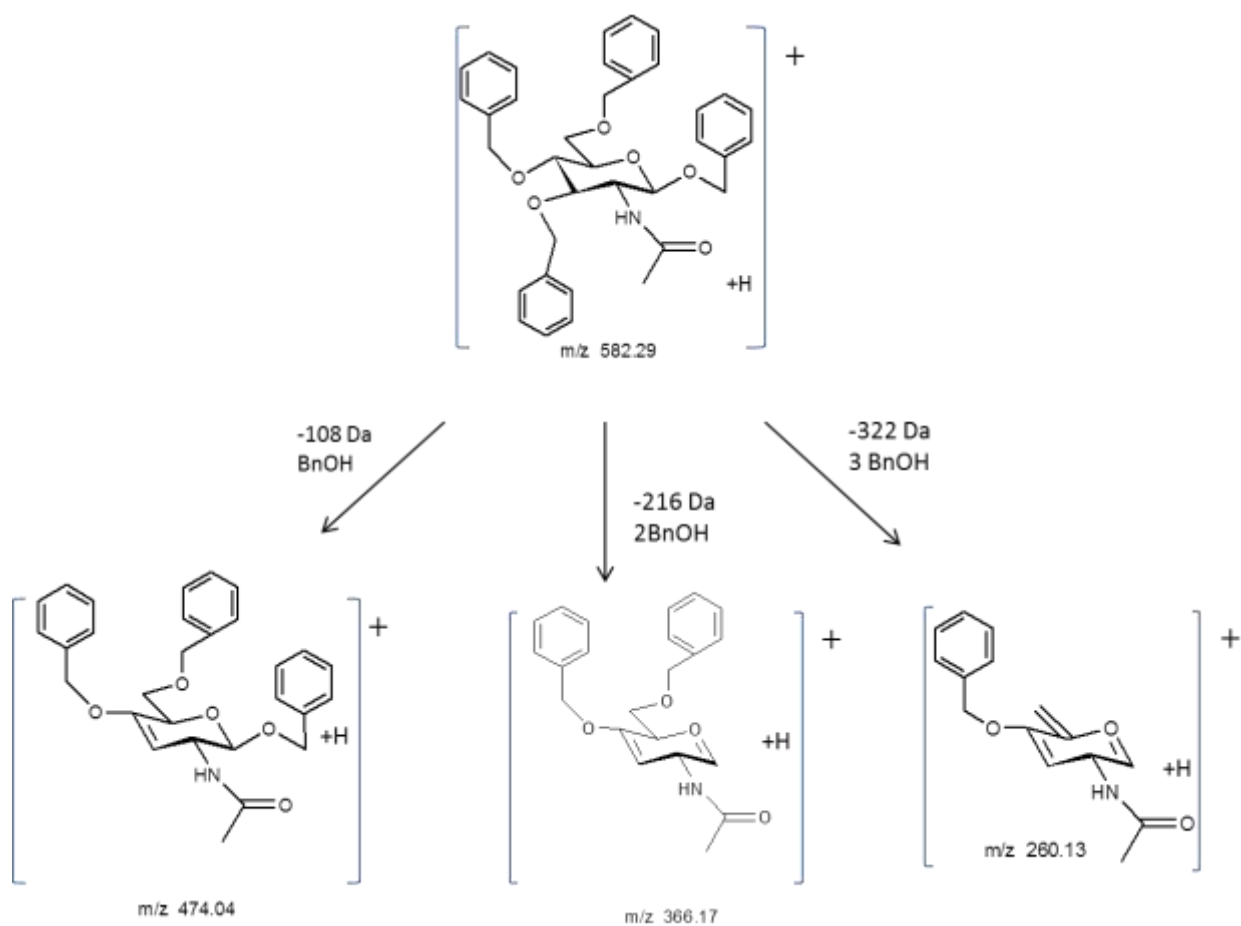
Figure 5.18: The low energy-CID-MS/MS fragmentations pathway for the precursor ion [M+H]$^+$ at *m/z* 582.29.

Similar to low CID-MS^3 of the QIT-MS instrument, the seconed-generation quasi-MS^3 at *m/z* 474.35 was measured using low energy-CID-MS^3, (Figure 5-19A). This product ion scan showed the presence of the product ions at *m/z* 366.03 and *m/z* 260.02, respectively. These product ions were respectively formed by elimination of one and two molecules of benzyl alcohol from the C-1, and the C-1 and C-2 positions, respectively (Figure 5.19B). However, the product ion at *m/z* 168.01 was only observes by the quasi-MS^3 of the QqTOF instrument, which indicates the loss of 3 molecule of benzyl alcohol from the C-3, C-4, and C-6 positions.
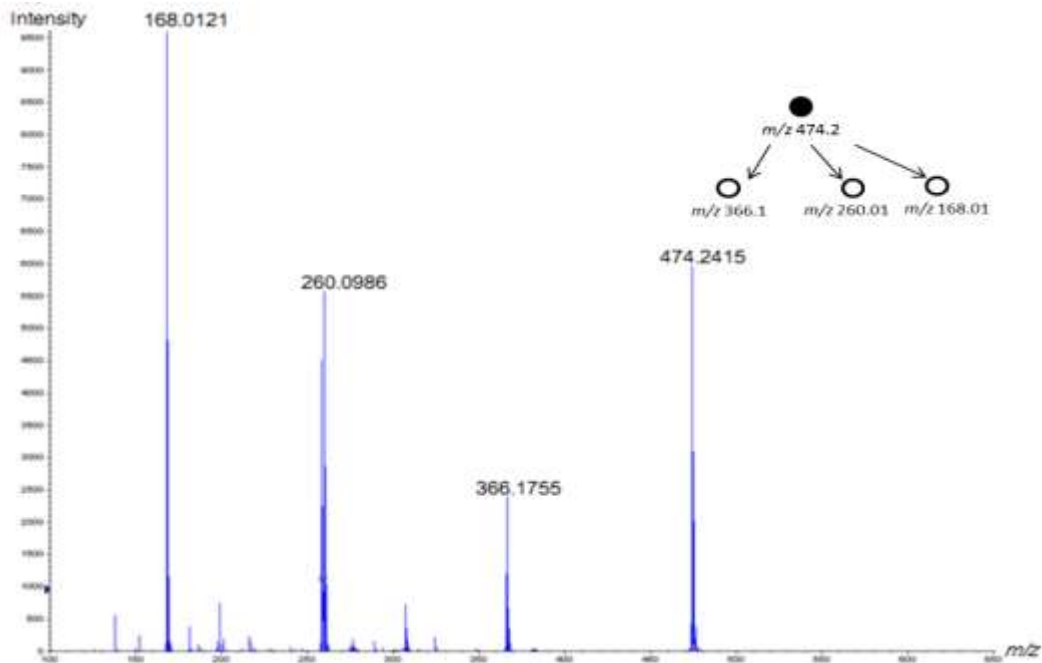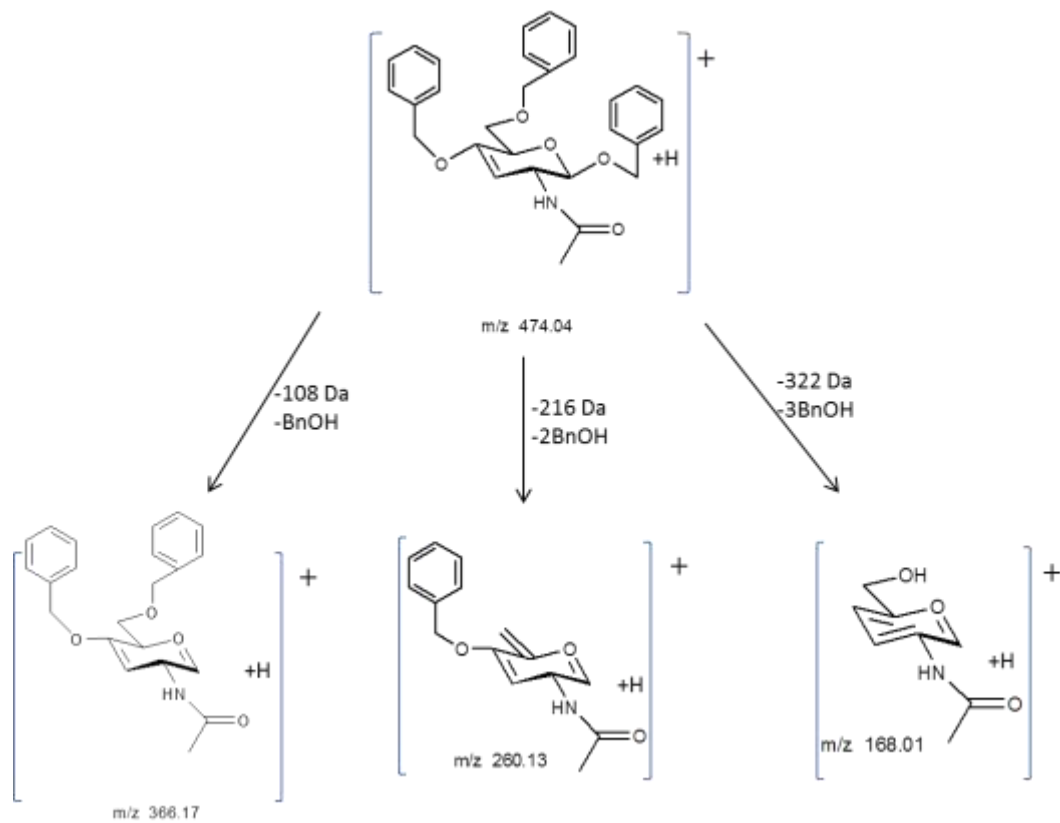
Figure 5.19: A) Quasi-MS^3 of the precursor ion [M+H]$^+$ at *m/z* 474.04 and B) is the quasi-MS^3 fragmentations pathway for the precursor ion [M+H]$^+$ at *m/z* 474.04.

5.4. Summary

The gas-phase MS/MS study was established for series synthetic glycosyl donor compounds of a 2-amino-2-deoxy-β-D-glucopyranosyl series.

Electrospray ionization was measured with two different MS instruments. ESI-QIT-MS gave the sodiated molecules, whereas analysis with the QqTOF-MS instrument showed both the sodiated and protonated molecules.

The gas-phase fragmentation routes of this series of compounds using tandem-in-time and tandem-in-space MS gave almost identical product ions. It was noted that all the same product ions series obtained from selected precursor ions in QIT-MS was identical to the product ion of QqTOF-MS. However, only the intensities of these product ions may vary in some cases.

Chapter 6

General conclusion:

Lipid A extracts are not merely composed of a single entity and are in reality a mixture of many structurally-related components. Due to the complex nature of lipid A, mass spectrometry was used to propose tentatively the precise molecular structure of such a biologically active extract. Tandem-in-time mass spectrometry using FT-ICR-MS^2 and tandem-in-space mass spectrometry using MALDI-TOF/TOF-MS/MS instruments was used to analyze the complex lipid A mixture composed of various structurally related components, without the need for any tedious separating techniques.

It was shown that the major component of the lipid A mixture, which was isolated by acid hydrolysis from the *A. liquaficiens* LPS, contained one phosphate group at the O-4' position. In addition, both D-GlcN units of the β-D-(1→6) disaccharides were *O-* and *N-*substituted with various fatty acids. These were identified as 12:0(3-OH) and 14(3-OH). The distribution of these fatty acids on the individual Lipid A molecules was established through the presence of the characteristic product ions in the FT-ICR-MS^2, namely the [Y-H]$^-$ and [C-H]$^-$ derived product ions. In the case of the MALDI-TOF/TOF-MSMS the presence of the unique diagnostic [C-H]$^-$ product ion was observed.

In addition, product ions originating from inner sugar fragmentations were observed in the SORI-CID and CID-TOF/TOF-MSMS analysis. Furthermore, MS/MS analysis of the [Y]$^-$ and [C]$^-$ ions clearly confirmed the presence of two 14:0(3-OH) fatty acids on the reducing end group, and one 14:0(3-O(14:0)) one 14:0(3-O(12:0)) on the non-reducing end group of the disaccharide. This was also evident by the generation of

product ions associated with distinctive losses of these fatty chains, either as neutral ketene, or as a free fatty acid.

On the other hand, the structures of the synthetic glycosyl donor residues composed of 2-amino-2-deoxy-β-D-glucopyranoside units were also evaluated in this thesis and their gas-phase fragmentation patterns were studied using tandem mass in time ESI-QIT-MSMS and tandem mass spectrometry in space ESI-QqTOF-MSMS. The CID-fragmentation pathways of the protonated and sodiated molecules were proposed.

References

1. Henderson, W.; McIndoe, J.S. *Mass Spectrometry of Inorganic, Coordination and Organometallic Compounds: Tools-Techniques-Tips.* John Wiley & Sons: England. **2005**.

2. Banoub, J. H.; Newton, R. P.; Esmans, E.; Ewing, D.F.; Mackenzie, G. *Chem. Rev.* **2005**, 105, 1869–1915.

3. Korfmacher, W.A. *Using Mass Spectrometry for Drug Metabolism Studies*. CRC Press: Boca Raton, FL. **2005**.

4. Cho,W.C. *Genom. Proteom. Bioinformat.* **2007**, 5, 77–85.

5. Hoffmann, E.; Stroobant, V. *Mass Spectrometry: Principles and Applications.* 3rd ed.; John Wiley & Sons: England. **2007**.

6. Fwkarasek, R. E. *Basic Gas Chromatography-Mass Spectrometry: Principle and Techniques:* Elsevier Science B.V. **1998**.

7. Gross, J. H. *Mass Spectrometry*. 2nd ed., Berlin – Heidelberg, Springer Verlag: 2011.

8. Dass, C. *Fundamentals of Contemporary Mass Spectrometry.* New York, Wiley-Interscience: 2007.

9. Desiderio, D. M.; Nibbering, N. M. *Mass Spectrometry: Instrumentation, Interpretation, And Applications*. John Wiley & Sons: **2009**.

10. Van Berkel, G. J.; Pasilis, S. P.; Ovchinnikova, O. *J. Mass Spectrom.* **2008**, 43, 1161-1180.

11. Venter, A.; Nefliu, M.; Cooks, R. G. *TrAC Trends in Anal. Chem.* **2008,** 27 (4), 284–290.

12. Chen, H.; Gerardo G.; Zenobi, R. *J. Am. Soc. Mass Spectrom.* **2009,** 20, 1947–1963.

13. Morris, H.R.; Panico M.; Barber M.; Bordoli R.S.; Sedgwick R.D.; Tyler A. *Biochem. Biophys. Res. Commun.* **1981**, 101(2), 623–31.

14. Ninomiya, S.; Ichiki, H.; Yamada, Y.; Nakata, T.; Seki, T.; J.; Matsuo, A. J. *Rapid Commun. Mass Spectrom.***2009**, 23, 1601–1606.

15. Alberici, R. M.; Simas, R. C.; Sanvido, G. B; Romao, W. Lalli, P.; Benassi, M.; Cunha, I. B. S.; Eberlin, M. N. *Anal. Bioanal. Chem.* **2010**, 398, 265–294.

16. Ifa, D. R.; Wu, C., Ouyang, Z.; Cooks, R. G.; *Analyst.* **2010**, 135, 669–681.

17. Caroline, S.; Carlito, C.; Lebrilla, B. *Biom. Applic. of Bioph.* **2010**, 3, 137-145

18. Fenn, J.B. *Angew Chem, Int.* **2003**, 42, 3871–3894.

19. Laskin, J.; Heath, B. S.; Roach, P. J.; Cazares, L.; Semmes, O. J. *Anal Chem.* **2012**, 84,141-148.

20. Nemes, P. ; Barton, A. A. ; Li, Y.; Vertes, A. *Anal. Chem.* **2008**, 80, 4575–4582.

21. Loo, J. A. *Mass Spectrom. Rev.* **1997**, *16*, 1-23.

22. Gaskell, S. J. *J. Mass Spectrom.* **1997**, *32*, 677-688.

23. Kebarle, P.; Tang, L. *Anal. Chem.* **1993**, *65*, 972-986.

24. Dole, M. L.; Mack, L. L.; Hines, R. L.; Mobley, R. C.; Ferguson, L. D.; Alice, M. B. *J. Chem Phys.* **1968,** 49, 2240–2249.

25. Gross, M. L.; Caprioli, *R. The Encyclopedia of Mass Spectrometry.* Eds, Elsevier Science, Oxford, 2003, Voll, 1-10.

26. Huang, M. Z.; Yuan, C. H.; Cheng, S. C.; Cho, Y. T.; Shiea, J. *Annu. Rev. Anal. Chem.* **2010**, 3, 43–65.

27. Aebersold, R.; Mann, M. *Nature*. **2003**, 422, 198–207.

28. Navas-Iglesias, N. N., Carrasco-Pancorbo, A., Cuadros-Rodríguez, L. *TrAc Trends in Anal. Chem.* **2009**, 28, 343-403.

29. Wang, Y.; Griffiths, W. J. *Chem. Soc. Rev.,* **2009**, 38, 1882-1896.

30. Zaia, J. *Chemistry&Biology.* **2008,** 15, 881–892.

31. Huang, M. Z.; Cheng, S. C.; Cho, Y. T.; Shiea, J. *Anal. Chim. Acta.* **2011**, 702, 1–15.

32. Zenobi, R.; Knochenmuss, R. *Mass Spectrom Rev.* **1998**, 17, 337–366.

33. Hay-Yan, J.; Wang, Shelley N.; Jackson, Amina S. Woods. *J. Am. Soc. of Mass Spectrom.* **2007**, 18, 567-577.

34. Jahouh, F.; Saksena, R.; Kováčb, P.; Banoub. J. *J. Mass. Spectrom.* **2012**, 47, 890–900.

35. Aebersold, R.; Mann, M. *Nature.* **2003**, 422, 198-207,

36. Domon1, B.; Aebersold,R.; *Science*, **2006**, 312 (5771), 212-217.

37. Burlingame, P. H.; Boyd, R. K.; Gaskell, S.J. *Anal. Chem.* **1996**, 68, 599R.

38. Soler, C.; Hamilton, B.; Furey, A.; James, K. J.; Mañes, J.; Picó, Y. *Analytica Chimica Acta.* **2006**, 571, 1 1–11.

39. Price, D.; Milnes, G. J. *Int. J. Mass Spectrum.* **1990**, 99, 1-39.

40. Cotter, R.J. *Anal Chem.* **1999**, 71, 445A-451A.

41. Mamyrin, B. A. *Int. J. Mass Spectrom. Ion Proc.* **1994**, 131, 1-19.

42. Paul, Wolfgang. *Reviews of Modern Physics.* 1990, 62 (3), 531–540.

43. Cooks, R. G.; Glish, G.L.; McLuckey, S.A.; Kaiser, R.E. *Chem. Eng. News.* **1991**, 69, 26.

44. March, R. E. and Hughes, R. J. *Quadrupole Storage Mass Spectrometry*. Wiley, New York 1989.

45. Wieboldt, R.; Campbell, D.; Henion, J. *LC/MS/MS Quantitation of Orlistat in Human Plasma with an ion Trap and a triple Quadrupole Spectrometer: A Comparative Study*. 45th ed.; ASMS Conference on Mass Spectrometry and Allied Topics, palm Springs, CA, 1-5, 1997.

46. Fishbane, P. M.; Gasiorowicz, S. G.; Thornton, S. T. *Physics for Scientists and Engineers.* 3rd ed.; Pearson Prentice Hall: 2005.

47. Marshall, A. G.; Hendrickson, C. L. *Int. J. Mass Spectrom. Ion Proc.* **2002**, *215*, 59 - 75.

48. Marshall, A. G.; Grosshans, P. B. *Anal. Chem.* **1991**, *63*, 215 - 229.

49. Pol, J.; Vidova, V.; Kruppa, G.; Kobliha, V.; Novak, P.; Lemr, K.; Kotiaho, T.; Kostiainen, V.; Havlicek, Volny, R. M. *Anal. Chem.* **2009**, 81, 8479–8487.

50. Yost, R. A.; Fetterolf, D. D. *Mass Specrtom. Rev*. **1983,** 2, 1-45.

51. Neubauer, G.; Mann, M. *Anal. Chem*. **1999**, 71, 235-242.

52. de Hoffmann, E. *J. Mass Spectrom.* **1996**, 31, 129-137.

53. Dass, C. *Mass Spectrom.* **1999**, 7, 95-98.

54. Jennings, K. *R. Int. J. Mass Spectrom. Ion Phys.* **1968**, 1, 227-235.

55. Zubarev, N. L.; Kelleher, F. W.; Mc Lafferty. *J. Am. Chem. Soc.* **1998**, 120, 3265–3266.

56. Syka, J. E.; Coon, J. J.; Schroeder, M. J.; Shabanowitz, J.; Hunt, D. F.; *Proc. Natl. Acad. Sci. U.S.A.* **2004**, 101, 9528–9533.

57. Mabud, Md. A.; Dekrey, M. J.; Cooks, R. G.; *Int. J. Mass Spectrom. Ion Proc.* **1985**, 67, 285-294.

58. Wysocki, V. H.; Ding, J. M.; Jones, J. L.; *J. Am. Soc. Mass Spectrom.* **1992**, 3, 27-32.

59. Harrison, A.G. *Mass Spectrom.* **1999**, 13, 1663-1670.

60. Cornish, T. J.; Cotter, R. J. *Rapid Commun. Mass Spectrom.* **1994**, 8, 781-758.

61. Spengler, B.; *J. Mass Spectrom.* **1997**, 32, 1019-1036.

62. Yergey, A. L.; Coorssen, J. R.; Backlund, P. S.; Blank, Jt.; P. S.; Humphrey, G. A.; Zimmerberg, J.; Cambell, J. M.; Vestal. M. L. *J. Am. Soc. Mass Spectrom.* **2002**, 13, 784-791.

63. Mechref, Y.; Novotny,V. M. *Anal. Chem.*, **2003**, **75** (18), 4895–4903.

64. Lewandrowski, U.; Resemann, A.; Sickmann. A. *Ana. Chem,* **2005**, 77 (10), 3274-3283.

65. Penn, S. G.; Cancilla, M. T.; Lebrilla, C. B. *Anal. Chem.* **1996**, 68, 2331–2339.

66. Bateman, R. H.; Caruthers, R. J.; Hoyes, B.; Jones, C.; Langridge, J. I.; Miller, A.; Vissers, J.B.C. *J. Am. Soc. Mass Spectrom.* **2002**, 13, 792-803.

67. Griffin, T.J.; Gygi, S.P.; Rist, B.; Aebersold R.; Loboda, A.; Jilkine, A.; Ens, W.; Standing, K.G. *Anal. Chem.* **2001**, 73, 978–986.

68. Jonscher, K. R.; Yates, J. R. *Anal. Biochem.***1997***,* 244, 1-15.

69. Cooks, R. G.; Kaiser, R. E. *Acc. Chem. Res.* **1992**, 23, 213-218.

70. Louris, J.N.; Cooks, R.J.; Syka, J.E.P.; Kelley, P.E.; Stafford, G.C.; Todd, J.F.J. *Anal. Chem.* **1987**, 59, 1677-1689.

71. March, R. E. *J. Mass Spectrom.* **1997**, 32, 351-369.

72. Hakansson, K.; Chambers, M. J.; Quinn, J. P.; McFarland, M. A.; Hendrickson, C. L.; Marshall, A. G. *Anal. Chem.* **2003**, 75, 3256-3262.

73. Rodriguez-Cruz, S. E.; Jockusch, R. A.; Williams, E. R. *J. Am. Chem. Soc.***1998**, 120, 5842 - 5843.

74. Rodriguez-Cruz, S. E.; Jockusch, R. A.; Williams, E. R. *J. Am. Chem. Soc.* **1999**, 121,8898 - 8906.

75. Dunbar, R. C. *Mass Spectrom. Rev.* **2004**, *23*, 127 - 158.

76. Hofstadler, H. A.; Wahl, J. H.; et al. *J. Am. Chem. Soc. Mass Spectrometry.***1994**, 5, 894-899.

77. Fridgen, T. D. *Mass Spectrom. Rev.* **2009**, 28, 586 - 607.

78. Polfer, N. C.; Oomens, J. *Mass Spectrom. Rev.* **2009**, 28, 468 - 494.

79. Polfer, N. C. *Chem. Soc. Rev.* **2011**, 40, 2211 - 2221.

80. Arora, A.; Rinehart, D.; Szabo, G.; Tamm, L. K. *J Biol Chem.* **2000**, 275, 1594–1600.

81. Miyadai, H.; Tanaka-Masuda, K.; Matsuyama, S.; Tokuda, H. *J. Biol. Chem.* **2004**, 279, 39807-39813.

82. Nikaido, H.; *Microbio.l Mo.l Biol. Rev.* **2003**, 67, 593–656.

83. Osborn, M.J.; Gander, J.E.; Parisi, E.; Carson, J. *J Biol Chem.* **1972,** 3973-3986.

84. Scott, J.R.; Barnett, T.C. *Ann. Rev. Microbiol.* **2006**, 60, 397-423.

85. Silhavy, T. J.; Kahne, D.; Walker, S. *Biol.* **2010**, 192, 3713-3721.

86. Choma, A.; Komaniecka, I.; Szewczuk, A. T.; Danihiewicz, W.; Spolnik, G. *Carbohydrate Research.* **2012**, 352, 126-136.

87. Matsuura, M. *Immunology*. **2013**, 154, 2131-2138.

88. Sohlenkamp, C.; Raetz, C. R. H.; Ingram, B. O. *Biochimica et Biophysica Acta.* **2013**, 1831, 1250-1259.

89. Sforza, S.; Silipo, A.; Molinaro, A.; Marchelli, R. ; Parrilli, M. ; Lanzetta, R. *J. Mass Spectrom.* **2004**, 39, 378-383.

90. Banoub, J. H.; El Aneed, A.; Cohen, A. M.; Joly, N. *Mass Spectrom Rev.* **2010**, 29, 606-650.

91. MacLean, L. L.; Perry, M. B.; Vinogradov, E. *Infect Immun.* **2004**, 72, 5925-5930.

92. Amor, k.; David, E.; Heinrichs, Frirdich, E.; Ziebell, K.; Johnson, P. R.; Whitfield, C. *Infect Immun.* **2000**, 68, 3, 1116–1124.

93. Kondakova, A.N.; Toukach, F.V.; Senchenkova, S.N.; Arbatsky, N.P.; Shashkov, A.S.; Knirel, Y.A.; Bartodziejska, B.; Zych, K.; Różalski, A.; Sidorczyk, Z. *Biochem.* **2003**, 68, 548–561.

94. Lukasiewicz, J.; Niedziela, T.; Jachymek, W.; Kenne, L.; Lugowski, C. *Glycobiology*. **2006**, 16, 538-550.

95. Sioud, S.; Jahouh, F.; Nashed, M.; Joly, N.; Banoub, J. H. *Rapid Commun in Mass Spectrom.* **2010**, 24, 2475-2490.

96. Michauda, J. P. et al, *PNAS*. **2013**, 110, 1941-1948.

97. Caroff, M.; Karibian, D. *Carbohydr.Res.* **2003**, 338, 2431-2447.

98. Li, B.; An, H. J.; Hedrick, J. L.; Lebrilla, C. B. *Methods Mol Biol.* **2009**, 534,1-13.

99. Zhang, J.; Schubothe, K.; Li, B.; Russell, S.; Lebrilla, C. B. *Anal Chem.* **2005**, **77**, 208–214.

100. Domon, B.; Costello, C. E. *Glyconjugate J.* **1988,** 5, 397-409.

101. Westphal, O.; Aepix, O.; Bister, F. *ZNaturforsch.* **1952**, 76, 148-155.

102. Pindur, U.; Mtiller, J.; F lo, C.; Witzel, H. *Chem. Soc. Rev.* **1987,** 16, 101-106.

103. Heyns, K.; Harrison, R.; Paulsen, H. *Chem. Ber.* **1967,** 100, 271-279.

104. Suami, T.; Ogawa, S.; Yoshizawa, T.; Umezawa, *S. Bull. Chem.* Soc. *Japan.* **1964,** 37,529-538**.**

105. Gigg, R.; Warren, C. D. J. *Chem. Soc.* **1965,** 1351-1357.

106. Hecker, *S.* J.; Minich, M. L.; Lackey, K. J. *Org. Chem.* **1990,** 55, 4905-4911.

107. Heyns, K.; Harrison, R.; Paulsen, H. *Chem. Ber.* **1967,** 100, 271-279.

108. Boullanger, P.; Jouineau, M.; Bouammali, B.; Lafont, D.; Descotes, G. *Carbohydr. Res.* **1990,** 202, 151-164.

109. Boullanger, P.; Banoub, J.; Descotes, G. *Can. J. Chem.* **1987,** 65, 1343.

110. Boullanger, P.; Lafont, D.; Banoub, J.; Descotes, G. *J. Carbohydr. Chem.* **1989,** 8, 343-1348.

111. Schultz, M.; Hermann, P.; Kunz, H. *Synlett* **1992,** 37, 4572-4581.

112. Imoto, M.; Yoshimura, H.; Shimamoto, T.; Sakaguchi, N.; Kusumoto, S.; Shiba, T. *Bull. Chem.* SOC. *Jpn.* **1987,** 60, 2205-2214.

113. Kiso, M.; Kito, T.; Murase, S.; Hasegawa, A. *Chem. Abstr.* **1989,** 39746-39753.

114. Higashi, K.; Nakayama, K.; Soga,T.; Shioya, E.; Poto, K.; Kusama, T. *Chem. Pharm. Bull.* **1990,** 38, 3280-3282.

115. Kolar, C.; Dehmel, K.; Wolk, H. *Carbohydr. Res.* **1990**, 206, 219-230.

116. Paulsen, H.; Helpap, B. *Carbohydr. Res.* **1991**, 216, 289-313**.**

117. Gunn, J. S. ; Lim, K. B. ; Krueger, J.; Kim, K. ; Guo, L.; et al. *Mol. Microbiol.* **1998**, 27, 1171–1182.

118. Christian, R. H.; Raetz, Guan Z.; Ingram, B. O.; Six, D. A.; Song, F.; Wang, X.; Zhao, J. *PMC*. **2009**, 50, S103–S108.

119. Visintin, A.; Halmen, K. A.; Latz, E.; Monks, B.G.; Golenbock, D.T. *Immunol, J.* **2005**,175,6465-64672.

120. Van, D. D.; Medzhitov, R.; Shaw, A.C.; *Trends Immunol.* **2006**, 27, 49–55.

121. Krziwon, C.; Zähringer, U.; Kawahara, K.; Weidemann, B.; Kusumoto, S.; et al. *Infect. Immun.* **1995**, 63, 2899-28905.

122. Babinski, K. J.; Ribeiro, A. A.; Raetz, C. R. H. *J. Biol. Chem.* **2002**, 277, 25937–25946.

123. Anderson, M. S.; Raetz, C. R. H. *J. Biol. Chem.* **1987**, 262, 5159–5169.

124. Williamson, J. M.; Anderson, M. S.; Raetz, C. R. H. *J. Bacteriol.***1991**,173, 3591-3596.

125. Wyckoff, T. J. O.; Lin, S.; Cotter, R. J.; Dotson, G. D.; Raetz, C. R. H. *J.Biol.Chem.* **1998**, 273, 32369-32372.

126. Jackman, J. E.; Raetz, C. R. H.; Fierke, C. A. *Biochemistry.* **2001**,40, 514–523.

127. Gennadios, H. A.; Whittington, D. A.; Li, X.; Fierke, C. A.; Christianson, D. W. *Biochemistry.* **2006**, 45, 7940-7948.

128. Gennadios, H. A.; Christianson, D. W. *Biochemistry.* **2006**, 45,15216–15223.

129. Vorachek-Warren, M. K.; Ramirez, S.; Cotter, R. J.; Raetz, C. R. H. *J. Biol. Chem.* **2002**, 277, 14194-14205.

130. Saitoh, S.; Akashi, S.; Yamada, T.; Tanimura, N.; Kobayashi, M. et al. *Int. Immunol.* **2004**, 16, 961–969.

131. Belunis, C. J.; Raetz, C. R. H. J. *Biol. Chem.* **1992**, 267, 9988–9997.

132. Brozek, K. A.; Raetz, C. R. H. J. *Biol. Chem.* **1990**, 265, 15410–15417.

133. Reynolds, C. M.; Kalb, S. R.; Cotter, R. J.; Raetz, C. R. H. J. *Biol. Chem.* **2005**, 280, 21202–21211.

134. Trent, M. S.; Raetz, C. R. H. J. *Endotoxin Res.* **2002**, 8, 158, 415-419.

135. Breazeale, S. D.; Ribeiro, A. A.; Raetz, C. R. H. *J. Biol. Chem.* **2002**; 277, 2886–2896.

136. Babinski, K. J.; Kanjilal, S. J.; Raetz, C. R. H. *J. Biol. Chem.* **2002**, 277, 25947-25956.

137. Babinski, K. J.; Ribeiro, A. A.; Raetz, C. R. H. *J. Biol. Chem,* **2002**, 277, 25937–25946.

138. Lukasiewicz, J.; Jachymek, W.; Niedziela, T.; Kenne, L.; Lugowski, C. *Lipid Research.* **2010**, 51, 564-574.

139. El Aneed, A.;Banoub, J. H. *Rapid Commun. Mass Sectrom.* **2005**, 19: 1, 1683-1695.

140. Wong, C. H. Carbohydrate-Based Drug Discovery. Wiley; 2003.

141. Klyosov, A. A.; Witczak, Z. J.; Platt, D. *Carbohydrate drug design*. 932. ACS; Washington: 2006.

142. Synowiecki, J.; Al-khateeb, N. A. *Critical Rev Food Sci Nutrition.* **2003**, 43, 145–171.

143. Poletti, L.; Lay, L. *Eur J Org Chem.* **2003**, 2999–3024.

144. Linhardt, R. J.; Toida, T. *Acc Chem Res.* **2004**, 37, 431–438.

145. Rossignol, D. P.; Hawkins, L. D.; Christ, W. J.; Kobayashi, S.; Kawata, T.; Lynn, M.; Yamatsu, I.; Kishi,Y. Brade, H.; Opal, S. M.; Vogel, S. N.; Morrison, D. C. *Endotoxin in Health and Disease*. **1999,** 699-717.

146. Kusumoto, S.; Oikawa, M. *Glycoscience: Chemistry and Chemical Biology*. Berlin - Heidelberg - New York: 2001.

147. Debenham, J.; Rodebaugh, R.; Fraser-Reid B. Liebigs Ann Recueil. **1997**, 791–802.

148. Aileen, F. G.; Bongat, Kamat, N. M.; Demchenko. V. A. *J Org Chem*. **2007**, 16; 72(4), 1480–1483.

149. Lin, L.; He, X.; Lindenmaier, M.; Yang, J.; Cleary, M.; Qiu, S.; Cordell, G. *Argric. Food Chem.* **2000**, 48(2), 354-365.